AD-A042 029 NAVAL RESEARCH LAB WASHINGTON D C F/G 17/1
PROCEEDINGS OF THE 25-26 FEB 1976 WORKSHOP ON MAGNETOSTRICTIVE --ETC(U)
JUN 77 R W TIMME
UNCLASSIFIED NRL-8137 NL

1 OF 2
ADA042029

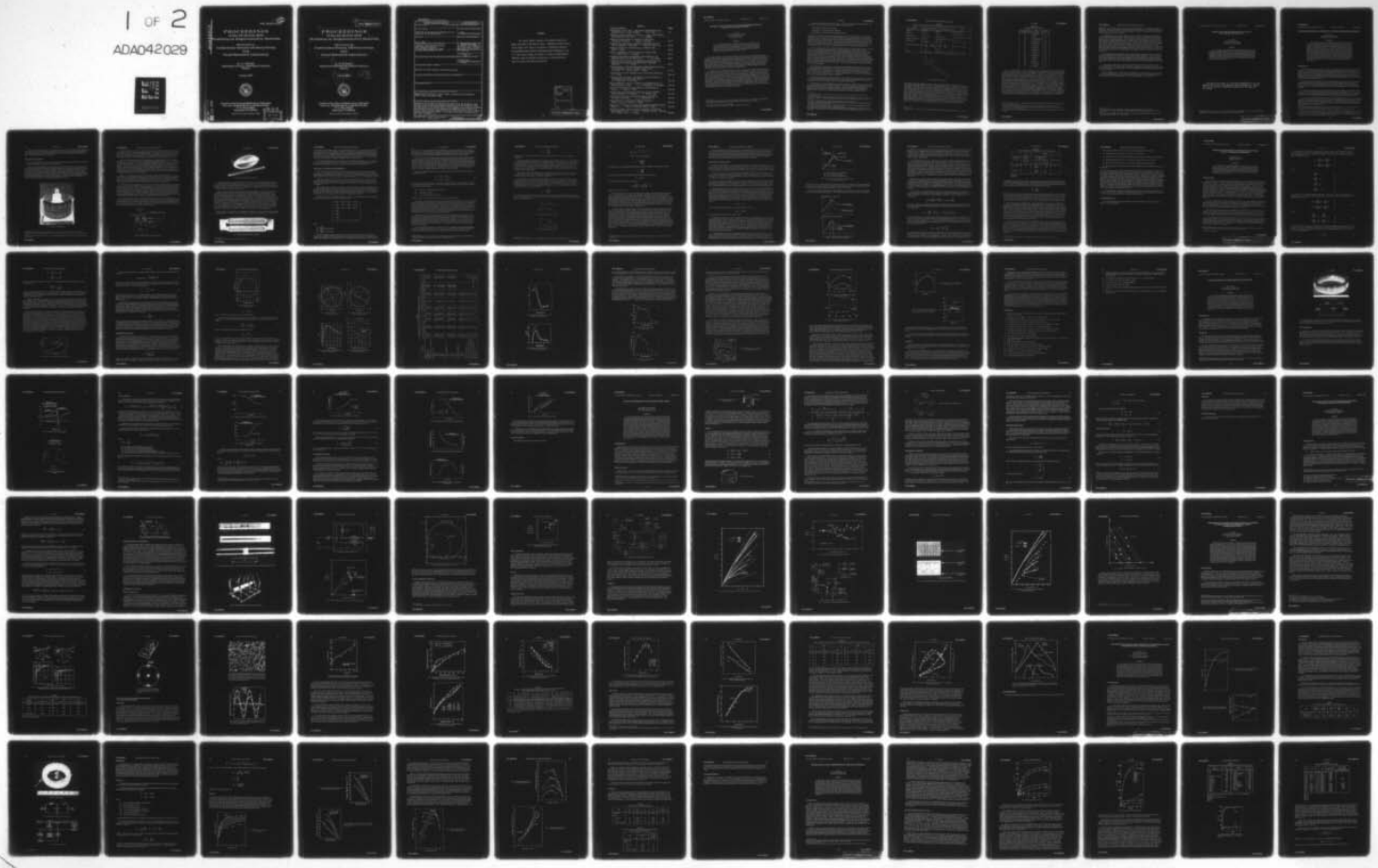

NRL Report 8137

PROCEEDINGS
of the 25-26 Feb 1976
Workshop on Magnetostrictive Materials

Sponsored by:
Underwater Sound Advisory Group
and
Naval Research Laboratory

R. W. TIMME
Materials Section, Standards Branch
Editor

1 June 1977

Underwater Sound Reference Division
NAVAL RESEARCH LABORATORY
P. O. Box 8337
Orlando, Fl 32806

(14) NRL Report 8137

(6)

PROCEEDINGS
of the 25-26 Feb 1976
Workshop on Magnetostrictive Materials

Sponsored by
Underwater Sound Advisory Group
and
Naval Research Laboratory

(10)

R. W. TIMME
Materials Section, Standards Branch
Editor

(11) 1 June 1977

(12) 171 p.

(9) Final rept.

Underwater Sound Reference Division
NAVAL RESEARCH LABORATORY
P. O. Box 8337
Orlando, Fl 32806

251 950

VP

UNCLASSIFIED

SECURITY CLASSIFICATION OF THIS PAGE *(When Data Entered)*

REPORT DOCUMENTATION PAGE		READ INSTRUCTIONS BEFORE COMPLETING FORM
1. REPORT NUMBER	2. GOVT ACCESSION NO.	3. RECIPIENT'S CATALOG NUMBER
4. TITLE *(and Subtitle)* Proceeding of the Workshop on Magnetostrictive Materials, 25-26 February 1976		5. TYPE OF REPORT & PERIOD COVERED Final 6. PERFORMING ORG. REPORT NUMBER
7. AUTHOR(s) R. W. Timme		8. CONTRACT OR GRANT NUMBER(s)
9. PERFORMING ORGANIZATION NAME AND ADDRESS Underwater Sound Reference Division Naval Research Laboratory P.O. Box 8337, Orlando, FL 32806		10. PROGRAM ELEMENT, PROJECT, TASK AREA & WORK UNIT NUMBERS PE: 62711N, Task: 14084, WU: M01-10.801 and PE: 61153N-11 Task: 5913, WU: S02-38.101
11. CONTROLLING OFFICE NAME AND ADDRESS		12. REPORT DATE 13. NUMBER OF PAGES 168
14. MONITORING AGENCY NAME & ADDRESS*(if different from Controlling Office)*		15. SECURITY CLASS. *(of this report)* Unclassified 15a. DECLASSIFICATION/DOWNGRADING SCHEDULE

16. DISTRIBUTION STATEMENT *(of this Report)*

Approved for public release; distribution unlimited

17. DISTRIBUTION STATEMENT *(of the abstract entered in Block 20, if different from Report)*

18. SUPPLEMENTARY NOTES

19. KEY WORDS *(Continue on reverse side if necessary and identify by block number)*

Magnetostrictive materials, sonar systems, underwater sound transducers, nickel alloys, rare earth alloys

20. ABSTRACT *(Continue on reverse side if necessary and identify by block number)*

A Magnetostrictive Materials Workshop was sponsored by the Underwater Sound Advisory Group and the Naval Research Laboratory on 25 and 26 February 1976. The objectives of the workshop were to bring together the scientists, engineers, and managers who are actively concerned with magnetostrictive materials to discuss recent advances, especially the rare earth-iron alloys, and to improve communication among disciplines. This issue of the Journal contains many of the papers presented.

DD FORM 1 JAN 73 1473 EDITION OF 1 NOV 65 IS OBSOLETE
S/N 0102-LF-014-6601

UNCLASSIFIED

SECURITY CLASSIFICATION OF THIS PAGE *(When Data Entered)*

FOREWORD

This report contains reprints of seventeen unclassified papers published in the Special Feature - Magnetostrictive Materials of the January 1977 issue of the Journal of Underwater Acoustics. The eighteenth paper entitled "Underwater Sound Transducers in the U. S. Navy: Past, Present, and Future" is classified CONFIDENTIAL; therefore, only the abstract of that paper is presented here so that this report may remain unclassified.

CONTENTS

U.S. Navy Journal of Underwater Acoustics Volume 27, No. 1 January 1977

INTRODUCTION TO THE THEME: WHAT FUTURE DO MAGNETOSTRICTIVE MATERIALS HAVE IN SONAR SYSTEMS?

R. W. Timme†
Underwater Sound Reference Division
Naval Research Laboratory
Orlando, Florida 32806

ABSTRACT

A Magnetostrictive Materials Workshop was sponsored by the Underwater Sound Advisory Group and the Naval Research Laboratory on 25 and 26 February 1976. The objectives of the workshop were to bring together the scientists, engineers, and managers who are actively concerned with magnetostrictive materials to discuss recent advances, especially the rare earth-iron alloys, and to improve communication among disciplines. This issue of the Journal contains many of the papers presented.

In February 1976, the Underwater Sound Advisory Group and the Naval Research Laboratory sponsored a small workshop on magnetostrictive materials and their relation to underwater sound. Fifty people directly involved in various aspects of this field attended the 2-day meeting at the Underwater Sound Reference Division in Orlando, Florida. The attendees were a cross section of a rather diverse group. Sonar system designers and engineers were present, as were basic physicists, material scientists, and program managers. Some were Government people, some were from industry, and some from universities, but all had the common interest of how magnetostrictive materials might be applied to satisfy Navy needs of generating and detecting underwater sound.

The purpose of the workshop was twofold: to discuss the question of "*What future do magnetostrictive materials have in sonar systems?*" and to improve communications among the various interested parties. This has not been the first such workshop or minisymposium. Similar meetings with similar objectives were held in 1966[1] and 1969.[2] The need for this meeting was largely a result of the recent discovery and development of rare-earth iron alloys having magnetostrictive properties far exceeding the more conventional nickel alloys. In fact, reports were being received from various research groups about alloys having coupling coefficients, strains, and power-handling capabilities exceeding, in some cases, the piezoelectric ceramics that had displaced the nickel alloys 20 or so years ago. Thus it was appropriate to reconvene for discussion of recent advances. Some of the attendees had also been present at the earlier meetings, but because time does take its toll, most of the attendees were relative newcomers and the establishment of lines of communication was needed.

†The Editors would like to thank Dr. R. W. Timme of NRL (Orlando), Chairman of the Workshop, for soliciting and editing the papers presented in this issue and for writing this very fine introduction to the theme.

[1]W. S. Cramer, ed., *JUA(USN)* 17, 199-346 (1967).
[2]F. S. Gardner, ed., *Proc. Met. Magnetoacoust. Mater. Workshop* (25 Aug. 1969).

Twenty-four formal presentations were made, 17 of which are the bulk of this Journal issue. The presentations can be divided into three rather different groups as follows:

1. Sonar transducer material requirements
2. Investigation of magnetostrictive nickel alloys
3. Investigation of magnetostrictive rare-earth iron alloys

The first session, chaired by Mr. Carey Smith (NAVSEA), opened with a discussion[3] of the historical development of Navy sonar by Dr. C. H. Sherman (NUSC). He presented the reasons why piezoelectric ceramics have been so much preferred over the conventional magnetostrictive alloys. He also discussed present and future Navy needs for sonar with references to specific numbers and systems and how new magnetostrictive alloys might be useful. A general impression received from Dr. Sherman's remarks was that the sonar engineers and designers are fairly content with piezoelectric ceramics and that any new material would have to possess clearly outstanding attributes before it would be widely accepted.

The next two papers by Dr. R. S. Woollett (NUSC)[4] and Dr. C. M. Davis (NRL)[5] were of a tutorial nature. They discussed the relations between basic material properties and operating transducer parameters and reviewed the properties of the conventional magnetostrictive materials. As a result of these two excellent presentations, the scientists understood more fully the operational implications of such properties as low elastic moduli, low permeability, and large magnetic fields, and the engineers understood better the need for studying such things as magnetocrystalline anisotropy and alloying techniques. Dr. Davis discussed one of the plagues of this business—investigators 20 years ago used different symbols to represent certain properties. The situation has been confused even more because some people, then as now, use electromagnetic units (emu), some use mks, and some use various combinations of the two. The reader may find it useful to review Table I in which the equivalences of the more unfamiliar parameters are summarized.

The second session, chaired by Dr. R. M. Bozorth, internationally known magnetician, concerned current investigations of conventional (i.e., non-rare-earth iron) magnetostrictive alloys. Only five papers were presented, which is indicative of the recent low level of effort in these materials. P. J. Lenart (NUSC)[6] and Drs. D. T. Peters (INCO),[7] E. L. Huston (INCO)[8], and J. A. Sinsky (NRL)[8] described work on nickel and nickel-cobalt alloys. C. L. LeBlanc (NUSC)[9] and Dr. E. L. Huston (INCO)[10] talked on the use of orthogonal magnetic fields in transducers.

The third group of papers was devoted entirely to the rare-earth iron alloys, which have been touted as the most significant breakthrough since the ceramics. These papers were presented in two sessions chaired by Dr. C. M. Davis, Jr. (NRL), and Dr. F. S. Gardner (ONR, Boston).

A slight digression may be appropriate at this point to answer the question "*What are a rare-earths?*" First of all, they are not "earths." They are a group of transition metals known as the lanthanide series and are found in the periodic chart as shown in Fig. 1. They are the 15 elements starting with lanthanum, atomic number 57, and ending with lutetium, atomic number 71. Each element in the lanthanide series has one more $4f$ electron than the preceding. They all have similar chemical

---

[3] C. H. Sherman, "Underwater Sound Transducers in the U.S. Navy: Past, Present, and Future," *JUA(USN)* **27**, (1977) (Confidential).
[4] R. S. Woollett, "Relation of Basic Material Properties to Operating Transducer Parameters," *JUA(USN)* **27** (1977).
[5] C. M. Davis, "Properties of Conventional Magnetostrictive Materials for Use in Underwater Transducers," *JUA(USN)* **27**, (1977).
[6] P. J. Lenart, "Nonlinear High-Drive Characteristics of Nickel Rings," *JUA(USN)* **27** (1977).
[7] D. T. Peters, "Comparison of the Magnetic and Magnetostrictive Properties of Cube-Textured and Conventional Nickel Transducer Materials," *JUA(USN)* **27** (1977).
[8] J. A. Sinsky, E. L. Huston, and D. T. Peters, "The Evaluation of Cube-Textured Nickel-Cobalt Magnetostrictive Ring Transducers During Low-Power Linear Drive," *JUA(USN)* **27** (1977).
[9] C. L. LeBlanc and C. H. Sherman, "Effect of Orthogonal Field Excitation of Nickel Rings," *JUA(USN)* **27** (1977).
[10] E. L. Huston, "Orthogonal Excitation of Magnetostrictive Materials for Improved High-Drive Characteristics," *JUA(USN)* **27** (1977).

TABLE I
Relations Between Parameters in the Electromagnetic (emu) and mks Systems of Units

Parameter	Unit in the emu System	Unit in the mks System	Relation
Current I	Abampere	ampere	1 abamp = 10 A
Potential V	abvolt	volt	1 abvolt = 10^{-8} V
Magnetic field H	oersted (Oe)	ampere-turn/meter	1 Oe = $(10^3/4\pi)$ (amp-turn)/m
Magnetic flux density B	gauss (G)	webers/meter^2 (= tesla (T))	1 G = 10^{-4} T
Permeability μ	oersted/gauss	henry/meter	1 Oe/G = $4\pi \times 10^{-7}$ H/m
Magnetostrictive constant d	$d = \frac{(\partial B)}{(\partial T)_H} = 4\pi \frac{(\partial S)}{(\partial H)_T}$	$d = \frac{(\partial B)}{(\partial T)_H} = \frac{(\partial S)}{(\partial H)_T}$	d (emu) = 10^3 d (mks)
	Oe^{-1}	m/A-turn	
Stress T	dynes/centimeter^2	newton/meter^2 (= pascal (Pa))	1 dyne/cm^2 = 10^{-1} Pa

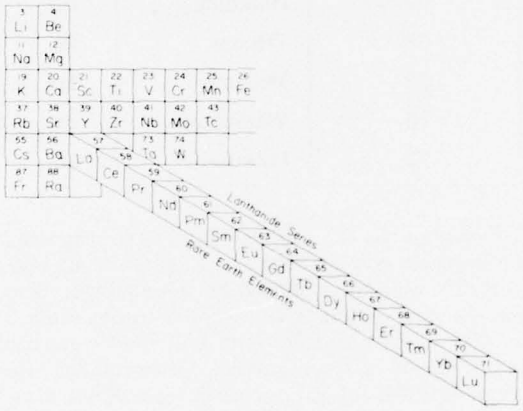

Fig. 1. Periodic chart of the elements

characteristics. Some are magnetic, some are not; some are magnetostrictive, some are not; and some have magnetic anisotropy, some do not. But, if they are magnetic, they are very magnetic. If they are magnetostrictive, the effect is huge. If they are anisotropic, the energies are tremendous. This series is truly a land of the giants. The second point to make about the rare-earth elements is that they are not rare. Dr. Gschneidner (Iowa State) pointed out in his presentation[11] that there are no availability problems with the rare-earth elements; in fact, there are many common elements (such as mercury, cadmium, iodine, and selenium) which are less abundant and several more (such as tungsten, molybdenum, tin, and lead) equally abundant. This, unfortunately, however, is not to say the rare earths are cheap. At present, the average cost of a 99.9% pure rare earth is about the same per kilogram as research grade lead zirconate titanate ceramic. Of course, this is much higher than the commercial grade ceramics from which transducers are made, but if a large market developed for the rare earths, then a substantial decrease in cost could occur. The lanthanide rare-earths are listed by name and symbol in Table II.

[11] K. A. Gschneidner, "Availability and Costs of Rare-Earth Metals—Especially the Heavy Lanthanides," *JUA(USN)* 27 (1977).

TABLE II
Lanthanide Rare-Earth Elements

Atomic Number	Element	Symbol
57	Lanthanum	La
58	Cerium	Ce
59	Praseodymium	Pr
60	Neodymium	Nd
61	Prometheum	Pm
62	Samarium	Sm
63	Europium	Eu
64	Gadolinium	Gd
65	Terbium	Tb
66	Dysprosium	Dy
67	Holmium	Ho
68	Erbium	Er
69	Thulium	Tm
70	Ytterbium	Yb
71	Lutetium	Lu

Dr. A. E. Clark (NSWC),[12] one of the discoverers of the large magnetostrictive effect in rare-earth iron alloys, opened the session on these new materials with an excellent review of the work leading to their discovery and a discussion of the promise offered by these alloys. Good progress has been made in characterizing the properties of the new materials; here contributions came from Drs. H. T. Savage (NSWC)[13] and R. W. Timme (NRL-USRD).[14] Data were presented comparing properties such as coupling coefficient, magnetostrictive constant, magnetostrain, permeability, effects of bias stress, elastic moduli, and power-handling capability for several rare-earth iron alloys, nickel, and ceramic. Dr. N. C. Koon (NRL), also one of the discoverers of these alloys, discussed some very recent data on a newly developed quaternary alloy that may be the best yet.[15] Alloy studies to achieve toughening in these somewhat brittle alloys were described by Dr. C. R. Crowe (NSWC).[16] Progress reports were presented, but are not published here, on single and polycrystalline growth by Dr. J. E. Milstein (NRL), on hot pressing techniques by Dr. H. J. van Hook (Raytheon), on plasma spray coatings by Dr. T. Taylor (Union Carbide), on vacuum-sintered and epoxy-encapsulated materials by D. A. E. Clark (NSWC), and on a samarium-nickel-iron composite by Dr. D. T. Peters (INCO). Dr. K. A. Gschneidner (Iowa State University) reviewed the availability and costs of the lanthanide rare-earth metals.[11] Actual prototype transducers, using rare-earth iron alloys as the active material, were described by Drs. J. E. Butler

[13]H. T. Savage and W. A. Ferrando, "Magnetomechanical Coupling, ΔE Effect, and Magnetization in Rare Earth-Iron Alloys," *JUA(USN)* **27** (1977).
[14]R. W. Timme, "Device-Oriented Material Measurements on Rare-Earth/Iron Alloys," *JUA(USN)* **27** (1977).
[15]N. C. Koon and C. M. Williams, "Extremely Low Anisotropy, High Magnetostriction Materials in a Quaternary Rare-Earth Iron System," *JUA(USN)* **27** (1977).
[16]C. R. Crowe, "Microstructure and Mechanical Properties of the Iron Rare-Earth Intermetallic Compounds," *JUA(USN)* **27** (1977).

(Raytheon),[17] R. R. Smith (NUC),[18] and O. L. Akervold (Honeywell).[19] The performance of these transducers suffered somewhat because their designs were undertaken before the material properties were fully known, but they were successful in demonstrating the potential of the materials and indicating in what areas special care would be necessary.

The workshop closed with an open discussion of the possibilities of applying the rare earth-iron alloys in underwater sound transducers. General opinion was that the rare earth-iron alloys, notably $Tb_{0.3}Dy_{0.7}Fe_2$, do have great potential. Many of the material design goals (e.g., strain, coupling, low eddy-current loss, and high-power capability) established by the sonar designers and engineers at the previous workshops in 1966 and 1969 have been met or exceeded. *But*, as is always the case, the price must be paid. For these materials that price not only includes cost but also the need of large magnetic fields and a brittleness similar to ceramic. In addition, some designers may be hesitant to accept magnetostrictive alloys simply because magnetic fields are inherently more difficult to route and control than electric fields. Before becoming discouraged, however, one should remember these materials have not been known very long and, at a similar point in development, ceramics were also looked upon with some doubt.

The continuing development program for rare earth-iron alloys is healthy and has an enthusiastic group of investigators and a multitude of avenues open for further improvement. The aforementioned need of large magnetic fields may be greatly reduced by the quaternary alloys, or permanent magnets may be used to provide the bias and thereby partially remove the need for large current-carrying coils. The problem of brittleness in ceramics has partially been solved, and similar techniques could be applied here.

At this point the outlook for a major fleet sonar system design using a rare-earth iron alloy is cloudy and premature. For many reasons ceramics are not threatened by competition from these alloys, but a complementary role is quite possible. At present, application in low-frequency, high-power projectors appears promising.

Thus the original question of "*What future do magnetostrictive materials have in sonar systems?*" was not definitely answered, nor was it expected to be. The purposes of the workshop, to discuss the question and to improve communications, were accomplished, however, to the benefit of all.

---

[17] J. L. Butler and S. J. Ciosek, "Development of Two Rare-Earth Transducers," *JUA(USN)* **27** (1977).
[18] R. R. Smith and J. C. Logan, "Design of a Transducer Using Rare-Earth Magnetostrictive Materials," *JUA(USN)* **27** (1977).
[19] O. L. Akervold, D. L. Hutchins, R. G. Johnson, and B. G. Koepke, "Rare-Earth Magnetostrictive Transducer and Material Development Studies," *JUA(USN)* **27** (1977).

U.S. Navy Journal of Underwater Acoustics Volume 27, No. 1 January 1977

UNDERWATER SOUND TRANSDUCERS IN THE U.S. NAVY: PAST, PRESENT, AND FUTURE* (U)

C. H. Sherman
New London Laboratory
Naval Underwater Systems Center
New London, Connecticut 06320

ABSTRACT

(U) Some aspects of the technical history of underwater sound transducers in the U.S. Navy are reviewed to explain the transition from magnetostrictive transducers to piezoceramic transducers. Present Navy use of transducers is then summarized in terms of the numbers and types of transducers that are being used for functions such as sonar and communications. Finally, estimates are made of Navy needs from transducers in the near future based on extension of present needs and on new sonar arrays now under development. The possibilities are also assessed for the use of new magnetostrictive materials in present and future Navy transducers.

The text of this paper is classified CONFIDENTIAL and has been omitted here so that this report may remain unclassified. Please refer to the Journal of Underwater Acoustics for the report by Dr. Sherman.

*Presented at the Workshop on Magnetostrictive Materials held under the sponsorship of the Underwater Sound Advisory Group and the Naval Research Laboratory, Orlando, Florida, 25-26 February 1976.

UNCLASSIFIED

U.S. Navy Journal of Underwater Acoustics Volume 27, Number 1 January 1977

RELATION OF BASIC MATERIAL PROPERTIES TO OPERATING TRANSDUCER PARAMETERS*

Ralph S. Woollett
Naval Underwater Systems Center
New London, Connecticut 06320

ABSTRACT

In evaluating materials for projector applications, a preliminary step is to measure their small-signal properties and then relate these properties to transducer performance by means of equivalent circuit analysis or distributed vibrator theory. However, no judgment of the material's capability can be made until the large-signal limits of the material's operating envelope are found. For magnetostrictive materials the saturation magnetostrictive strain is the most decisive high-level property, but the hysteresis and winding losses sustained in driving to high strains are also of first-order importance. Because the magnetostrictive materials will be in competition with piezoelectric ceramics, it is important that all properties of the two classes of materials be expressed on a common basis to the maximum extent possible. When the rare-earth compounds enter the evaluation arena, new aspects of the design problem come to the fore. With these materials heat transfer design must be given high priority, and the design must accommodate a volume of copper conductor that probably exceeds the volume of the magnetic core. These practical problems as well as the traditional material criteria will influence the final judgment.

INTRODUCTION

At the last magnetostriction workshop in 1969[1] I was assigned a topic similar to the present one, namely, to relate material properties to transducer performance and thereby reveal the areas where improvements in materials were most needed. I concluded then that the highest priority in materials development should be given to increasing the saturation magnetostrictive strain λ_s, because this property was limiting the power capability of magnetostrictive transducers and thereby making them noncompetitive.[2] It appeared that dramatic improvements could not be expected from alloy systems then in use; so our hopes lay in breakthroughs in magnetic research.

It was astounding how rapidly these requested breakthroughs came about. Rare-earth compounds† that are magnetostrictive at room temperatures were in 1969 only something to be speculated about. Fortunately, Earl Callen was at the meeting and did the speculation. Today these compounds are a well-documented reality,[3] and they have provided values of saturation magnetostriction beyond my wildest imaginings.

It is only the influence of these new materials that allows this presentation to be any different from the one delivered in 1969, because design and analysis procedures have not changed much in the interim. Therefore, in addition to reviewing once again the material properties that are important to the transducer designer, I will try to indicate ways in which use of the new materials would change design parameters.

The big challenge that the rare-earth elements present to the designer is the need for very much higher magnetic fields than that to which he has been accustomed. This feature requires that the volume of copper conductor be increased by an order of magnitude or more over that used with the older materials and requires that great emphasis be put on heat transfer design. The volume of the winding will more likely than not exceed the volume of the magnetic core.

*Presented at the Workshop on Magnetostrictive Materials held under the sponsorship of the Underwater Sound Advisory Group and the Naval Research Laboratory, Orlando, Florida, 25-26 February 1976.

†A brief discussion of the rare-earth metals is given by Dr. Timme in his Introduction to the Theme in this issue.

[1] F. S. Gardner, ed., "Proceedings of the Metallic Magnetoacoustic Materials Workshop," ONR Boston Branch (25 Aug. 1969).
[2] R. S. Woollett, "Magnetostrictive Material Requirements for Sonar Transducers," *JUA(USN)* **20**, 679-690 (1970).
[3] H. T. Savage, A. E. Clark, and J. M. Powers, "Magnetomechanical Coupling and ΔE Effect in Highly Magnetostrictive Rare Earth-Fe_2 Compounds," *IEEE Trans. Magn.* **mag-11**, 1355-1357 (1975).

My review is organized as follows: first, I will describe various types of magnetostrictive transducers; then, I will review the small-signal material properties that are used in the initial phase of transducer design; finally, I will talk about the large-signal power limits of the material and how this information is used to establish the final capability of the design.

TYPES OF TRANSDUCERS[4-6]

Some of the configurations in which magnetostrictive materials can be used will now be described to illustrate qualitatively the important design considerations.

Figure 1 shows a free-flooding nickel ring transducer. The rings vibrate with a uniform breathing motion and radiate sound from both their inside and outside surfaces. They are normally used at radial resonance, and the size of the resonant ring is slightly less than one wavelength in the water. Because the nickel core is noncorrosive, it requires no protection from the seawater. The excellent strength of the laminated nickel rings and the elegant simplicity of this configuration has made the magnetostrictive ring a popular transducer type—the only one that survived the competition of the piezoceramics for very long. The winding is intended to be acoustically transparent. It does not contact the vibrating core, and hence does not contribute to the mechanical impedance of the ring.

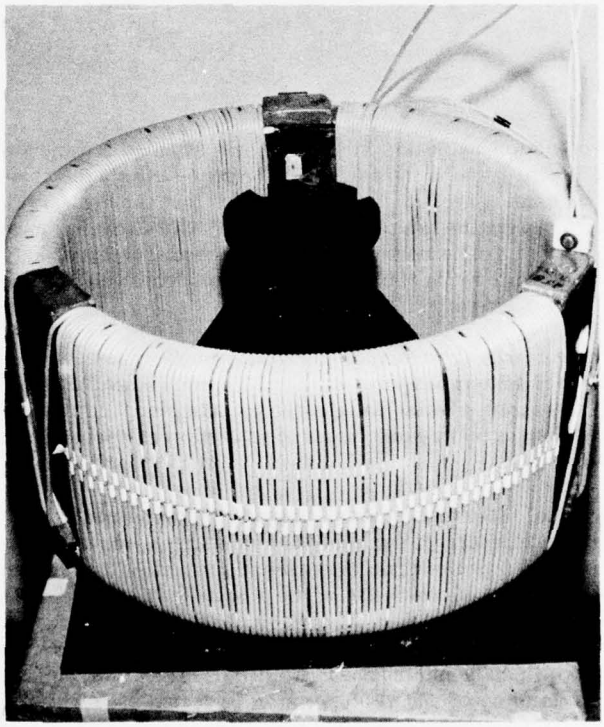

Fig. 1. Nickel scroll ring transducer

[4]R. S. Woollett, "Power Limitations of Sonic Transducers," *IEEE Trans. Sonics Ultrason.* **su-15**, 218-229 (1968).
[5]T. F. Hueter, "Twenty Years in Underwater Acoustics: Generation and Reception," *J. Acoust. Soc. Am.* **51**, 1025-1040 (1972).
[6]C. H. Sherman, "Underwater Sound—A Review. 1: Underwater Sound Transducers," *IEEE Trans. Sonics Ultrason.* **su-22**, 281-290 (1975).

If instead of nickel, the rings were made out of one of the rare-earth compounds, such as $TbFe_2$, they would be capable of much higher broadband power. Unfortunately, in the course of the development of the new materials, the great strength advantage of the magnetostrictive metals slipped away. The $TbFe_2$ ring would be brittle and fragile. We hope that other rare-earth compounds will be developed that will regain the strength advantage—even if the price is lower magnetostrictive activity.

The very thick winding required on a rare-earth metal core could hardly be made acoustically transparent. It would be necessary then to consolidate the winding with the core for the vibrations to be transmitted to the water. If a rubbery consolidating compound was used, the winding would add mass but not much stiffness, and the resonance frequency would go down. The mechanical losses would be increased. If, on the other hand, a rigid consolidating compound was used, both mass and stiffness would be added and the change in resonance frequency would be less. The added stiffness would decrease the effective electromechanical coupling factor of the resonator. The possibilities for heat transfer are good in the free-flooding arrangement. Techniques for circulating liquid through the consolidated winding would have to be explored.

Figure 2 is a schematic illustration of a longitudinally vibrating composite transducer. The resonator consists of two laminated magnetostrictive bars joined at the front to a radiating head and at the rear to a counterbalancing tail mass. Magnetostrictive resonators of this type have been completely superseded in the United States by piezoceramic versions. The increase in power promised by the rare-earth compounds would tend to put the magnetostrictive type back in the competition.

Because the conductive windings are not in the path of vibratory power flow, they can be isolated from the cores by spacing. Then the thick coil required for a rare-earth model would not affect the mechanical behavior of the resonator. Permanent magnets have sometimes been used in these structures, but their reluctance degrades performance, and they could not provide a strong enough field for the rare earth compounds. A dc bias current is, therefore, required. Transducers of this type are usually used in pulsed sonar systems; it would be desirable to pulse the bias current along with the signal to reduce heating and conserve power. The need for providing a bias power supply and associated circuitry would penalize the magnetostrictive designs in any competition with the piezoceramics.

The transducer shown in Fig. 3 is called a flextensional type because it uses both flexural and extensional vibrations. The driving member is the axial ceramic stack; it induces flexural vibrations in the surrounding metal shell. The flextensional transducer is smaller than the types described previously for the same resonance frequency. Of course, the smaller size is accompanied by a decrease in power, but the resulting performance will be optimum for some applications.

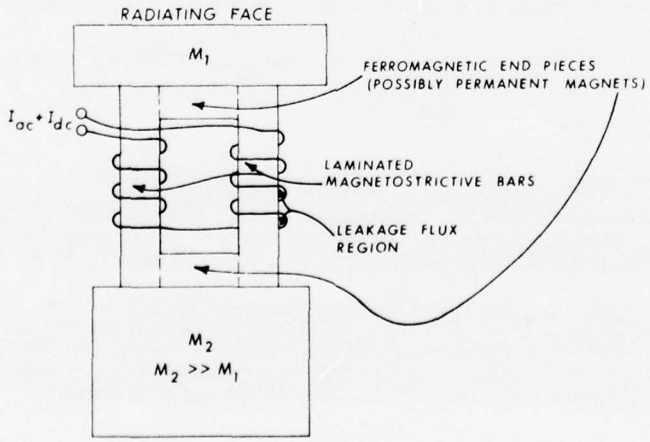

Fig. 2. Longitudinal vibrator transducer (tonpilz)

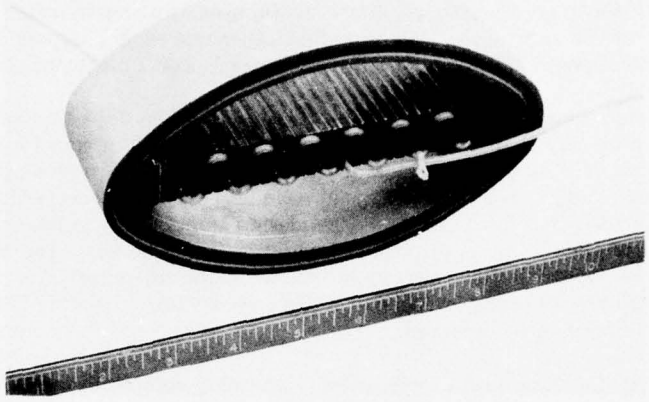

Fig. 3. Piezoelectric flextensional transducer

No magnetostrictive version of this transducer has been built to my knowledge, but the configuration is obviously suitable for magnetostrictive drive. In the latter case the oval shell would be ferromagnetic to provide the flux return path for the central bar. As in the longitudinal vibrator transducer, the winding coil can be isolated from the core. The heavy coil required for a rare-earth core would then not affect the vibratory behavior of the transducer.

Figure 4 shows a flexurally vibrating magnetostrictive bar assembly.[7] The two bars flex inwardly and outwardly together, forming a balanced vibrator. Flexural vibrators are advantageous for low-frequency use because they are more compact than extensionally vibrating types and more compact even than the flextensional type. To generate flexural motion, it is necessary for the magnetostrictive strains in the opposite sides of a bar to be of opposite polarity. In the arrangement shown, each bar is slotted, and separate windings are put on the two halves of each bar. Then an attempt is made to restore the integrity of the bars by filling the slots with aluminum spacers and epoxy. This nickel vibrator is about 1 m long and resonates at 300 Hz. It is intended to radiate from the outer surfaces of the bars; it would be incorporated in a housing designed to retain air in the space between the bars. Although this is a very rugged device, its power capability is too low because of the low saturation magnetostriction of the available metals. Piezoceramic flexural bars have swept the field of competition. The fragility of the ceramic has been overcome to a large extent by the use of compressive prestress.

Because improved very-low-frequency transducers are urgently needed, a good place to put the rare-earth compounds to use would be in the construction of flexural bars, assuming that a compound could

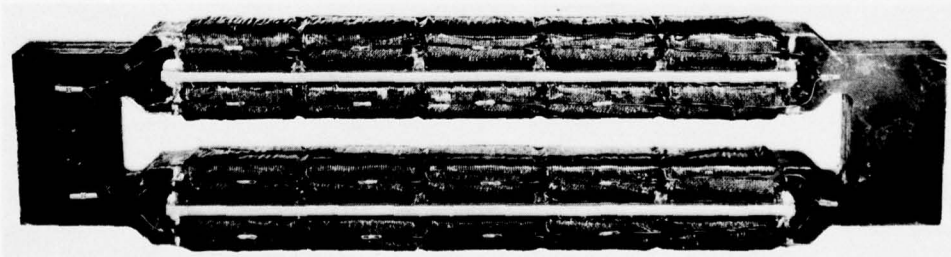

Fig. 4. Co-Ni double-bar flexural-mode transducer

[7]R. S. Woollett, U. S. Patent No. 3,174,130 (issued 16 Mar. 1965).

be developed with reasonable strength. A simpler arrangement than the one shown would be desirable at the start, and it is, in fact, possible to avoid the slotted bars and complicated windings and just use a single coil on each bar. To generate flexure in that case, bilaminar bars employing two dissimilar materials would be used. One material would have positive magnetostriction and the other negative magnetostriction for the best results. Flexure could still be produced, but less effectively, if one of the laminations was inert, composed, for example, of stainless steel or a strong ceramic.

In the flexural bar transducer, the coils must be consolidated with the magnetic cores to allow the vibration to be transmitted to the water. The massive coils required for a rare-earth transducer will affect the vibratory behavior with results similar to those discussed for the ring transducer.

SMALL-SIGNAL PIEZOMAGNETIC PROPERTIES

I will now turn to the quantitative aspects of evaluating magnetostrictive materials for transducer applications. The transducers under consideration are primarily high-power projectors. The prospects for magnetostrictive hydrophones at this time are pretty dim. It is assumed that the material is operated with a magnetic bias so that for small signals, at least, the transducer acts as a linear transmission system.

Small-signal properties will be discussed first. These properties enable one to calculate to a first approximation resonance frequency, bandwidth, efficiency, and input power factor. They cannot, of course give any information on the power capability of the transducer. Power limits will be discussed at length later.

Biased magnetostrictive materials operating in the linear regime may be called piezomagnetic in the same sense that prepoled electrostrictive ceramic materials are called piezoelectric. The material may be described by linear equations of state (or constitutive equations), which are analogs of the piezoelectric equations of state. There are four forms in which these equations may be written. I will be using the form in which stress and magnetic field intensity are the independent variables.

Equation (1) shows the piezomagnetic equations of state for a polycrystalline material, which apply when the ac magnetic field is colinear with the dc bias field:

$$\left.\begin{aligned}
S_1 &= s_{11}^H T_1 + s_{12}^H T_2 + s_{13}^H T_3 + d_{31} H_3 , \\
S_2 &= s_{12}^H T_1 + s_{11}^H T_2 + s_{13}^H T_3 + d_{31} H_3 , \\
S_3 &= s_{13}^H T_1 + s_{13}^H T_2 + s_{33}^H T_3 + d_{33} H_3 , \\
S_4 &= s_{44}^H T_4 , \\
S_5 &= s_{44}^H T_5 , \\
S_6 &= s_{66} T_6 \\
B_3 &= d_{31} T_1 + d_{31} T_2 + d_{33} T_3 + \mu_{33}^T H_3
\end{aligned}\right\} \qquad (1)$$

where

S = strain,
H = magnetic field intensity,
T = stress,
B = magnetic flux density.

If the ac field had a component normal to the dc field, shear strains would be produced piezomagnetically and additional terms would appear in the equations, but this type of exciting field is not used in sonar transducers. In the equations, S_1 to S_3 are extensional strains and T_1 to T_3 are extensional

strains and T_1 to T_3 are extensional stresses. Similarly S_4 to S_6 are shear strains, and T_4 to T_6 are shear stresses. By convention, the x_3 coordinate axis coincides with the direction of the bias magnetization. However, the bias magnetization and the resulting static strain do not appear in the equations; the variables that are shown are the small signal incremental values of stress, strain, and field.

The s coefficients (with double subscripts) in the equations of state are elastic moduli measured at constant field intensity, the d coefficients are piezomagnetic moduli, and μ_{33}^T is the incremental permeability measured at constant (or zero) stress. The values of all the coefficients depend on the particular value of the bias magnetization that is chosen for the operating point. There are eight independent coefficients in this set, but in engineering applications they are not all used or measured. The notation is that of the IEEE Standards,[8] which is a big improvement over the unsystematic and ambiguous notation used in some of the older literature. The parallelism of these equations with those of piezoelectricity is a big help to transducer designers who wish to work in both fields.

Equation (2) shows the equations of state reduced to the simple form that is adequate for most transducer applications:

$$\left.\begin{aligned} S_3 &= s_{33}^H T_3 + d_{33} H_3 \\ B_3 &= d_{33} T_3 + \mu_{33}^T H_3 \end{aligned}\right\} . \tag{2}$$

These equations apply to slender bars or thin rings, in which lateral stress can be neglected. Shearing stresses are also presumed to be absent. We are left with three coefficients that are of practical interest in small-signal transducer design:

s_{33}^H = reciprocal of Young's modulus, constant H,

d_{33} = piezomagnetic modulus,

μ_{33}^T = incremental permeability, constant T.

In addition, we are interested in the density of the material and its resistivity.

The influence of these properties on transducer design will now be reviewed. The elastic compliance modulus s_{33}^H together with the density ρ determines the speed of sound in the material. A small sound velocity (large s_{33}^H) is often desired because it can result in a compact resonator for a given frequency. In the case of a ring transducer resonating at a given frequency, for example, an ordinary nickel ring would be 60% larger in diameter than a PZT-4 ceramic ring; a cube-textured nickel ring, however, would be only 26% larger; and a rare-earth $TbFe_2$ ring would be about the same size as the ceramic one. A large compliance modulus also leads to low specific acoustic impedance for the material and this helps the designer to achieve low mechanical Q and large bandwidth.

Turning to the incremental permeability μ_{33}^T, we note that a high value of permeability would enable us to use a winding with few turns and still achieve the normal electrical impedance level. On the other hand, high permeability tends to produce high eddy-current loss; so we would not want the permeability raised unless the resistivity of the material was also raised. As a practical matter, the incremental permeability of nickel, which lies in the range 30 to 100 relative to free space, appears to be satisfactory. The rare-earth compounds have low permeability, which requires that large coils be used, as mentioned earlier.

A high piezomagnetic modulus d_{33} obviously is desired. To judge the small-signal piezomagnetic activity of a material, one should not look at d_{33} alone, but rather combine the three coefficients of the equations of state as shown in Eq. (3) to yield the electromechanical coupling factor k_{33}.

[8]Technical Committee on Transducers and Resonators of the IEEE Group on Sonics and Ultrasonics, "IEEE Standard on Magnetostrictive Materials: Piezomagnetic Nomenclature," IEEE Standard (1971).

$$k_{33}^2 = \frac{d_{33}^2}{s_{33}^H \mu_{33}^T} . \tag{3}$$

The values of the coupling factor always lie between zero and one; hence, it is easy to judge their significance.

The electromechanical coupling factor is analogous to the coupling coefficient of a mutual inductor. Its fundamental character is brought out by its energy definition. When energy is put into a transducer electrically, k_{33}^2 gives the fraction of the input energy that appears in mechanical form, stored in the elastic displacement. It is thus a basic index of energy conversion capability of the transducer. For nickel, $k_{33} \approx 0.3$ at optimum bias. For the cobalt-nickel alloys, values exceeding 0.5 have been obtained at optimum bias. Most aspects of transducer performance (especially bandwidth) improve with an increase in the coupling factor.

Figure 5 gives values of the piezomagnetic parameters for annealed nickel.[9] The curves show the way these parameters vary with bias flux density. Evidently these parameters cannot be treated as constants unless the swing of the ac flux density is kept small.

As an example of how the piezomagnetic parameters are used in a transducer design, an electromechanical circuit is shown in Fig. 6 for a ring transducer. The ring is assumed to be vibrating with uniform radial motion. The circuit relates the electrical variables voltage and current to the mechanical variables radial velocity and force. The classical analogy is used, with velocity analogous to current. Starting at the left of Fig. 6 we have the blocked inductance L_b, that is determined by the number of turns—the dimensions, and the permeability:

$$L_b = \frac{n^2 bh\mu_{33}^S}{2\pi a} .$$

The electrical and mechanical portions of the circuit are coupled by an electromechanical gyrator, whose ratio α is determined by the piezomagnetic modulus and the compliance modulus along with the number of turns and the dimensions:

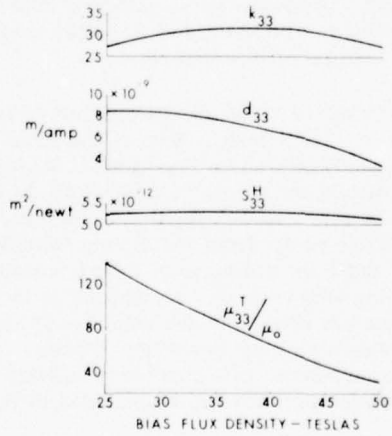

Fig. 5. Piezomagnetic parameters for nickel

[9]"Magnetostriction Transducers," Vol. 13, National Defense Research Council, Div. 6 (NTIS PB77669, 1946).

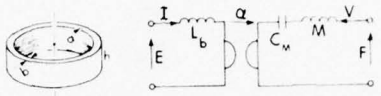

Fig. 6. Circuit for a ring transducer

$$\alpha = -\frac{nbhd_{33}}{aS_{33}^{H}} .$$

The compliance C_M is determined by the dimensions and the compliance modulus of the material:

$$C_M = \frac{aS_{33}^{H}}{2\pi bh} .$$

The mass M of the vibrator is determined by the dimensions and the density:

$$M = 2\pi abh\rho .$$

The angular resonance frequency ω_r is given by

$$\omega_r = \sqrt{\frac{1}{MC_M}} = \frac{1}{a}\sqrt{\frac{1}{\rho s_{33}^{H}}} = \frac{C^H}{a} .$$

Where C^H is the sound velocity.

The right-hand side of the circuit is terminated in the radiation impedance when the transducer is in water. It is then possible to calculate the small-signal performance of the transducer by circuit analysis. However, the circuit as shown omits all losses. A mechanical loss resistance should be estimated and added to the right-hand mesh of the circuit. The eddy-current loss angle should be calculated from lamination thickness and the permeability and resistivity of the material. To account for the calculated eddy-current effects in the circuit, one would add resistance to the left-hand mesh and also make the gyrator ratio a complex number. The small-signal efficiency could then be calculated. The result gives a preliminary view of the dissipation problem, but the more important efficiency is the one effective at high levels, which is lower because of hysteresis loss.

A tuning condenser is normally added at the electrical input of the circuit to improve the power factor of the transducer's impedance. The circuit is then in the form of a bandpass filter, and according to the theory of Mason,[10] its bandwidth about resonance is determined by the effective electromechanical coupling factor. Specifically the fractional bandwidth $\Delta f/f_r$ is approximately equal to the coupling factor k for the electrically tuned transducer that has a radiation load close to optimum. Mason's goal is to extract the available power from the driving amplifier over the widest possible frequency band and deliver it to the radiation resistance at a fairly constant level over the band. He is thus as concerned with the operating efficiency of the amplifier as he is with the transducer, and in his specified band the tuned transducer will present to the amplifier an impedance of high-power factor and fairly constant magnitude. If, however, an amplifier of greater than conventional capacity is employed, then, by a more or less brute force approach, it is possible to operate over a bandwidth that exceeds the Mason criterion. A description of this approach will be included in the later discussion of large-signal operation.

[10] W. P. Mason, "Electromechanical Transducers and Wave Filters," (D. Van Nostrand Co., Inc., New York, 1948), 2nd ed., pp. 230-238.

For the longitudinally vibrating transducer, an electromechanical circuit may be obtained also, but it is more complicated than the one shown for the ring in Fig. 6 in that it contains transcendental impedance functions in the mechanical mesh rather than the lumped parameter elements shown for the ring. However, approximations for the longitudinal vibrator are possible for the frequency region about resonance, and the circuit is than reduced to the form shown here. The relations between material properties and transducer performance are similar for both types of vibrators.

LARGE-SIGNAL POWER LIMITS

Operation of the materials at high power and limits that are encountered will be discussed in this section. One problem, which may be very formidable, is heating. I will bypass that problem by assuming that the signal has a low duty cycle and that the designer is very talented in heat transfer design. Also, it will be assumed that the operating depth is great enough that cavitation does not have to be considered.

Figure 7 shows source level or power output curves applicable to either electric or magnetic transducers. The low frequency resonator is illustrated, for which the radiation resistance is proportional to the square of the frequency. The same design principles apply to higher frequency transducers, although the slopes of the curves will be modified.

A stress limit exists in the region of resonance, where the material may fail from fracture or fatigue. Off-resonance, the source level is determined by the maximum blocked force that may be generated in the material by magnetostriction or electrostriction. This force is ultimately limited by magnetic saturation in the magnetostrictive case and by voltage breakdown in the electrostrictive or piezoelectric case.

An alternative to the concept of a limiting blocked force is the concept of a limiting free displacement, where the free displacement is generated magnetostrictively or electrostrictively. This free displacement ξ_f is derived from the blocked force F_b by multiplying the latter by the compliance C_M. The stress limit line has a slope that is the same as the slope of the low-frequency response and a height relative to the response given by the ratio of the fatigue-limited displacement to the free displacement resulting from the magnetostriction or electrostriction, as shown on the graph. For a simple transducer with uniform strain distribution, the displacement is simply the strain multiplied by the length of the active material. Thus the maximum free displacement may be related to the saturation magnetostrictive strain λ_s:

$$\max \xi_f = \ell \lambda_s ,$$

and the fatigue limited displacement may be related to fatigue stress $T_{\max}$:

$$\xi_{\max} = \ell s_{33}^H T_{\max} .$$

For more complex vibrators, similar relations hold.

In summary, the source level out of the region of resonance for a magnetostrictive vibrator may be expressed in terms of either the maximum blocked force, the maximum free displacement, or the saturation magnetostrictive strain λ_s. This leads to the important conclusion that the ultimate limit on source level is the saturation magnetostrictive strain λ_s, except in a narrow band about resonance where the fatigue limit of the material may be the determining factor. In order for this saturation limit to be a practical operating limit, it is necessary, of course, to have a material with a narrow hysteresis loop so that it may be driven near saturation without encountering astronomical values of hysteresis loss. Another factor determining how close we can approach the ultimate power limit is the amount of waveform distortion that can be tolerated.

A transducer that is heavily loaded by radiation may not encounter the stress limit even at resonance. An optimum Q_M for power is defined as the Q_M that causes the stress limit and the electric or magnetic force limit to be equal at resonance, as shown by the tangency of the curves in Fig. 7. For broad bandwidths we must operate near the base of the resonance curve. Note that lowering Q_M does

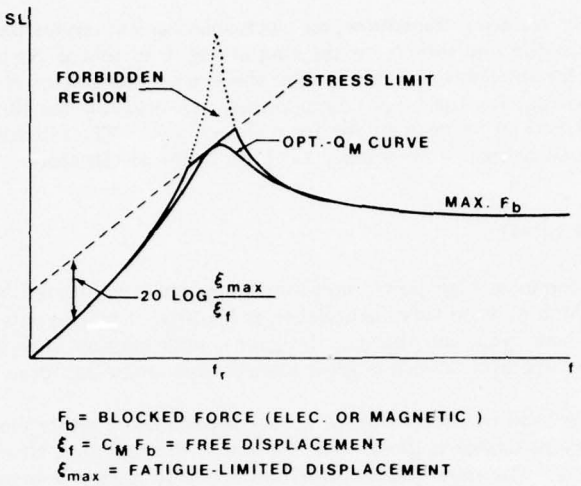

Fig. 7. Source level curve, showing limits caused by allowable stress and attainable driving force

not broaden the base; it simply lowers the undesired peak. Hence we should not be too firmly wedded to the idea that low Q_M is required for broadband. The troublesome peak may be reduced by electrical equalization at the amplifier input when design for low Q_M is impractical.

In Fig. 8 narrowband and broadband operating conditions are compared. The source level envelope represents the power limits shown in Fig. 7. Any chosen operating curve must lie within the confines of

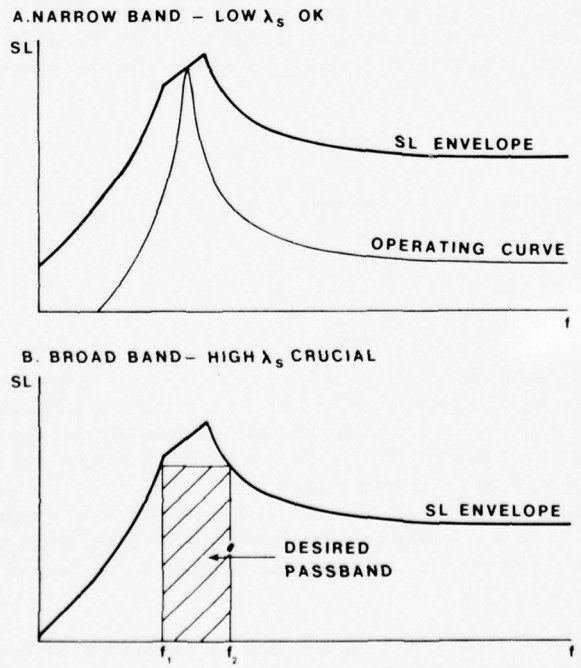

Fig. 8. Source level (SL) envelope with possible operating regions: (a) narrowband and (b) broadband

this envelope. In the narrowband case (Fig. 8(a)) the transducer has a high Q_M and the fatigue or fracture properties of the material are crucial. A high-saturation magnetostriction is not needed; nickel, for example, should be adequate. In the example illustrated the material has a high-saturation magnetostriction, but the transducer operates with a driving field very much below saturation, thus not fully using the material. Only rarely do transducer specifications call for such a narrowband that the material is stress limited as illustrated here.

A very broadband case is shown in Fig. 8(b). The top of the required passband remains below the stress limit, and the achievable power is determined entirely by the saturation magnetostriction λ_s. In trying to synthesize a flat-topped response as shown, a number of techniques can be used, including adding a tuning condenser to the transducer, using input equalizers ahead of the power amplifier, and using acoustoelectrical feedback. The graph depicts the transducer's ability to supply acoustic power over a chosen band, but it does not provide any insight into the problem of extracting this power from the amplifier. To minimize this problem we should aim for a fractional bandwidth no greater than the coupling factor k, but this criterion of Mason's is hard to apply because k is not constant over the large field excursions employed. If we exceed Mason's criterion, the extra bandwidth is purchased at the price of a larger amplifier, capable of supplying reactive power at the band edges and tolerating impedance mismatches.

The discussion so far has centered around saturation magnetostriction, with some attention paid to coupling factor. Permeability also is an important consideration for high-power operation. The lower the permeability, the more copper will be needed in the winding to drive to saturation flux density and the greater will be the heat problem. Low permeability is thus undesirable. Dr. Arthur Clark (NSWC), however, has pointed out that when very high magnetostrictive strain is achieved, low permeability tends to follow and that this phenomenon is required by conservation of energy. Thus, high driving fields are inevitable.

To show that a very high driving field is required to achieve high magnetostrictive strain (at least in the rare-earth materials), consider a simple transducer with uniform strain distribution and neglect magnetic nonlinearity. The material is biased halfway to saturation so that its operating point is specified as follows:

$$\text{electrical}\left(\frac{B_{\max}}{2}, \frac{H_{\max}}{2}\right); \quad \text{mechanical}\left(\frac{\lambda_s}{2}\right)$$

where $B_{\max}$ and $H_{\max}$ are maximum values (close to saturation) of the flux density and field intensity respectively. Equation (4) shows the relation between the input and output energy densities, μ_e and μ_{em}, respectively:

$$\mu_{em} = \frac{1}{8}\frac{\lambda_s^2}{s_{33}^H} = \frac{k^2}{1-k^2}\,\mu_e = \frac{k^2}{1-k^2}\,\frac{1}{8}\,B_{\max}H_{\max}\,. \tag{4}$$

The converted energy μ_{em} is proportional to λ_s^2 and will be large if the objective of a high value for λ_s has been achieved. The input energy, proportional to the BH product, must be even larger because of imperfect coupling, evidenced by $k < 1$. Because the maximum flux density $B_{\max}$ is limited by saturation, the burden of providing the large input energy falls on H. To show this explicitly, one can solve for $H_{\max}$ and obtain Eq. (5):

$$H_{\max} = \frac{1}{B_{\max}}\,\frac{1-k^2}{k^2}\,\frac{\lambda_s^2}{s_{33}^H}\,. \tag{5}$$

The saturation flux density for the rare-earth compound $TbFe_2$ is about 8200 G (0.82 T); so this value along with the other properties can be substituted into Eq. (5) to determine what values of driving field are required by the conservation of energy principle. The results of the calculation are included in the 3d column of Table I. The table shows magnetic fields required to achieve selected high-strain values

TABLE I
Electric and Magnetic Fields Required to Generate Large Strains

Peak-to-Peak Strain λ ($\lambda < \lambda_s$)	PZT-4 rms Electric Field E_3 ($k = 0.7$) (kV/cm)	$TbFe_2$		
		Peak-to-Peak Magnetic Field H_{max} ($k = 0.4$, $B_{max} = 8200$ G)		Permeability
		Oe	10^4 A/m	
333×10^{-6}	4	[a]670 [b]1,600	[a]5.3 [b]13	12
900×10^{-6}	11	[a]4,800 [b]4,800	[a]38 [b]38	1.7

[a]Calculated.
[b]Measured.

and compares $TbFe_2$ with PZT-4 ceramic. The coupling factor appropriate to large-signal drive was assumed to be somewhat smaller than the maximum value measured under small-signal conditions for $TbFe_2$. The gross permeability (relative to that in free space μ_0) corresponding to the maximum H values is shown and is seen to be very low, as calculated from the equation

$$\frac{\mu}{\mu_0} = \frac{B_{max}}{H_{max}} .$$

The calculations are of value in showing the inevitability of the high driving fields, but more accurate numbers are obtained from direct measurements. The calculated H for 900 part per million (ppm) strain agrees with the measured value, but the calculated H for 330 ppm is low by over a factor of 2; this is probably because the flux density at this strain is not near saturation as was assumed. All the numbers, whether calculated or measured, convey the same impression of very high magnetic fields.

PZT-4 will produce the 330 ppm strain at an rms driving field of 4 kV/cm (10 V/mil), which is a value often used by designers, although it is considered by some to be higher than desirable. For 900 ppm strain, 11 kV/cm is required. This is much higher than is used in practice, but it has been suggested by Berlincourt[11] as a possible driving field. To use this field would require that much more space be devoted to insulation than is needed at present. Cooling of the ceramic would be a problem, and low duty cycle would be a necessity. The analogous problems in using $TbFe_2$ at 900 ppm strain would be providing room for the great volume of conductor that would be required and cooling the winding and core. Neither the PZT-4 nor the $TbFe_2$ design task would be easy, but if a requirement for extraordinarily high-power densities were to arise, the designer would have to decide which is the lesser evil: providing insulation to contain electric fields of 11 kV/cm or providing conductors to generate magnetic fields of 4800 Oe (3.8×10^5 A/m).

Should we really be concerned about achieving high-power densities, or can we get along nicely using nickel for scrolls and using PZT at 2 to 3 kV/cm for other configurations? Having been, for 25 years, on the receiving end of requests for less weight, less volume, and more power (all adding up to more watts/kilogram) there has never been any doubt in my mind that we need greater power densities. But there are others who are preoccupied with some of the better present systems and are so well satisfied with the results obtained that they seem puzzled by attitudes such as mine. To lay to rest any doubts that materials researchers might be engaged in unnecessary endeavors, I have listed some pertinent applications:

[11]W. P. Mason, ed., "Physical Acoustics" (Academic Press, Inc., New York, 1964), Vol. 1, Part A, p. 255.

- Long range surveillance might use 50 tons (45 Mg) of magnetostrictive material.
- Submarine add-on system space, if not weight, is very limited.
- Towed active systems and variable depth sonar require low drag, sometimes neutral buoyancy.
- Air-transported systems such as active sonobuoys, and dipped sonar must be light.
- Systems constrained by ejection ports must pass through torpedo or signal tube.
- Very-low-frequency projectors have poor radiation loading; therefore, high demands are put on the material.

For these applications, power densities will probably never be high enough to make the transducer user lose interest in further gains, provided they are not exorbitantly priced. Long-range surveillance, employing large high-power arrays, may someday come to life again. If it does, reductions in the weight of the transducers will ease deployment and maintenance problems. Transducers to be added to submarines have volume restrictions because spaces outside the pressure hull are limited and drag increases must be avoided. In towed systems, restrictions on both weight and volume limit the performance attainable with conventional materials. Air-transported systems will always benefit from less weight if accomplished with no decrease in performance. Systems planners are continually coming up with ingeneous schemes for devices that must be launched through torpedo tubes or signal tubes yet have impressive sonar performance. Very-low-frequency projectors normally are required to be much less than a wavelength in dimensions. Therefore they have low radiation resistance and require large magnetostrictive or electrostrictive displacements to radiate significant power.

It is concluded that the search for materials with greater power capability is indeed justified. At the same time it must be recognized that the transducer designer has a very demanding list of properties that the material must possess before it will displace existing materials.

ACKNOWLEDGMENTS

This work was supported by the NAVSEA Sonar Technology Division, SEA 06H1-2 with C. C. Walker as the Project Manager.

U.S. Navy Journal of Underwater Acoustics Volume 27, Number 1 January 1977

PROPERTIES OF CONVENTIONAL MAGNETOSTRICTIVE MATERIALS FOR USE IN UNDERWATER TRANSDUCERS*

Charles M. Davis, Jr.
Naval Research Laboratory
Washington, D.C. 20375

ABSTRACT

The properties of conventional magnetostrictive materials are presented and compared. The criteria considered for comparison are (a) the ability to transfer energy between the electrical and mechanical systems, (b) the open circuit voltage produced by an applied mechanical pressure, (c) the maximum power-handling capacity, (d) frequency limitations caused by eddy currents, and (e) ease and expense of fabrication. The materials discussed include nickel, 2V-permendur, Alfenol, the permalloys, a Mn-Co-Ni alloy, Co-Cr-Ni alloys, and various ferrites.

INTRODUCTION

Prior to 1946, nickel, 2V-permendur, and 45 permalloy were the only magnetostrictive materials available for transducers.[1] (Actually, in 1943 the Japanese began to use hot rolled Al-Fe alloys, but because of the war did not publish this information.) In 1950 Sussman and Ehrlich[2] reported on the transducer properties of an iron, cobalt, and chromium alloy named "Hiperco." In the same year Masumoto and Otomo[3] published information about the dynamic magnetostrictive properties of an Al-Fe alloy named "Alfer." In 1953 Nachman and Buehler[4] developed a method of warm-rolling Alfer below the crystallization temperature. Alloys processed in this manner are essentially "cold-rolled" and therefore exhibit grain orientation. They are referred to as "Alfeno." In 1954 the dynamic magnetostrictive activity of these alloys was investigated by Davis, Robey, and Ferebee.[5,6] In 1956 Davis, Helms, and Ferebee[7,8] investigated the Ni-Fe alloys containing from 35% to 67.5% nickel (permalloys). Clark reported on the dynamic magnetostriction of Ni-Co alloys in 1956[9] and the Ni-Co-Cr alloys in 1961.[10]

A variety of magnetostrictive ferrites have been considered. The cobalt-substituted nickel ferrites were investigated at the RCA Laboratory;[11] the Philips Research Laboratory;[12] and elsewhere.[13] The effect of replacing a portion of the nickel by ferrous iron was described by Davis and Ferebee.[14,15] Kikuchi[16] considered the Ni-Zn and Ni-Cu ferrite systems. C. M. Van der Burgt and A. L. Stuijts[17] as well as Brockman[18] have described a number of magnetostrictive ferrites.

The rare-earth iron alloys currently being considered are a significant new class of magnetostrictive materials. The nomenclature being used to describe the properties of these alloys is consistent with existing IEEE standards on piezoelectric crystals[19] and differs from that used in Refs. 1-17. In the next section, design considerations are discussed in terms of both the old and the new nomenclature.

To evaluate magnetostrictive materials, the following factors will be considered: (a) the ability to transfer energy between the electrical and mechanical systems, (b) the open circuit voltage produced by an applied mechanical pressure, (c) the maximum power-handling capacity, (d) frequency limitations caused by eddy currents, and (e) the ease and expense of fabrication. The relative importance of the factors depends somewhat on the application.

*Presented at the Workshop on Magnetostrictive Materials held under the sponsorship of the Underwater Sound Advisory Group and the Naval Research Laboratory, Orlando, Florida, 25-26 February 1976.

[1]See reference list on page 51.

A magnetostrictive material, when subjected to a change in magnetic state, undergoes a change in mechanical state or visa versa. The mathematical approach used until recently expressed the change in stress T and magnetic field H that resulted from a change in magnetic induction B and mechanical shape S by the differential relations

$$\left.\begin{aligned} dT &= \left(\frac{\partial T}{\partial B}\right)_S dB + \left(\frac{\partial T}{\partial S}\right)_B dS \\ dH &= \left(\frac{\partial H}{\partial B}\right)_S dB + \left(\frac{\partial H}{\partial S}\right)_B dS \end{aligned}\right\} \tag{1}$$

where

$$\left.\begin{aligned} \left(\frac{\partial T}{\partial B}\right)_S &= -\lambda\,, \\ \left(\frac{\partial T}{\partial S}\right)_B &= E_B\,, \\ \left(\frac{\partial H}{\partial B}\right)_S &= \frac{1}{\mu_r}\,, \\ \left(\frac{\partial H}{\partial S}\right)_B &= -4\pi\lambda\,. \end{aligned}\right\} \tag{2}$$

The symbol λ is the "so-called" dynamic magnetostriction constant, E_B is the Young's Modulus at constant B, and μ_r is the blocked or reversible permeability. The presently adopted nomenclature can be defined by the relations

$$\left.\begin{aligned} dB &= \left(\frac{\partial B}{\partial H}\right)_T dH + \left(\frac{\partial B}{\partial T}\right)_H dT \\ dS &= \left(\frac{\partial S}{\partial H}\right)_T dH + \left(\frac{\partial S}{\partial T}\right)_H dT \end{aligned}\right\} \tag{3}$$

where

$$\left.\begin{aligned} \left(\frac{\partial B}{\partial H}\right)_T &= \mu_T\,, \quad \left(\frac{\partial B}{\partial T}\right)_H = d\,, \\ \left(\frac{\partial S}{\partial H}\right)_T &= \frac{d}{4\pi}\,, \quad \left(\frac{\partial S}{\partial T}\right)_H = S^H\,. \end{aligned}\right\} \tag{4}$$

The symbol μ^T is the permeability at constant T, d is effective piezomagnetic strain constant, and S^H is the elastic compliance at constant H. The 4π that appears in Eqs. (2) and (4) is the result of the use of the emu system of units. Solving for dB and dS in Eq. (1) and comparing with Eqs. (2), (3), and (4) yields the following relations:

$$\mu^T = \frac{\mu_r}{1 - k^2}\,, \tag{5}$$

$$S^H = \frac{1}{E_B(1-k^2)} = \frac{1}{E_H}, \tag{6}$$

$$d = \frac{4\pi\lambda\mu_r}{E_H} = 4\pi\lambda\mu_r S^H \tag{7}$$

where E_H is the Young's modulus at constant H. The electromechanical coupling coefficient k, given by the expression

$$k^2 = \frac{4\pi\lambda^2\mu_r}{E_B} = \frac{d^2}{4\pi S^H \mu^T}, \tag{8}$$

is the most important single factor used to characterize magnetostrictive materials. For a sample freely vibrating with no losses or radiation, it can be shown that k^2 is either the fraction of the stored magnetic energy that is converted to mechanical energy or the fraction of the stored mechanical energy that is converted to magnetic energy.[2]

To optimize hydrophone performance, it is necessary to maximize the open circuit voltage resulting from a change in stress. Because the induced voltage is proportional to the magnetic flux change, the parameter d provides a criterion for the evaluation of hydrophone materials. (See Eq. (4).) For conventional materials, E_H remains constant to within a few percent. It follows from Eq. (7) that $\lambda\mu_r$ represents an alternate figure of merit for hydrophone performance. In the case of rare-earth iron alloys, E_H changes by more than a factor of 2 with magnetic bias, and $\lambda\mu_r$ cannot be used to replace d for hydrophone evaluation.

Several processes contribute to a change in magnetization: domain-wall motion, nucleation of domains of reverse magnetization, and rotation out of easy direction.[20] Processes such as 180° domain-wall motion, which predominate on the steep portion of the magnetization curve, account for only a small portion of the observed magnetostriction.[21] In this region a given change in flux produces very little change in stress and thus results in a small value of λ. Rotation out of easy direction is the mechanism that accounts for the major portion of the magnetostrictive effect. For the materials listed in the introduction, this mechanism predominates between the knee of the magnetization curve and saturation and results in a larger value of λ in this region. On the other hand, the value of μ_r decreases when rotations out of the easy direction predominate. Because there is no sharp division in the region where one or the other of these mechanisms occur, the value of λ would be expected to increase and μ_r to decrease continuously as saturation is approached. This is in agreement with the results shown in Fig. 1 for nickel. In the same figure the variation in $\lambda\mu_r$ with bias is shown. A similar curve is expected for d. On the basis of the observed variation of λ and μ_r, it is possible to explain the maxima that occur as a function of bias for k^2 as well as $\lambda\mu_r$.

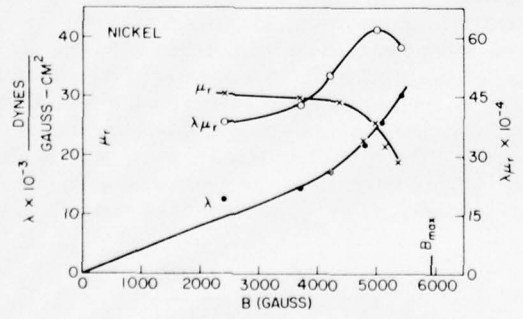

Fig. 1. Variation of λ, μ_r, and $\lambda\mu_r$ with magnetic induction

The maximum output power that a magnetostrictive material is capable of providing is given by the expression[1]

$$\text{maximum power} = \frac{Q_m T_{\max}^2 \omega \times 10^7}{E_B} \tag{9}$$

where ω is the angular frequency, Q_m is the mechanical Q, and $T_{\max}$ is the maximum stress. Using the expression for λ given in Eq. (2), the value of $T_{\max}$ can be determined from the area under the λ versus B curve such as in Fig. 1. The resulting expression is

$$T_{\max} = -\int_0^{B_{\max}} \lambda \, dB \, . \tag{10}$$

Because Q_m and in most cases ω are determined primarily by the transducer design and not by the magnetostrictive material used, the power developed in a magnetostrictive material is proportional to $T_{\max}^2/E_B$. From Eq. (10) it is seen that the maximum power achievable is determined not only by λ but also by $B_{\max}$.

Finally, the power-handling capacity of a transducer is, from a practical standpoint, often limited by both the resultant heating and ease of cooling. The latter is less of a problem for magnetostrictive alloys than for ceramics because of the large thermal conductivity of metals. For conventional magnetostrictive alloys, heating results primarily from eddy-current losses. This may not be the case in rare-earth iron alloys operated in a biased state where copper loss could predominate. The frequency at which the skin depth becomes equal to $\sqrt{2}$ times the lamination thickness t is defined as the characteristic frequency f_c. The product $f_c t^2$ is given by[1]

$$f_c t^2 = \frac{10^9 \rho_e}{2\pi^2 \mu_r} \tag{11}$$

where ρ_e is the electrical resistivity in ohm-centimeters and t is in centimeters. To simplify fabrication, it is desirable that $f_c t^2$ be made large. The value of ρ_e is essentially a constant of the material while μ_r is strongly influenced by processing, construction techniques, and operating conditions. Thus for a given value of ρ_e, to increase $f_c t^2$, it is necessary to reduce μ_r. This, however, decreases the value of k and $\lambda\mu_r$, and d, thus processing is a tradeoff. The aim is to achieve as large a value of λ as possible while settling for a value of μ_r that will provide simultaneously sufficiently large k, $\lambda\mu_r$, d, and $f_c t^2$.

EXPERIMENTAL DETAILS

To determine all the parameters in Eq. (8), it is necessary to measure at least three of them independently. The most convenient to measure are μ_r, E_B, and k. For toroidal samples oscillating in the radial extensional mode, lumped parameter techniques may be employed. The three parameters can be determined by the motional-impedance method.[1] This consists of measuring the electrical impedance versus frequency. The mechanical impedance appears as an added electrical impedance at the input terminals. For the case of large Q_m, the various electrical, magnetic, and mechanical parameters can be obtained from the impedance locus. The total impedance in air of a 12.5 Alfenol ring stack is shown in Fig. 2. (The number preceding Alfenol refers to the percentage of aluminum.) The value of μ_r obtained from the blocked (or clamped) reactance, $(X_b)_{\omega_0}$, measured at resonance, is given by the expression

$$\mu_r = \frac{(X_b)_{\omega_0} a \times 10^9}{4\pi f_0 N^2 b \ell} \tag{12}$$

where f_0 is the resonant frequency in hertz, N is the number of turns, b is the wall thickness, a is the mean radius, and ℓ is the height. All dimensions are given in centimeters. The expression for E_H is

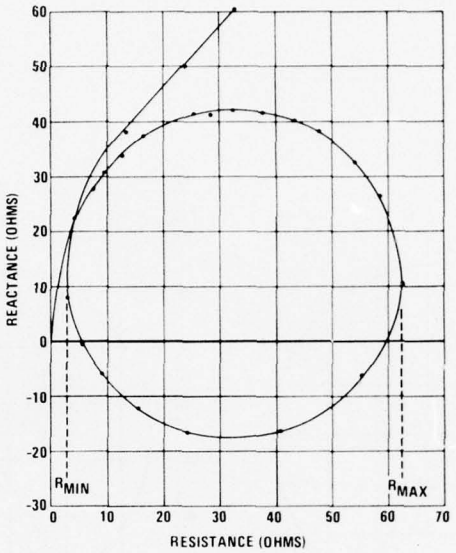

Fig. 2. Total impedance in air of a 12.5 Alfenol ring stack

$$E_H = 4\pi^2 f_0^2 a^2 \rho \tag{13}$$

where ρ is the density. Using Eq. (6), E_B is obtained from E_H.

Subtracting the blocked impedance R_b from the total impedance R_i yields the motional impedance shown in Fig. 3. The effective electromechanical coupling coefficient k_{eff} can be calculated from the relation

$$\frac{k_{\text{eff}}^2}{1 - k_{\text{eff}}^2} = \frac{D}{(X_b)\omega_0 Q_m} \tag{14}$$

where D is the diameter of the motional impedance circle and

$$Q_m = \frac{f_0}{f_2 - f_2}.$$

In the cases considered here, k_{eff} and k are equal to within a few percent; values of k reported subsequently are in reality k_{eff}. Finally, the value of $f_c t^2$ can be obtained from the angle lag ψ. The motional impedance circle of 40 permalloy is shown in Fig. 4. In this case eddy-current losses are more significant, as evidenced by the larger value of ψ.

Warm rolling aluminum-iron alloys below the recrystallization temperature results in grain orientation. Furthermore, when alloys in the range from 10- to 20-Alfenol are slow cooled, they form an ordered structure.[4] Quenching from above 600°C yields a disordered structure. The magnetostrictive activity associated with the ordered phase is greater than with the disordered. The values of k_{eff} at optimum polarizing field, designated hereafter as k_{max}, corresponding to the ordered phase are shown in Fig. 5 and listed in Table I. The corresponding values of the parameters for the disordered phase are also included in Table I. The largest value of k_{max} for the ordered phase is 0.30 (for 12.5 Alfenol) and for the disordered phase is 0.12 (for 13.8 Alfenol). The higher values of k_{max} observed for the ordered phase result mainly from the higher values of λ. Values of λ, μ_r, and $\lambda\mu_r$ are plotted in Fig. 6 for the ordered phase. Comparisons between μ_r and μ^T and between $\lambda\mu_r$ and d are given in Figs. 7 and 8, respectively.

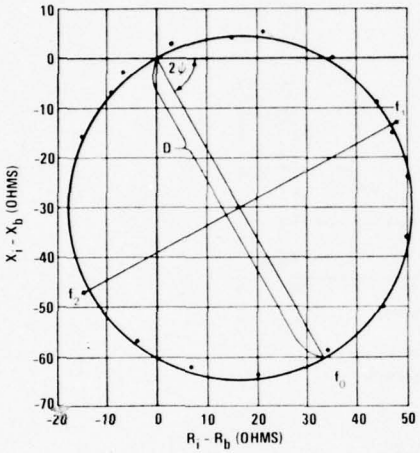

Fig. 3. Motional impedance in air of a 12.5 Alfenol ring stack

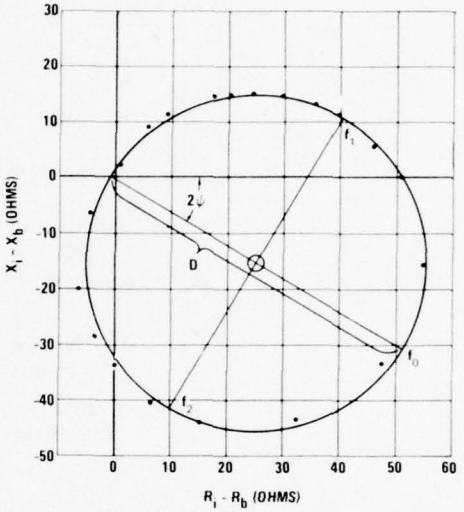

Fig. 4. Motional impedance in air of a nickel ring stack (40 permalloy)

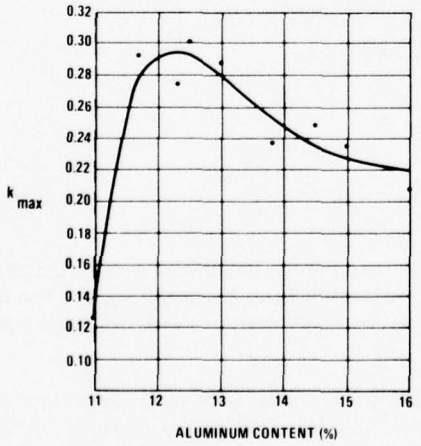

Fig. 5. Variation in k_{max} of Alfenol (ordered phase) versus aluminum content

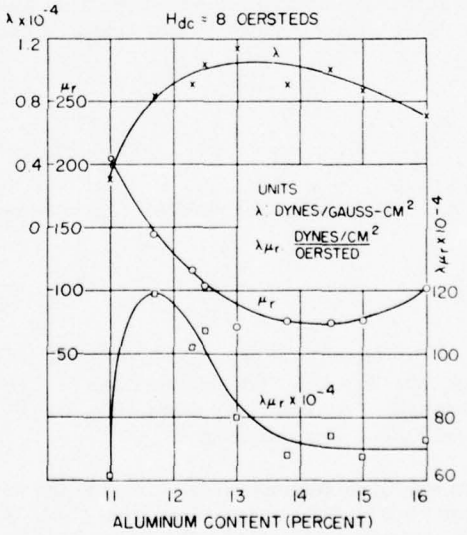

Fig. 6. Variation of λ, μ_r and $\lambda\mu_r$ for Alfenol versus aluminum content

TABLE I
A Comparison of the Properties of Various Magnetostrictive Materials

Material	k_{max}	$\lambda \times 10^{-4}$ (dyne/(cm^2 – G))	μ_r	μ^T	$d \times 10^7$ (G^{-1})	$E_B \times 10^{-12}$ (dyne/cm^2)	$S^H \times 10^{12}$ (cm^2/dyne)	T^2_{max}/E_B (dyne/cm^2)	f^2_{ct} (cycle-cm^2)
Nickel	0.31	2.75	22	24	39	2.1	0.53	3,560	16.8
2V-permendur	0.35	1.65	80	90	78	2.4	0.47	5,100	24.5
Hiperco	0.17	0.80	75	77	37	≈2.1	0.49	4,400	12.9
0.5% Ma, 4.5% Co, and 95% Ni	0.37	3.45	22	25	45	2.4	0.47	–	–
Permalloys (% Ni):									
37.5	0.24	0.73	123	130	86	1.4	0.76	1,380	20.0
40.0	0.38	1.18	107	124	131	1.4	0.83	–	22.6
42.5	0.35	1.28	101	115	115	1.6	0.71	1,510	18.7
46.5	0.32	1.19	90	100	93	1.6	0.69	810	18.7
50.0	0.33	1.27	86	96	90	1.7	0.66	2,640	15.5
52.5	0.32	1.41	73	81	80	1.8	0.62	3,210	14.8
55.0	0.20	0.99	63	66	43	1.9	0.55	3,370	18.1
Alfenol (ordered; % Al):									
11.0	0.15	0.39	184	188	61	1.5	0.68	890	23.9
11.7	0.29	0.69	183	204	160	1.1	1.01	3,380	41.3
12.6	0.30	1.03	104	114	88	1.7	0.65	2,330	58.0
13.0	0.28	1.31	58	63	70	1.5	0.73	3,850	68.4
13.8	0.24	0.91	76	81	67	1.4	0.76	1,780	75.5
14.5	0.25	1.01	73	78	66	1.5	0.71	2,166	81.3
Alfenol (disordered; % Al):									
11.7	0.07	0.27	69	69	18	1.3	0.80	–	–
13.0	0.07	0.21	130	131	22	1.6	0.64	–	–
13.8	0.12	0.36	130	132	40	1.5	0.67	–	–
14.3	0.09	0.34	81	82	22	1.6	0.65	–	–
4.5% Co and 95.5% Ni	0.51	1.41	122	165	135	2.2	0.62	–	4.5
1.4% Co, 2.3% Cr, and 96.3% Ni	0.37	1.39	92	107	85	2.2	0.53	–	16.8
2.4% Co, 0.8% Cr, and 96.8% Ni	0.43	1.69	76	93	90	2.2	0.56	–	12.3
$Ni_{0.967}Co_{0.027}Fe^{2+}_{0.06}Fe^{3+}_2O_4$	0.38	3.3	19	22	52	1.8	0.65	2,560	27,000.0
$Tb_{0.3}Dy_{0.7}Fe_2$	0.60	7.8	2.8	4.3	71	0.6	2.60	–	1,090.0

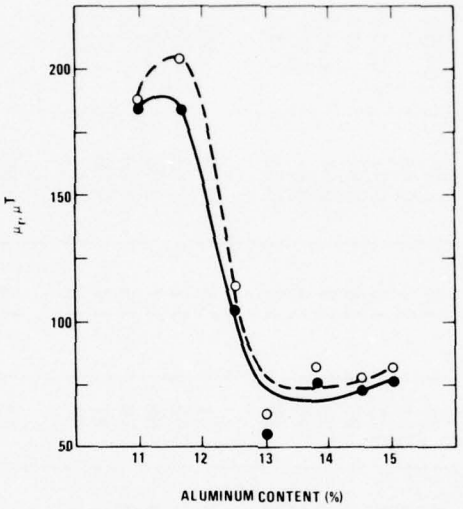

Fig. 7. Variation in μ_r (●—●) and μ^T (○—○) for Alfenol versus aluminum content

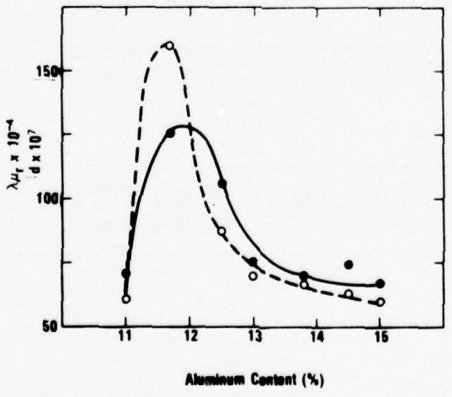

Fig. 8. Variation in $\lambda\mu_r$ (●—●) and d (○—○) for Alfenol versus aluminum content

In both cases qualitative if not quantitative agreement is observed. Values of these parameters as well as the corresponding moduli are given in Table I for these and other magnetostrictive systems considered.

The variation in k_{max} with nickel content for permalloy is shown in Fig. 9. The peak value is 0.376 and occurs for 40 permalloy. A second maximum of 0.35 is observed for approximately 50 permalloy. The maximum value of $\lambda\mu_r$ occurs for 42.5 permalloy as shown in Fig. 10. The large decrease in k_{max} for samples with less than 40% nickel is caused by the rapid decrease in Curie temperature in this range (30 permalloy is nonmagnetic at room temperature).[20] The other large decrease in k_{max}, which occurs for samples with more than 52.5% nickel, appears to be associated with the strain sensitivity of these alloys.

In 1950, Gaugler[22] investigated the effect of tension and magnetic annealing on the Ni-Fe series. His results indicate that applying tension to these materials in the range from 30% to 52.5% nickel aligns the magnetic domains perpendicular to the direction in which the tension is applied, while in the region from 52.5% to 85% nickel, the tendency is toward parallel alignment. Because of the magnetostrictive effect, the application of a static magnetic field to Ni-Fe alloys in the region below approximately 80% nickel produces a stress in the direction of the applied field, and in the regions above 52.5% nickel this stress aligns the magnetic domains in the same direction as the field. A change in magnetization, such as would accompany an ac field superimposed on the dc field and in the same direction would then be

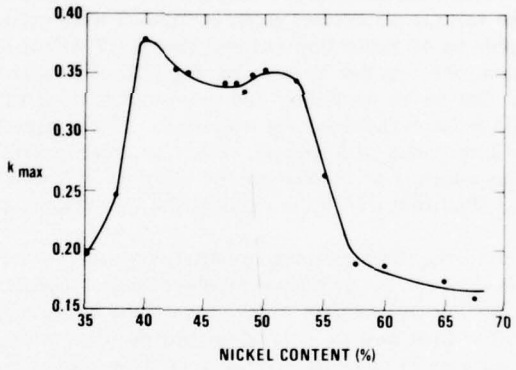

Fig. 9. Variation in k_{max} of permalloy versus nickel content

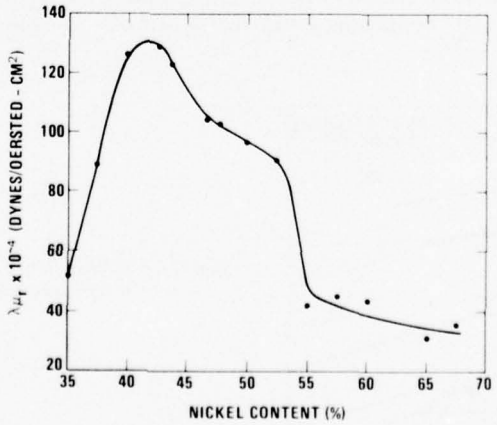

Fig. 10. Variation in $\lambda\mu_r$ of permalloy versus nickel content

caused in large part by the motion of 180°C Bloch walls.[23] Because 180° Bloch wall motions produce no change in strain, the value of k_{max} should be small.

Both the rapid cooling and magnetic annealing of Ni-Fe alloys in the range from 40% to 52.5% nickel resulted in a slight lowering of the value of k_{max}, the greatest decrease being about 10%. For materials having greater than 52.5% nickel, the effect of magnetic annealing was more pronounced. The greatest effect was observed for 65% nickel, in which case k_{max} was reduced to such an extent that it could not be measured. Magnetic annealing raised the value of the maximum permeability by a factor of 70. Because no grain orientation was observed, a possible explanation is that of domain orientation. In such a case the primary magnetization mechanism is 180° Bloch wall motion, and a considerable reduction in k_{max} would follow. This is in agreement with the observations. Thus a possible explanation of the decrease in k_{max} and $\lambda\mu_r$ above 52.5% nickel is the occurrence of domain orientation produced by the strain associated with the dc bias.

The value of k_{max} corresponding to various cobalt-chromium-nickel alloys is shown in Fig. 11. A peak value of 0.5 is observed for the 4.5% cobalt-nickel alloy. Chromium-nickel alloys exhibit a peak value of approximately 0.37 for 2.2% chromium. A ridge of high values of k_{max} occurs along the dotted line joining these compositions. Clark[10] suggests that this is caused by a minimum in the magnetocrystalline-anisotropy constant along this line. Additions of chromium increase the electrical resistivity ρ_e as shown by the dashed lines in Fig. 11. An addition of 1% chromium lowers the Curie temperature approximately 50°C, while a 3% addition of cobalt raises the Curie temperature by the same amount. Using the values of k_{max}, d, and ρ_e given by Clark[10] for the alloys indicated as dark circles in Fig. 11 and taking E_B to be 2.18×10^{12} dynes/cm^2, the various parameters given in Table I were calculated. The 4.5% Co alloy exhibits a value of d comparable to 40 permalloy but less than 11.7 Alfenol and might therefore be suitable for hydrophone applications. As can be seen by Eq. (11), the large value of μ_r results in a very small value for $f_c t^2$ (one-fifth that of 40 permalloy and one-tenth that of 11.7 Alfenol) and would necessitate the use of thin laminations for high-frequency operation. Clark suggests that the 1.4% Co and 2.3% Cr alloy, because of the large value of k and ρ_e, would be more suitable for use in high-frequency transducers. However, this suggestion is not borne out by the data in Table I where the value of $f_c t^2$ for this alloy is seen to be less than that of 2V-permendur, the permalloys, and the Alfenols.

Van der Burgt[13] investigated the dynamic magnetostrictive properties of cobalt-substituted nickel ferrites. As in the case of the Co-Cr-Ni alloys discussed, the effect of cobalt on the magnetostrictive properties is apparently associated with its effect on the crystalline anisotropy constant. The first-order anisotropy constant of cobalt ferrite is known to be large and positive, while that of nickel ferrite is negative and approximately an order of magnitude smaller. Consequently, by adding a small amount of cobalt ferrite in solid solution with nickel ferrite, it is possible to produce a ferrite with an anisotropy constant of zero.[17] At room temperature this composition is obtained when approximately 2-1/2% of the nickel has been replaced by cobalt as shown in Fig. 12. Ferebee and Davis[15] considered the effect of divalent ion substitution on these ferrites. The resulting value of k_{max} is shown in Fig. 13 for both slow-cooled and quenched samples containing 0.027 moles of CoO per mole of ferrite. The value of

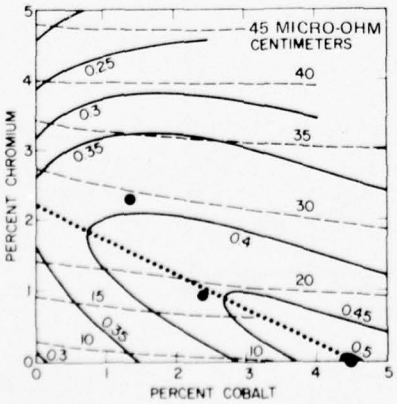

Fig. 11. Variation in k_{max} (—) and ρ_e (- - -) for chromium-cobalt-nickel alloys

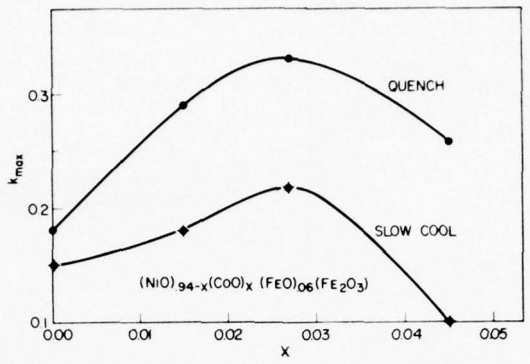

Fig. 12. Variation in k_{max} in cobalt-nickel-ferrous-ferrite versus cobalt content

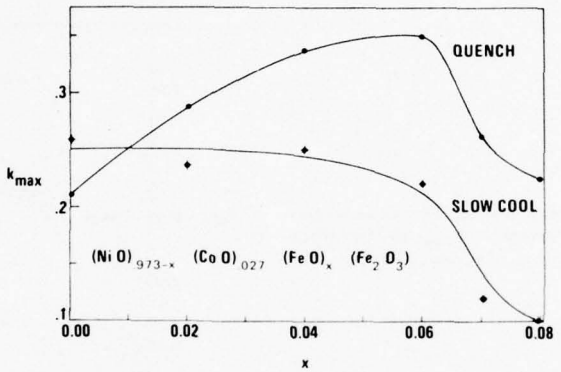

Fig. 13. Variation in k_{max} in cobalt-nickel-ferrous-ferrite versus divalent iron content

k_{max} reached 0.36 for quenched samples containing between 0.05 and 0.06 mole of FeO per mole of ferrite. Other relevant parameters are given in Table I. The values of $f_c t^2$ exceed those obtained with conventional metallic alloys by 500 to 1,700 times. Therefore, transducers constructed of these ferrites could be operated at frequencies in the megahertz range without excessive eddy-current losses. As a class, however, the ferrites suffer because of the tendency for brittle fracture to occur.

Brockman[18] has investigated the ferrite series $(Ni_{0.9}Zn_{0.1})_{0.90-x}Co_xCu_{0.1}Fe_2O_4$. These ferrites exhibit values of k_{max} versus temperature that peak, presumably because of the net crystalline anisotropy going through zero. The results corresponding to x equal to 0.024 are shown in Fig. 14. By sandwiching two different compositions in this series with peaks at 5° and 18°C, an element was produced that exhibited a value of k_{max} equal to approximately 0.3 from 0° to 20°C, as shown in Fig. 15.

Various parameters exhibited by the $Tb_{0.3}Dy_{0.7}Fe_2$ alloy[24] are given in Table I for the purpose of comparison. While the value of μ_r is smaller by an order of magnitude than that exhibited by the other materials, the large value of λ and small value of E_B combine as shown by Eq. (8) to yield a larger value of k_{max} than previously observed. The large values of λ and S^H are not sufficient to overcome the small value of μ_r as shown by Eq. (7), with the result that the value of d for this alloy is less than that of many of the alloys listed, but comparable to that of nickel. The expectation is that processing techniques can be developed that will increase the value of μ_r. This might improve the value of d but decrease that of $f_c t^2$ as shown by Eq. (11). For the present sample, the value of $f_c t^2$ is larger by nearly two orders of magnitude than that exhibited by any of the other alloys, with the result that at a given frequency, laminations of this rare-earth iron alloy could be made 5 to 10 times as thick as for the more conventional alloys. The use of thicker laminations would facilitate fabrication. In the case of the rare-earth/iron alloys, the need to simplify fabrication might outweigh the advantage of increasing the value

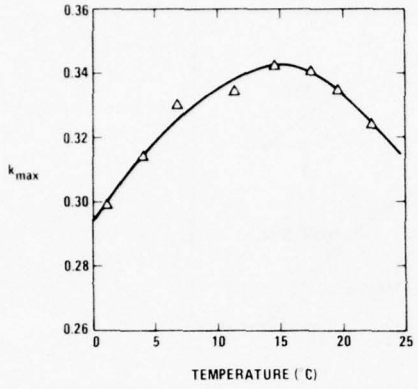

Fig. 14. Variation in k_{max} versus temperature in $Ni_{0.788}Zn_{0.088}Co_{0.024}Cu_{0.1}Fe_2O_4$

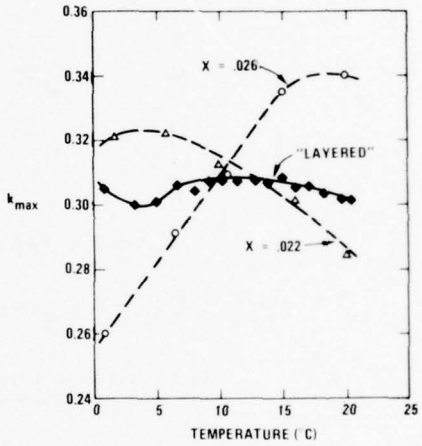

Fig. 15. The effect of layered fabrication on the temperature dependence of k_{max} for the ferrite series $(Ni_{0.9}Zn_{0.1})_{0.9-x}Co_xCu_{0.1}Fe_2O_4$

of d. Finally, while the value of T_{max}^2/E_B is not given in Table I for this alloy, the measurements of Timme[25] indicate that the power-handling capacity of these materials far exceeds that of the other alloys.

In the summary that follows, the properties of only the more conventional alloys are compared. Further discussion of the rare-earth iron alloys is left for those papers that deal explicitly with that class of alloys.

SUMMARY

Within each family of conventional magnetostrictive materials considered, there is a range of compositions with values of k_{max} sufficiently large for use in underwater transducers. The largest values are exhibited by the Co-Cr-Ni alloys.

The maximum power-handling capacity of 2V-permendur was the largest measured. Those of Alfenol, nickel, and the nickel-iron alloys are approximately equal. The addition of divalent iron to the cobalt-substituted nickel ferrites significantly improves their maximum power-handling capacity. When 6% of the nickel is replaced by ferrous iron, the maximum power-handling capacity is 70% that of nickel. Two additional factors must be considered when designing transducers for high-power applications: brittle fracture in ferrites and heating caused by eddy-current losses in alloys.

Eddy-current losses in magnetostrictive transducers result in an upper frequency limit of approximately 300 kHz for Alfenol and 100 kHz for the other alloys. By making use of ferrites, however, it should be possible to construct magnetostrictive transducers capable of operating into the megahertz frequency range. In addition, the use of ferrites in magnetostrictive transducers simplifies fabrication by eliminating the necessity of laminar construction.

The 11.7 Alfenol is especially promising as both a projector and receiver because of the high values of d, $f_c t^2$, T_{max}^2/E_B, and Curie temperature. An added advantage of Al-Fe alloys is that they contain no nickel or cobalt, each of which is a strategic material. In the case of cobalt, the United States is dependent on mines in Africa for its supply. The U.S. supply of nickel during wartime is reasonably secure because most of it comes overland from Canada. However, in wartime, demand for nickel would increase at a rate much faster than that of the overall economy because of its use in steels and other alloys.

In view of the fact that among the conventional alloys discussed there are several exhibiting distinct advantages over nickel, it is appropriate to ask why these have not been adopted for use. Part of the answer is that while some advantage could be realized by their use, alloys such as Alfenol are not generally available. The advantage that would be realized by their adoption would not justify or support a special purpose industry for their production. Also, the processing techniques involved are in many cases considerably more difficult than that required for nickel. Finally, the emergence of barium titanate and lead zirconates diverted interest away from magnetostriction. Clearly what is needed to revive interest in magnetostriction is an alloy with properties equal or superior to those of these ceramics. The rare earth-iron alloys might be just such a class of materials.

REFERENCES

1. "Design and Construction of Magnetostrictive Transducers," Summary Technical Report, NDRC, Div. 6, Vol. 13, p. 327.
2. H. Sussman and S. L. Ehrlich, *J. Acoust. Soc. Am.* **22**, 499 (1950).
3. H. Masumoto and G. Otomo, *Sci. Rep. Res. Inst. Tohoku Univ. Ser. A* **2**, 413 (1950).
4. J. F. Nachman and W. J. Buehler, *J. Appl. Phys.* **25**, 307 (1954).
5. C. M. Davis, I. L. Robey, and S. F. Ferebee, *J. Acoust. Soc. Am.* **26**, 936(A) (1954).
6. C. M. Davis and S. F. Ferebee, *J. Acoust. Soc. Am.* **28**, 156(A) (1956).
7. C. M. Davis, H. H. Helms, and S. F. Ferebee, *J. Acoust. Soc. Am.* **28**, 780(A) (1956).
8. C. M. Davis, H. H. Helms, and S. F. Ferebee, *J. Acoust. Soc. Am.* **29**, 431 (1957).
9. C. A. Clark, *Brit. J. Appl. Phys.* **7**, 355 (1956).
10. C. A. Clark, *J. Acoust. Soc. Am.* **33**, 930 (1961).
11. "Final Development Report for Sonar Search Systems," Bureau of Ships Contract No. NObsr-49016, Phase II (Sept. 1952).
12. E. W. Gorter, *Philips Res. Rep.* **9**, 295 (1954).
13. C. M. Van der Burgt, *J. Acoust. Soc. Am.* **28**, 1020 (1956).
14. C. M. Davis and S. F. Ferebee, *J. Acoust. Soc. Am.* **29**, 1256(A) (1957).
15. S. F. Ferebee and C. M. Davis, *J. Acoust. Soc. Am.* **30**, 747 (1958).
16. Y. Kikuchi, et al., *J. Acoust. Soc. Am.* **29**, 569 (1957).
17. C. M. Van der Burgt and A. L. Stuijts, *Ultrasonics* **1**, 199 (1963).
18. F. G. Brockman, *JUA(USN)* **17**, 319 (1967).

19. Technical Committee on Transducers and Resonators of the IEEE Group on Sonics and Ultrasonics, "IEEE Standard on Magnetostrictive Materials: Piezomagnetic Nomenclature," IEEE Standard 319-1971 (1971).

20. R. M. Bozorth, *Ferromagnetism* (D. Van Nostrand Co., Inc., New York, 1953).

21. E. W. Lee, *Rep. Prog. Phys.* **18**, 205-210 (1955).

22. E. A. Gaugler, thesis, Univ. of Maryland (1950).

23. F. Bloch, *Z. Phys.* **74**, 295-335 (1932).

24. A. E. Clark, "Introduction to Highly Magnetostrictive Rare-Earth Materials," *JUA(USN)* **27**, 109-125 (1977).

25. R. W. Timme, "Device-Oriented Material Measurements on Rare-Earth Iron Alloys," *JUA(USN)* **27**, 139-146 (1977).

U.S. Navy Journal of Underwater Acoustics Volume 27, No. 1 January 1977

NONLINEAR HIGH-DRIVE CHARACTERISTICS OF NICKEL RINGS*

Peter J. Lenart
Naval Underwater Systems Center
New London, Connecticut 06320

ABSTRACT

The electrical input impedances and acoustic radiation characteristics of magnetostrictive scroll-wound ring transducers were measured and the data reduced to obtain information on the transducer's material parameters as a function of high-drive fields. Nickel 200-A scrolls approximately 12.33 in. (31.32 cm) in diameter and 0.917 in. (2.33 cm) in height were used in making these measurements. The experimental data were obtained from both in-air excitation of the rings as well as from in-water excitation. Quantities derived were the relative reverse permeability, the elastic compliance, the piezomagnetic strain constant, and the material electromechanical coupling coefficient. The data will be compared to the theoretical model, NRL EIGSHIP, a computer program of a mathematical analysis of the electroacoustic performance of a single finite-length magnetostrictive circular cylinder submerged in an unbounded medium and radiating sound.

INTRODUCTION

In many applications of magnetostrictive transducers, the level of operation is low enough to assure that the performance of the transducer is essentially linear. However, when that same transducer is driven at higher power levels to make fuller use of its capabilities, then nonlinear behavior can be expected and must be taken into account. As is usually the case with nonlinearities, the experimental approach of addressing the problem is perhaps the most certain method of determining the characteristics of the device in question. This presentation makes use of such an approach to garner the information on high-drive material properties of one type of magnetostrictive transducer.

APPARATUS

In a study program, two scroll-wound nickel 200-A transducers were prepared for measurement (Fig. 1). The active core consisted of 67 turns of nickel strip material 0.917 in. (2.33 cm) in height by 0.010 in. (0.025 cm) in thickness. The mean diameter of the ring is 12.334 in. (31.32 cm) and is toroidally wound with 216 turns of No. 10 polyethylene-jacketed wire. The ratio of the average cross-sectional area enclosed in the toroidal windings to the cross-sectional area of the ring core is 3.137:1.000.

The rings were simultaneously excited by a dc magnetizing current and an ac driving current (Fig. 2). The dc current used for all the measurements was 6.5 A producing a field of 18 Oe (1,432 A/m) and was chosen from preliminary measurements so as to maximize the electromechanical coupling coefficient. The ac drive currents were varied to correspond to excitation fields of from 2.75 to 13.8 Oe (219 to 1,098 A/m). Both the in-air and in-water impedance measurements were done by continuous wave methods. The input electrical resistance and reactance were measured by a Dranetz Complex Impedance-Admittance Meter with a High Power Impedance Measurement Adaptor.

*Presented at the Workshop on Magnetostrictive Materials held under the sponsorship of the Underwater Sound Advisory Group and the Naval Research Laboratory, Orlando, Florida, 25-26 February 1976.

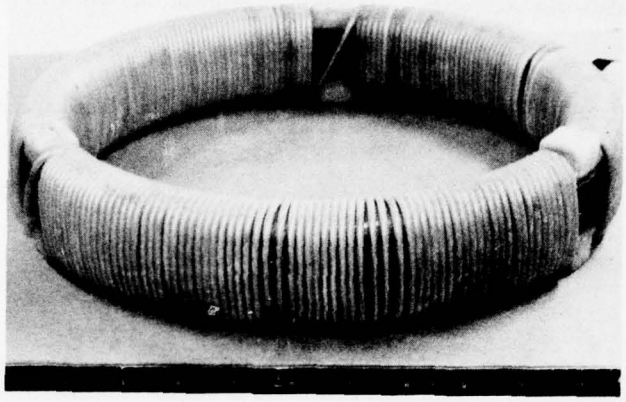

Fig. 1. Nickel scroll transducer

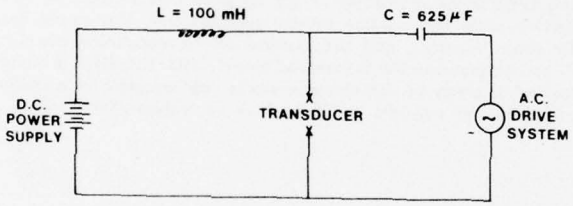

Fig. 2. Blocking circuit used for the measurements

To minimize any temperature effects on the material properties and their effect on the in-water data, all measurements were made at the Naval Underwater System Center's Millstone Research Annex where the water temperature at depth was 63°F (17°C).

THE EXPERIMENT

At each one of several excitation fields both the input reactance as well as resistance were measured individually versus frequency over the frequency range from 2.0 to 7.0 kHz. Figure 3 shows the actual data taken for one of the rings at an excitation field of 11 Oe (875 A/m). Interpolation curves are shown corresponding to the blocked reactance and resistance quantities. Subtracting the blocked quantities from the input quantities produces the motional impedance diagram for the transducer (Fig. 4).

It is, of course, from these motional circles that the basic information, such as the resonant frequency f_0, the quality factor Q, and the effective electromechanical coupling coefficient k, is obtained. Data are required to calculate the core material parameters and the effect that increasing the excitation fields has on them.

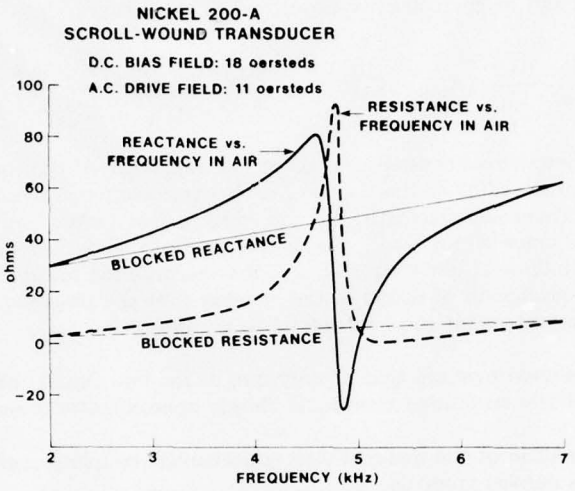

Fig. 3. Example of measured input impedance

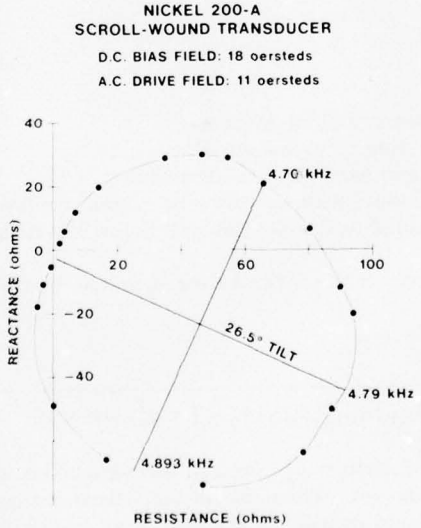

Fig. 4. Example of motional impedance diagram

DATA ANALYSIS

In the analysis of the data at the various excitation fields, the approach used was basically that of Sinsky,[1] making use of Butterworth and Smith's expression for the total electrical impedance Z_T as a function of a the electrical and magnetostrictive properties of a transducer[2]:

$$Z_T = r_w + \frac{jfN^2 4\pi \times 10^{-7}}{a}\,(A_{\text{coil}} - A_0) + \frac{jfN^2\mu_{33}^S A_0 \chi}{a} + \left(\frac{\mu_{33}^S N g_{33} A_0 \chi}{a S_{33}^B}\right)^2 \left(\frac{1}{R_m + jX_m}\right) \tag{1}$$

where g_{33} is the piezomagnetic stress constant, r_w is the d.c. resistance of the toroidal ring. N is the number of turns, a is the mean radius of the core, A_0 is the cross sectional area of the ring core. μ_{33}^S is the reverse permeability at constant strength, χ is the eddy current vector, and R_m and X_m are the mechanical resistance & reactance respectively. Certain assumptions were made, namely that the dc resistance of the toroidal windings is less than 1 Ω, and that because the metal strip thickness of the ring is much less than the wavelength of sound in the material over the frequency band of interest, then the real part of the eddy-current factor can be assumed to be unity.

Although the data presented here are that of only one of the two scrolls that were measured, the data from the second identically structured transducer closely approximates these results.

Figure 5 shows the variation of the material electromechanical coupling coefficient k_{33} versus increasing magnetic field, as derived from Eq. (2):

$$k_{33}^2 = \frac{k^2}{(1 - L_0/L_f)(1 - A_0/A_{\text{coil}})} \tag{2}$$

where

$$\frac{k^2}{1 - k^2} = \frac{D_z}{Q_z X_b}\ ,$$

D_z is the diameter of the impedance circle in ohms,
Q_z is the quality factor of the ring being measured,
X_b is the core reactance at the radial resonance frequency,
L_0 is the inductance of the winding with the transducer core removed,
L_f' is the free inductance measured at frequencies well below the radial resonance of the ring.

With the eddy-current factor assumed to be unity, the equation can be reduced further to the form of Eq. (3):

$$k_{33}^2 = \frac{k^2}{1 - [(A_{\text{coil}}/A_0/[(A_{\text{coil}}/A_0 - 1 + \mu_{33}^T/4\pi \times 10^{-7})]}\ . \tag{3}$$

The reversible permeability at constant stress μ_{33}^T used in this expression was obtained from the low-frequency core reactance versus frequency. What should be noticed is that the relatively high value of k_{33} at 2.75 Oe (219 A/m) rolls off and appears to level off at an excitation field of 11 Oe (875 A/m).

---

[1] J. A. Sinsky, "An Experimental Description of a Free-Flooded Finite-Length Radiating Magnetostrictive Ring Transducer," NRL Report 7887 (June 1975).

[2] S. Butterworth and F. D. Smith, "The Equivalent Circuit of the Magnetostriction Oscillator," *Proc. Phys. Soc. Lon.* 43 (No. 2), 166 (1931).

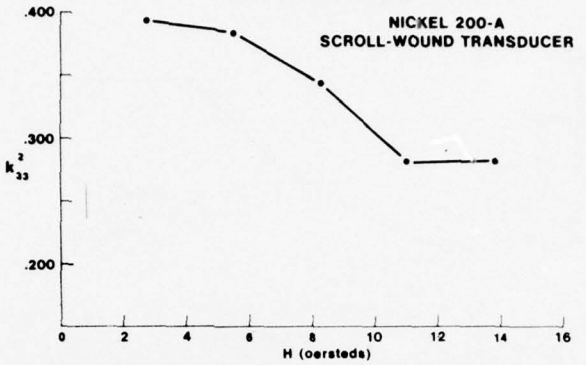

Fig. 5. Material coupling coefficient as a function of excitation field

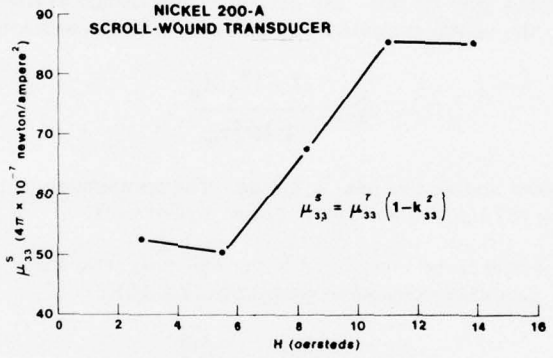

Fig. 6. Permeability at constant strain as a function of excitation field

Using the values for material coupling coefficient and the reversible permeability at constant stress at each driving field condition allows us to compute the reversible permeability at constant strain μ_{33}^S (Eq. (4)):

$$\mu_{33}^S = \mu_{33}^T (1 - k_{33}^2) \tag{4}$$

where

$$\mu_{33}^T = \frac{r_m}{A_0 N^2} \frac{dX_c}{df} + \left(1 - \frac{A_{coil}}{A_0}\right) 4\pi \times 10^{-7}$$

and X_c is the curve reactance. The permeability increases from a low value of approximately 50 units at 5.5 Oe (438 A/m) to a high value of 85 at 11 Oe (875 A/m) (Fig. 6), exhibiting the same relative behavior that was reported for nickel ring stacks by the National Defense Research Committee.[3] Should the scroll continue to behave relatively the same as the stacks, one could expect that the permeability would fall off appreciably at still higher ac excitation fields.

[3]National Defense Research Committee, "The Design and Construction of Magnetostriction Transducers," Summary Technical Report (Div. 6, NDRC, Washington, D.C., 1946), Vol. 13, p. 350.

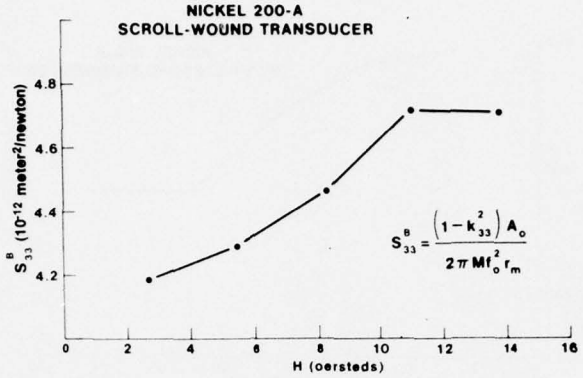

Fig. 7. Elastic compliance as a function of excitation field

If we again assume the eddy-current factor to be unity, the motional impedance is at a maximum when the mechanical reactance goes to zero. By definition this occurs at the radial resonance frequency f_0, allowing us to compute the elastic compliance (Fig. 7) from the expression in Eq. (5):

$$s^B_{33} = \frac{(1 - k^2_{33})A_0}{2\pi M f^2_0 r_m} \quad . \tag{5}$$

M is the mass of the ring core and in this case is 3.4 kg. The compliance increases steadily to a value of 4.7×10^{-12} Pa^{-1} at 11 Oe (875 A/m), and then appears to level off.

The last material parameter to be considered is the piezomagnetic stress constant g_{33} (Fig. 8), which is derived in terms of the previously considered properties (Eq. (6)):

$$g_{33} = \frac{k_{33}}{\sqrt{1 - k^2_{33}}} \sqrt{\frac{s^B_{33}}{\mu^T_{33}}} \quad . \tag{6}$$

As can be seen here, the stress constant falls off rapidly from 10 to 6×10^{-5} A/N as the field increases to 11 Oe (875 A/m).

CONCLUDING REMARKS

From a transducer designer's point of view, the following question may be legitimately posed: What effect does all of this have on the in-water performance of a scroll-wound transducer? To answer that question, in-water impedance data at the same dc and ac excitation levels were taken and analyzed.

Considering the effect that increasing the ac excitation field has upon the resonant frequency f_0 of the device, we notice that f_0 decreases steadily to a point at 11 Oe (875 A/m) where it appears to bottom out (Fig. 9). However, taking the resonance at a field of 2.75 Oe (219 A/m) as a reference, the maximum percent decrease in f_0 is on the order of only 1%. From this it appears that the change in resonant frequency is not a major concern.

Now, however, if we take a look at maximum motional resistance R_{max} taken from the R versus f data at the resonant frequencies corresponding to each ac excitation field, we do notice a rather substantial fluctuation in maximum resistance (Fig. 10). In fact, using the maximum resistance at a driving field of 2.75 Oe (219 A/m) as a reference, the variation in maximum resistance reached a high of approximately 40% at an ac magnetizing field of 11 Oe (875 A/m). One must certainly take this change into account when considering the ultimate acoustic behavior of the transducer.

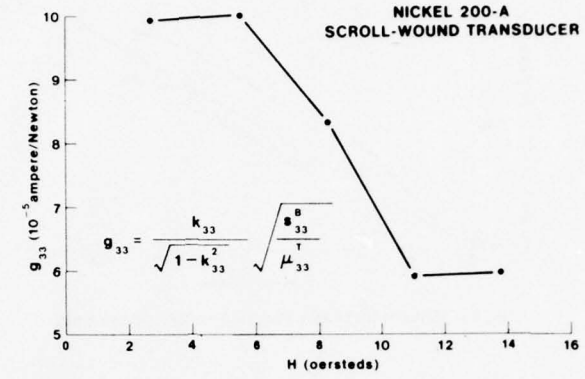

Fig. 8. Piezomagnetic constant as a function of excitation field

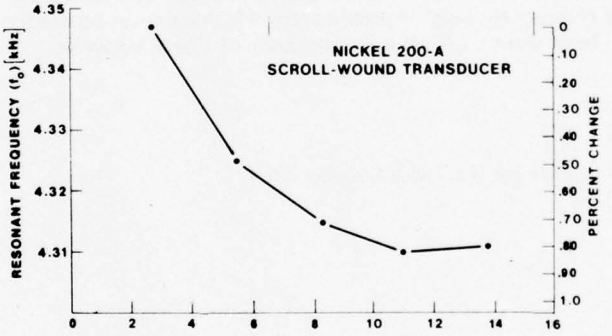

Fig. 9. Resonant frequency as a function of excitation field

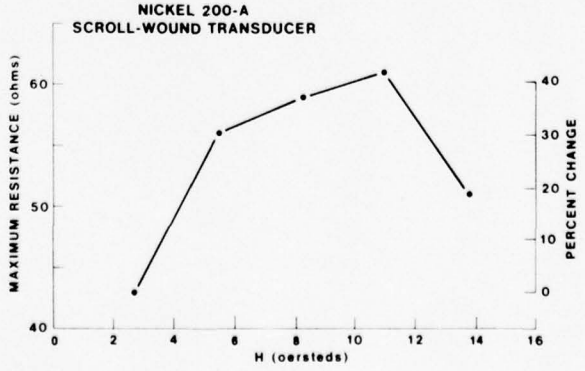

Fig. 10. Maximum motional resistance as a function of excitation field

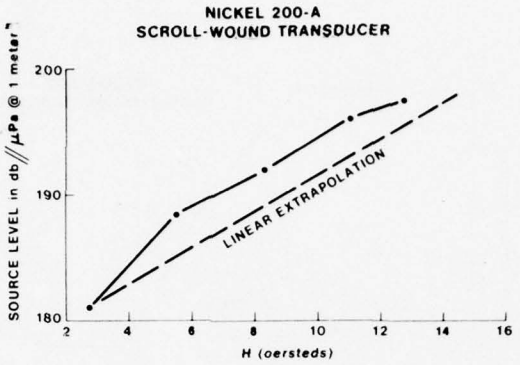

Fig. 11. Source level as a function of excitation field

Source level information gathered from the transmitting current responses of the transducer at the various excitation fields does, in fact, show the nonlinear, in-water behavior of these scrolls (Fig. 11). At 11 Oe (875 A/m) the source level has increased by 15 dB rather than the theoretical value of 12 dB (a 3-dB difference) when compared to the source level at 2.75 Oe (219 A/m).

To summarize, the in-air impedance measurements reveal that the magnetostrictive material properties vary substantially as the ac excitation field is increased. The corresponding water data show that the resonant frequency changes by only approximately 1%, maximum resistance fluctuates by as much as 40%, and the source level shows a 3-dB gain over that of linear behavior.

ACKNOWLEDGMENT

This program was funded by NAVELEX Code 3204.

U.S. Navy Journal of Underwater Acoustics Volume 27, Number 1 January 1977

EFFECT OF ORTHOGONAL FIELD EXCITATION OF NICKEL RINGS*

C. L. LeBlanc and C. H. Sherman
Naval Underwater Systems Center
New London, Connecticut 06320

ABSTRACT

A linear magnetostrictive theory is used to investigate the alternating small signal characteristics of a thin-walled nickel ring transducer operating in the radial mode with orthogonal magnetic fields for polarization and excitation. The concept of using orthogonal fields, described by Edson and Huston (*J. Acoust. Soc. Am.*, May 1974), is studied from this linear viewpoint, and values for the effective electromechanical coupling coefficient are presented in terms of the material coupling coefficient k_{33} derived by applying collinear polarization and excitation magnetic fields along the axis of principal strain. Although the effective coupling was found to depend quite heavily on the orientation of the resultant driving and bias magnetic fields, no case was encountered where the effective coupling exceeded k_{33}. However, initial measurements made by Huston on a length expander nickel scroll in the form of a tube indicated that the low-level coupling coefficient increased approximately 16% when the transducer was driven orthogonally. Similar measurements on a nickel ring transducer did not substantiate this finding and gave results in approximate agreement with theory. Thus no definite conclusion can be drawn from the preliminary low-level experimental results. Nevertheless, it is expected that orthogonal excitation will have genuine advantages under large signal driving conditions. Two special cases of high-amplitude drive are discussed: linearized drive and unpolarized drive.

INTRODUCTION

Magnetostrictive scroll transducers have been in use for over 20 years. In all this time the first new approach for driving these scrolls is the orthogonal drive concept described by Edson and Huston in their article "High-Performance Magnetostrictive Transducers."[1] Our investigation[2] of the orthogonal drive concept will show that the low-level coupling coefficient for an orthogonally driven nickel scroll in the form of a ring cannot exceed the coupling for a conventionally driven scroll but that high-amplitude orthogonal drive may give better linearity and more acoustic power output than high-amplitude conventional drive. Improved linearity and increased power output of orthogonally driven scrolls have been substantiated by measurements made by Huston. However, his low-level coupling coefficient measurements indicated a 16% increase when the transducer was driven orthogonally, which disagrees with our derived results. The measurements were made on a length expander nickel tube whereas the theory was developed by considering the radial displacement of a ring transducer.

PHYSICAL MODEL

Figure 1 depicts a thin-wall scroll transducer approximating a ring with two windings: an exterior toroidal winding, which is the one used in conventional scrolls, and an interior solenoidal winding

*Presented at the Workshop on Magnetostrictive Materials held under the sponsorship of the Underwater Sound Advisory Group and the Naval Research Laboratory, Orlando, Florida, 25-26 February 1976.

[1] A. P. Edson and E. L. Huston, "High-Performance Magnetostrictive Transducers," *J. Acoust. Soc. Am.* **55**, 1076-1079 (1974).

[2] C. L. LeBlanc and C. H. Sherman, "Use of Orthogonal Fields in Magnetostrictive Scroll Transducers," NUSC TM TD12-75-72 (2 Mar. 1972).

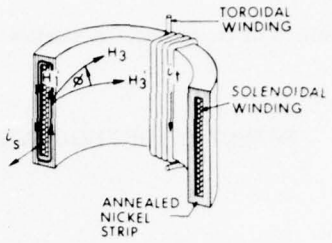

Fig. 1. Orthogonal-drive magnetostrictive scroll transducer

completely surrounded by magnetostrictive material. Bias and alternating currents can be superimposed in both windings. Current i_t in the toroidal winding produces a closed circumferential magnetic field H_3'. Current i_s in the solenoidal winding produces an axial magnetic field H_1', which forms a closed path as outlined by the solid closed line with connecting arrows. This latter field is perpendicular to the H_3' circumferential field; thus the term "orthogonal drive." The resultant magnetic field is H_3 and is inclined at an angle ϕ to the H_3' field. To gain a better understanding of orthogonal drive, the scroll transducer was analyzed using linear, small-signal magnetostrictive theory. The objective was to determine the effective electromechanical coupling coefficient and to see if orthogonal drive provided a higher coupling than conventional drive.

THEORY

It is conventional to write the linear, small-signal equations of state in a coordinate system with the X_3 direction parallel with the bias magnetization direction in the material. Figure 2 demonstrates this type of coordinate system. The resultant bias magnetization vector H_3 is inclined at an angle ϕ such that the tangent of ϕ is the ratio of the physically applied orthogonal bias fields, $H_1'(\mathrm{dc})$ and $H_3'(\mathrm{dc})$. The first step in the analysis is to write the constitutive equations of state for polarized polycrystalline material with magnetostrictive symmetry in the unprimed coordinate system. Because the unprimed system is rotated through the angle ϕ to the primed system, which fits the scroll geometry and by which the scroll motion can be described, the original equations of state must be transformed to the primed system for practical analysis. The transformation is accomplished using tensor analysis, and the transformed equations in the primed coordinate system that apply to a simple magnetostrictive ring transducer with magnetic isotropy are—

$$S_3' = s_{33}^{H'} T_3' + d_{13}' H_1' + d_{33}' H_3' , \tag{1}$$

$$B_1' = d_{13}' T_3' + \mu_{33}^{T'} H_1' , \tag{2}$$

$$B_3' = d_{33}' T_3' + \mu_{33}^{T'} H_3' , \tag{3}$$

which relate strain S' and magnetic induction B' to stress T' and magnetic intensity H'. Assuming that the mechanical stress and strain, as well as the magnetic intensity and induction, are uniform throughout the material (which is an appropriate assumption for a short, cylindrical, thin-walled ring transducer), then the static and dynamic coupling coefficients can be considered equal.

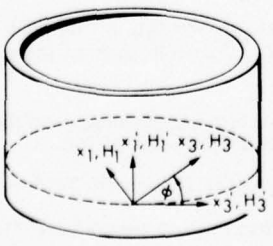

Fig. 2. Coordinate system

The coupling coefficient is evaluated, using an energy approach defined in the "IEEE Standards on Piezoelectric Crystals,"[3] by calculating the piezomagnetic strain and induction energy densities. The first step in determining specific energies is to multiply Eq. (1) by the only existing stress component—the T_3' circumferential stress (in other words, all other stress components have been set equal to zero for the thin-walled ring operating in its fundamental radial hoop mode). Then Eqs. (2) and (3) are multiplied by their respective alternating magnetic field components H_1' and H_3'. The resulting expression for the magnitude of the effective electromechanical coupling coefficient k' becomes

$$k' = \left| \frac{\overbrace{[d_{31}\sin^3\phi + (d_{33} - d_{15})\sin\phi\cos^2\phi]}^{d'_{13}} H' + \overbrace{[d_{33}\cos^3\phi + (d_{31} + d_{15})\sin^2\phi\cos\phi]}^{d'_{33}}}{\{\underbrace{[s_{33}^H\cos^4\phi + s_{11}^H\sin^4\phi + (2s_{13}^H + s_{55}^H)\sin^2\phi\cos^2\phi]}_{s_{33}^{H'}}\underbrace{\mu_{33}^T}_{\mu_{33}^{T'}}[1 + H'^2]\}^{1/2}} \right| . \quad (4)$$

The relationships between the primed coefficients and the unprimed coefficients, the ones usually measured and published as the material constants, are found by comparing the appropriate bracketed expressions. H' represents the ratio of the alternating magnetic field components, H_1' to H_3', and can be either positive or negative depending on whether the field components are in phase or 180° out of phase.

If it is now assumed that the material is isotropic elastically, there is no change in volume upon magnetization, and the elastic and piezomagnetic shear coefficients have relationships similar to their piezoceramic counterparts, then Eq. (4) reduces to the form

$$\frac{k'}{k_{33}} = \left| \frac{\left(\cos\phi - H' \frac{\sin\phi}{2}\right)}{(1 + H'^2)^{1/2}} \right| , \quad (5)$$

where k_{33} is the material coupling coefficient associated with a conventionally driven scroll.

A more comprehensive study of the coupling coefficient for arbitrary phase between H_1' and H_3' was undertaken, but the final result for maximum coupling reduced to Eq. (5). Because many cases, ranging from H' equals zero to infinity, are possible in Eq. (5), only specific cases will be plotted to demonstrate the behavior of the coupling coefficient versus H' and the angle ϕ.

Figure 3 shows the coupling coefficient ratio k'/k_{33} plotted as a function of the bias direction ϕ for various driving signal ratios H'. The upper left plot shows that the coupling factor varies as the cosine of ϕ when H' equals zero (or when the only active driving field is the H_3' field). For this case when ϕ equals zero, the driving field is parallel with the H_3'(dc) bias vector and the S_3' strain, and maximum coupling is achieved. This case represents the conventionally driven scroll. When ϕ equals 90°, the driving field H_3' is perpendicular to the magnetic bias vector, which is now in the x_1' direction, and the result is zero coupling. The plot in the upper right-hand corner shows that the coupling factor varies as one-half the sine of ϕ when H' is infinite (or when the only active driving field is the H_1' field). When ϕ equals zero, the driving field is perpendicular to the magnetic bias vector, which is in the x_3' direction, and the result is again zero coupling. When ϕ equals 90°, the driving field H_1' is parallel with the magnetic bias vector in the x_1' direction but is perpendicular to the S_3' strain, resulting in a perpendicular coupling coefficient half the material coupling coefficient k_{33} under the assumptions outlined previously.

The two lower plots represent cases of more practical interest. On the left the resultant driving and bias magnetic fields are always parallel with one another, and thus the values for the coupling ratio

[3]"IRE Standards on Piezoelectric Crystals: Determination of the Elastic, Piezoelectric, and Dielectric Constants—the Electromechanical Coupling Factor, 1958," *Proc. IRE* **46** (No. 4) (Apr. 1958).

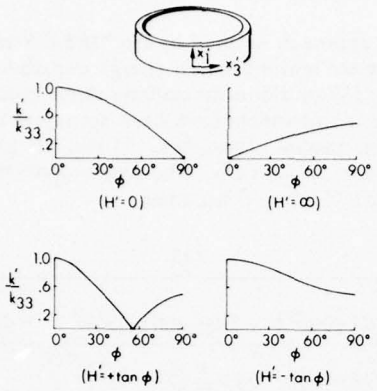

Fig. 3. Coupling ratio versus bias direction

at ϕ equal to 0° and 90° are unity and one-half, respectively, for the thin-walled ring operating in the radial mode. Because the parallel and transverse piezomagnetic contributions to the S'_3 strain oppose one another in this case, the coupling factor goes to zero at ϕ roughly equal to 55°, when the magnitude of the net individual contributions are equal. On the right the orientation between the resultant driving and bias magnetic fields varies continuously with the angle ϕ, and the resultant fields are parallel at ϕ equals 0°, mutually perpendicular at ϕ equals 45°, and again parallel at ϕ equals 90°. However, in this case, on each half cycle of the driving signal the parallel and perpendicular piezomagnetic contributions to the S'_3 strain are additive; thus no null for the coupling ratio is observed.

Another case of interest is when the resultant driving and bias magnetic fields are mutually perpendicular to one another for all values of the angle ϕ. This takes place when H' equals the negative cotangent of ϕ. Although this plot is not shown, the coupling ratio was found to vary as (3/4) sin 2ϕ and had a maximum value of three-quarters at ϕ equal to 45° and a value of zero at ϕ equal to 0° and 90°.

The results of the analysis indicated that, although the effective coupling was found to depend quite heavily on the orientation of the resultant driving field with respect to the resultant bias magnetization field, there was no case where the effective coupling coefficient for the orthogonally driven scroll exceeded k_{33}—the coupling coefficient for a conventionally driven scroll.

EXPERIMENTAL RESULTS

Results of initial, low-level coupling coefficient measurements on the two prototype orthogonal scroll transducers will be described. One transducer was a nickel ring with windings as shown in Fig. 1 and a radial resonance at 11.4 kHz. The transverse coupling coefficient measured when the driving and bias magnetic fields were both in the axial direction, perpendicular to the S'_3 strain, was found to be 0.12. The coupling coefficient measured when the driving and bias magnetic fields were both in the circumferential direction, parallel with the S'_3 strain, was 0.23, which is approximately the value of k_{33} for nickel. The approximate factor of 2 between the measured coupling values is consistent with the conditions assumed in deriving Eq. (5) from Eq. (4).

Two values of the effective electromechanical coupling coefficient were measured on the ring transducer under orthogonal drive conditions. In the first case the driving fields were adjusted to correspond to $H' = -\cot\phi$ such that the resultant driving field was perpendicular to the resultant bias field and $k' = 0.21$ was measured. Because for this case theory indicates

$$k' = (3/4)k_{33} \sin 2\phi ,$$

the value of ϕ, which could not be measured directly, must have been about 45°. In the second case, the driving fields were adjusted to correspond to $H' = \tan\phi$ such that the resultant driving field was parallel with the resultant bias field (this case is shown in the lower left plot of Fig. 3), and $k' = 0.10$

was measured. This value is also roughly consistent with $\phi = 45°$. Thus, the measurements on the ring transducer agree approximately with the theory.

The second transducer was a toroidally wound nickel tube suspended inside a solenoidal winding and had a length resonance at 6.8 kHz. Measurements on this transducer were made by Huston. The effective coupling coefficient measured with the driving and bias magnetic fields parallel with one another and collinear with the axis of principal strain (longitudinal) was only 0.088. This low coupling value is to be expected because of flux leakage and nonuniform stress and strain in the tube at resonance, and, in addition, the fact that a half-wavelength, ceramic, dummy load transducer had been epoxied to one end of the tube for high-power measurements. When the effective orthogonal coupling coefficient was measured on this composite device for the condition $H' = -\cot\phi$, a value of $k' = 0.102$ was found, suggesting that orthogonal driving can increase the coupling factor.

It must be noted that all the coupling coefficient values given for the ring are maximum values determined at optimum bias current levels, which were different for each measurement, while both measurements for the tube were made at the same bias. Thus no definite conclusions can be drawn from these preliminary experimental results.

HIGH-AMPLITUDE DRIVE

The coupling coefficient is only one of several criteria used to estimate transducer performance. It is associated with low-level, linear characteristics. The primary advantages advocated for orthogonal drive were associated with high-amplitude drive characteristics. Two cases of high-amplitude orthogonal drive of scroll transducers will be discussed to demonstrate potential advantages of this new concept over high-amplitude conventional drive.

The relation between the useful circumferential strain S_3' and the S_3 strain in the direction of magnetization is

$$S_3' = \frac{1}{2} S_3(3\cos^2\phi - 1)\,, \tag{6}$$

where ϕ is the angle between S_3' and S_3 as shown in Fig. 4.

Although the relation given in Eq. (6) is a static one, it will be assumed that it holds dynamically. The square-law relationship between strain and magnetic induction,

$$S_3 = S_s\left(\frac{B}{B_s}\right)^2 \tag{7}$$

(where subscript s designates saturation), in conjunction with the normalization criteria

$$\left.\begin{aligned} S &= \frac{S_3'}{S_s} \\ b &= \frac{B}{B_s} \end{aligned}\right\} \tag{8}$$

is used in Eq. (6) to derive

$$S = b_x^2 - \frac{1}{2} b_y^2\,, \tag{9}$$

which gives the normalized strain in terms of the normalized Cartesian components of induction b_x and b_y.

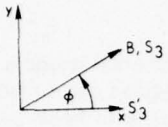

Fig. 4. Cartesian representation of strain

Let the components of induction be given by

$$\begin{aligned} b_x &= b_{px} + u(t) \\ b_y &= b_{py} + v(t) \end{aligned} \tag{10}$$

where b_{px} and b_{py} are fixed bias components and $u(t)$ and $v(t)$ are driving components. Inserting these components in the normalized strain formula yields

$$S = \left(b_{px}^2 - \frac{1}{2}\, b_{py}^2\right) + [2b_{px}u(t) - b_{py}v(t)] + \left[u(t)^2 - \frac{1}{2}\, v(t)^2\right]. \tag{11}$$

Applying the condition

$$v(t) = \sqrt{2}\; u(t) \tag{12}$$

eliminates the bracketed term with the squared, time-dependent functions on the extreme right-hand side of Eq. (11). The expression for the strain then reduces to

$$S = \left[b_{px}^2 - \frac{1}{2}\, b_{py}^2\right] + [2b_{px} - \sqrt{2}\; b_{py}]\, u(t). \tag{13}$$

Because both bracketed terms in Eq. (13) are constants, the strain is a linear function of the magnetic induction $u(t)$. In addition, the bias components can be adjusted to maximize the peak-to-peak strain to a value of the square root of two times saturation strain. In a conventionally biased scroll, the peak-to-peak strain cannot exceed saturation strain, and there is considerable second harmonic distortion.

The other case of interest is unpolarized orthogonal drive. Let the driving components of induction be given by

$$\begin{aligned} b_x &= b_o \sin(\omega t) \\ b_y &= b_o \cos(\omega t) \end{aligned} \tag{14}$$

These conditions cause the resultant magnetic induction vector to be constant in magnitude and to rotate at an angular frequency ω. Inserting these expressions into the normalized strain formula yields

$$S = \frac{1}{4}\, b_o^2 - \frac{3}{4}\, b_o^2 \cos(2\omega t). \tag{15}$$

Driving to saturation induction makes b_o equal unity, and then the S_3' strain has a fixed component of one-quarter saturation strain with an alternating component of three-quarters saturation strain. Therefore, the peak-to-peak strain is 1-1/2 times the saturation strain. When a conventional scroll is driven unpolarized, the peak-to-peak strain cannot exceed saturation strain. In both cases the strain varies at twice the frequency of the driving magnetic induction.

SUMMARY

It has been shown theoretically that the coupling coefficient for an orthogonally driven scroll is no greater than that for a conventionally driven scroll. Although initial experimental results are not conclusive, some of the results may not be consistent with the theoretical approach. While this possible discrepancy remains to be resolved, it has been shown theoretically that polarized orthogonal drive gives higher linear strain amplitude than conventional polarized drive and that unpolarized orthogonal drive gives higher strain amplitude than conventional unpolarized drive. For the latter cases, orthogonal drive has the potential for about 3 dB more acoustic power.

ACKNOWLEDGMENTS

This work was supported by the NAVSEA Sonar Technology Division, SEA 06H1-2, with C. C. Walker as Project Manager.

U.S. Navy Journal of Underwater Acoustics Volume 27, No. 1 January 1977

ORTHOGONAL EXCITATION OF MAGNETOSTRICTIVE MATERIALS FOR IMPROVED HIGH-DRIVE CHARACTERISTICS*

E. Lee Huston
Paul D. Merica Research Laboratory
The International Nickel Company, Inc.
Suffern, New York 10901

ABSTRACT

This paper discusses the effects of high-drive-level orthogonal excitation fields on magnetostrictive transduction. A nonlinear model valid for isotropic, square-law magnetostrictive materials is used to review theoretical predictions. A piston-type transducer was constructed from Ni-200 and fitted with toroid-wound and solenoid-wound coils. This prototype device was evaluated using both conventional and orthogonal modes of excitation. Power tests were conducted with output power levels up to 50 W/cm^2 of active core area by driving the piston into a tuned ceramic dummy load. Device efficiency in excess of 50% was obtained at 5 W/cm^2 output power. As the output power was increased, orthogonal excitation consistently provided higher efficiency and linearity than conventional excitation. In addition, device linearity improved with increasing drive level for the orthogonal tests. Self-biased excitation was obtained by driving the two coils plus a pair of diodes in parallel. For self-biased excitation, device efficiency increased with drive level, exceeding 30% at 40 W/cm^2 output power.

INTRODUCTION

It has been customary to design and build magnetostrictive transducers so that the axes of excitation and static magnetic polarization coincide with the axis of mechanical or acoustic output. The possibility of achieving increased power density or improved linearity by off-axis excitation has been previously recognized.[1-3] A detailed analysis[4] of off-axis excitation provided the following conclusions:

- A 125% increase occurs in the available power density capability of the core.

- "Square-law" distortion is eliminated. These improvements are independent of the transducer core material and may conveniently be achieved by the simultaneous application of two mutually perpendicular magnetic excitation fields to the transducer core. This configuration has been termed "orthogonal excitation."[5,6] It was also recognized that orthogonal excitation offers a novel method for self-biased operation. To verify these predictions, a prototype piston transducer was constructed and evaluated at high-drive levels using both conventional and orthogonal modes of excitation. The experimental results are the subject of this paper and are presented after a brief review of pertinent magnetostriction theory.

*Presented at the Workshop on Magnetostrictive Materials held under the sponsorship of the Underwater Sound Advisory Group and the Naval Research Laboratory, Orlando, Florida, 25-26 February 1976.

[1] Fried Krupp AG, German patent application K159,470 (1945).
[2] H. H. Rust and E. Bailites, *Acustica* 2, 132-135 (1952).
[3] H. H. Rust and E. Bailites, German patent 910,603 (1954).
[4] A. P. Edson and E. L. Huston, *J. Acoust. Soc. Am.* 55, 1076-1079 (1974).
[5] A. P. Edson, U.S. patent 3,753,058 (14 Aug. 1973).
[6] A. P. Edson, U.S. patent RE 28,381 (1 Apr. 1975).

Magnetostrictive transduction is achieved principally through linear magnetostriction: a change of physical dimensions at constant volume in response to a change in the state of magnetization. The magnitude of the strain is a function of both the net induction B and the direction of strain measurement. If the material is *isotropic*, the strain at right angles to net induction is opposite in sign and half as large as that parallel to the axis of induction. At constant induction, the angular dependence of the magnetostrictive strain, $\Delta l(\phi)/l$, may be written as

$$\frac{\Delta l(\phi)}{l} = 0.5 \left(\frac{\Delta l}{l}\right) (3 \cos^2 \phi - 1), \tag{1}$$

where $(\Delta l/l)_o$ is the strain along the axis of net induction. For many materials, magnetostrictive strain $(\Delta l/l)_o$ is proportional to the square of net induction up to the saturation strain, $(\Delta l/l)_s$, at technical saturation B_s. Equation (1) may then be rewritten as

$$\frac{\Delta l(\phi, B)}{l} = 0.5 \left(\frac{\Delta l}{l}\right)_s (3 \cos^2 \phi - 1) \left(\frac{B}{B_s}\right)^2 \tag{2}$$

This math model permits calculation of the magnetostrictive strain or stress of an *isotropic square-law* transducer material when the net induction is inclined at any angle ϕ to the axis of loading.

It is apparent from Eq. (2) that oscillating saturation induction between coincidence ($\phi = 0$) and quadrature ($\phi = 90^\circ$) with the mechanical output axis will result in the magnetostrictive strain varying between $+ (\Delta l/l)_s$ and $- 0.5 (\Delta l/l)_s$. This 50% increase in peak-to-peak strain increases the available magnetostrictive strain energy density to 2-1/4 times that obtainable from conventional uniaxial operation. By simultaneously varying both the magnitude and orientation of the net induction, an endless spectrum of magnetostrictive strain waveforms is possible. The additional degree-of-freedom variable orientation is the essential difference between orthogonal and conventional modes of excitation.

The induction changes encountered during orthogonal excitation may be conveniently shown in the two-dimensional induction diagram of Fig. 1. For the case shown, the induction components along the x and y axes have the parametric form

$$\left.\begin{aligned} B_x &= B_{px} + B_{ox} \sin(\omega t) \\ B_y &= B_{py} + B_{oy} \sin(\omega t). \end{aligned}\right\} \tag{3}$$

The B_p values represent static or bias inductions, while the B_o values are time varying. This system of equations represents a straight line in the induction plane. The line is the trace of the net induction vector $\mathbf{B} = \mathbf{B}_x + \mathbf{B}_y$. The prototype device that achieves this induction change will be discussed presently. Further analysis of orthogonal excitation is greatly simplified by representing the instantaneous net induction as the sum of a fixed induction $\mathbf{B}_m$ applied along the axis of mechanical output and a time-varying induction $\mathbf{B}_e$ applied at a fixed excitation angle ϕ_e, as also illustrated in Fig. 1. The operating conditions for any transducer are thus determined by specifying B_m, ϕ_e, and a range of values for B_e. Using this new set of variables, the magnetostrictive strain waveform, Eq. (2), may be rewritten as

$$\frac{\Delta l(\phi, B)}{l} = B_s^{-2} \left(\frac{\Delta l}{l}\right)_s [B_m^2 + B_m B_e \cos \phi_e + B_e^2 (1.5 \cos^2 \phi_e - 0.5)]. \tag{4}$$

The B_e values are time varying. Accordingly, B_e^2 contains a term in $\sin^2(\omega t)$, and such a term leads to the familiar "square-law" distortion. However, the coefficient of the B_e^2 term depends upon the excitation angle and vanishes at 125.4°. Thus the linearity of the output magnetostrictive-strain waveform may be controlled independent of the amplitude of the strain. This is a significant departure from conventional excitation.

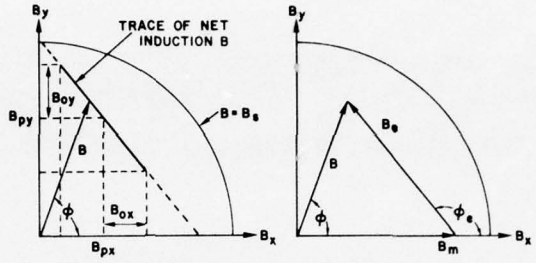

Fig. 1. Two-dimensional induction diagram showing the correspondence between the two sets of induction components

PROTOTYPE DEVICE CONSTRUCTION

A piston-type magnetostrictive transducer was designed and built for operation with either conventional or orthogonal excitation to permit a direct comparison of the two modes. The device is simply a 0.304-m (12-in.) long tube. It was made by winding up, in scroll fashion, a 2.0×10^{-4} m (8-mil) thick sheet of annealed Ni-200 covered with Thermoset Type 316 epoxy. The outside diameter of the tube was 3.49×10^{-2} m (1.37 in.), and the active cross-sectional area of nickel was 1.34×10^{-4} m^2 (0.21 $in.^2$). After drying at room temperature, a 54-turn toroidal winding was wound through the tube and epoxied to the tube walls. The device at two stages of construction is shown in Fig. 2. The toroid coil produces a magnetic field directed around the circumference of the tube. The entire assembly was then suspended inside the solenoid coils shown in Fig. 3. The solenoid coil produces a magnetic field along the length of the device. This field is perpendicular to the toroid field. Two solenoid coils were wound concentrically—one to provide conventional dc bias and the second, ac excitation. The resonant frequency for the length or piston mode of the assembled device was 7050 Hz. No flux return path was provided for the solenoid windings.

The output power generated by this device was measured by a dummy load technique. To accomplish this, an aluminum (2017T4)-ceramic (EC64) composite stack (Fig. 2) of the same resonant frequency was constructed. The stack was epoxied to one end of the magnetostrictor and can be seen protruding from the end of the solenoid coils in Fig. 3. The active cross section of the ceramic stack was more than 7.5 times that of the nickel magnetostrictor.

One orthogonal excitation circuit used to test this prototype device is shown in Fig. 4. The two solenoid coils and the toroid coil with its perpendicularly directed fields are shown schematically. Direct current bias is applied to the toroid and one solenoid and is blocked by the capacitor from the second solenoid. Alternating current power is applied to the toroid and second solenoid, while being blocked by a choke from the bias solenoid. Operation of this circuit requires both ac and dc power supplies; self-biased excitation will be discussed separately. The test circuit reduces to conventional excitation by simply disconnecting the toroid leg.

EXPERIMENTAL RESULTS

Induction Measurements

When the device is driven with the circuit shown in Fig. 4, the ac and dc magnetic fields interact in a special way. At one instant they reinforce each other in the axial direction (solenoid) and are in opposition in the circumferential direction (toroid). One-half cycle later they are adding in the toroid and subtracting in the solenoid. This interplay of magnetic fields results in both a change in magnitude and orientation of the core induction. As discussed in the introduction, it is convenient to show the core induction as a two-dimensional diagram. In Fig. 5, the x-axis represents core induction along the axial direction, while the circumferential induction is given along the vertical axis. The bias induction produced by a 1.8-A dc current is shown as $\mathbf{B}_p$. The trace of the net induction vector in response to a

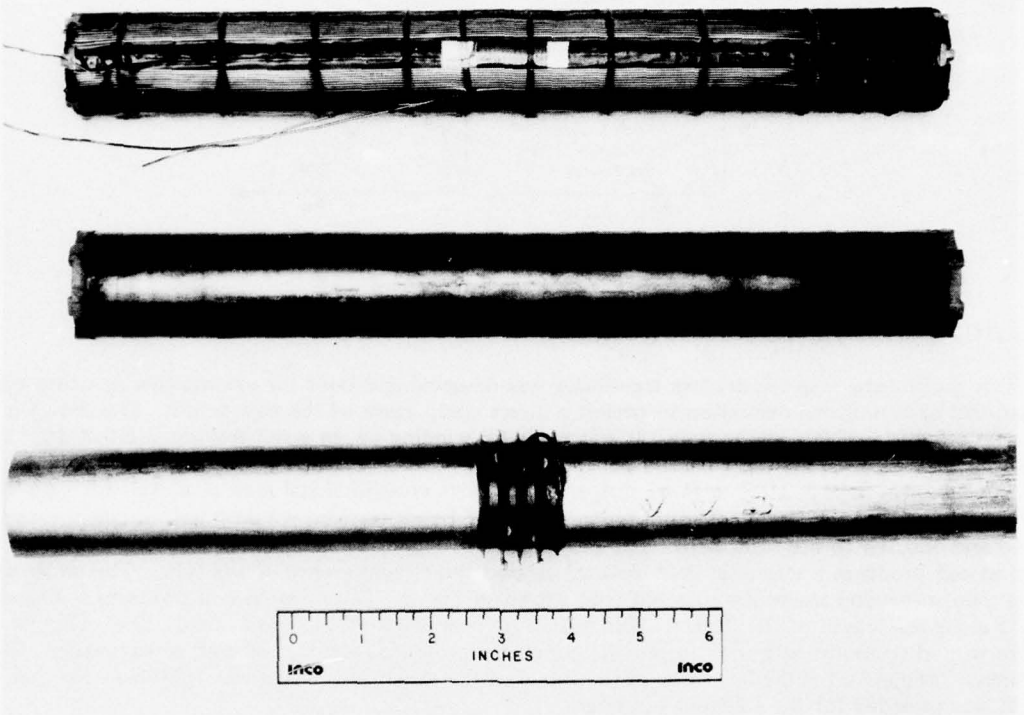

Fig. 2. Prototype piston transducer at two stages of construction and the aluminum-ceramic composite dummy load

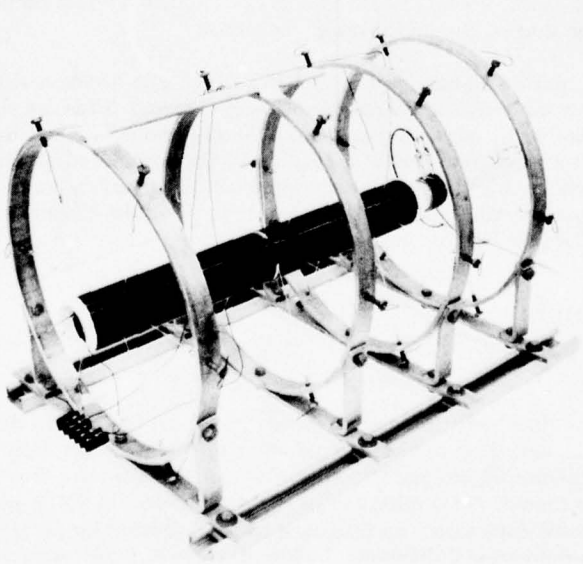

Fig. 3. Transducer mounted in solenoid coil ready for testing

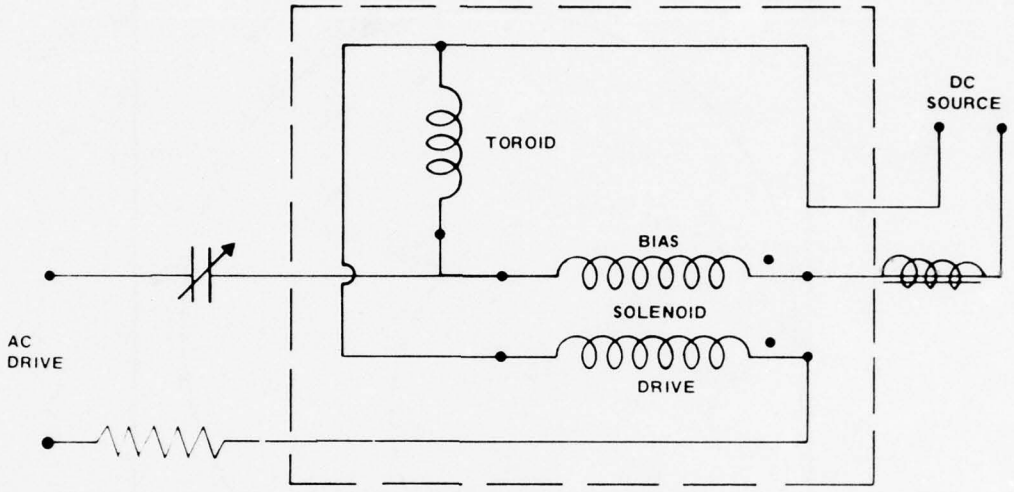

Fig. 4. Schematic orthogonal excitation circuit

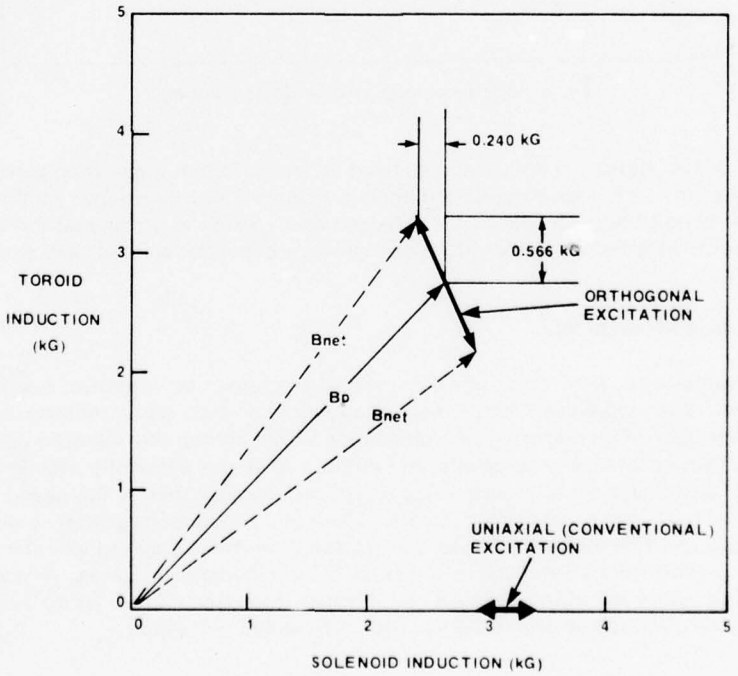

Fig. 5. Induction diagram obtained at 1.8-A bias and 38-W/cm^2 ac input

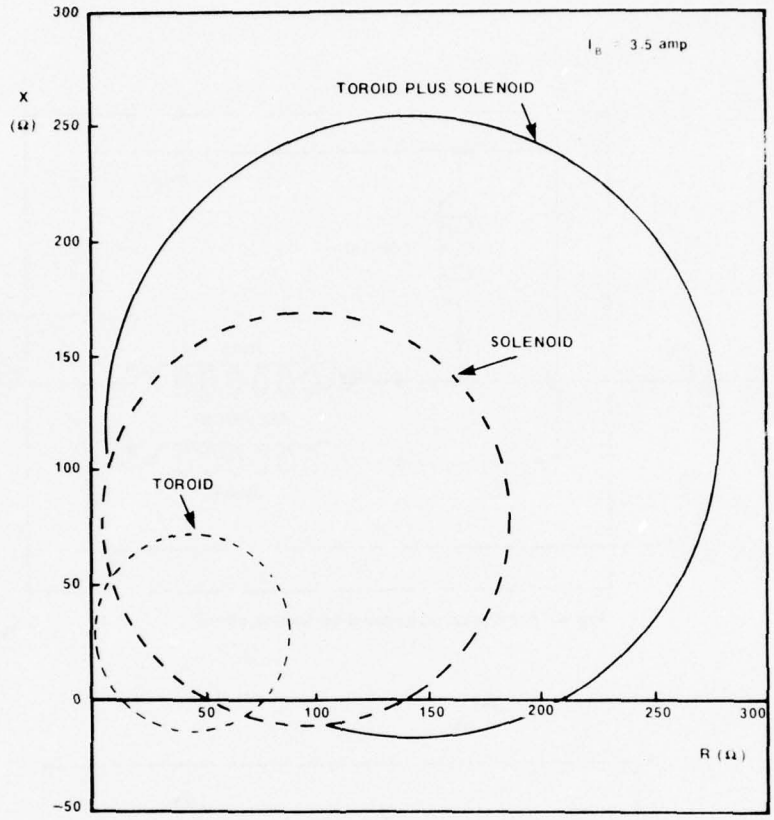

Fig. 6. Impedance loops measured at 3.5-A bias

38-W/cm^2 ac input is also shown. The trace is inclined at an excitation angle of approximately 115° to the output axis (solenoid). The corresponding induction change for conventional excitation at the same set of bias and drive conditions is shown on the solenoid axis. These experimental induction measurements present a graphic illustration of the difference between conventional and orthogonal excitation.

Low-Power Impedance Measurements

Impedance measurements were made as a function of frequency to determine coupling. For orthogonal excitation, three impedance loops may be measured at each bias condition, as shown in Fig. 6. These loops are obtained by measuring the impedance of the toroid and solenoid coils separately and then together. During these measurements, the dummy load was physically attached to the magnetostrictor but electrically open circuited. This reduces coupling due to the added end mass but otherwise does not interfere with the measurements. The same resonant frequency is obtained from all curves, and the toroid and solenoid impedances add (at the same frequency) to give the total impedance. Electromechanical coupling coefficients calculated from total impedance loops are shown in Fig. 7. The experimental coupling values are plotted against the net bias induction. Contrary to LeBlanc & Sherman's analysis[7], higher values of coupling were attained with orthogonal excitation.

[7]C. L. LeBlanc and C. H. Sherman, NUSC TM TD 12-75-72 (2 Mar. 1972).

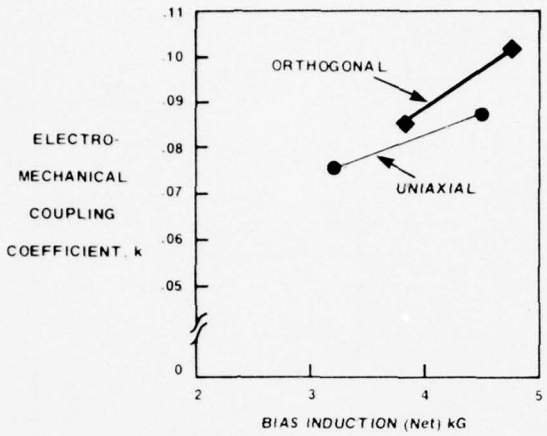

Fig. 7. Coupling coefficients measured as a function of bias induction and excitation mode

Power Measurements

To compare the power and efficiency capabilities of these two excitation modes, the test circuit shown in Fig. 8 was employed. The tests were run pulsed, and the input power measured with the Fluke VAW meter. The dummy load was terminated with a tuned resistive load. Output power was obtained from the voltage drop across the resistive load. For each input power test, excitation frequency and resistive load were varied to obtain maximum power output (i.e., maximum efficiency). Experimental results are summarized in Fig. 9. These are high-power tests far in excess of the 0.5 W/cm^2 cavitation threshold for water. The three sets of curves refer to three different bias levels. Without exception, orthogonal excitation gives equal or greater output power. At low bias, the curves flatten, showing signs of apparent saturation. At high bias, output power in excess of 50 W/cm^2 at an efficiency greater than 40% was obtained.

Linearity

During the power tests, drive voltage is mainted as a sinusoid and the dummy load has a high mechanical Q and low-output power density, so that the output voltage is also a sinusoid. The drive current then must contain the nonlinearities of the magnetic field to strain transformation. The effect of the excitation mode on linearity is thus obtained by comparing drive current waveforms. Current waveforms from a number of tests were Fourier analyzed and a linearity index was formed from the coefficients. This index is unity for a pure sinusoid with the same frequency as the drive voltage and falls off as the harmonic content increases. The results of this analysis are shown in Fig. 10 for comparative tests at 1.8-A bias. "Square-law" distortion is evident for conventional excitation even at 10 W/cm^2. However, linearity actually increases for orthogonal excitation at output power levels in excess of 30 W/cm^2.

Self-Biased Excitation

The drive circuit permitting self-biased excitation of the prototype device is shown in Fig. 11. Two fast-acting diodes (IN 3881) have been added and the toroid and one solenoid drive coil connected in parallel. The dc power supply and the second solenoid coil are not used. The resistors are simply current shunts. The diodes act like rectifiers in a resistive circuit—passing current in only one direction. However, because the circuit is reactive, current is not interrupted. The current waveforms measured during a 67-W/cm^2 input power test are shown in Fig. 12. The total drive current is shown at the top

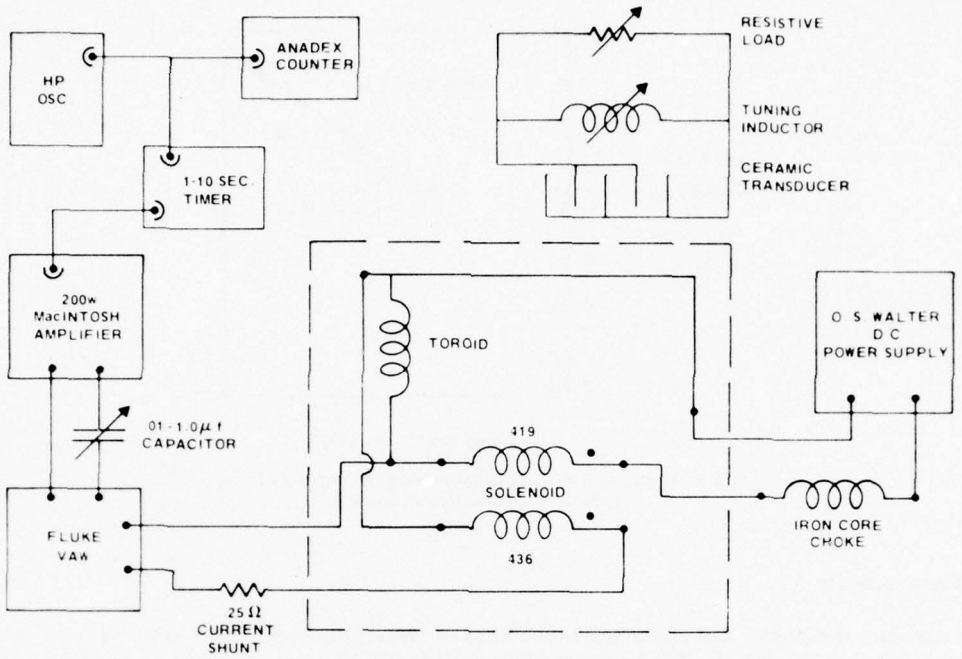

Fig. 8. Schematic of circuit employed for power tests

and the toroid and solenoid components below. The positions of the origins indicate that each component has acquired a dc bias and is phased at 180° with respect to the other. The lack of symmetry in these components is due to an impedance mismatch of 57% between the two coils.

The results of power tests using this drive circuit are shown in Fig. 13. Tests were performed to 40 W/cm^2 output, and the measured points (solid triangles) are superimposed on the earlier data. Self-biased excitation is indeed capable of high-power operation. In fact, the device efficiency was observed to increase with increasing output power density. The reason for this can be seen on the schematic induction plot shown in Fig. 14. At low drive levels, operation is near the origin of induction space—an inherently low efficiency region. Efficiency improves as the device is driven to higher working induction levels. The straight line shows the expected net induction trace for matched toroid and solenoid impedance.

SUMMARY

Experimental data obtained from one prototype piston transducer operated alternately in conventional and orthogonal modes of excitation have been presented. Increased power density capability and improved device linearity were demonstrated for orthogonal excitation in agreement with theoretical predictions. A modest increase in the coupling coefficient was also achieved. This increase is believed to result from an increase in the contribution of magnetic domain rotations to the net induction change. Self-biased operation at high-power levels was also demonstrated. Thus, orthogonal excitation of a magnetostrictive core does, in fact, offer many improvements over conventional operation. These improvements are independent of the magnetostrictive core material and complement the current material development effort.

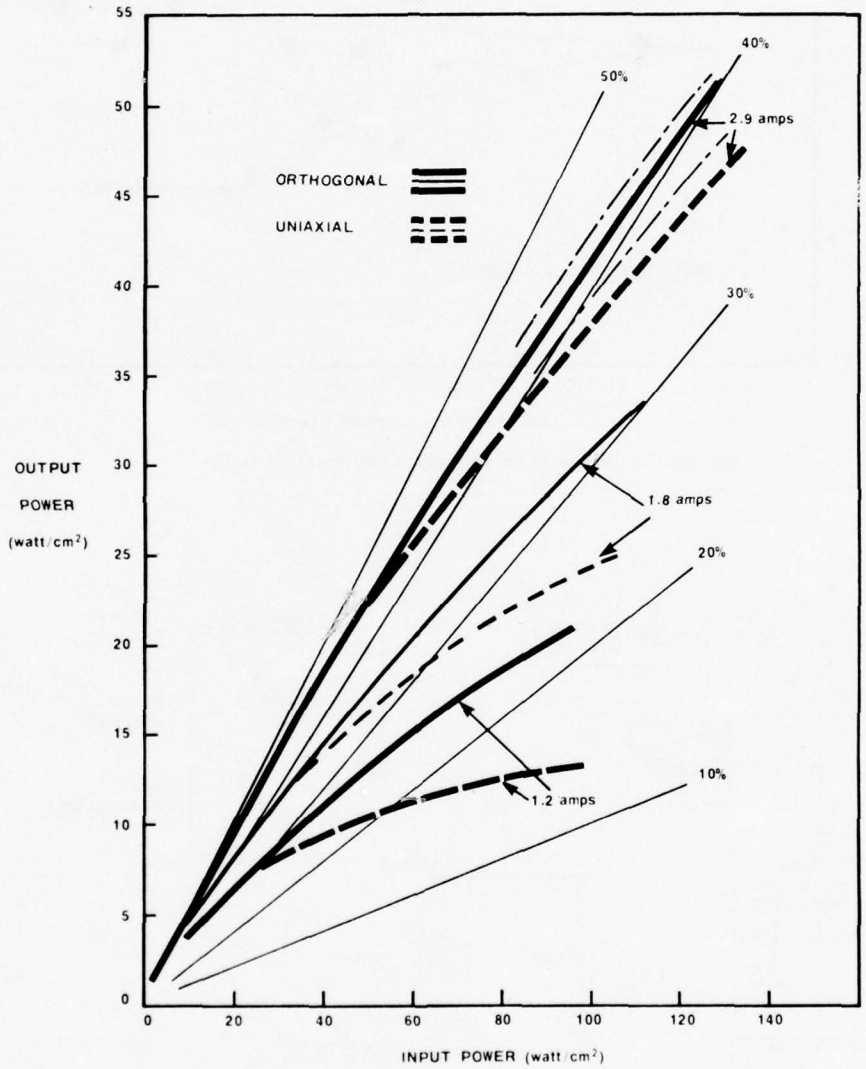

Fig. 9. Efficiency curves measured as a function of bias level and excitation mode

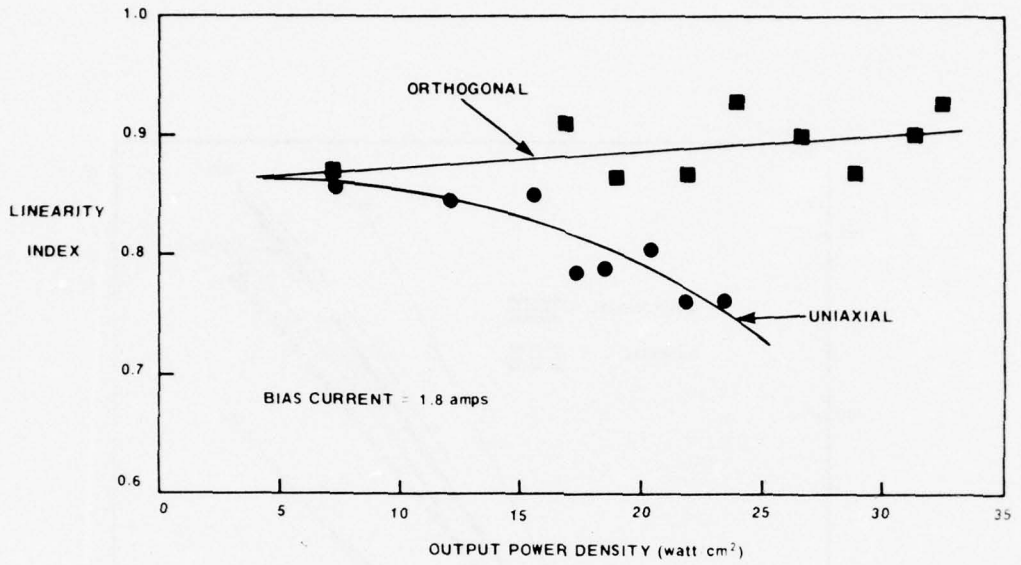

Fig. 10. Comparison of linearity measurements at 1.8-A bias

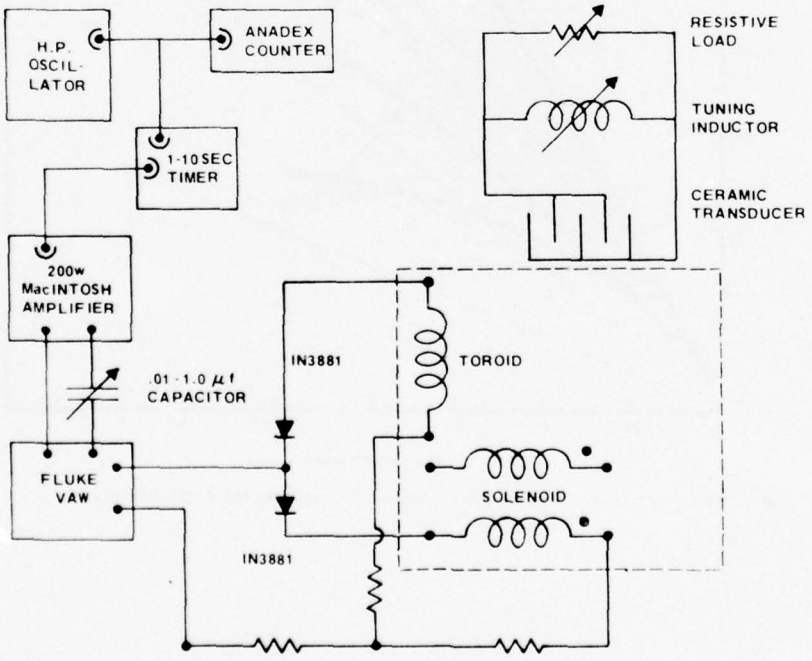

Fig. 11. Schematic of circuit employed for self-biased tests

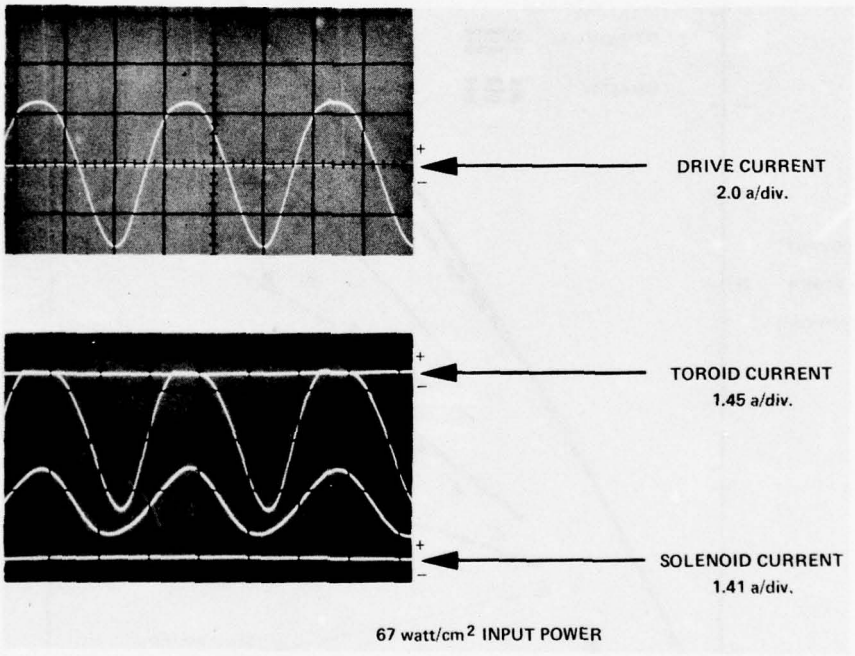

Fig. 12. Current waveforms measured during self-biased excitation at 67-W/cm^2 input power

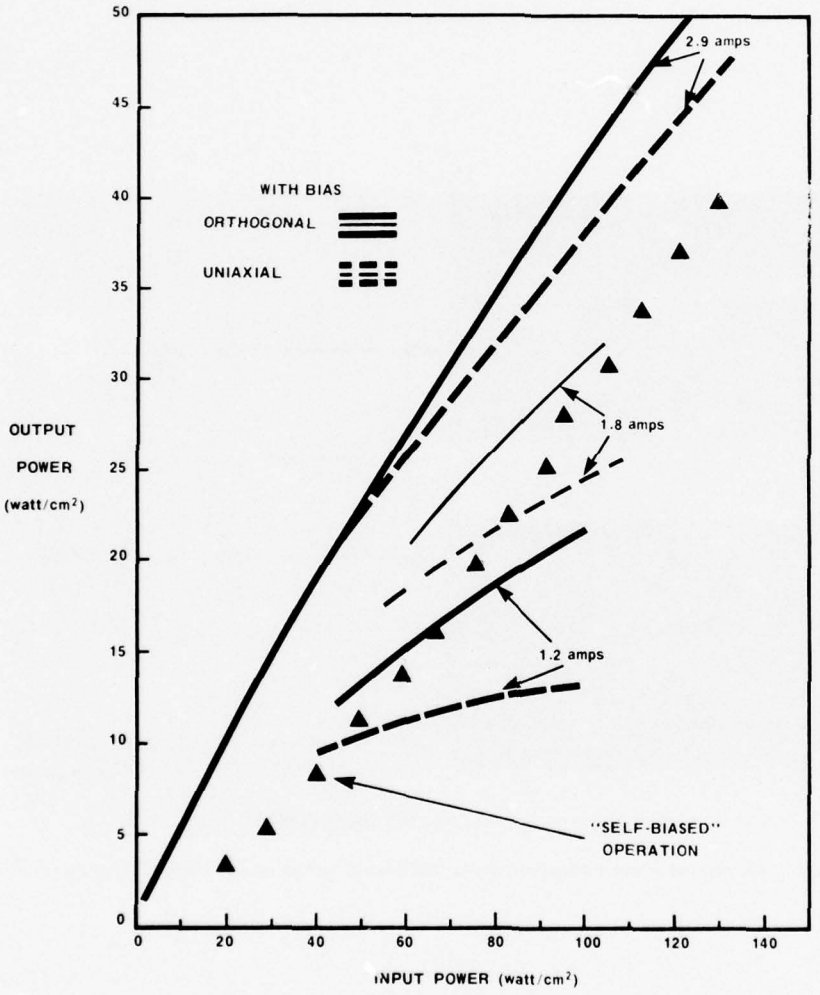

Fig. 13. Efficiency curve for self-biased excitation compared with earlier measurements

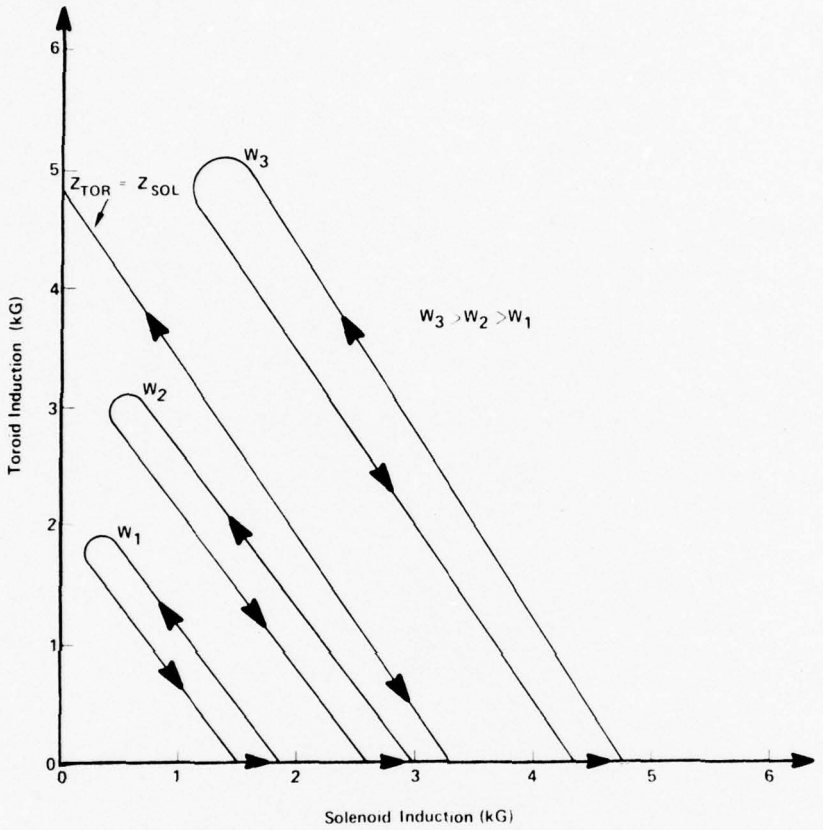

Fig. 14. Schematic induction diagram for self-biased excitation

Hueter's review[8] of magnetostrictive transducers concluded that the natural advantages of these devices—reliability, ruggedness, corrosion resistance, and low impedance—were compromised by low coupling, low power density, poor linearity, and the need for dc bias. The results of this investigation indicate that the disadvantages are, at least in part, a consequence of the method of excitation. The extent to which orthogonal excitation can be used to improve device performance needs to be experimentally determined. Research areas of particular importance are core material and core design for compatibility with orthogonal fields, the effect of impedance mismatch, and the effect of excitation angle. To the author's knowledge, no research in these areas is currently in progress.

[8]T. F. Hueter, *J. Acoust. Soc. Am.* **51** (No. 3, Part 2), 992 (1972).

U.S. Navy Journal of Underwater Acoustics Volume 27, No. 1 January 1977

COMPARISON OF THE MAGNETIC AND MAGNETOSTRICTIVE PROPERTIES OF CUBE-TEXTURED AND CONVENTIONAL NICKEL TRANSDUCER MATERIALS*

D. T. Peters
Paul D. Merica Research Laboratory
The International Nickel Company, Inc.
Suffern, New York 10901

ABSTRACT

The anisotropies in the elastic, magnetic, and magnetostrictive properties of nickel have been considered, with the conclusion that a cube-on-face texture (100) ⟨100⟩ nickel sheet would be expected to result in a 50% increase in the magnetostrictive strain energy density and a 21% decrease in sound velocity compared to conventional randomly oriented nickel sheet. This paper describes the results of measurements comparing the magnetic and magnetostrictive properties of tape-wound ring scrolls of cube-textured nickel and randomly oriented nickel. The expected increase in strain energy density and decrease in sound velocity were observed. These improved characteristics were found with an equivalent coupling coefficient in the two materials and a nearly linear response of magnetostrictive strain to applied field in the cube-textured nickel. Low-power linear drive measurements by Sinsky at NRL are also described. In this work, larger reverse permeabity (μ_{33}^{T}) and piezomagnetic strain constant (d_{33}) values at all induction levels were found for the randomly oriented material, while the textured nickel showed slightly larger coupling coefficient (k_{33}) and increased piezomagnetic constant (g_{33}) values. Cube-textured nickel is shown to be an attractive new material for consideration by the transducer engineer for a number of applications.

INTRODUCTION

Nickel processed to have a very high degree of the cube-on-face crystallographic orientation in polycrystalline sheet for use as a core material in magnetostrictive transducers has been described in two recent publications.[1,2] This paper summarizes the results of the work by The International Nickel Company, Inc. (INCO), to develop an improved pure nickel core material and the results of INCO and NRL studies comparing the cube-textured nickel with conventional nickel. The paper by Sinsky et al. in this issue describes the properties of nickel-cobalt alloys in the cube-textured condition.

Because the magnetic properties of materials are generally quite anisotropic, substantial improvements to various properties have been effected in several systems. Well-known examples would include the silicon-iron transformer materials, nickel-iron and cobalt-iron soft magnetic alloys, and the alnico and barium ferrite permanent magnet alloys.

*Presented at the Workshop on Magnetostrictive Materials held under the sponsorship of the Underwater Sound Advisory Group and the Naval Research Laboratory, Orlando, Florida, 25-26 February 1976.

[1]E. L. Huston, D. T. Peters, and G. D. Sandrock, "Magnetic and Magnetostrictive Properties of Cube Textured Nickel for Magnetostrictive Transducer Applications," *IEEE Trans. Magn.* mag-9(4), pp. 636-640 (Dec. 1973).
[2]E. L. Huston and J. A. Sinsky, "Comparison of Cube-Textured and Conventional Nickel Magnetostrictive Ring Transducers During Low-Power Linear Drive," *J. Acoust. Soc. Am.* 58(5), pp. 1082-1089 (Nov. 1975).

The magnetostrictive response of nickel exhibits a pronounced crystallographic dependence. Saturation values of the magnetostrictive strain $(\Delta l/l)_s$, measured in the ⟨100⟩ and ⟨111⟩ directions have been reported by Lee[3] to be -45.9×10^{-6} and -24.3×10^{-6}, while Yamamoto and Nakamichi[4] give the values -54.1×10^{-6} and -22.4×10^{-6}, respectively. Young's modulus E is also quite anisotropic: 13.9×10^{11} and 30.7×10^{11} dyne/cm^2 in the ⟨100⟩ and ⟨111⟩ directions, respectively.[5] However, the magnetostrictive strain energy density (proportional to $E(\Delta l/l)_s^2$) is also anisotropic, and it is this quantity that indicates ultimate power capabilities for transducer applications. Combining the available data leads to the prediction of a 24% to 51% increase, with respect to random values: $(\Delta l/l)_s = -32.8 \times 10^{-6}$ (Ref. 3) to -35.1×10^{-6} (Ref. 2) and $E = 21.9 \times 10^{11}$ dyne/cm^2 (Ref. 5) for the magnetostrictive strain energy in the ⟨100⟩ direction. Thus the available power density of nickel for magnetostrictive applications can be enhanced by crystallographic texturing.

The magnetocrystalline anisotropy must also be taken into account. The anisotropy constants for nickel at room temperature[6] are approximately $K_1 = -45{,}000$ erg/cm^3 and $K_2 = 23{,}000$ erg/cm^3; i.e., the "easy" direction of magnetization in nickel is in the [111] crystallographic direction. Therefore, cube-textured nickel will have a lower permeability in the plane of the sheet than randomly oriented polycrystalline material. This suggests at first glance that the increased power density in cube-textured nickel might only be available at a significant sacrifice in magnetomechanical efficiency. But, because the coupling coefficient can be taken as a measure of the conversion of magnetic energy to mechanical energy, it is not entirely apparent that a sacrifice in efficiency is inevitable in cube-textured nickel.

Figure 1 illustrates the main crystallographic directions in iron and nickel and the effect of anisotropy on the magnetization curves.[7] Table I gives a comparison of the elastic and magnetostrictive properties of single and polycrystalline nickel as a function of crystal direction and in the polycrystalline state. The figure of merit FM is defined as $E(\Delta l/l)_s^2$.

Figure 2 shows the orientation of a unit cube of nickel in a cube-textured sheet and the resulting X-ray pole figure. The {100} ⟨100⟩ texture, commonly termed the "cube-on-fact" or simply "cube" texture, has ⟨100⟩ crystal directions in both the rolling and transverse direction. In addition to X-ray diffraction measurement of the relative intensity of diffraction maxima, one can detect the presence of the cube texture by the shape of etch pits, as shown in the photomicrograph of Fig. 3. When it is established that the cube texture is present, its degree of perfection can be measured quite conveniently by determining the first anisotropy constant K_1 by torque magnetometry. The amplitude of the maxima of the torque curve will vary from zero in a random polycrystalline aggregate to a maximum of one-half of the first anisotropy constant K_1 of a single crystal of the material in a perfectly cube-oriented sheet. Torque curves for nickel with three levels of cube texture are shown in Fig. 4. The value of the first anisotropy constant of the polycrystalline materials, $(K_1)_p$, is taken as a measure of the amount of cube texture.

The cube texture is obtained by a heavy cold reduction followed by a high-temperature anneal. In nickel, the grain size before the cold working operation, impurity content, annealing time and temperature, sheet thickness, and other factors are important and must be controlled to obtain a high degree of cube orientation.

[3] R. M. Bozorth and R. W. Hamming, *Phys. Rev.* **89**, 865 (1953).
[4] M. Yamamoto and T. Nakamichi, *J. Phys. Soc. Japan* **2**, 228 (1958).
[5] C. J. Smithells, *Metals Reference Book* (Plenum Press, Inc., New York, 1967), 4th ed., Vol. III, p. 708.
[6] S. Chikazumi, *Physics of Magnetism* (John Wiley & Sons, Inc., New York, 1966), p. 130.
[7] R. M. Bozorth, *Ferromagnetism* (D. Van Nostrand Co., Inc., New York, 1953), p. 475.

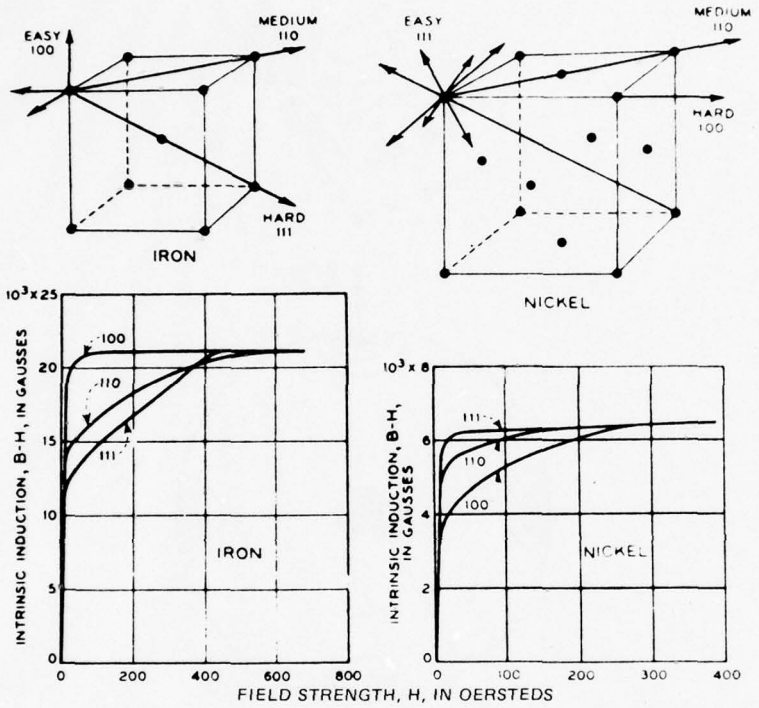

Fig. 1. Crystallographic directions in cubic nickel and iron crystals and the primary magnetization curves in those directions (from Bozorth, Ref. 7)

TABLE I
Comparison of Elastic and Magnetostrictive Properties of Single and Polycrystalline Nickel

Crystal Orientation	E (10^{11} dyne/cm^2)	$(\Delta l/l)_s$ (10^{-6})	FM[a] (10^3 dyne/cm^2)	FM / FM (polycrystalline)
⟨100⟩	13.9	-54.1	4.07	1.36
⟨110⟩	23.5	-29.6	2.06	0.69
⟨111⟩	30.7	-22.4	1.54	0.51
Polycrystalline	21.92	-37	3.00	1.00

[a]Figure of merit FM = $E(\Delta l/l)_s^2$

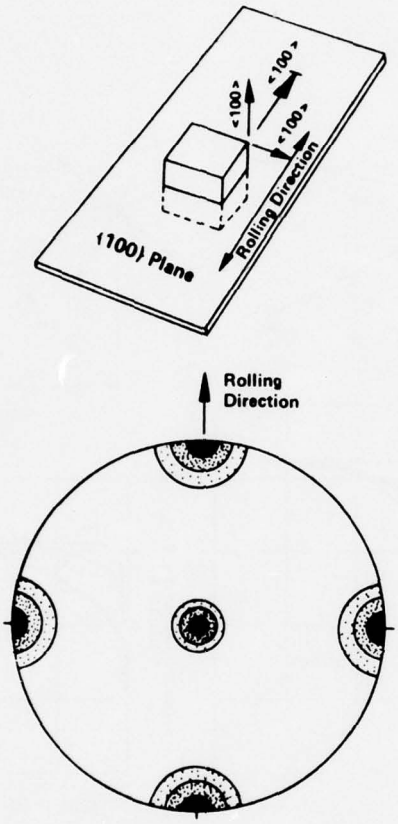

Fig. 2. Orientation of a unit cube of nickel in a cube-textured sheet and the resulting X-ray diffraction pole figure ($\{100\}\langle 100\rangle$ texture)

MAGNETIC AND MAGNETOSTRICTIVE PROPERTIES OF CUBE-TEXTURED NICKEL

INCO Results

Saturation magnetostrictive strain λ_s as a function of the degree of cube orientation (expressed as $(K_1)_p$) is plotted in Fig. 5. A linear increase with the degree of cube texture is indicated. The strain was measured on 1-in. (2.5-cm) disks punched from the 0.020-cm thick sheet by strain gages. Only the strain resulting from a 90° rotation of the specimen in the magnetic field was recorded. (A more complete description of experimental methods can be found in Ref. 1 and 2.) The strain obtained from the 90° rotation technique is 3/2 the saturation value $(\Delta l/l)_s$. This technique is independent of the initial domain distribution, eliminating the difficulty frequently encountered in uniaxial saturation strain measurements. The values of $(\Delta l/l)_s$ obtained for the random and fully textured samples are -37×10^{-6}, respectively. Both values are in good agreement with the data reported by Yamamoto and Nakamichi.[4] When these experimental values are used to calculate the available magnetostrictive strain energy, a 51% increase is obtained for the fully $\{100\}$ $\langle 100\rangle$ textured nickel sheet.

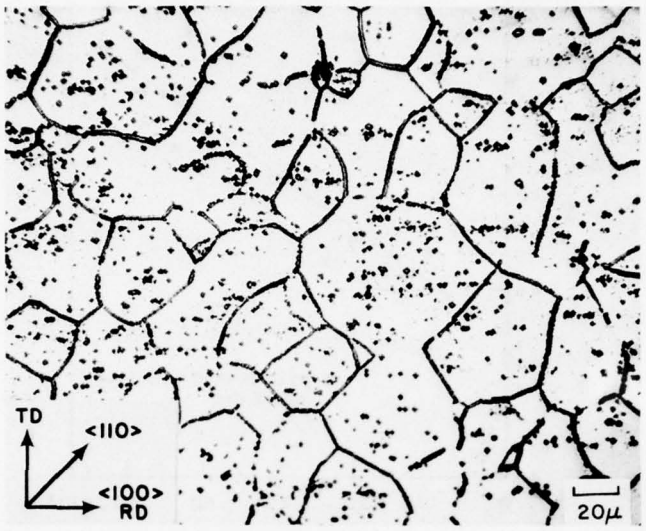

Fig. 3. Optical micrograph of the sample with $(K_1)_p$ = -47,600 erg/cm^3. This specimen was electrolytically etched to show dislocation etch pits. The edges of the etch pits are formed by ⟨110⟩ directions in each grain. The close alignment of the grains with one another and with the rolling direction is evident and in agreement with the large value of $(K_1)_p$ obtained from the torque curve.

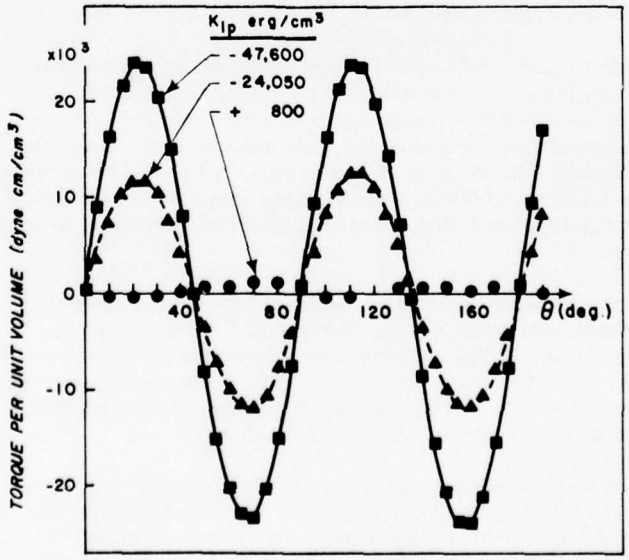

Fig. 4. Torque curves obtained for three polycrystalline nickel disks. The values for $(K_1)_p$, the first magnetocrystalline anisotropy constant, were derived from these data.

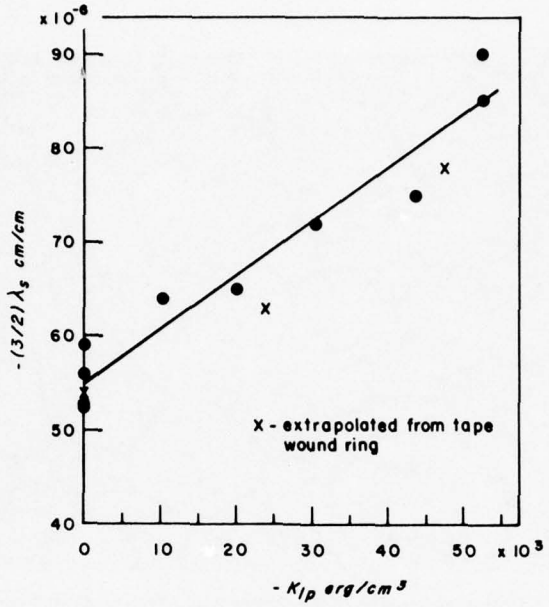

Fig. 5. Three-halves saturation magnetostrictive strain plotted as a function of $(K_1)_p$ for polycrystalline nickel sheet

The static magnetostrictive strain measured with fully textured and random tape-wound rings is shown as a function of applied field in Fig. 6. The larger strain of the fully textured ring is not evidenced until a field in excess of 100 Oe (8,000 A/m) is applied. However, the strain of the textured ring increases almost linearly with field over the entire range from 0 to 150 Oe (0 to 12,000 A/m), implying reduced distortion of the output strain waveform for large-field excitation.

The results of static magnetic measurements on the three tape-wound rings are shown in Fig. 7. Remanence and coercivity values increase with $(K_1)_p$. The primary magnetization curves show little difference for induction levels B below about 3,500 G. Above this level, however, the textured samples require larger applied fields to attain the same induction as the random sample. For the fully textured samples, the applied field must be increased by a factor of 2 to maintain the same induction level in the range from 4,500 to 5,500 G. This magnetic hardness at high induction levels is consistent with domain theory and the fact as noted above that the ⟨100⟩ directions in nickel are the "hard" magnetization directions.

A number of dynamic measurements were made on tape-wound rings (D_{avg} = 5.5 cm) of the textured, partially textured, and random nickel sheet at INCO. The magnetic hardness of the textured samples at high induction levels is also apparent in the reversible permeability data shown in Fig. 8. These data were obtained at 5,000 Hz, a frequency f well below mechanical resonance (21 to 28 kHz, depending on the degree of texture). The relatively high reversible permeability at low induction for this particular specimen of fully textured nickel is anomalous.

A summary of data from impedance measurements on the small tape-wound scrolls is given in Table II. The symbol H_p is the magnetic polarization field required to produce the desired induction level. Data obtained from remanent operation (H_p = 0) are also included. The large values of Q_{em}, greater than 29 in all cases, indicate that the rings were well consolidated and that epoxy and ringcase did not contribute significant mechanical losses to the radial vibration mode.

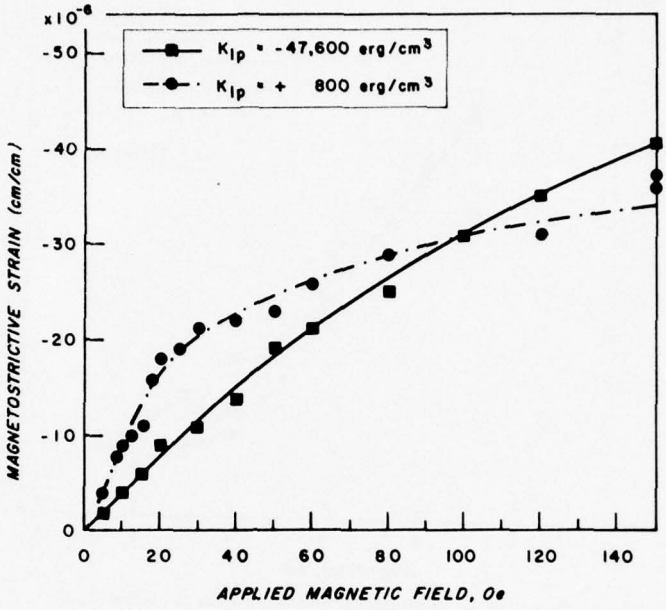

Fig. 6. Static magnetostrictive strain of tape-wound nickel ring samples measured as a function of the applied magnetic field

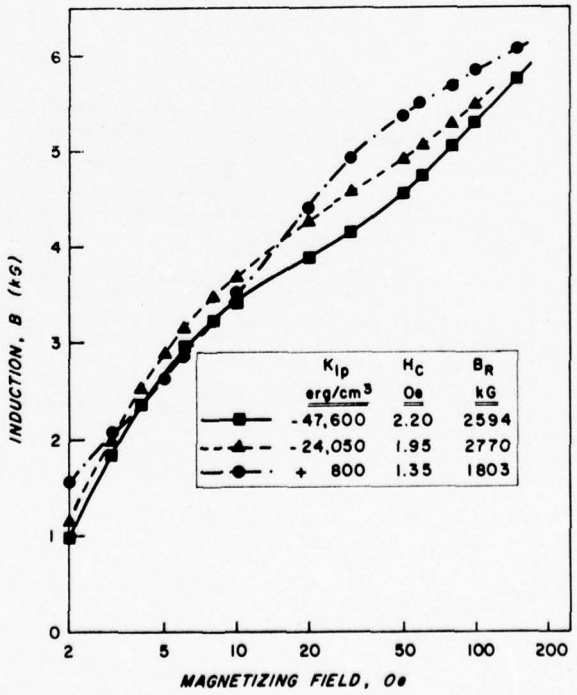

Fig. 7. Primary magnetization curves for the polycrystalline tape-wound nickel ring samples

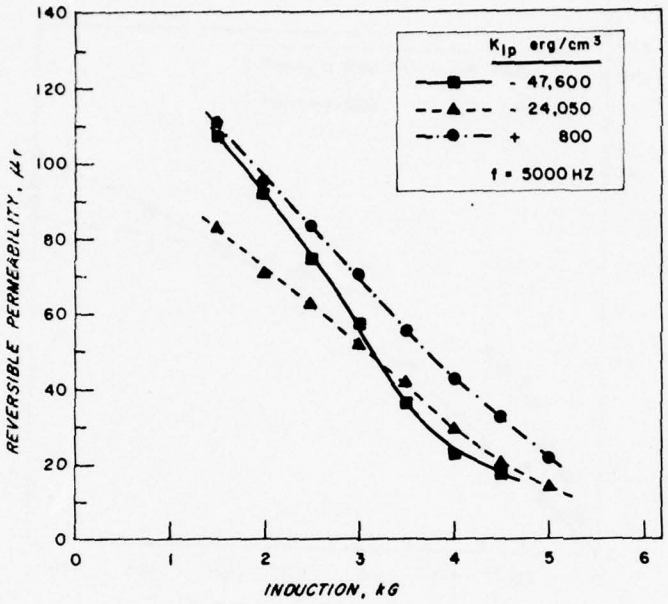

Fig. 8. Reversible permeability at 5000 Hz for the polycrystalline tape-wound nickel ring samples

TABLE II
Summary of Data Obtained From Impedance Measurements on Three Tape-Wound Nickel Ring Transducers With Different Values of $(K_1)_p$

B (kG)	$(K_1)_p$ = +800 erg/cm^3					$(K_1)_p$ = -24,050 erg/cm^3					$(K_1)_p$ = -47,600 erg/cm^3				
	H_p (Oe)	f_{em} (Hz)	Q_{em}	Q_e	k	H_p (Oe)	f_{em} (Hz)	Q_{em}	Q_e	k	H_p (Oe)	f_{em} (Hz)	Q_{em}	Q_e	k
2.0	3.0	27,730	70.2	2.17	0.127	3.2	23,695	62.4	3.04	0.142	3.3	21,630	88.3	2.22	0.139
2.5	4.5	27,620	50.3	2.54	0.175	4.0	23,660	53.8	3.42	0.171	4.3	21,615	69.1	2.88	0.168
3.0	6.8	27,510	40.5	2.89	0.214	5.5	23,595	43.7	4.86	0.214	6.5	21,580	54.6	3.79	0.215
3.5	10.0	27,370	29.1	3.45	0.259	8.0	23,520	39.9	7.32	0.242	11.0	21,485	47.7	5.88	0.268
4.0	14.8	27,250	29.5	5.80	0.284	14.5	23,395	41.1	13.1	0.281	22.5	21,465	62.6	14.2	0.264
4.5	21.3	27,310	34.8	6.15	0.277	25.9	23,400	48.3	15.8	0.252	43.6	21,410	75.1	10.8	0.263
5.0	32.0	27,485	65.5	9.81	0.231	55.7	23,525	84.0	17	0.203	—	—	—	—	—
Remanent	0	27,575	89.0	1.74	0.104	0	23,600	59.7	2.39	0.156	0	21,640	83.9	1.92	0.139

[a]1 Oe = 79.57747 A/m.

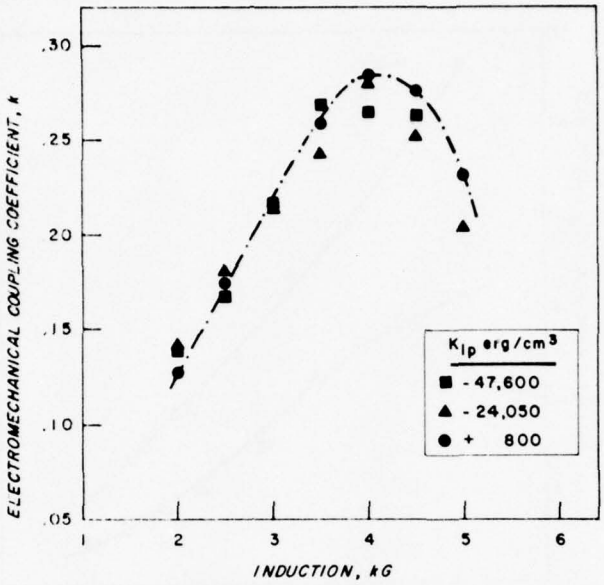

Fig. 9. Electromechanical coupling coefficient measured as a function of induction for the three tape-wound nickel ring specimens

For convenience, the coupling coefficients given in Table II are plotted as a function of induction in Fig. 9. The random ring, $(K_1)_p$ = 800 erg/cm^3, has a maximum value of 0.284 at 4,000 G. This compares favorably with a value of 0.30 reported by Clark.[8] The textured rings show essentially the same result indicating that the {100} ⟨100⟩ texture has little effect on the coupling coefficient.

NRL Results

Joel Sinsky, then at the Naval Research Laboratory, has measured the electrical input impedance of both random nickel (Ni-200) and cube-textured nickel scroll-wound rings.[2] He expressed the results of the measurements in terms familiar to acoustic engineering, namely μ_{33}^T, d_{33}, k_{33}, and g_{33}. A thorough analysis of the impedance data to obtain these quantities, based on Butterworth and Smith's approximate expression for the total electrical input impedance of a magnetostrictive ring transducer in air,[9] is presented in the Huston and Sinsky paper.[2] The impedance measurements on each ring were obtained under conditions of low-power linear excitation to permit analysis with the conventional piezomagnetic equations of state. The data were plotted as a function of bias induction to facilitate comparison of the two materials.

The reversible permeability of the cube-textured nickel (CTNi) and random nickel (Ni-200) rings determined at NRL is shown in Fig. 10. The lower reversible permeability of the cube-textured ring implies that the input core impedance, which is proportional to μ_{33}^T, is correspondingly less than that of the Ni-200 ring for the same core cross section and frequency. Also, eddy-current losses and, therefore, internal heating losses, again proportional to μ_{33}^T, will be less in the cube-textured material compared to the conventional randomly oriented nickel.

The material electromechanical coupling coefficients k_{33}, shown in Fig. 11, are strongly dependent upon the bias induction level and are generally similar to the INCO data of Fig. 9. A maximum value of 0.282 is attained by CTNi at 4.5 kG and exceeds the maximum attained with the Ni-200 ring by about

[8] C. A. Clark, *J. Acoustical Soc. Am.* **33**, 930 (1961).
[9] S. Butterworth and F. D. Smith, "The Equivalent Circuit of the Magnetostriction Oscillator," *J. Phys. Soc. Lon.* **43**(2), 166 (1931).

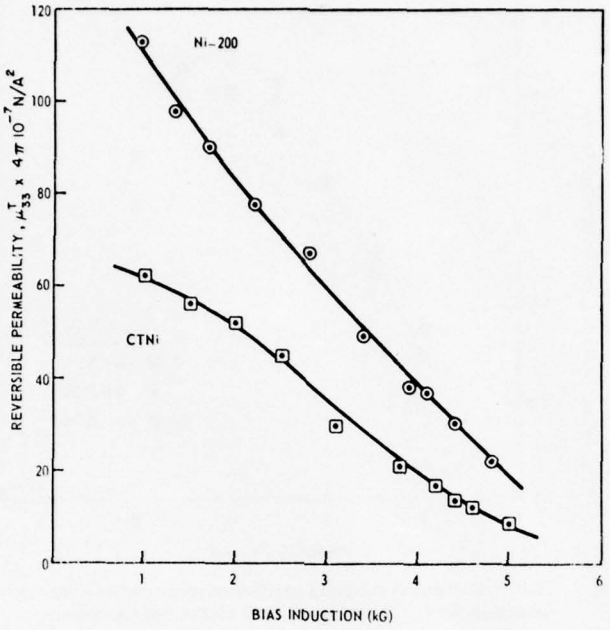

Fig. 10. Reversible permeability of the two nickel rings as a function of the bias induction

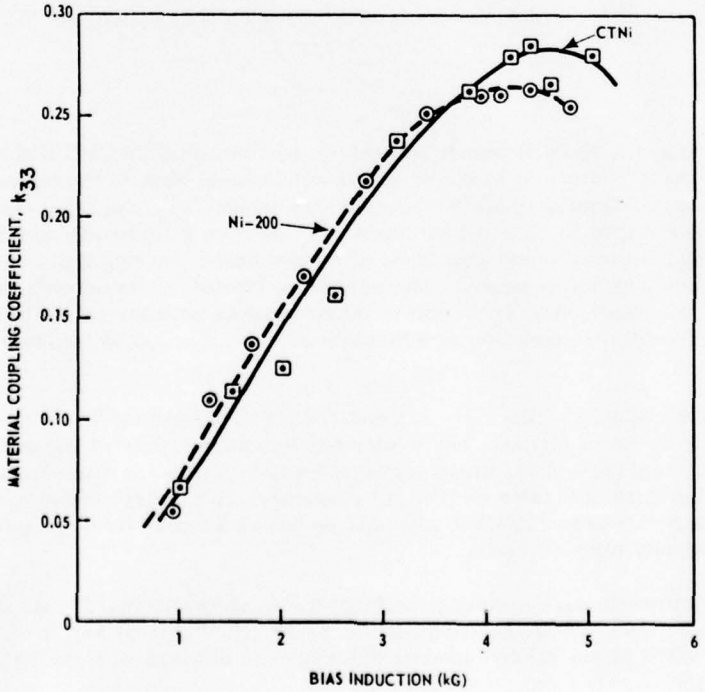

Fig. 11. Material coupling coefficient k_{33} of the two nickel rings as a function of the bias induction

TABLE III
Elastic Compliance and Modulus of Cube-Textured and Ni-200 as a Function of Introduction

CTNi			Ni-200		
B (kG)	S_{33}^B (10^{-12} m^2/N or Pa^{-1})	E (10^{11} Pa)	B (kG)	S_{33}^B (10^{-12} m^2/N or Pa^{-1})	E (10^{11} Pa)
2.5	8.16	1.22	2.8	5.04	1.99
3.1	7.98	1.25	3.4	4.98	2.01
3.8	7.86	1.27	3.9	4.94	2.02
4.4	7.75	1.29	4.4	4.91	2.04

7%. In the linear analysis, k_{33}^2 is a measure of the energy conversion capability of a piezomagnetic material. Its magnitude "gives the fraction of input electrical energy that appears in mechanical form, stored in the elastic displacement."[10] The coupling coefficient is also often used as an indication of the bandwidth capability of a piezomagnetic material.

The elastic properties shown in Table III for the two nickel rings are significantly different. Cube-textured nickel exhibits a 37% larger elastic compliance with a corresponding 37% lower Young's elastic modulus. This is a direct result of elastic anisotropy, which for the nickel lattice is softest in [100] directions. The lower modulus for CTNi results in a 21% reduction in sound velocity. In practical terms, this means that for a specified resonance frequency, a CTNi ring can be built with a 21% smaller diameter than its Ni-200 counterpart, with a resulting weight and material saving. Smaller size rings with the same resonant frequency are advantageous for elements of an array. A more densely packed ring array results in a reduction of the interelement spacing and a greater angular dispersion of all the minor lobes from the main beam of the array radiation pattern. On the other hand, if a CTNi ring array was built with the same interelement spacing used in a Ni-200 ring array and the resonance frequencies of the rings in each array were identical, then the smaller size CTNi rings would be acoustically less visible and have smaller interelement forces than the larger Ni-200 rings.[2]

The piezomagnetic strain constant d_{33} (Fig. 12) is higher by about 8% at optimum bias induction for the Ni-200 ring. The piezomagnetic constant d_{33} is the proportionality constant between the mechanical strain and the applied magnetic field at constant stress. Magnetostrictive strain is directly related to magnetic domain rotation and, consequently, the induction change resulting from the applied field. Because the CTNi ring exhibits about a 50% lower permeability, a reduction in d_{33} greater than the observed 8% value is expected unless the magnetostrictive strain of CTNi is larger than Ni-200. The increased magnetostrictive strain of CTNi is readily apparent in the comparison of g_{33} values shown in Fig. 12. This piezomagnetic constant reflects the proportionality between strain and induction. At 5 kG, g_{33} for CTNi is more than twice the value for Ni-200.

It is felt that the NRL dynamic data of Figs. 10, 11, and 12 complement the INCO static magnetostrictive strain measurements reported in this paper and demonstrate with low-power tests the claim for increased power-handling capability of cube-textured nickel. Actual transducer performance at high-power densities can only be determined by experiments at high-drive levels.

Some testing in water was also done at NRL on the CTNi and Ni-200 rings.[2] The water resonant frequency of the CTNi ring was approximately 20% lower than that of the Ni-200 ring, as was the case in air. Transmitting efficiencies calculated for the in-water impedance circles of the two materials show

[10]R. S. Woollett, "Magnetostrictive Material Requirements for Sonar Transducers," *JUA(USN)* **20**, 679 (1970).

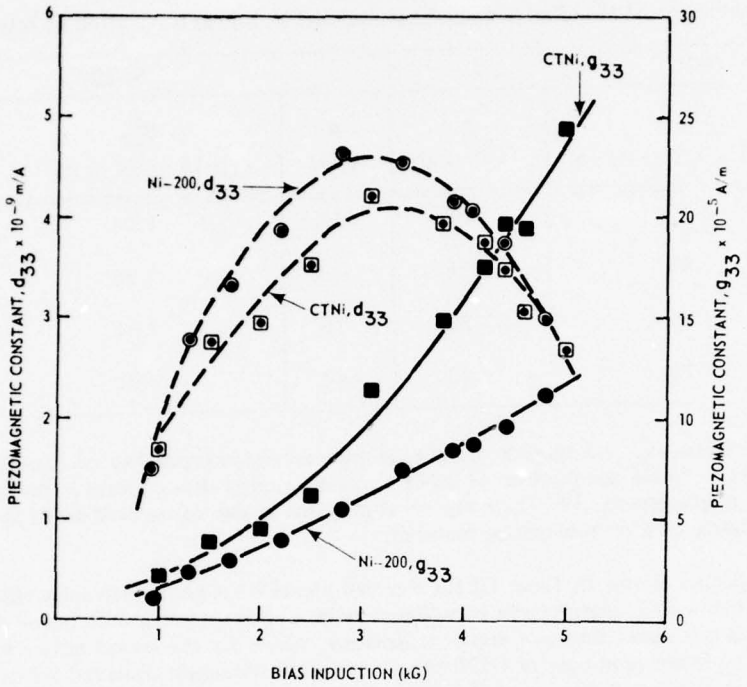

Fig. 12. Piezomagnetic constants d_{33} and g_{33} as functions of bias induction for the two nickel rings

them both to operate at greater than 75% efficiency when driven with a 15-mA excitation signal. The transmitting efficiencies of the rings were also calculated directly from the ratio of the outgoing acoustic power to the incoming electrical power for each ring. The outgoing acoustic power was found by numerically integrating under the far-field directivity patterns, as shown in Fig. 13. For detectable far-field transmission, the rings were driven at currents of 100 mA. The efficiencies determined by this method were 59% for the CTNi ring and 66% for the Ni-200 ring. The efficiencies are high because the ac driving currents were small. The purpose of doing the calculations was to indicate that at low-power drive the efficiencies of the two rings were comparable.

The maximum far-field transmitting response is 2 dB lower for the CTNi ring than for Ni-200 at the 100-mA drive level. Comparisons at constant drive voltage (constant induction swing) would increase the response of CTNi relative to Ni-200 because of the 50% lower reversible permeability of the CTNi ring.

CONCLUSION

The side-by-side comparison of cube-textured and conventional random nickel free-flooded ring transducers demonstrates that substantial magnetic and magnetostrictive property changes result from the introduction of the cube-on-face crystallographic texture in nickel. The changes are in three principal categories: magnetic permeability, elastic modulus, and power-handling capability. For a given set of transducer conditions, random nickel offers higher reversible permeability, increased electrical impedance, and higher eddy-current losses. The increased elastic compliance (lower Young's modulus) of cube-textured nickel permits a 21% size reduction for the same resonant frequency. Further, the increased strain energy density of cube-textured nickel improves the power-handling capability of nickel magnetostrictive transducers. This crystallographic texture has little effect on the material electromechanical coupling coefficient. It is hoped that this comparison will aid the transducer engineer in his selection of a core material for a particular transducer application.

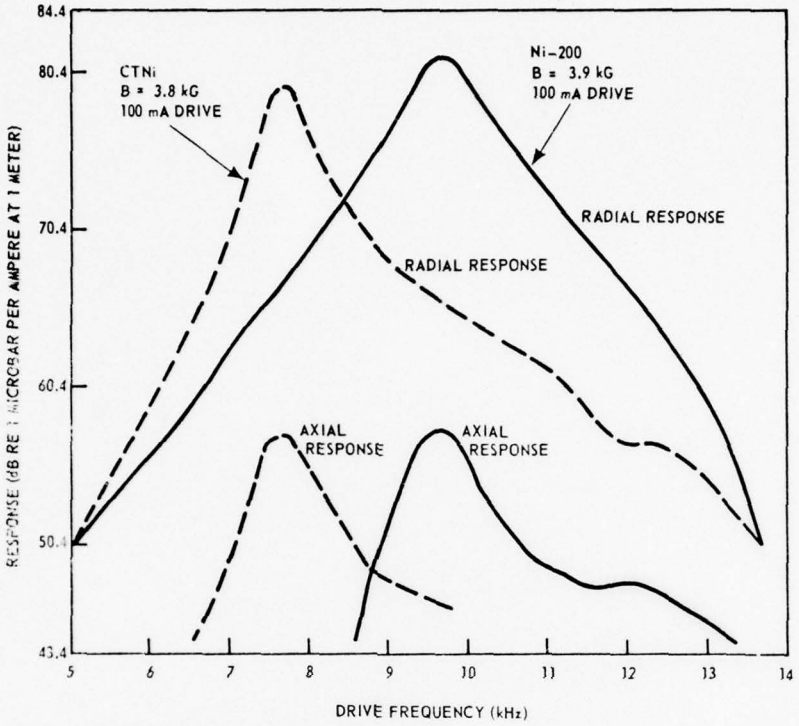

Fig. 13. Far-field transmitting current response of the nickel rings in water. The upper curves are for pressures measured in the plane of the rings, and the lower curves are for pressures measured on the axis of the rings.

ACKNOWLEDGMENT

The NRL work quoted were supported by the Naval Electronics Systems Command, Code 320.

U.S. Navy Journal of Underwater Acoustics Volume 27, Number 1 January 1977

THE EVALUATION OF CUBE-TEXTURED NICKEL-COBALT MAGNETOSTRICTIVE RING TRANSDUCERS DURING LOW-POWER LINEAR DRIVE*

J. Sinsky
Naval Research Laboratory
Washington, D.C. 20375
E. L. Huston and D. T. Peters
The International Nickel Company, Inc.
Suffern, New York 10901

ABSTRACT

The magnetic and magnetostrictive properties of four scroll-wound ring transducers made from "cube-on-face" textured nickel-cobalt alloys were measured and compared to the corresponding properties of a conventional Nickel-200 ring transducer. The transducers were separately excited in air at low-power linear drive levels with varying amounts of bias induction. Larger reversible permeability (μ_{33}^T) was obtained for all cobalt levels. An increase in the material coupling coefficient (k_{33}) of approximately 50% was obtained for 3% and 4.5% cobalt over that for Nickel-200. Values obtained for the piezomagnetic constant (g_{33}) were also generally higher for the nickel-cobalt alloys than for Nickel-200. A 20% reduction in sound velocity was also observed. A broad range of magnetic and magnetostrictive property improvements are thus affected by the combination of cobalt additions to and cube texturing of the conventional nickel alloy.

INTRODUCTION

In previous reported work[1-3] the magnetic and magnetostrictive properties of a magnetostrictive scroll-wound ring transducer made from cube-textured nickel (CTNi) were measured and compared to the corresponding properties of a ring transducer made from conventional Nickel-200 (Ni-200). In this paper, we report on similar measurements of properties of four scroll-wound ring transducers made from CTNi-cobalt alloys and their comparison with those of the same Ni-200 ring. The addition of cobalt to nickel reduces the magnetocrystalline anisotropy and thereby increases reversible permeability μ_{33} and coupling k_{33}. This reduction in anisotropy[4] is shown in Fig. 1.[4] Complete compensation of the magnetic anisotropy is attained with about 4.5% cobalt. Cobalt also reduces the magnetostrictive strain of nickel[5] as shown in Fig. 2. However, at 4.5% cobalt the saturation magnetostrictive strain in the [100] direction is −47 ppm, some 10 ppm larger than the value for random polycrystalline nickel. Thus, the addition of cobalt to CTNi should provide attractive combinations of magnetic and magnetostrictive properties for transducer applications.

As an extension of earlier work, scroll-wound ring transducers were produced from CTNi strip containing 1.5%, 3.0%, and 4.5% cobalt by weight and evaluated at low-power-drive conditions. The advantages indicated by this investigation of the CTNi-cobalt alloys over conventional Ni-200 are increased saturation strains, a 50% increase in material coupling coefficient, and a 40% reduction in Young's modulus.

*Presented at the Workshop on Magnetostrictive Materials held under the sponsorship of the Underwater Sound Advisory Group and the Naval Research Laboratory, Orlando, Florida, 25-26 February 1976.

[1]E. L. Huston, D. T. Peters, and G. D. Sandrock, "Magnetic and Magnetostrictive Properties of Cube Textured Nickel for Magnetostrictive Transducer Applications," *IEEE Trans. Magn.* **mag-9**(4), 636 (Dec. 1973).
[2]J. A. Sinsky, "Comparison of a Cube-Textured-Nickel and a Nickel-200 Magnetostrictive Ring Transducer," NRL Report 7779 (Aug. 1974).
[3]E. L. Huston and J. A. Sinsky, "Comparison of Cube-Textured and Conventional Nickel Magnetostrictive Ring Transducers During Low-Power Linear Drive," *J. Acoust. Soc. Am.* **58**, 1082 (1975).
[4]S. Chikazumi, *Physics of Magnetism* (John Wiley & Sons, Inc., New York, 1964), p. 145.
[5]Ibid, p. 174.

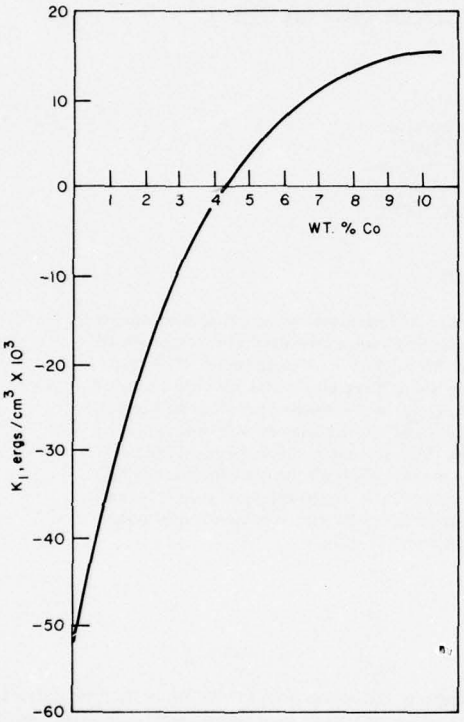

Fig. 1. The effect of cobalt on the magnetocrystalline anisotropy of nickel-cobalt alloys

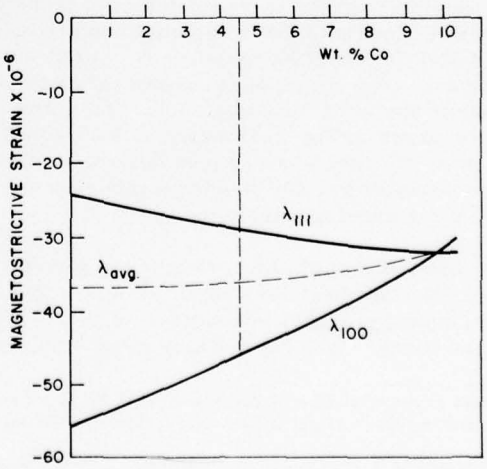

Fig. 2. The effect of cobalt on the saturation magnetostrictive strain of nickel-cobalt alloys

APPARATUS

The core materials were CTNi-cobalt strips 8 mils (2×10^{-4} m) thick produced from elemental metal powders. These powders were first blended and isostatically compacted to form billets that were then sintered, extruded, and hot rolled to yield fully dense bands approximately 0.01 m thick. The bands were cold rolled to final thickness and annealed for 360 s at temperatures exceeding 1,000°C in a reducing atmosphere to produce the cube-on-face texture. Finally, the strips were air annealed for 2 hr at 815°C to provide an insulating oxide coating on all surfaces. Nickel-cobalt strips containing three different cobalt levels at 1.5%, 3.0%, and 4.5% by weight produced in this manner, and a high degree of cube-on-face texture was confirmed by X-ray diffraction, etch pit, and torque magnetometry techniques. The degree of texture was later verified by sound velocity measurements.

All ring cores were scroll wound, which means that they were made by winding the metal strip about a mandrel. A bonding agent, Thermoset Type 316 epoxy, which cures at room temperature, was applied to the strip prior to winding to consolidate the laminations. The nickel-cobalt (4.5% Co) core, consolidated with Thermoset Type 316 epoxy, was designated 4-1/2% Ni-Co OLD. A second nickel-cobalt (4.5% Co) transducer, designated 4-1/2% Ni-Co NEW, was consolidated with Thermoset Type 346 epoxy. The latter bonding agent is a filled epoxy with minimum volume change on curing. To remove geometrical effects, all the CTNi-cobalt rings were built to the same dimensions. The diameter was selected to give approximately the same resonance frequency as the Ni-200 ring. Table I gives the average dimensions of the cores. The expression A_c/A_0 is the ratio of the average cross-sectional area enclosed in the windings to the cross-sectional area of the ring core and is used in the leakage flux correction.

The ring transducers used were wire wound and each of the cores was separately mounted as shown in Fig. 3. The mounting structure was designed to hold a core in a fixed position in the windings while providing the least possible clamping of the core and to be acoustically invisible in the excitation frequency range of interest.

Each ring was simultaneously excited by a dc magnetizing current and an ac driving current. The blocking circuit that isolated the ac current source from the dc current source is diagramed in Fig. 4.

The circuit block diagram of the transducer driving system is shown in Fig. 5. The in-air impedance measurements were done with a continuous wave (CW); therefore, the pulse timing generator and the transmitter gate in the driving system were switched off. The Pulse Vector Immittance Meter measures the input electrical resistance and reactance of the transducer and blocking circuit under conditions of CW or pulsed current excitation. The dc magnetizing current was varied during the experiment to provide varying induction-field levels in the ring cores. The level of the ac drive current, however, was held constant at 15 mA rms for the entire experiment by a current normalizer. The rings were demagnetized between changes of the level of the dc magnetizing current.

TABLE I
Average Dimensions and Masses of the Finished Cores

Rings	Outside Diameter (m)	Inside Diameter (m)	Height (m)	Mean Radius (m)	Mass (kg)	$\frac{A_c}{A_0}$
Cube-textured						
Nickel-cobalt	0.111	0.100	0.021	0.053	0.305	8.7
Nickel-200	0.138	0.125	0.019	0.066	0.434	8.6

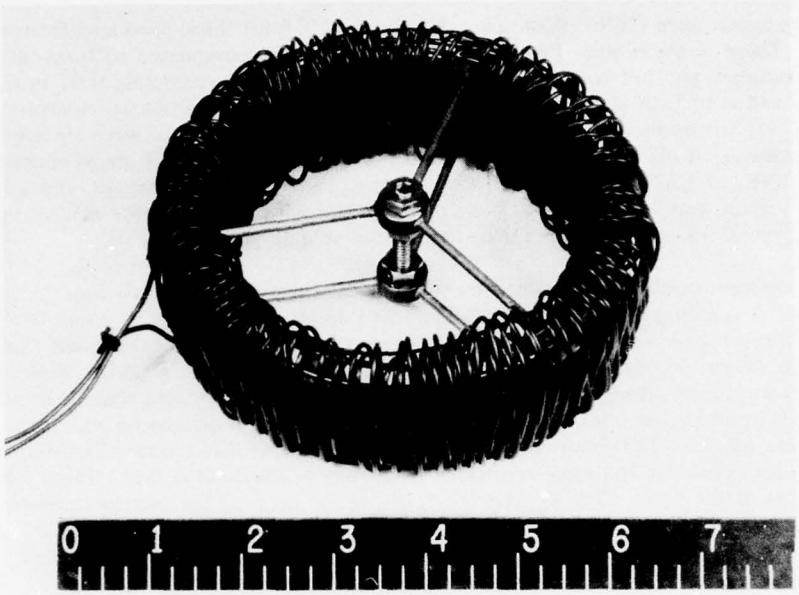

Fig. 3. A ring transducer

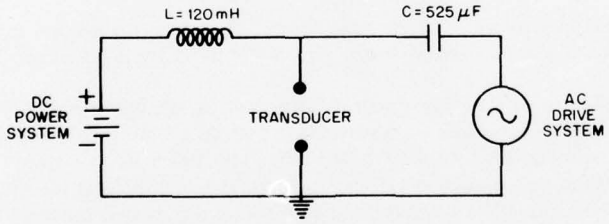

Fig. 4. Blocking circuit to isolate the current sources

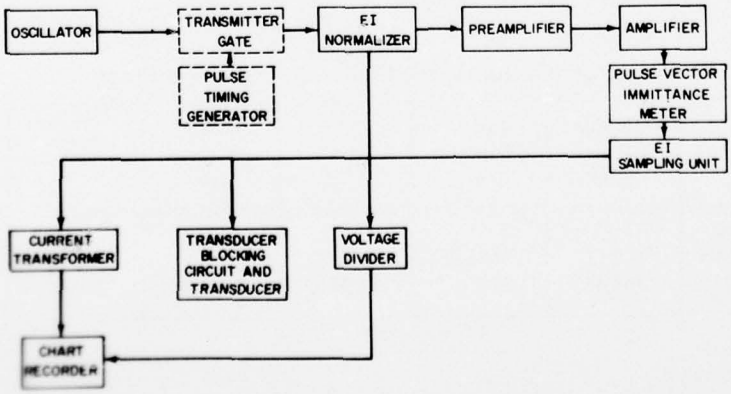

Fig. 5. Transducer driving system

EXPERIMENT

An experimental run on a ring transducer corresponded to input electrical impedance measurements at various frequencies of ac excitation for a single value of dc magnetizing current. A total of 9 or 10 runs was made on the rings, and the values of magnetic field intensity and induction field level are shown in Fig. 6 for the CTNi-cobalt rings and the Ni-200 ring. The magnetic field intensity was calculated from the dc magnetizing current, the number of turns, and the mean radius. The induction field level was obtained by using these *B-H* curves for the ring cores. A direct comparison of the variation of the magnetostrictive parameters of the rings versus induction field is thereby facilitated. All the CTNi-cobalt cores have higher levels of saturation induction than the Ni-200 core. The saturation induction levels for the CTNi-cobalt cores increase with increasing cobalt content.

ANALYSIS

The impedance data were analyzed with a Butterworth and Smith equivalent circuit with leakage flux correction for a magnetostrictive ring oscillator.

The relationships between stress and strain and between magnetic field intensity and magnetic induction field for magnetostrictive material are

$$B_3 = d_{33}T_3 + \mu_{33}^T H_3$$

$$S_3 = s_{33}^B T_3 + g_{33}B_3 ,$$

where

B_3 = the circumferential magnetic induction field,
d_{33} = the piezomagnetic constant,
T_3 = the circumferential stress,
μ_{33}^T = the reversible permeability at constant T,
H_3 = the circumferential magnetic field intensity,
S_3 = the circumferential strain,
s_{33}^B = the elastic compliance at constant B.

These relationships define four of the properties of the rings that are sought: μ_{33}^T, s_{33}^B, d_{33}, and g_{33}.

The reversible permeability is obtained from a plot of the low-frequency core reactance versus frequency. The equation for μ_{33}^T, where dX_c/df is the slope of the low-frequency core reactance versus frequency, is given by

$$\mu_{33}^T \approx \frac{a}{A_0 N^2} \frac{dX_c}{df} + 4\pi \times 10^{-7}\left(1 - \frac{A_c}{A_0}\right),$$

where a is the mean radius of the core and N is the number of lum. The effective electromechanical coupling coefficient k is calculated from

$$\frac{k^2}{1 - k^2} = \frac{D_z}{X_c Q_z}$$

where D_z is the diameter of the motional impedance circle in ohms, Q_z is the quality factor of the transducer, and X_c is the core reactance at the radial resonance frequency. The material electromechanical coupling coefficient k_{33} is given by

$$k_{33}^2 = \frac{k^2}{1 - \{(\alpha - 1)/[\alpha - 1 + (\mu_{33}^T/4\pi \times 10^{-7})]\}},$$

where $\alpha = A_c/A_0$. The piezomagnetic strain constants and the elastic compliance are given by

$$d_{33} = \frac{k_{33}}{\sqrt{1 - k_{33}^2}} \sqrt{\mu_{33}^T s_{33}^B},$$

$$g_{33} = \frac{d_{33}}{\mu_{33}^T},$$

$$s_{33}^B = \frac{(1 - k_{33}^2)A_0}{2\pi M f_0^2 a}.$$

Where M is the mass of the ring core.

RESULTS

Figure 7 is a plot of the reversible permeability for three different cobalt levels. Permeability increases with increasing cobalt content. Figure 8 shows that the reversible permeability of CTNi-cobalt (4-1/2% Co) is higher than that of Ni-200. This is also true of the other nickel-cobalt rings. This result shows that the CTNi-cobalt rings are magnetically softer than conventional nickel, which we also saw from the shape of the primary induction curves. These cobalt-added CTNi rings are unlike the cube-textured pure nickel ring, which had a reversible permeability approximately 50% lower than the conventional nickel ring. The higher permeabilities also imply higher blocked reactance values for cores of the same dimensions although they are accompanied by higher eddy-current losses.

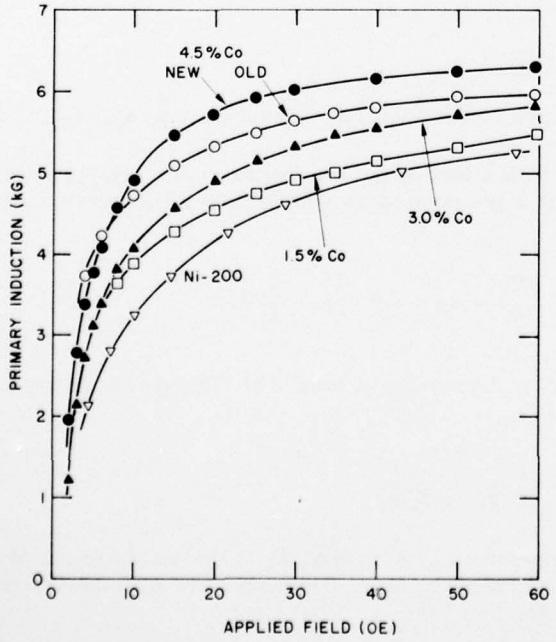

Fig. 6. Primary induction curves for the test specimens

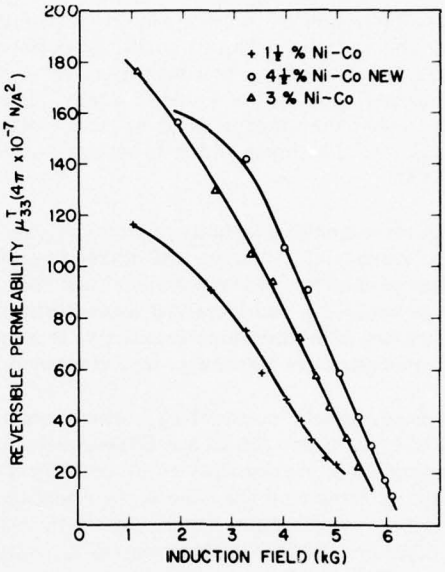

Fig. 7. Reversible permeability of three nickel-cobalt rings as a function of bias induction

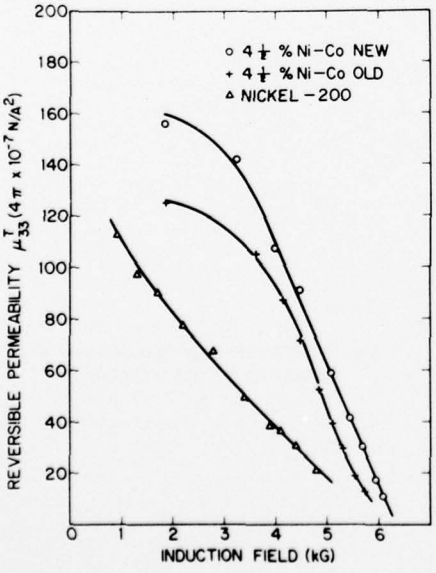

Fig. 8. Reversible permeability of 4-1/2% nickel-cobalt rings compared to that of a nickel-200 ring as a function of bias induction

The differences between the two curves for CTNi-cobalt (4-1/2% Co) are attributed to residual bonding strains during consolidation, as mentioned earlier. The CTNi-cobalt (4-1/2% Co) alloy is particularly sensitive to residual strains because of its very small magnetocrystalline anisotropy. The epoxy used to consolidate the 4-1/2% Ni-Co OLD core imparted a stress bias to the core that had to be overcome by the applied magnetizing field. As a result, its primary induction curve is reduced along with its reversible permeability. Only the 4-1/2% Ni-Co NEW alloy will be represented in subsequent curves.

Figure 9 is a plot of material electromechanical coupling coefficient versus bias induction field for the rings. The electromechanical coupling coefficients all peak at between 4 and 5 kG. Note that the CTNi-cobalt (3% Co) ring gave a maximum value of 0.387 and that the maximum values are approximately the same regardless of cobalt content. The maximum value of k_{33} for the CTNi-cobalt alloys is about 50% higher than that of Ni-200. This increase in coupling coefficient is due, not to the cube texturing, but to the cobalt addition because the k_{33} for cube-textured pure nickel was about the same as for Ni-200.

The piezomagnetic constants d_{33} and g_{33} are plotted in Figs. 10 and 11, respectively. The piezomagnetic constant d_{33} increases with increasing cobalt content, and the CTNi-cobalt (4-1/2 Co) maximum value is approximately 3.4 times greater than that of Ni-200. This large increase reflects both the higher reversible permeability and increased magnetostrictive strain in the CTNi-cobalt materials. Insofar as d_{33} is a measure of hydrophone sensitivity, this improved level of properties enhances the possibility of using a magnetostrictive transducer in a combined active/passive mode.

The piezomagnetic constant g_{33}, which relates the magnetic stress produced by a change in induction field level, is higher for all the CTNi-cobalt materials, but it decreases with increasing cobalt content (for induction fields greater than approximately 4 kG). This reflects the increased strain energy density of the material caused by the cube-on-face texture. Strain energy density is then diminished by adding cobalt. These dynamic data demonstrate with low-power drive the possibility for increased power-handling capability of CTNi-cobalt materials. Actual transducer performance at high-power densities can

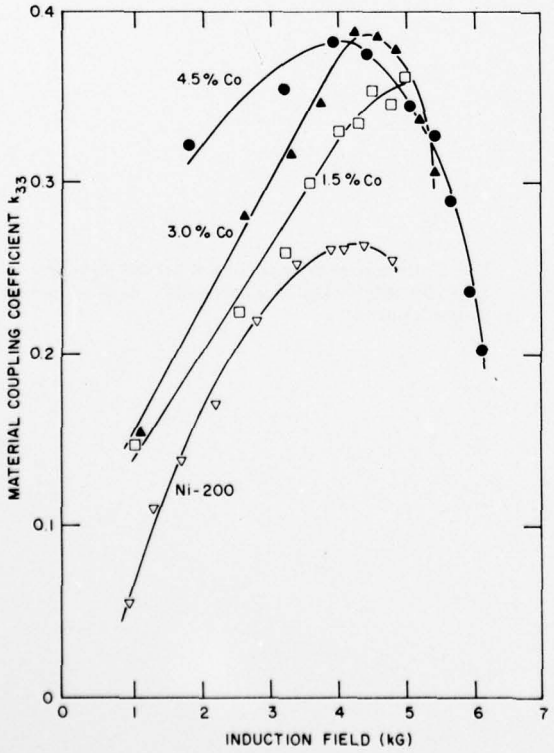

Fig. 9. Material coupling coefficient as a function of bias induction

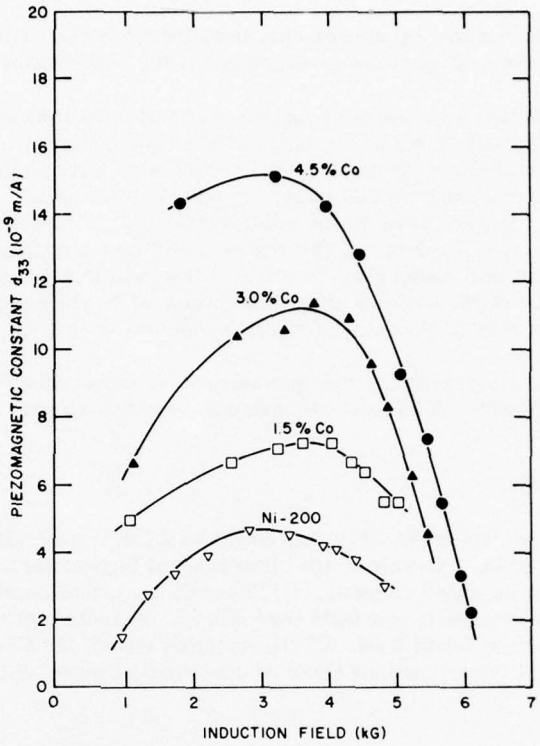

Fig. 10. Piezomagnetic constant d_{33} as a function of bias induction

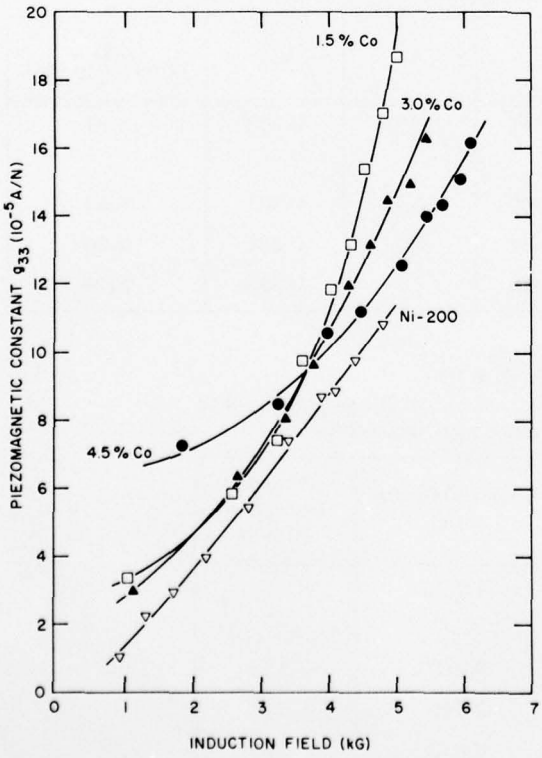

Fig. 11. Piezomagnetic constant g_{33} as a function of bias induction

only be determined by experiments at high-drive levels. These experiments are planned in the near future as the next phase of investigation of the cube-textured-nickel and nickel-cobalt cores.

Table II is a summary of material parameters at optimum bias levels. Note that the radial resonance frequency values of the cores, including the larger Ni-200 core, are within 10% of each other. The values of Q, or figures of merit, decline with increasing cobalt level because of increasing permeability, which corresponds to increasing eddy-current losses. Thus CTNi-cobalt has a broader bandwidth in air with higher coupling. In water, however, it is expected that the bandwidth is primarily determined by water loading. In this regard it will be interesting to compare the performance of these CTNi-cobalt and nickel cores in water at low- and high-power drive levels. The symbol s_{33}^{B} is the elastic compliance of the material and is the inverse of Young's modulus. Sound velocity in the material is the square root of the ratio of Young's modulus to density.

Table III gives the sound velocities in the nickel-cobalt materials and compares these values with those of Ni-200. A 17% to 24% decrease in sound velocity is observed.

SUMMARY

The relative effect of adding cobalt to CTNi is qualitatively the same as cobalt additions to conventional nickel. Therefore, the advantages of high-power density and lower sound velocity are combined with increased coupling. CTNi-cobalt has higher permeability, higher coupling coefficient, and higher piezomagnetic constants than Ni-200. A desired set of properties can be achieved by selecting an appropriate cobalt level. Of the materials tested, the CTNi-cobalt (3% Co) appears to offer an optimum set of properties over those of conventional nickel in that it displays a higher strain energy density

TABLE II
Ring Parameters at Optimum Bias Levels

Ring	B (kG)	f_0 (Hz)	Q	k_{33}	s_{33}^{B} ($\times 10^{-12}$ m^2/N)
Nickel-200	4.4	11,511	91	0.263	4.91
CTNi:					
1-1/2% Co	5.0	11,869	55	0.361	6.82
3% Co	4.3	11,384	20	0.387	7.36
4-1/2% Co NEW	4.0	10,910	13	0.382	8.70

TABLE III
Sound Velocities in the Nickel-Cobalt Rings Compared to the Sound Velocity in Nickel-200

Ring	Sound Velocity (m/s)	Percent Less Than Ni-200
Nickel-200	4,754	–
CTNi:		
1-1/2% Co	3,910	17
3% Co	3,749	21
4-1/2% Co NEW	3,633	24

while attaining the highest material electromechanical coupling coefficient (0.387), a 21% reduction in sound velocity, and a factor of 2 increase in d_{33}. Furthermore, the CTNi-cobalt (3% Co) is not sensitive to the residual fabrication strains as was evidenced by the CTNi-cobalt alloy containing 4-1/2% cobalt.

ACKNOWLEDGMENTS

Appreciation is expressed to G. Sandrock of The International Nickel Co. for valuable discussions and contributions to the research, to J. Sosler for preparation of the transducer cores and preliminary measurements on them, to D. Gregan and D. Dorsey of the Naval Research Laboratory for assistance in preparing the transducers, and to J. Neeley for assistance in taking the measurements. The authors are grateful to the Naval Electronic Systems Command, Code 320, for partial support of the work.

U.S. Navy Journal of Underwater Acoustics Volume 27, No. 1 January 1977

INTRODUCTION TO HIGHLY MAGNETOSTRICTIVE RARE-EARTH MATERIALS*

A. E. Clark
Naval Surface Weapons Center
Silver Spring, Maryland 20910

ABSTRACT

Since 1963, it has been known that the rare-earth elements possess extraordinary magnetostrictions ($\approx 10{,}000 \times 10^{-6}$), far in excess of those characteristics of the magnetic transition metals and alloys. These magnetostrains, however, are available only at cryogenic temperatures. Within the last few years, very high magnetostrictive strains (exceeding 2500×10^{-6}) have been achieved at room temperature in rare-earth alloys containing terbium (Tb) and iron (Fe). These alloys possess the largest known room temperature magnetostrictions and maintain the largest known magnetomechanical coupling factor ($k \approx 0.6$) over wide ranges in applied field. Recently both positive and negative magnetostrictive materials have been examined. In this paper, an introduction to the highly magnetostrictive rare-earths is given. Measurements on polycrystals and single crystals are presented. The importance of grain orientation in the fabrication of transducer elements is established.

INTRODUCTION

While the magnetostrictive phenomena of magnetic metals was known for many years, the importance of magnetostrictive materials as transducer elements dates to the discovery of the magnetostriction oscillator by Pierce[1†] and Vincent[2] in 1928. Metallic transducers quickly emerged as cheap, high-power, rugged devices, far superior to the then available piezoelectric materials. Their superiority, however, declined in the 1940's when an effort to develop synthetic piezoelectric crystals was highly successful. Barium titanate and the lead zirconate titanates emerged that possessed lower losses and far higher magnetomechanical couplings. These materials rapidly replaced the magnetostrictive materials even though the magnetostrictive metals remained the most robust and easiest to bond. In view of the advances in piezoelectric ceramics, a seminar on *Magnetostrictive Materials and Their Application to Underwater Sound* was convened in 1966 to assess the role of magnetostrictive transducers. The potential of magnetostrictive ferrites and transition metal alloys, such as Ni-Co, Fe-Co, and Fe-Al, was discussed.[3] Again in 1969 a workshop entitled *Metallic Magnetoacoustic Materials*, was held specifically to determine the state of the art of magnetostrictive materials.[4] At this time the low-temperature magnetostrictive properties of the rare-earth elements[‡] were just emerging and were presented in their budding form.

Extensive research on the magnetostrictive properties of the rare-earths was being performed in the early 1960's at the Naval Ordnance Laboratory by Clark, Bozorth, and DeSavage[5] and at Iowa State University (Ames Laboratory) by Alstad, Legvold, and Rhyne.[6] At this time it was widely recognized that the rare-earths possessed many extraordinary magnetic properties, properties attributed to the unfilled $4f$ electron shells. Of particular interest were the heavy rare-earth metals, which crystallize into

*Presented at the Workshop on Magnetostrictive Materials held under the sponsorship of the Underwater Sound Advisory Group and the Naval Research Laboratory, Orlando, Florida, 25-26 February 1976.
†References listed on page 123.
‡A brief discussion of the rare-earth metals is given by Dr. Timme in his Introduction to the Theme in this issue.

the hexagonal close-packed (n.c.p.) structure and possess unusual magnetic ordering configurations. Huge atomic moments were found, as high as $10\mu_b$, which dwarfed the conventional values of $0.6\mu_b$ and $2.2\mu_b$ for Ni and Fe, respectively. Enormous magnetic anisotropies (difficulty of magnetization rotation) were also measured for these elements. In 1963 and 1964, a breakthrough in magnetostrictive materials occurred with the measurement of the basal plane magnetostrictions of Dy and Tb at low temperatures. These values still remain today the largest known magnetostrictions ($\approx 1\%$). The observed basal plane strains are 100 to 10,000 times the value of typical magnetostrictions. Enormous magnetic anisotropies inhibited the measurement of other magnetostriction constants and those of other elements. Efforts were made to understand both the temperature dependences of the magnetostrictions as well as their atomic origin.[7,8] The application of these materials to magnetostriction vibrators, however, was severely restricted because of the relatively low ordering temperatures of the rare-earths. Only Gd, which is essentially nonmagnetostrictive, possesses a Curie point as high as room temperature.

A search for magnetostrictive materials with high magnetostriction at room temperature was started. In this search the highly magnetostrictive rare-earths Tb and Dy were combined with the magnetic transition metals Ni, Co, and Fe.[9,10] The largest magnetostriction by far was found in $TbFe_2$.[11] Of all the known rare-earth-transition metal compounds, the iron compounds have the largest magnetostriction at room temperature. Of all rare-earth-iron compounds, the rare-earth-Fe_2 compounds have the strongest exchange interactions and the highest ordering temperatures. It is this strong exchange, coupled with the high concentration of rare-earth ions in these compounds that increases the magnetostrictive and anisotropic properties of the rare-earth elements, heretofore available only at cryogenic temperatures, to room temperature. Large magnetocrystalline anisotropies (greater than 10^7 ergs/cm^3) and magnetostriction constants (greater than 2,000 ppm) persist in these compounds in spite of the high cubic point symmetry at the rare-earth site. This high symmetry effectively shorts out one of the two magnetostriction constants, yielding a spectacular $\lambda_{111} >> \lambda_{100}$ anisotropy, unknown in any other material.[12]

This paper presents an overview of the magnetostriction studies of the highly magnetostrictive rare-earth alloys, dealing with binary compounds, magnetic anisotropy, the importance of ternary and quaternary compounds, unusual ΔE effects, directions for improved material development and fabrication techniques.

BINARY RARE-EARTH IRON ALLOYS

The first compound found to exhibit a huge magnetostriction at room temperature is $TbFe_2$.[9,11] This compound still possesses the largest known room temperature magnetostriction. In Fig. 1 the room temperature magnetostriction, $\lambda_\parallel - \lambda_\perp$ is plotted against applied field H for five Tb_xFe_{1-x} samples. All possess unusually large magnetostrictions. The value of $\lambda_\parallel - \lambda_\perp$ denotes the fractional change in length parallel to the magnetic field minus the fractional change perpendicular to the magnetic field. (In nontextured materials, $\lambda_\parallel - \lambda_\perp = (3/2, \lambda_s$.) All three intermetallic compounds shown exhibit huge magnetostrictions: 194 ppm for Tb_2Fe_{17}, 1,040 ppm for $TbFe_3$ and 2,630 ppm for $TbFe_2$ at 25 kOe (99 MA/m). For a 3 at. % Tb in Fe sample (not shown) the magnetostriction is far from saturation with $(\lambda_\parallel - \lambda_\perp)/H = 6.5 \times 10^{-10}$/Oe. Both $Tb_{0.03}Fe_{.97}$ and Tb_2Fe_{17} display large volume magnetostrictions. In $Tb_{0.03}Fe_{0.97}$, $\Delta V/VH = 88 \times 10^{-10}$/Oe, in Tb_2Fe_{17}, $\Delta V/VH = 37 \times 10^{-10}$/Oe. The Tb-rich alloys, while also exhibiting large magnetostrictions, are substantially more rugged in the cast state than are the compounds $TbFe_2$, $TbFe_3$, and Tb_2Fe_{17}.

Figure 2 shows our early measurements of the field dependence of the magnetostriction for the RFe_2 compounds (R = Sm, Tb, Dy, Er, and Tm). The outstanding compounds are $TbFe_2$ and $SmFe_2$. They stand out as parallel giants with room temperature magnetostrictions greater than 2,000 ppm (for $SmFe_2$, $\lambda < 0$; for $TbFe_2$, $\lambda > 0$). This is because of the large magnetoelastic energy of the rare-earth iron alloys (Sm—most prolate in form; Tb—most oblate in form)[7,13] and the large iron-iron and rare-earth-iron exchange constants that maintain the rare-earth sublattic magnetization relatively intact at room temperature so that the magnetostriction does not fall appreciably from its low-temperature value.

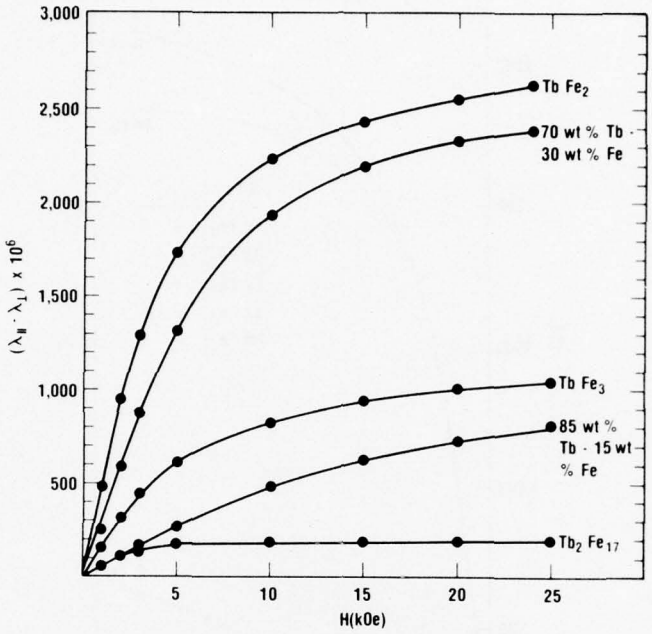

Fig. 1. Magnetostriction of Tb-Fe alloys

The slow increase in magnetostriction with field observed for $DyFe_2$ indicates a large magnetocrystalline anisotropy. In the next section it is shown that indeed the anisotropy is large, with values of anisotropy $|K| \approx 10^7$ ergs/cm^3 at room temperature.

The magnetostriction of $ErFe_2$ $TmFe_2$, and, to a lesser extent, $TbFe_2$ and $SmFe_2$ saturate at relatively low fields, while that of $DyFe_2$ is far from saturation. Because the magnetic moment is parallel to the [111] crystallographic direction in $TbFe_2$, $SmFe_2$, $ErFe_2$, and $TmFe_2$, and parallel to the [100] direction in $DyFe_2$, this suggests that $\lambda_{111} >> \lambda_{100}$. This is indeed the case as is shown below.[12] The increasing magnetostriction with increasing field in the case of $DyFe_2$ arises from the rotation of the magnetization away from the easy [100] axes, thereby sensing λ_{111}; whereas the magnetostriction of the Tb, Er, Sm, and Tm compounds arises directly from λ_{111}. (λ_{100} and λ_{111} denote the single crystal magnetostriction constants of cubic crystals.)

In Table I we compare the values of the magnetostriction of some of the RFe_2 compounds that exhibit high magnetostriction with those of transition metals, oxides, and other rare-earth-transition metal compounds. (Some of the rare-earth meterials are not entirely single phase, and longer annealing may further increase the magnetostriction.)

Single crystal magnetostriction measurements have been made to identify the source of the magnetostriction. In Fig. 3, values of λ_{111} are shown for $TbFe_2$ and $ErFe_2$. In both crystals, [111] is the easy magnetization direction. Attempts to measure λ_{100} with fields up to 25 kOe (1.99 MA/m), proved fruitless in both cases. Although some rotation of the magnetization away from the easy [111] direction occurs, no λ_{100} was detected. On the other hand, $DyFe_2$ and $HoFe_2$ possess [100] easy. Hence in these compounds, λ_{100} is sensed at remanence. Surprisingly, we find $\lambda_{100} = 0 \pm 4 \times 10^{-6}$ for $DyFe_2$.[12] Similarly, a small value (however, not equal to zero) is found for $HoFe_2$.[18] This highly anisotropic magnetostriction establishes the importance of grain orientation. A poorly oriented polycrystal yields $\lambda_s \approx 0$; an isotropic polycrystal, $\lambda_s = 0.6\lambda_{111}$; and an oriented polycrystal, $\lambda_s = \lambda_{111}$. The importance of grain orientation cannot be underestimated. The effect is twofold beneficial. An oriented polycrystal will exhibit, in addition to the obvious increase in magnetostriction, far lower internal losses at grain boundaries. For a good transducer material we need easy domain wall motion

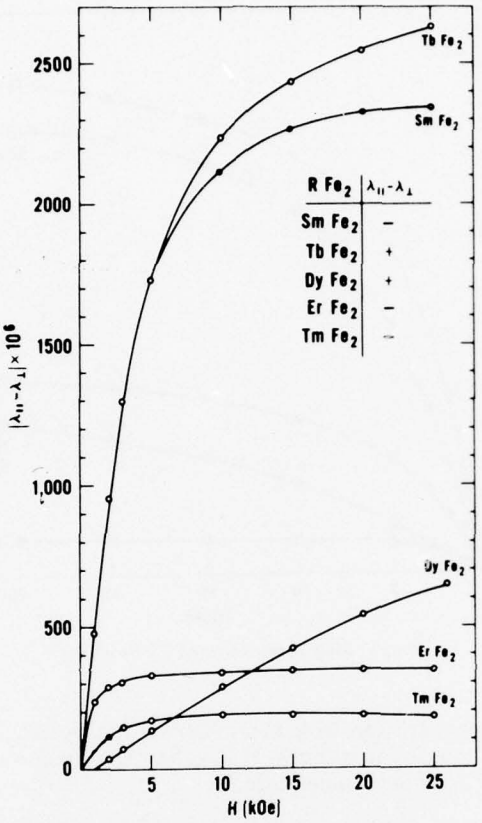

Fig. 2. Magnetostriction of RFe_2 compounds

and low internal stresses at grain boundaries. The first can be achieved by sufficiently high material purity and low magnetic anisotropy, and the second by preferential grain orientation.

An atomic model of magnetostriction, based upon the high symmetry of the rare-earth-element site in the Laves phase C15 structure, is described in Ref. 12. On the basis of this model, an internal distortion is coupled to the external [111] strain, yielding a very large λ_{111}. On the other hand, the high symmetry shorts out the potentially huge λ_{100}.

There are a total of 15 lanthanide rare-earth elements. In the following discussion we will point out the ones suitable for magnetostrictive transduction. In Table II are listed the rare-earth elements in order of the increasing number of $4f$ electrons. (La with no $4f$ electrons and Lu with a full shell of fourteen $4f$ electrons are omitted.) It is possible to calculate the intrinsic ($T = 0$ °K) magnetostriction of each 3+ rare-earth ion for a particular compound (assuming its existence) given the magnetostriction of at least one compound (e.g., Tb^{3+} in $TbFe_2$). The theory uses the Stevens' equivalent operator method. Using the measured room temperature magnetostriction of $TbFe_2$ and $ErFe_2$ and assuming single-ion temperature dependences,[8] we calculated intrinsic values of $5{,}000 \times 10^{-6}$ and $-1{,}770 \times 10^{-6}$, respectively, for $TbFe_2$ and $ErFe_2$.[21] According to Stevens, the ratio of the intrinsic magnetostriction of one rare-earth ion to another is given by the ratio of $\alpha J(J - 1/2)\langle r_f^2 \rangle$ where α is the lowest order Stevens' factor, J is the ground state angular momentum for the 3+ ion, and $\langle r_f^2 \rangle$ is the average radius squared of the $4f$ electron shell. In Table II, the values of α, J and $\langle r_f^2 \rangle$ are given along with the calculated values of λ_{111} for RFe_2 compounds. Note that the largest positive magnetoelastic interactions belong to $CeFe_2$, $PrFe_2$, $TbFe_2$, and $DyFe_2$; the largest negative interactions occur in $SmFe_2$,

TABLE I
Magnetostrictions of Some Polycrystalline Materials at Room Temperature[a]

Material	$10^6\lambda_s$	Material	$10^6\lambda_s$
Fe	-9[b]	$TbFe_2$	1,753
Ni	-35[b]	$TbFe_2$ (sputtered)	308
Co	-62[b]	$Tb_{0.3}Dy_{0.7}Fe_2$	1,068
Sm, Tb, Dy, and Ho	≈0[c]	$DyFe_2$	433
Fe_3O_4	40[d]	$HoFe_2$	85[f]
$CoFe_2O_4$	-110[d]	$ErFe_2$	-229
$NiFe_2O_4$	-26[d]	$TmFe_2$	-123
$Y_3Fe_5O_{12}$	-2[e]	$TbFe_{1.6}Co_{0.4}$	1,487
Tb_2Co_{17}	47	$TbFe_{1.6}Ni_{0.4}$	1,151
YCo_3	0.4	85% Tb-15% Fe	539
$TbCo_3$	65	70% Tb-30% Fe	1,590
Tb_2Ni_{17}	-4	$TbFe_3$	693
YFe_2	1.7	Tb_2Fe_{17}	131
$SmFe_2$	-1,560		

[a]Fro the rare-earth compounds, λ_s denotes (2/3) $(\lambda_\parallel - \lambda_\perp)$ at 25 kOe (1.99 MA/m).
[b]See Ref. 14.
[c]Nonmagnetic at room temperature.
[d]See Ref. 15.
[e]Ref. 16.
[f]Ref. 17.

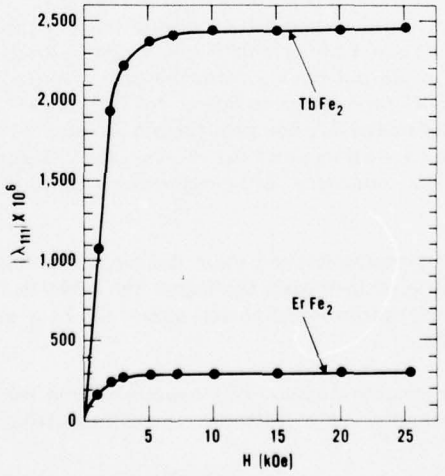

Fig. 3. Magnetostriction of single crystal $TbFe_2$ and $ErFe_2$. For $TbFe_2$, $\lambda_{111} > 0$; for $ErFe_2$, $\lambda_{111} < 0$.

TABLE II
Magnetostriction of RFe_2 Compounds

R	$\alpha \times 10^{2}$[a]	J	$\langle r_f^2 \rangle$[b]	$\lambda_{111} \times 10^{6}$[c] Calculated, 0 K	$\lambda_{111} \times 10^{6}$ Experimental, Room Temperature
Ce	-5.72	5/2	1.20	6,800	—
Pr	-2.10	4	1.086	6,300	—
Nd	-0.643	9/2	1.001	2,300	—
Pm	0.772	4	0.942	-2,000	—
Sm	4.13	5/2	0.883	-3,600	-2,100[c]
Eu	0	0	0.834	0	—
Gd	0	7/2	0.785	0	—
Tb	-1.01	6	0.756	5,000	2,460[d]
Dy	-0.635	15/2	0.726	4,800	1,260[c]
Ho	-0.222	8	0.696	1,850	185[e]
Er	0.254	15/2	0.666	-1,770	-300[d]
Tm	1.01	6	0.639	-4,250	—
Yb	3.18	7/2	0.613	-4,070	—

[a]Ref. 13.
[b]Ref. 19.
[c]Ref. 18.
[d]Ref. 20.
[e]Ref. 12.

$TmFe_2$, and $YbFe_2$. No magnetostriction is predicted for $GdFe_2$ and $EuFe_2$ on the basis of this model. The elements Ce and Yb are not useful magnetostrictly because Ce is often found in its quadrivalent state Ce^{4+} and Yb in its divalent state Yb^{2+}, yielding zero magnetostriction. The compound $PmFe_2$ is radioactive, and $PrFe_2$ and $NdFe_2$ do not readily form the cubic Laves phase compound. This leaves $TbFe_2$ and $DyFe_2$ as the two most promising candidates for high room-temperature (positive) magnetostriction. The element Dy is eliminated for practical reasons because [100] is the easy magnetization direction and $\lambda_{100} \approx 0$. (See the following section.) For negative magnetostriction, $TmFe_2$ and $SmFe_2$ appear to be most promising. The compound $SmFe_2$ emerges because of its high Curie temperature and much lower cost.

Values of λ_{111} at room temperature depend upon the rare-earth sublattice magnetization at this temperature. The higher the Curie temperature, the higher the sublattice magnetization and the higher the magnetostriction. Room temperature experimental values for λ_{111} are given in the table for $SmFe_2$, $TbFe_2$, $DyFe_2$, $HoFe_2$, and $ErFe_2$.

As pointed out earlier, the saturation values of magnetostriction for a polycrystal λ_s depend upon the degree of orientation of crystallites. For isotropic crystallite distribution,

$$\lambda_s = \frac{2\lambda_{100} + 3\lambda_{111}}{5}$$

Because $\lambda_{100} \approx 0$, it follows that $\lambda_s \approx 0.6\lambda_{111}$. For preferential orientation,

$$0.6\lambda_{111} < \lambda_s < \lambda_{111}.$$

The values of λ_{111} can be compared to the values for polycrystals in Fig. 2 and Table I.

AD-A042 029 NAVAL RESEARCH LAB WASHINGTON D C F/G 17/1
PROCEEDINGS OF THE 25-26 FEB 1976 WORKSHOP ON MAGNETOSTRICTIVE --ETC(U).
JUN 77 R W TIMME
UNCLASSIFIED NRL-8137 NL

2 OF 2
ADA042029

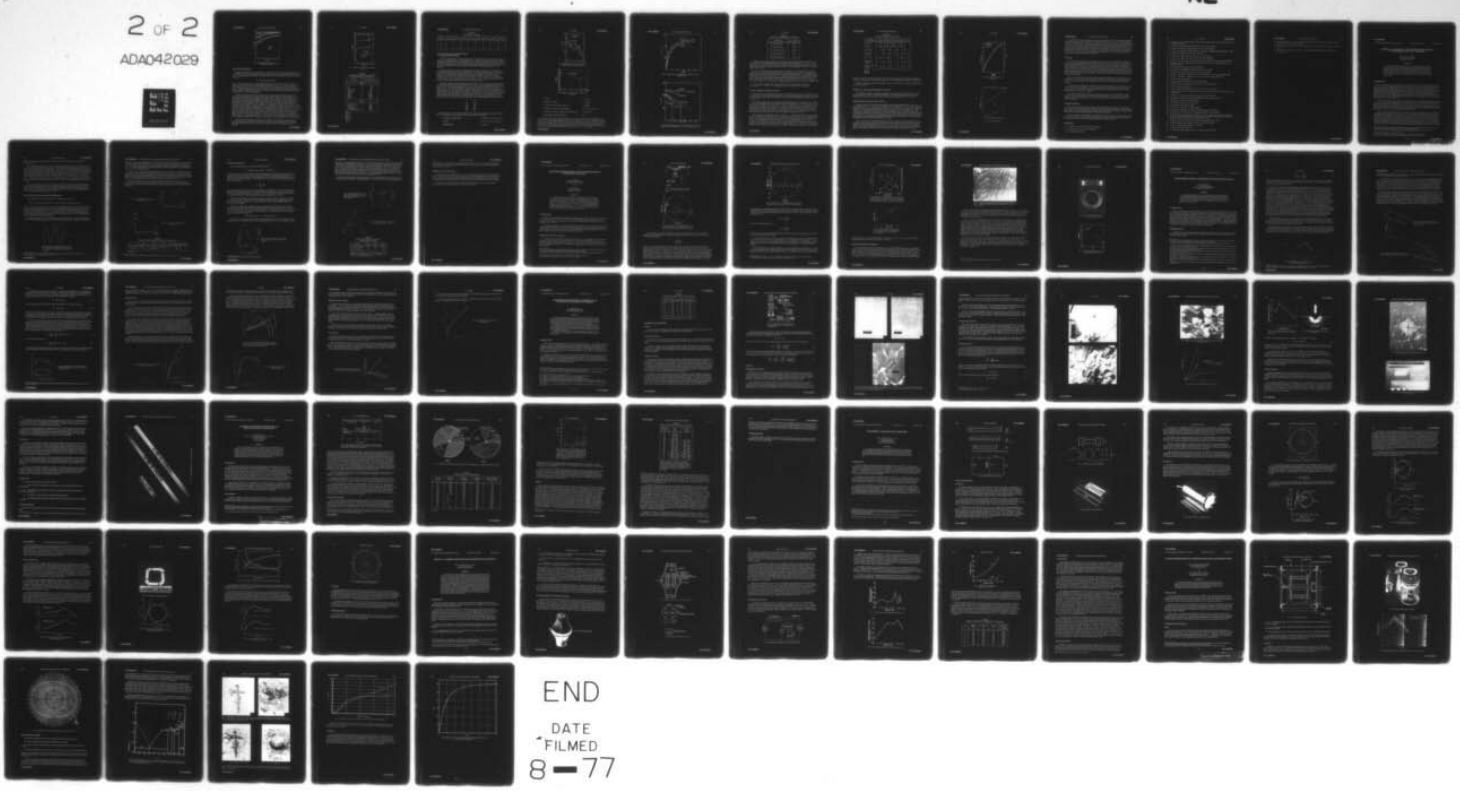

END

DATE FILMED
8-77

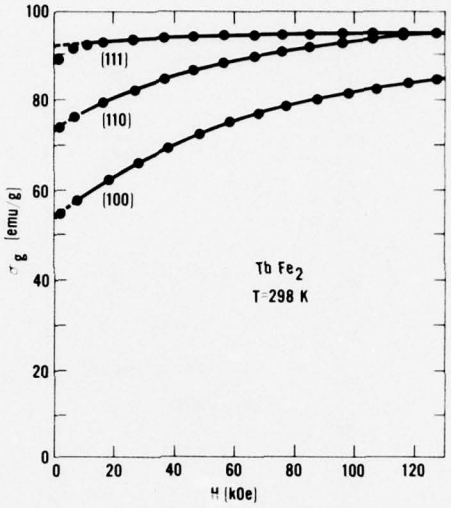

Fig. 4. Room temperature magnetic moment σ_g of single crystal $TbFe_2$

MAGNETIC ANISOTROPY

Magnetic anisotropy refers to the difference in energy required to rotate the magnetization from one crystalline direction to another crystalline direction. This energy is often expressed in direction cosines (α_j's) of the magnetization with respect to the crystalline axes. For cubic crystals, the lowest order, the expression is

$$K = K_1 (\alpha_1^2\alpha_2^2 + \alpha_2^2\alpha_3^2 + \alpha_3^2\alpha_1^2).$$

If $K_1 < 0$, the energy is lowest when the magnetization points along the [111] direction; if $K_1 > 0$, [100] is the preferred direction of magnetization. When [111] is easy, λ_{111} is sensed at remanence; when [100] is easy, λ_{100} is sensed. The total expression for the anisotropy is in general an infinite series. As higher order terms are taken into account, other directions may become easy and the magnetostriction referred to that direction is sensed. In some cases (e.g., $HoFe_2$ and some ternary alloys) the easy direction is a function of temperature.

Magnetic anisotropy values were determined both by magnetization measurements and magnetic torque measurements.[22,23] Both methods employ single crystals. Using the former method, the anisotropy can be calculated from magnetization measurements along various crystallographic directions. This method is useful when the anisotropy is very large. Torque methods are more accurate and are particularly useful for moderate and low magnetic anisotropies. The largest recorded anisotropy of a cubic crystal at room temperature is that of $TbFe_2$.[21] It is negative. The largest known positive anisotropy is that of $DyFe_2$.[22] Figure 4 illustrates the magnetization curves for $TbFe_2$ at room temperature along the three principal crystallographic directions in fields up to 120 kOe (9.5 MA/m).[24] Note that even at this huge field, the moment cannot be aligned along its hard [100] direction. The anisotropy energy is too high. Similar curves exist for $DyFe_2$. For $ErFe_2$, the anisotropy at room temperature is smaller because of its lower Curie temperature. However, it becomes enormous at low temperatures. Figure 5 shows the magnetization curves versus H for $ErFe_2$ at 4.2 K. From these measurements we estimate that K_1 (at 4 K) is approximately -5×10^8 ergs/cm^3, the largest known cubic magnetic anisotropy. Comparable magnitudes are calculated for anisotropies of $TbFe_2$ and $DyFe_2$ at this temperature.

Table III lists the anisotropy constants of some cubic metals and ferrites at room temperature. Here the large difference between the anisotropies of the RFe_2 compounds and the cubic transition metal alloys is clearly shown. In the next section a method to reduce the magnetic anisotropy is described.

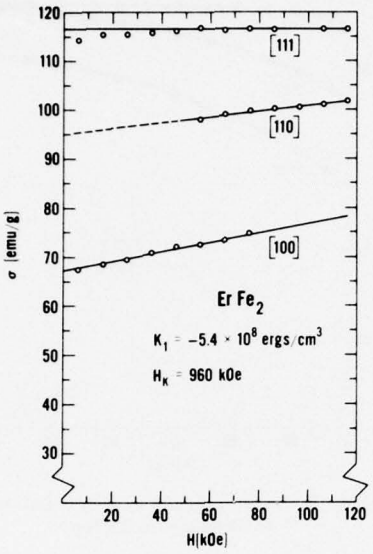

Fig. 5. Magnetic moment of single crystal $ErFe_2$ at 4.2 K

TABLE III
Anisotropy Constants of Some Cubic Metals and Ferrites at Room Temperature

Material	$10^{-4}K_1$ (ergs/cm^3)
Metal	
Fe	45[a]
Ni	-5[a]
70% Fe-Co	-43[b]
65% Co-Ni	-26[c]
$ErFe_2$	-330
$DyFe_2$	2,100
$TbFe_2$	-7,600
$HoFe_2$	360[d]
Ferrite	
$Ga_{0.44}Fe_{2.54}O_4$	-81[e]
$CoFe_2O_4$	260[f]
$Co_{0.8}Fe_{2.2}O_4$	290[g]
$Co_{0.3}Zn_{0.2}Fe_{2.2}O_4$	150[g]

[a]Ref. 25.
[b]Ref. 26.
[c]Ref. 27.
[d]Ref. 23.
[e]Ref. 28.
[f]Ref. 29.
[g]Ref. 30.

TABLE IV
Polarity of λ, K_1 and K_2

Quantity	$PrFe_2$	$SmFe_2$	$TbFe_2$	$DyFe_2$	$HoFe_2$	$ErFe_2$	$TmFe_2$	$YbFe_2$
λ	+	-	+	+	+	-	-	-
K_1	+	-	-	+	+	-	-	+
K_2	-	0	+	-	+	-	+	-

MAGNETOSTRICTION OF PSEUDOBINARY LAVES PHASE COMPOUNDS

For many magnetostrictive transducer applications the figure of merit contains the ratio of the square of the magnetostriction to the anisotropy energy.[4] One therefore looks for materials with small anisotropy energy, as well as the large magnetostriction. Table IV contains the signs of λ, K_1, and K_2 for the RFe_2 compounds, from our measurements and from theoretical estimates. The symbols K_1 and K_2 are the coefficients of the two lowest terms in the magnetic anisotropy expression for cubic materials.

Using this table we can construct pseudobinary compounds in such a way as to minimize the magnetic anisotropy while maintaining a large positive (or negative) magnetostriction. The procedure is to select compounds with the same magnetostriction sign (if possible) but with opposite signs of anisotropy. Attractive ternary compounds yielding a positive magnetostriction are $Tb_{1-x}Dy_xFe_2$ (Terfenol-D), $Tb_{1-x}Ho_xFe_2$,[31] and $Tb_{1-x}Pr_xFe_2$ (Terfenol-P). The compounds of negative magnetostriction are $Sm_{1-x}Ho_xFe_2$ (Samfenol-H), $Sm_{1-x}Dy_xFe_2$, and $Sm_{1-x}Yb_xFe_2$. In each case x can be chosen to maximize λ^2/K_t where K_t equate the sum of the K values.

The largest saturation magnetostrictions have been found in the Terfenol-D and Terfenol-P systems. The Terfenol-D system has been investigated in detail. Figure 6 shows the magnetostriction of polycrystalline arc-cast and annealed samples of $Tb_{1-x}Dy_xFe_2$ for fields 10 and 25 kOe (of 800 and 1,990 kA/m). Near $x = 0.7$, the magnetostriction at these fields exhibits a peak reflecting the near-zero magnetic anisotropy at this concentration. Figure 7 illustrates how the value of the saturation magnetostriction constant λ_{111} varies with Dy concentration. The constant λ_{111} was determined by x ray techniques, using a method developed to accurately pinpoint the value of x for anisotropy sign reversal.[12] It was shown that the magnetostrictive properties of this alloy system degrade rapidly as x becomes greater than 0.75. This is reflected in the rapid drop[32] of the magnetomechanical coupling factor k_{33}:

x	k_{33}
0.5	0.48
0.7	0.53
0.74	0.6
0.76	0.4
0.8	0.23

$Tb_{0.27}Dy_{0.73}Fe_{1.95}$ is the material presently used in the prototype devices developed at USRD/NRL, NUC, Raytheon, and Honeywell. Some of its properties are as follows:

- Saturation magnetostriction — $\lambda_s = 1{,}000 \times 10^{-6}$ to $1{,}110 \times 10^{-6}$
- $d\lambda/dH$ — $d = 8 \times 10^{-9}$ to 10×10^{-9} m/A
- Magnetization — $M = 0.98$ T

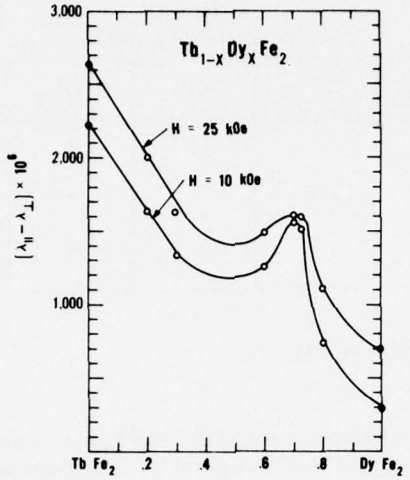

Fig. 6. Magnetostriction of $Tb_{1-x}Dy_xFe_2$ at fields of 800 and 1,990 kA/m (10 and 25 kOe)

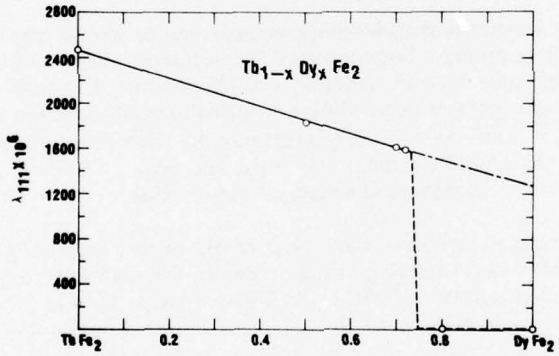

Fig. 7. Magnetostriction constant λ_{111} determined by x ray method

- Density — $\rho = 9.2$ g/cm^3
- Resistivity ($TbFe_2$) — $\rho = 60\ \mu\Omega\cdot$cm
- Sound velocity (16 kA/m (200 Oe)) — $v = 2{,}300$ m/s
- Young's modulus (16 kA/m (200 Oe)) — $E = 5 \times 10^{10}$ N/m^2 (Pa)
- Magnetomechanical coupling (16 kA/m (200 Oe)) — $k = 0.52$ to 0.6
- Permeability (16 kA/m (200 Oe)) — $\mu_r^s = 4$

The magnetostrictive properties of a new alloy, $Tb_{-x}Pr_xFe_2$, are now being investigated. The element Pr has a huge intrinsic magnetostriction and is far less expensive than Tb. However, it does not crystallize in the cubic $PrFe_2$ structure. Figure 8 shows magnetostriction versus H for two $Tb_{1-x}Pr_xFe_2$ alloys. Initial results indicate that only 20% to 30% $PrFe_2$ can be added to $TbFe_2$ before 2d phase material appears. The highest measured d constant, $d\lambda/dH$, occurs for $Tb_{0.9}Pr_{0.1}Fe_2$. Determination of λ_{111} by x ray indicates an almost constant value of λ_{111} for $1 > x > 0.7$. See Fig. 9.

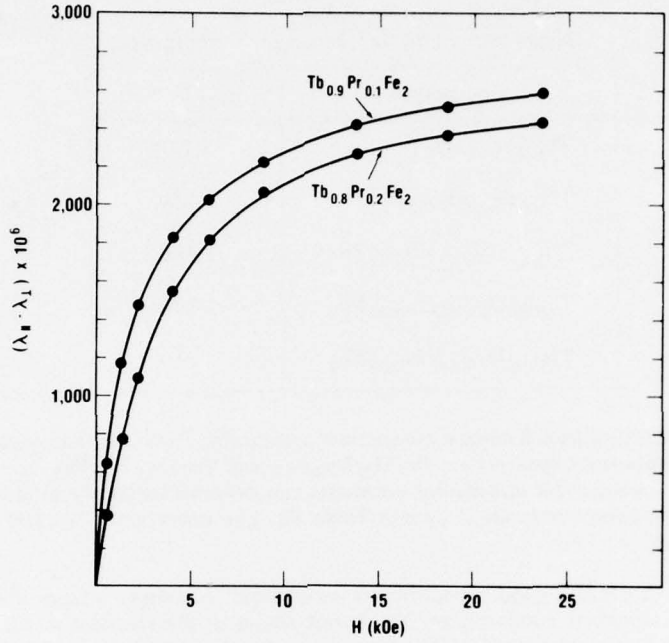

Fig. 8. Magnetostriction of $Tb_{0.9}Pr_{0.1}Fe_2$ and $Tb_{0.8}Pr_{0.2}Fe_2$ versus magnetic field

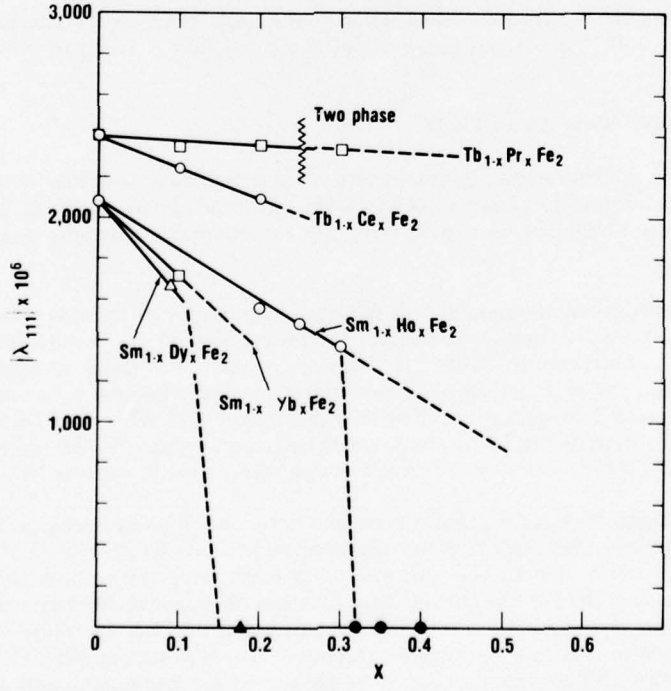

Fig. 9. Magnetostriction constant λ_{111} for some ternary-rare-earth/Fe_2 compounds. For Tb compounds, $\lambda_{111} > 0$; for Sm compounds, $\lambda_{111} < 0$

TABLE V
Magnetostriction of Quaternary Compounds

Compound	$\lambda_{111} \times 10^6$
$Tb_{0.3}Pr_{0.1}Dy_{0.6}Fe_2$	1,750
$Tb_{0.3}Pr_{0.2}Dy_{0.5}Fe_2$	1,760
$Tb_{0.26}Dy_{0.53}Ho_{0.21}Fe_2$	1,460
$Tb_{0.23}Dy_{0.35}Ho_{0.42}Fe_2$	1,135
$Tb_{0.19}Dy_{0.18}Ho_{0.63}Fe_2$	810

Positive magnetostriction pseudobinary compounds containing three rare-earth elements have also been examined. Two important systems are $Pr_xTb_yDy_zFe_2$ and $Tb_xDy_yHo_zFe_2$ ($x + y + z = 1$). In both systems, the two lowest order anisotropy constants can be simultaneously minimized, if necessary. Values of λ_{111} for some compounds are shown in Table V. The uncertainty is $\pm 100 \times 10^{-6}$. All compounds have [111] easy.

It is more difficult to find a good pseudobinary compound to achieve a large λ^2/K for negative magnetostriction. An important compounent, Yb, is not found in the trivalent state. However, compounds can be selected that compensate both anisotropy and magnetostriction. Two important pseudobinaries are $Sm_{1-x}Dy_xFe_2$ and $Sm_{1-x}Ho_xFe_2$. Unfortunately, in this case both λ and K_1 have opposite signs. However, the anisotropy can be compensated with small additions of Dy and Ho, leaving a $|\lambda|$ greater than $1{,}000 \times 10^{-6}$. Figure 9 shows values of λ_{111} for $Sm_{1-x}Ho_xFe_2$. The $Sm_{1-x}Dy_xFe_2$ system is not completed. For $Sm_{1-x}Ho_xFe_2$, compensation occurs near $x = 0.3$, where $\lambda_{111} \approx 1{,}200 \times 10^{-6}$.

In view of this, a bender bar (or magnetostriction multiplier) configuration composed of $Tb_{0.27}Dy_{0.73}Fe_2$ ($\lambda > 1{,}000 \times 10^{-6}$) and $Sm_{0.7}Ho_{0.3}Fe_2$ ($\lambda < 1{,}000 \times 10^{-6}$) is proposed.

ELASTIC ENERGIES AND THE ΔE EFFECT

Room temperature sound velocities, densities, and moduli are listed in Table VI for $TbFe_2$, $ErFe_2$, YFe_2, and $TbFe_3$. Longitudinal and shear velocities were measured ultrasonically at 7 MHz. The moduli are midway between those of the soft rare-earth elements and the stiffer magnetic transition metals such as Fe and Ni.

The moderate magnitudes of the moduli and the huge magnitudes of the magnetostrictions combine to yield very large magnetoelastic forces and energies for these compounds. Values for λ_s; $E\lambda_s$; and the energy density, $(1/2)E\lambda_s^2$, are shown in Table VI. They are compared to those of elemental Ni, a typical magnetostrictive material. The quantity $E\lambda_s$ is a measure of the force exerted by a constrained bar of the material that is magnetized to saturation. The energy density, $(1/2)E\lambda_s^2$, represents the amount of magnetic energy that can be transformed to elastic energy per unit volume of the material. For $TbFe_2$, this energy is about 1,000 times that of earlier magnetostrictive materials, such as Ni.

Closely related to magnetostriction is the "ΔE effect"; i.e., the fractional change in Young's modulus between the magnetically saturated state and the unmagnetized state. Because of the huge magnetostrictive effects in the RFe_2 compounds, a large "ΔE effect" at room temperature occurs.[36] We observe the change in resonant frequency at constant current as a function of magnetic field in a thin bar of $Tb_{0.3}Dy_{0.7}Fe_2$ resonanting near 15 kHz. From this we calculated the corresponding sound velocity and modulus. The dependence of Young's modulus on magnetic field is shown in Fig. 10. We find that the modulus increases by about 150%. This increase is by far the largest known and reflects a sound velocity

TABLE VI
Elastic and Magnetoelastic Properties[a]

Property	$TbFe_2$	$ErFe_2$	YFe_2	$TbFe_3$	Ni
v_l (m/s)	3,940	4,120	4,340	4,230	—
v_s (m/s)	1,980	2,180	2,720	2,340	—
ρ (g/cm^3)	9.0	9.7	6.7	9.4	—
$E \times 10^{-10}$ (N/m^2)	9.4	12.1	12.7	13.1	21[b]
$\lambda_s \times 10^6$	1,750	-229	—	693	-33[c]
$E\lambda_s \times 10^{-7}$ (N/m^2)	17	2.8	—	9	0.7
$E\lambda_s^2/2) \times 10^{-3}$ (J/m^3)	145	3.2	—	32	0.1

[a]Ref. 33.
[b]Ref. 34.
[c]Ref. 35

change of ≈ 60% upon magnetic saturation. Thus, these compounds may have potential as adjustable frequency resonators, filters, and acoustic delay lines, as well as for high-power energy converting devices.

Detailed compliance and magnetomechanical coupling measurements are reported by Savage[37] and Timme[38] in this journal.

RESISTIVITY AND MAGNETORESISTANCE OF $TbFe_2$

The electrical resistivity is an important parameter for many applications.[39] Figure 11 shows the electrical resistivity of $TbFe_2$ as measured by Savage.[39] The transverse magnetoresistivity at room temperature is almost linear in fields to 800 kA/m (10 kOe), yielding $\Delta\rho/\rho H = 7.5 \times 10^{-9}$ m/A.

FABRICATION OF TRANSDUCER ELEMENTS

Improved magnetic and magnetostrictive properties depend upon grain orientation. This is convincingly shown by $\lambda_{111} >> \lambda_{100}$. Grain orientation has two profound effects: (1) increased saturation magnetostriction λ_s and (2) decreased internal strains at grain boundaries. The benefit of the first effect is obvious. Complete grain alignment would achieve an increase in λ_s of approximately 50%. The second effect is perhaps far more significant. Presently the biggest obstacles to higher permeability and coupling factor are the large internal strains commonly developed at grain boundaries in highly magnetostrictive materials. These internal strains depend upon the state of magnetization. During the process of magnetization, internal energies are developed that produce no useful external work. The overall effect is to degrade the high intrinsic permeability and d constant.

Thus, the method used to fabricate transducer elements, if possible, should be adaptable to grain orientation. The transducer alloys also should be as free as possible from imperfections, such as voids and inclusion, that inhibit rapid domain wall motion. Other criteria are low cost; ability to produce large sizes and various configuration; and, in some cases, the ability to laminate and construct bimetallic elements. The transducer elements should also have adequate toughness and resistance to shock.

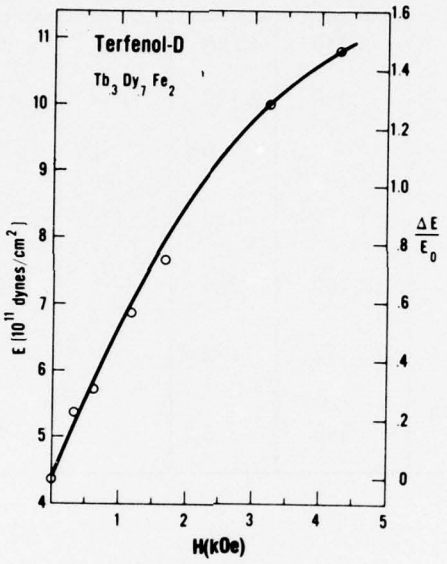

Fig. 10. Elastic modulus and ΔE effect in Terfenol-D

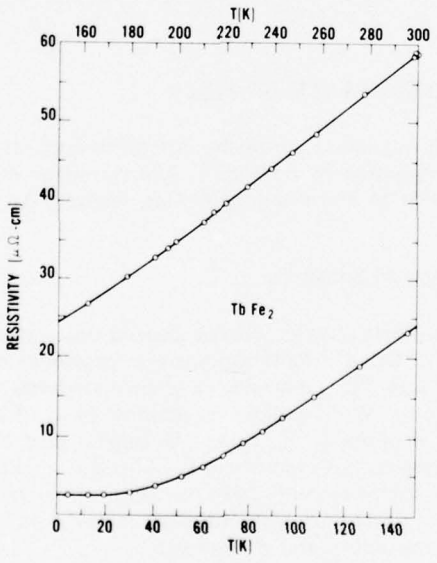

Fig. 11. Resistivity of $TbFe_2$

It is unlikely that all these desirable features can be embodied in one method. Powder metallurgy has the great advantage that it is adaptable to grain orientation and size control. Powder metallurgy techniques similar to those necessary here have already been employed for permanent magnet fabrication. At present vacuum sintering of grain-oriented powders is being performed at the Naval Surface Weapons Center. Dense materials have already been prepared by vacuum hot press methods at Raytheon. Arc-plasma deposition, another attractive technique, has the advantage of simplicity and ease of laminating. Rings have been produced by arc-plasma deposition at Union Carbide. These methods, and others, such as arc-casting, vacuum casting, epoxy encapsulation, and particulate composites are presently being explored and are reported elsewhere in this journal.

SUMMARY

The rare-earth intermetallic compounds have opened up a new era in magnetostrictive materials. Only a few years ago magnetostrictions of 1,000 ppm were nonexistent. Today we have many materials with these magnetostrictions at room temperature and above. These materials rely on two highly magnetoelastic rare-earth elements: Tb and Sm, plus the element iron, which lifts the magnetostriction to room temperature. Alloys have been developed with coupling factors equivalent to those of piezoelectric ceramics ($k \cong 0.6$), far greater than typical magnetostrictive materials. Many static and dynamic properties of these alloys have been investigated. They include magnetostriction elastic moduli, permeability, magnetomechanical coupling, anisotropy, and resistivity. Some prototype transducers have been designed and constructed.

The rare-earth alloys are not yet optimized for transducer performance. New systems are under investigation. Giant strides are expected by grain orientation and the reduction of imperfections. Substantial increases in permeability and coupling factor are forecast. Toughened samples also appear imminent.

New transduction configurations and methods of excitation are expected to emerge because of the new features of rare-earth materials. An attractive possibility uses bimetallic strips of highly magnetostriction materials. One can also envision the possibility of composite transducers containing both magnetostrictive and piezoelectric materials.

Magnetostrictive materials, of course, are not limited to their use in sonar transducers. Valves, actuators, and resonators are expected to employ rare-earth materials. As interest in the rare-earth elements for these applications grows, the research base will widen and ultimately yield still further-improved materials.

ACKNOWLEDGMENTS

The author would like to thank his many coworkers, particularly Henry Belson, Howard Savage, James Cullen, Nobu Tamagawa, and Dale McMasters, who helped shape this program. He also acknowledges the many helpful discussions with Earl Callen (American University), James Rhyne (NBS), Norman Koon (NRL), Robert Timme (USRD/NRL), and Jack Butler (Raytheon).

The research phase of this program was sponsored by the Office of Naval Research and the Naval Surface Weapons Center. The development of materials for sonar transducers was jointly sponsored by the Naval Sea Systems Command and the Naval Electronics Systems Command.

REFERENCES

1. G. Pierce, *Proc. Am. Acad. Arts Sci.* **63**, 1 (1928).
2. J. Vincent, *Proc. Phys. Soc.* **41**, 477 (1929).
3. See *JUA(USN)* **17** (1967).

4. F. Gardner, ed., Proc. Metallic Magnetoacoust. Mat. Workshop, (Boston, 1969). Sponsored by the Office of Naval Research.

5. A. Clark, R. Bozorth, and B. DeSavage, *Phys. Rev. Lett.* **5**, 100 (1963).

6. J. Alstad, S. Legvold, and J. Rhyne, *Phys. Rev. Lett.* **10**, 509 (1963).

7. N. Tsuya, A. Clark, and R. Bozorth, *Proc. Int. Conf. Magn.* (Nottingham, England, 1964), p. 250.

8. E. Callen and H. Callen, *Phys. Rev.* **129**, 578 (1963).

9. A. Clark and H. Belson, *AIP Conf. Proc.*, No. 5, p. 1498 (1972).

10. N. Koon, A. Schindler, and F. Carter, *Phys. Lett.* **37A**, 413 (1971).

11. A. Clark and H. Belson, *Phys. Rev.* **B5**, 3642 (1972); also *IEEE Trans. Magn.* **mag-8**, 477 (1972).

12. A. Clark, J. Cullen, O. McMasters, and E. Callen, *AIP Conf. Proc.*, No. 29 (1976) p. 192; also NSWC/WOL/75-177.

13. K. W. H. Stevens, *Phys. Soc. Lon.* **65**, 209 (1952).

14. R. M. Bozorth, *Ferromagnetism* (Van Nostrand, New York, 1951).

15. J. Smit and H. P. Wijn, *Ferrites* (Wiley, Inc., New York, 1959).

16. A. Clark, R. DeSavage, W. Coleman, E. Callen, and H. Callen, *J. Appl. Phys.* **34**, 1296 (1936).

17. N. Koon, A. Schindler, C. Williams, and F. Carter, *J. Appl. Phys.* **45**, 5389 (1974).

18. N. Koon, private communication.

19. A. Freeman and R. Watson, *Phys. Rev.* **127**, 2058 (1962).

20. A. Clark, J. Cullen, and K. Sato, *AIP Conf. Proc.* No. 24 (1975), p. 670.

21. N. Koon, private communication.

22. A. Clark, J. Cullen, and K. Sato, *AIP Conf. Proc.* No. 10, p. 1015 (1974).

23. A. Clark, H. Belson, and N. Tamagawa, *Phys. Lett.* **42A**, 160 (1972); also *AIP Conf. Proc.*, No. 10, p. 749 (1973).

24. C. Williams, N. Koon, and J. Milstein, *AIP Conf. Proc.*, No. 29 (1976).

25. Magnetic fields were obtained at the NRL High Field Facility, Washington, D.C.

26. U. Hoffman, *Z. angew. Phys.* **22**, 106 (1967).

27. L. W. McKeehan, *Phys. Rev.* **51**, 136 (1937).

28. J. W. Shih, *Phys. Rev.* **50**, 376 (1936).

29. R. F. Pearson, *J. Appl. Phys.* **31**, 160S (1960).

30. R. Perthel, G. Elbinger, and W. Keileg, *Phys. Status Solidi* **17**, 151 (1966).

31. F. M. Bozorth, E. R. Tilden, and A. J. Williams, *Phys. Rev.* **99**, 1788 (1955).

32. The anisotropy and magnetostriction of the $Tb_{1-x}Ho_xFe_2$ system has been widely investigated by N. C. Koon and C. M. Williams, "Extremely Low Anisotropy, High Magnetostriction Materials in a Quaternary Rare-Earth Iron System," *JUA(USN)* **27**, 127-132.

33. H. Savage, A. Clark, and J. Powers, *IEEE Trans. Magn.* **mag-11**, 1355 (1975).

34. A. Clark, H. Belson, and R. Strakna, *J. Appl. Phys.* **44**, 2913 (1973).

35. "Nickel," The International Nickel Co., Inc., 1951.

36. J. J. Went, *Physica* **17**, 98 (1951).

37. A. Clark and H. Savage, *IEEE Trans. Sonics Ultrason.* **su-22**, 50 (1975).

38. H. T. Savage and W. A. Ferrando, "Magnetomechanical Coupling, ΔE Effect, and Magnetization in Rare-Earth Iron Alloys," *JUA(USN)* **27,**

39. Robert W. Timme, "Device-Oriented Material Measurements on Rare-Earth Iron Alloys," *JUA(USN)* **27**, 139-146.

40. H. Savage (Naval Surface Weapons Center, White Oak, Silver Spring, Md. 20910), private communications.

U.S. Navy Journal of Underwater Acoustics Volume 27, Number 1 January 1977

EXTREMELY LOW ANISOTROPY, HIGH MAGNETOSTRICTION MATERIALS IN A QUATERNARY RARE-EARTH–IRON SYSTEM*

N. C. Koon and C. M. Williams
Naval Research Laboratory
Washington, D.C. 20375

ABSTRACT

We have measured the single crystal magnetostriction and anisotropy constants of a number of compounds in series $Ho_xTb_yDy_{1-x-y}Fe_2$, with emphasis on those compositions where the total anisotropy is low enough that the samples can be easily magnetized in any crystallographic direction. Of particular interest is the composition $Ho_{0.58}Tb_{0.20}Dy_{0.22}Fe_2$, where both of the lowest order anisotropy constants are very close to zero. For this composition the most important factor limiting the low field magnetostriction of a polycrystalline specimen is probably internal strain due to highly anisotropic magnetostriction.

INTRODUCTION

One of the central problems in making use of high magnetostriction rare-earth iron (RFe_2)† intermetallic compounds as magnetostrictive transducer elements has been that the pure (binary) compounds possess extremely large magnetic anisotropy, which means that high magnetic fields are needed to achieve large strains in polycrystalline specimens. The main successes thus far in developing improved materials have come by combining rare-earth elements that have the same sign of magnetostriction but different easy directions of magnetization in the Laves structure. These include combinations of $TbFe_2$ ([111] is easy) with $DyFe_2$ ([100] is easy)[1] and $TbFe_2$ with $HoFe_2$ ([100] is easy).[2] Great improvement in the low field magnetostrictive properties occurs for compositions where the [111] and [100] directions are almost equally easy.

For such compounds, however, the magnetic anisotropy is not necessarily zero, although in general it is lower than the binary compounds by a considerable margin. Even further reduction in the anisotropy can be achieved by combining more than two rare-earth elements, as we have shown for the Ho-Tb-Dy Fe_2 system. The anisotropy can be made so low, in fact, that the dominating factor affecting the low field magnetostriction of a polycrystal is probably the fact that the magnetostriction is highly anisotropic ($|\lambda_{111}| >> |\lambda_{100}|$), resulting in large internal strains.

Analysis of anisotropy and magnetostriction data on ternary and quarternary RFe_2 compounds is simplified by two important facts. The first is that the anisotropy and magnetostriction are predominantly single ion in origin, a well-established fact. The second is that the rare-earth elements interact only with the iron sublattice, not with the other rare-earth elements.[3] This means that a given rare-earth spin in the Laves structure will contribute essentially the same amount to the magnetization, anisotropy, and magnetostriction regardless of which other rare-earths are present. This is not true near the ordering temperatures (500 to 700 K), but for room temperature and below it should be obeyed extremely well. Once the magnetostriction and anisotropy of the pure (binary) compounds are established,

*Presented at the Workshop on Magnetostrictive Materials held under the sponsorship of the Underwater Sound Advisory Group and the Naval Research Laboratory, Orlando, Florida, 25-26 February 1976.
†A brief discussion of the rare-earth metals is given by Dr. Timme in his Introduction to the Theme in this issue.

[1] A. E. Clark, *AIP Conf. Proc.*, No. 18, p. 1015 (1974).
[2] N. C. Koon, A. I. Schindler, C. M. Williams, and F. L. Carter, *J. Appl. Phys.* **45**, 5389 (1974).
[3] R. M. Nicklow, N. C. Koon, C. M. Williams, and J. B. Milstein, *Phys. Rev. Lett.* **36**, 532 (1976).

therefore, the properties of any combination of them is linearly proportional to the respective concentrations.

The combination $Ho_xTb_yDy_{1-x-y}Fe_2$ is a particularly interesting one because for $TbFe_2$ [111] is easy, while for $DyFe_2$ and $HoFe_2$ [100] is easy. From Mössbauer[4] and anisotropy measurements[5] it is known that as a function of composition $Dy_xTb_{1-x}Fe_2$ exhibits a transition from [111] easy to [100] with no intermediate [110] easy composition. For $Ho_xTb_{1-x}Fe_2$, on the other hand, the transition goes from [111] to [110] and then to [100]. From this information alone it is possible to deduce that if the anisotropy is described by the usual K_1 and K_2, then near the "compensation" compositions, K_1 passes through zero, while for the $Dy_xTb_{1-x}Fe_2$ system, $K_2 < 0$, and for the $Ho_xTb_{1-x}Fe_2$ system, $K_2 > 0$. Clearly, by combining the zero K_1 composition of $Ho_xTb_{1-x}Fe_2$ and $Dy_xTb_{1-x}Fe_2$, it should be possible to produce a composition where $K_1 = K_2 = 0$. This is essentially what we have been able to show.

Similar measurements as a function of composition have been made of the single crystal magnetostriction constants, and the values of those constants appropriate to $TbFe_2$, $DyFe_2$, and $HoFe_2$ have been estimated. The significant point is that because the magnetostriction and anisotropy depend in different ways upon the angular part of the rare-earth $4f$ electron wave functions, the magnetostriction can be quite large when the anisotropy is very small.

SINGLE CRYSTAL MAGNETOSTRICTIVE PROPERTIES

The magnetostriction of a single crystal in the usual expansion is given by

$$\frac{\delta \ell}{\ell} = \frac{3}{2}\lambda_{100}(\alpha_1^2\beta_1^2 + \alpha_2^2\beta_2^2 + \alpha_3^2\beta_3^2) + 3\lambda_{111}(\alpha_1\alpha_2\beta_1\beta_2 + \alpha_1\alpha_3\beta_1\beta_3 + \alpha_2\alpha_3\beta_2\beta_3) + \ldots,$$

where the values of α are the direction cosines of the magnetization and the values of β are the direction cosines of the measuring direction. In the absence of high-order terms, the strain along [111] is described entirely by the term involving λ_{111}, and that along [100] is described entirely by the term involving λ_{100}. In the event that $\lambda_{100} = \lambda_{111}$, the magnetostriction is isotropic in the sense that the observed strain does not depend on the orientation of the crystal axes, but only on the angle between the measuring direction and the magnetization.

The highly anisotropic nature of magnetostriction in the $Ho_xTb_yDy_{1-x-y}Fe_2$ system is illustrated in Fig. 1. where the strain along [111] in a $Ho_{0.59}Tb_{0.19}Dy_{0.22}Fe_2$ crystal is plotted as a function of

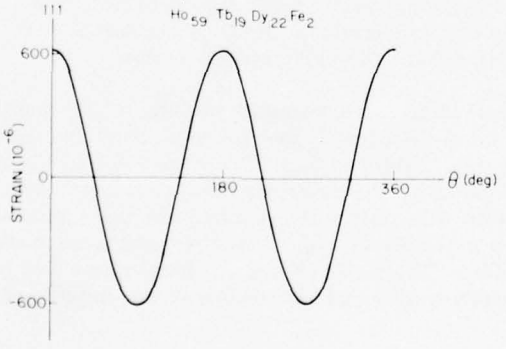

Fig. 1. Magnetostrictive strain along the [111] direction as a function of the angle between the [111] and the direction of the magnetization. The axis of rotation is [110].

[4]U. Atzmony, M. P. Dariel, E. R. Bauminger, D. Libenbaum, I. Nowik, and S. Ofer, *Phys. Rev.* **7**, 4220 (1973).
[5]C. M. Williams and N. C. Koon, *Phys. Rev.* **B11**, 4360 (1975).

the angle of rotation of the magnetization in the $1\bar{1}0$ plane. The peak-to-peak strain is approximately 1200×10^{-6}. When the measuring direction is [100], however, the peak-to-peak strain is less than 40×10^{-6}, which is too small to plot on the same scale. Although λ_{100} is generally much smaller than λ_{111}, it can be measured reliably in crystals with [100] easy, then extrapolated to those compositions where it cannot be measured directly.

In Figs. 2 and 3 we plot the room temperature values of λ_{111} and λ_{100} as a function of composition in $Ho_xTb_{1-x}Fe_2$. Insofar as it has been checked, the values appear to be in direct proportion to composition, as expected. One surprising feature, however, is that λ_{100} appears to change sign between $HoFe_2$ and $TbFe_2$, going through zero at about $x = 0.83$. It is interesting to note also that this is rather close to the composition where the lowest order anisotropy constant passes through zero.

By taking our results on the low anisotropy composition together with the value of λ_{111} for $TbFe_2$ and λ_{100} for $DyFe_2$ measured by Clark,[6] we summarize the room temperature magnetostriction measurements in Table I. Because of uncertainties in the extrapolation process, rather large error limits are quoted.

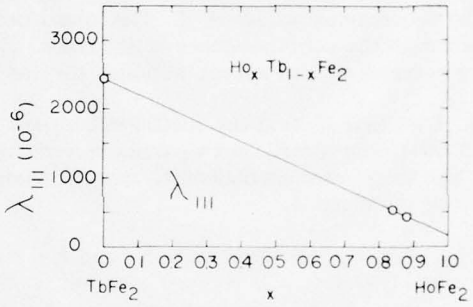

Fig. 2. λ_{111} as a function of composition x for $Ho_xTb_{1-x}Fe_2$

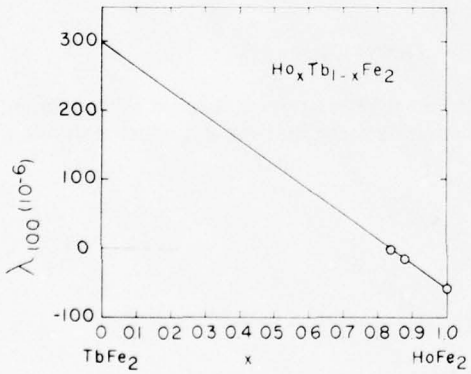

Fig. 3. λ_{111} as a function of composition x for $Ho_xTb_{1-x}Fe_2$

TABLE I
Magnetostriction Constants of Selected RFe_2 Compositions

	$HoFe_2$	$TbFe_2$	$DyFe_2$	$Ho_{0.58}Tb_{0.20}Dy_{0.22}Fe_2$
λ_{111} (10^{-6})	185 ± 20	[a]2,460	1,060 ± 150	820 ± 50
λ_{100} (10^{-6})	−59 ± 6	300 ± 100	[a]0 ± 4	22 ± 10

[a]From Ref. 6.

[6]A. E. Clark, J. R. Cullen, O. D. McMasters, and E. R. Callen, *AIP Conf. Proc.*, No. 29, p. 192 (1976).

MAGNETIC ANISOTROPY

The conventional expansion of magnetic anisotropy energy is

$$E = K_1(\alpha_1^2\alpha_2^2 + \alpha_1^2\alpha_3^2 + \alpha_2^2\alpha_3^2) + K_2\alpha_1^2\alpha_2^2\alpha_3^2 + \ldots ,$$

where the values of α are the direction cosines of the magnetization. Unfortunately the elements of this expansion do not form an orthonormal set, and if terms of other than lowest order are present, the meaning of the various coefficients becomes ambiguous. Because we observed higher order terms in the data on low anisotropy $Ho_xTb_yDy_{1-x-y}Fe_2$ compounds, it was necessary to use another expansion set, the Kubic harmonics[7]:

$$E = \sum_{\varrho} \kappa_{\varrho} H_{\varrho} .$$

In this expansion the values of H_{ϱ} are the Kubic harmonics and the values of κ_{ϱ} are coefficients analogous to the conventional values of K. The lowest order term appearing is κ_4, which can be identified with K_1, although the correspondence is not exact. Next is κ_6, which can be identified similarly with K_2. Higher order terms also appear, although they are less important than κ_4 and κ_6.

In Fig. 4 we have plotted the coefficients κ_4 and κ_6 for $Ho_xTb_{1-x}Fe_2$ as a function of composition. The lowest order coefficient κ_4 varies very rapidly with composition, crossing through zero near $x = 0.87$. The sixth-order coefficient κ_6 remains relatively constant, increasing slightly toward the Ho-rich side of the diagram.

Based on the simple analysis using K_1 and K_2, we expected that K_2 and hence also κ_6 would change signs and therefore pass through zero somewhere between the low anisotropy compositions of $Ho_xTb_{1-x}Fe_2$ and $Dy_xTb_{1-x}Fe_2$. We assumed that the zero κ_4 composition of $Dy_xTb_{1-x}Fe_2$ occurred at $x = 0.7$, and that the one for $Ho_xTb_{1-x}Fe_2$ occurred at $x = 0.86$. We then grew a series of single crystals with compositions defined by

$$x(Ho_{0.86}Tb_{0.14}Fe_2) + (1 - x)(Dy_{0.7}Tb_{0.3}Fe_2) .$$

The results of our anisotropy measurements at room temperature for a series of compounds having different values of x are shown in Fig. 5. The interesting data are that for κ_6, which exhibits a linear

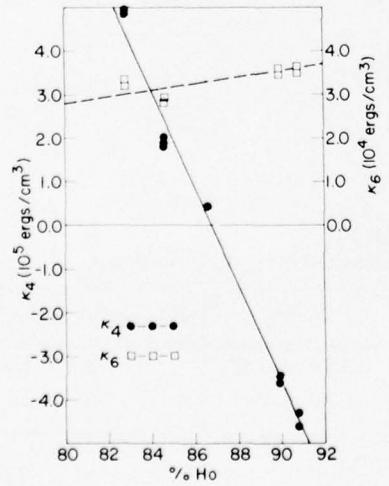

Fig. 4. Anisotropy coefficients κ_4 and κ_6 for $Ho_xTb_{1-x}Fe_2$ as a function of atomic Ho percent

[7]F. M. Mueller and M. G. Priestly, *Phys. Rev.* **148**, 638 (1966).

drop with x, crossing through zero at about $x = 0.32$. The data show that κ_4 for the measured samples is larger than κ_6. However, that simply reflects how much the predicted compositions missed the actual zero κ_4 line. By using the data it is possible to calculate the composition where both κ_4 and κ_6 are zero, as well as the composition lines where κ_4 and κ_6 are separately zero. For ease of visualization these are displayed on a composition diagram in Fig. 6. The extrapolated values of κ_4 and κ_6 for $HoFe_2$, $TbFe_2$, and $DyFe_2$ are given in Table II. The numbers quoted are linear extrapolations of the data and do not include nonlinear corrections due to such mechanisms as magnetostriction. The large error limits are due again to the uncertainty of the extrapolation process.

By varying the composition, small amounts about the zero composition of $Ho_{0.58}Tb_{0.22}Fe_2$, the anisotropy can be controlled to a remarkable degree. It is possible to choose any of the three principal

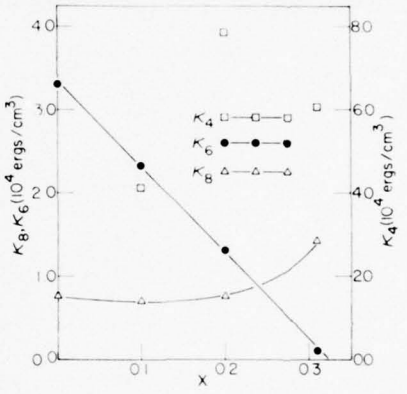

Fig. 5. Anisotropy coefficients κ_4 and κ_6 as a function of composition x, where x is defined by $x(Ho_{0.80}Tb_{0.14}Fe_2) + (1 - x)(Dy_{0.7}Tb_{0.3}Fe_2)$

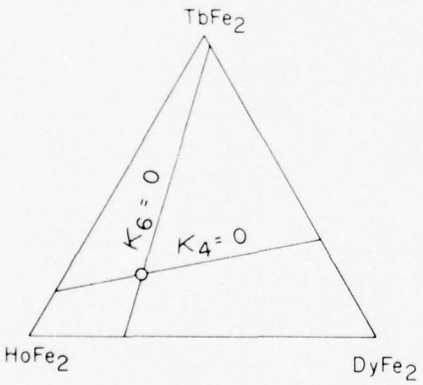

Fig. 6. Locus of $\kappa_4 = 0$ and $\kappa_6 = 0$ compositions for the system $Ho_xTb_{1-x-y}Fe_2$

TABLE II
Extrapolated Anisotropy Coefficients[a]
for Binary RFe_2 Compound

Coefficient	$HoFe_2$	$TbFe_2$	$DyFe_2$
κ_4 (10^6 ergs/cm^3)	−1.5	9.7	−4.7
κ_6 (10^4 ergs/cm^3)	3.9	0.3	−10.7

[a]Approximate compositions for $\kappa_4 = 0$: $Ho_{0.87}Tb_{0.13}Fe_2$ and $Tb_{0.33}Dy_{0.67}Fe_2$. Approximate composition for both $\kappa_4 = 0$ and $\kappa_6 = 0$: $Ho_{0.58}Tb_{0.20}Dy_{0.22}Fe_2$.

axis directions on the easy direction of magnetization. Because λ_{111} is by far the largest magnetostriction constant, it will probably be desirable, for example, to insure that in a polycrystalline transducer element the [111] is easy.

SUMMARY AND CONCLUSIONS

In the quaternary system $Ho_xTb_yDy_{1-x-y}Fe_2$, the anisotropy can be reduced to a relatively low level, comparable to that of nickel, while retaining a very large magnetostriction. Because the magnetostriction is highly anisotropic, however, it appears likely that in the polycrystalline state the internal strain energies caused by highly anisotropic magnetostriction will be larger than the anisotropy energies.

One possible way of reducing these internal strain energies would be to use single crystals or textured polycrystals with the [111] axes along the strain direction.

U.S. Navy Journal of Underwater Acoustics Volume 27, No. 1 January 1977

MAGNETOMECHANICAL COUPLING, ΔE EFFECT AND MAGNETIZATION IN RARE-EARTH IRON ALLOYS*

H. T. Savage
Naval Surface Weapons Center
Silver Spring, Maryland 20910

and

W. A. Ferrando
American University
Washington, D.C. 20016

ABSTRACT

The magnetomechanical coupling in bars of highly magnetostrictive $Tb_xDy_{1-x}Fe_{2-\delta}$ was determined as a function of bias field, x, and δ. A unique method for measurement of the complex permeability was developed. We find high coupling ($0.5 \leq k \leq 0.6$) over a wide range of applied fields (50 to 500 Oe), Young's modulus at constant field changes from 4.5 to 11.0 × 10^{10} Pa as the bias changes from 0 to 4.5 kOe corresponding to a change in sound velocity greater than 50%. Toroids of arc-cast rings were also measured yielding magnetomechanical coupling $k_{33} > 0.4$. A study of the magnetization process has begun. In single crystal $DyFe_2$, the domains are about μm wide on a (100) surface. The widths are much smaller in polycrystalline $Tb_{0.2}Dy_{0.73}Fe_2$.

INTRODUCTION

We have previously reported[1] coupling factor measurements in $Tb_xDy_{1-x}Fe_{2-\delta}$† where the values of x lie between 0 and 1. The term δ is a measure of the deviation from stoichiometry, i.e., $\delta = 0$ designates the stoichiometric compound. We will use the following symbol to designate a particular formula: $(x, 1 - x, 2 - \delta)$.

Our measured largest value of the coupling factor k_{33} was 0.6. This is the largest ever reported for a magnetostrictive material. We stated at that time that larger values of k_{33} would be observed in grain-oriented material. We still believe that is true. The paper will report further measurements of k_{33} as well as initial domain studies and material preparation techniques.

APPARATUS AND DATA ANALYSIS

A schematic of the measurement apparatus is shown in Fig. 1. It is basically a system to measure the complex susceptibility as a function of frequency. Because the permeability is so low in polycrystalline material, a separate pickup coil must be used. This avoids the leakage flux inherent in the method of Butterworth and Smith.[2] The operational amplifier puts out the sum of an ac drive and a dc bias current.

*Presented at the Workshop on Magnetostrictive Materials held under the sponsorship of the Underwater Sound Advisory Group and the Naval Research Laboratory, Orlando, Florida, 25-26 February 1976.
†A brief discussion of the rare-earth metals is given by Dr. Timme in his Introduction to the Theme in this issue.

[1]H. T. Savage, A. E. Clark, and J. M. Powers, *IEEE Trans. Magn.* mag-11, 1355 (1975).
[2]S. Butterworth and F. D. Smith, *Proc. Phys. Soc. Lon.* 43, 166 (1931).

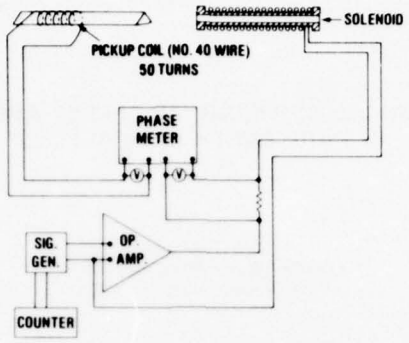

Fig. 1. Measurement apparatus; the sample slides into the solenoid for the actual measurement

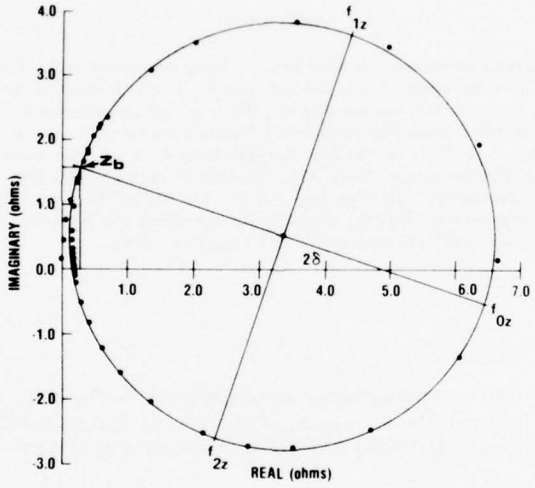

Fig. 2. Impedance circle for $Tb_{0.3}Dy_{0.7}Fe_2$ at a bias of 150 Oe (12 kA/m). The ac drive is 2 Oe (160 A/m) rms. The circle tilts at twice the loss angle δ ($\delta \simeq 10^{\circ}$).

Two voltages, one proportional to **B** and the other to **H**, are produced. The two voltmeters measure the magnitude of the two voltages and the phase meter measures the phase ϕ between them. This defines an impedence

$$Z = \left| \frac{V_1}{V_2} \right| e^{i\phi}$$

where V_2 is proportional to **H**, and V_1 proportional to **B**. The system works for toroids or bars. A typical set of data is shown in Figs. 2 and 3. Figure 2 is the plot of the real part of Z versus the imaginary part. Figure 3 is a similar plot of $1/Z$. The data that generate most of each circle come from different frequency ranges. The admittance circle is the easiest to interpret because it is not tilted by eddy currents and hysteresis. However, it is more difficult to measure. A low-distortion, high-stability signal generator is necessary. Our values for k_{33} are somewhat higher when derived from the admittance circle than those derived from the impedance circle. We have always reported impedance circle values because impedance circles are usually used in connection with magnetostrictive transducers. The value

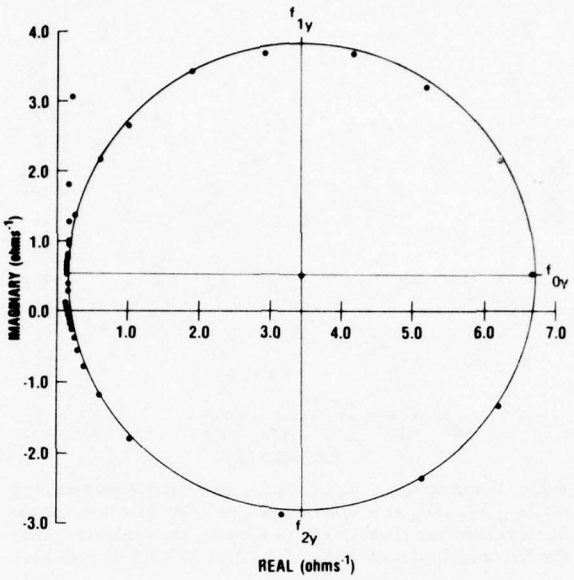

Fig. 3. Admittance circle for $Tb_{0.3}Dy_{0.7}Fe_2$ at a bias of 150 Oe. The same data were used to generate this circle as the one in Fig. 2.

of the admittance & impedance method is that when coupled with a single strain measurement, all the parameters necessary for a linear description of the material are available. Figure 4 shows the data that can be gained from impedance and admittance circle data on a (0.3, 0.7, 2) bar. The Q value for the admittance circle is

$$Q_y = \frac{f_{0y}}{f_{1y} - f_{2y}}$$

and that for the impedance circle is

$$Q_z = \frac{f_{0z}}{f_{2z} - f_{1z}} \ .$$

Q_y gives just the intrinsic material losses while Q_z includes eddy-current and hysteresis losses,[3] which can be determined from the loss angle δ.

In our material, bars with a cross section of 0.1 in. (2.5 mm) on a side have a loss angle of about 10° at 10 kHz. Figure 5 shows the resonant frequency at constant $\mathbf{B}(f_s)$ and constant $\mathbf{H}(f_p)$. This change in resonant frequency with magnetic field is called the ΔE effect. It corresponds to a change in Young's modulus of 150%, the largest ever reported at room temperature.[4] In a magnetostrictive material.

The determination of the blocked reactance Z_b is the most difficult part of the analysis. We have computer routines that make expanded plots of the data. From these we can find the crossing of the high- and low-frequency parts of the circle and hence Z_b. A computer routine is then used to locate the

[3]"Magnetostriction Transducers," Vol. 13, National Defense Research Council, Div. 6, DDC No. 77669 (1946).
[4]A. E. Clark and H. T. Savage, *IEEE Trans. Sonics Ultrason.* su-22(1), 50 (1975).

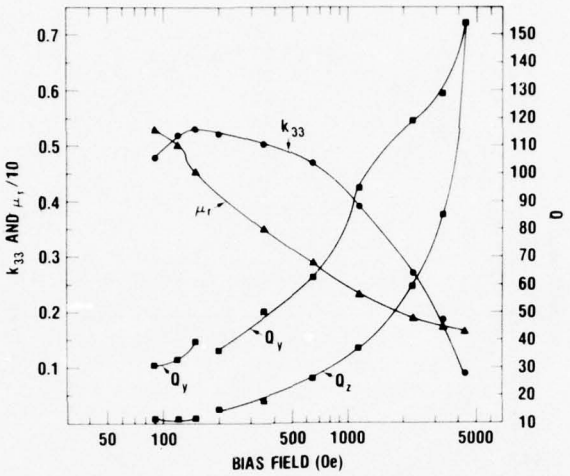

Fig. 4. Coupling factor k_{33}, Q factor, and relative permeability in $Tb_{0.3}Dy_{0.7}Fe_2$ as a function of bias field. The three points for bias field less than 180 Oe (14 kA/m) were measured after the bar was shortened from 3.9 to 2.52 in. (9.9 to 6.40 cm).

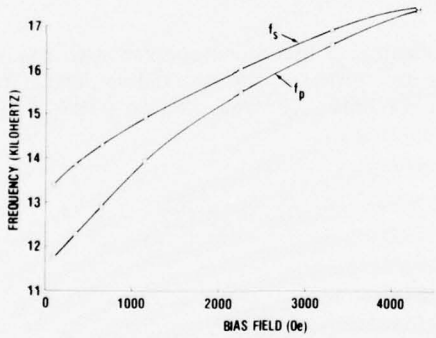

Fig. 5. Resonant frequency (at constant induction and constant field) versus bias field of a 3.9-in. (9.9-cm) long bar of $Tb_{0.3}Dy_{0.7}Fe_2$ (1 Oe = 79.58 A/m).

center of the circle. Around resonance $(f/f_{0y})^2$ is factored out of the admittance circle data. This significantly changes the location of the center of the circle.

RESULTS ON PRESENT MATERIALS

Our metallography has shown considerable amount of Widmanstätten precipitates. An example is shown in Fig. 6. We do not know the effects of this precipitate, which we believe to be $TbFe_3$. It has masked our efforts to observe domains. A sample used for domain studies was annealed for 2 weeks at 1075° C in addition to the usual 1 week at 850° C. The sample was then cooled to 600° C in 3 hr. This is faster than usual. The Widmanstätten precipitate disappeared. We believe that its disappearance was due to the fast cool rather than the long anneal. The sample quality was much better than usual.

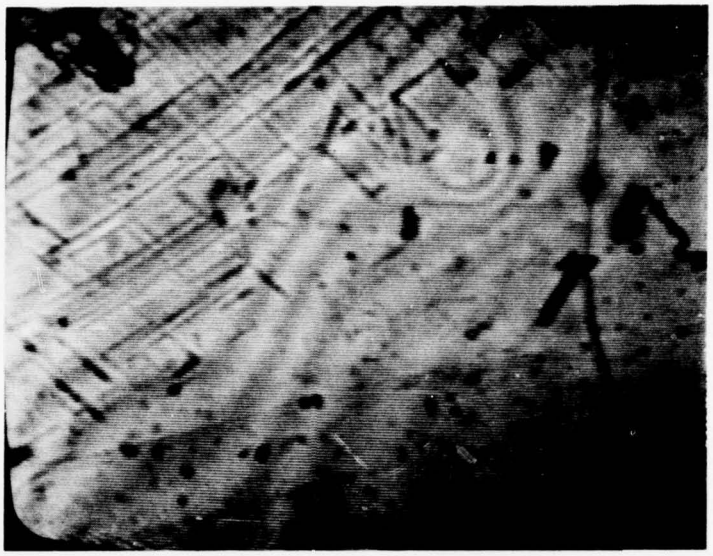

Fig. 6. An example of a Widmanstätten precipitate is shown in the upper left corner. It has a cross-hatched pattern with regular angles. The stripes are about 1 μm wide.

We have also succeeded in preparing a high-quality ring (shown in Fig. 7) that is 2 in. (5 cm) in o.d., about 1.5 in. (38 cm) in i.d., and 1/4 in. (6.3 cm) thick.[5] An earlier attempt led to a cracked ring in which k_{33} was measured to be 0.44. The sample had two resonances (one due to the crack) and had high eddy-current losses. We expect the present ring to show a higher coupling coefficient after a reduction in cross-sectional area.

In Fig. 8 we see the coupling factor plotted versus relative Dy concentration. At approximately (0.73, 0.27, 2) the easy axis changes from ⟨111⟩ to ⟨100⟩. This should be the approximate concentration of minimum anisotropy. Because λ_{100} is so small, the coupling factor diminishes drastically when the easy axis is ⟨100⟩. The curve also shows a possible trend toward lower coupling as the Tb content increases. However, we have measured a (0.50, 0.50, 2) bar and find it to have a maximum coupling of about 0.5. We had originally assumed that a lower anisotropy should lead to higher coupling. The results on the (0.50, 0.50, 2) bar indicate that the trend toward lower k_{33} with higher anisotropy is not as strong as anticipated. Internal losses in the material may be a strong function of anisotropy, however. The bar with the highest coupling coefficient had Q_y = 200, 4 times as high as any other at the bias field of maximum coupling.

Finally, we want to comment on the initial results of our domain study. On a (100) surface in $DyFe_2$, we find the walls lying in ⟨100⟩ direction with the moment in a ⟨100⟩ direction. The domains are about 300 μm wide. This is as seen in Si-Fe. In polycrystalline and oriented single crystals (0.27, 0.73, 2) the situation is different. Basically the domains are long and narrow in almost all of our observations. A typical width is around 2 μm. The length seems to be limited only by crystalline geometry and imperfections.

[5]Prepared by D. McMasters and K. Gschneidner of Iowa State University.

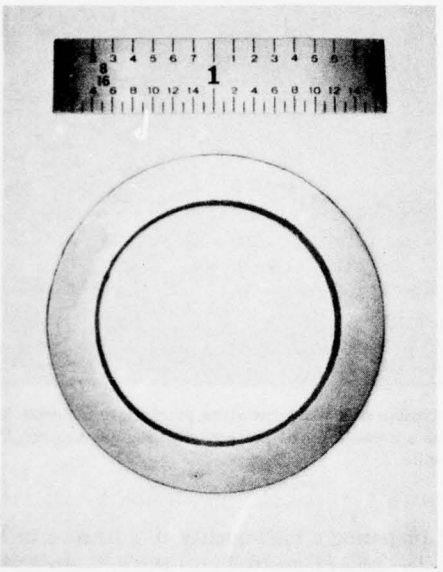

Fig. 7. Arc-cast ring. It has a width of about 0.125 in. (3.2 mm) after grinding

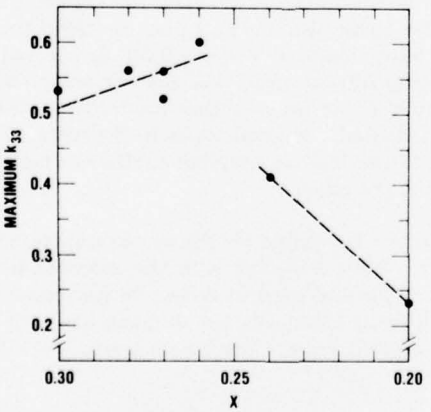

Fig. 8. Maximum coupling factor versus Tb-Dy concentration for $Tb_xDy_{1-x}Fe_2$

U.S. Navy Journal of Underwater Acoustics Volume 27, Number 1 January 1977

DEVICE-ORIENTED MATERIAL MEASUREMENTS ON RARE-EARTH/IRON ALLOYS*

Robert W. Timme
Naval Research Laboratory
Underwater Sound Reference Division
Orlando, Florida 32806

ABSTRACT

Engineering application of rare-earth/iron magnetostrictive alloys requires knowledge of the material macroscopic characteristics that are often difficult to calculate from the more basic material properties. This is a report on those device-related properties such as permeability, magnetomechanical coupling, hydrophone factor, high- and low-power drives, and the effects of bias stress. Comparisons are made between nickel, Tb-Ho-Fe, and Tb-Dy-Fe alloys.

INTRODUCTION

Recent investigations of the physical properties of the rare-earth iron magnetostrictive alloys† have given strong indications that the terbium-dysprosium-iron[1-3] and terbium-holmium-iron[4-7] systems are good possibilities for underwater transducer application. However, successful engineering application of these rare-earth iron alloys to transducers requires specific knowledge of material macroscopic characteristics that are often difficult to calculate from the more basic material properties. The purpose of this paper is to present experimentally determined values for the magnetomechanical coupling, permeability, hydrophone constant, effects of low- and high-power drive, and effects of stress. Comparisons will be made between the Tb-Ho-Fe alloys, Tb-Dy-Fe alloys, nickel, and ceramic. The experimental technique used for these measurements has been described in another paper.[6]

LOW-POWER DRIVE

Probably the most universally accepted characteristic used for evaluation of a material is the coupling constant k_{33} because it is a measure of the potential efficiency for energy conversion. The coupling is calculated as follows

*Presented at the Workshop on Magnetostrictive Materials held under the sponsorship of the Underwater Sound Advisory Group and the Naval Research Laboratory, Orlando, Florida, 25-26 February 1976.

†A brief discussion of the rare-earth metals is given by the author in his Introduction to the Theme in this issue.

[1] A. E. Clark, "Magnetic and Magnetoelastic Properties of Highly Magnetostrictive Rare-Earth/Iron Laves Phase Compounds," *AIP Conf. Proc.*, No. 18, pp. 1015-1018 (1974).

[2] H. T. Savage, A. E. Clark, and J. M. Powers, "Magnetomechanical Coupling and ΔE Effect in Highly Magnetostrictive Rare Earth-Fe_2 Compounds," *IEEE Trans. Magn.* **mag-11**(S).

[3] A. E. Clark and H. T. Savage, "Giant Magnetically Induced Changes in the Elastic Moduli in $Tb_{0.3}Dy_{0.7}Fe_2$," *IEEE Trans. Sonics Ultrason.* **su-22**, 50-52 (1975).

[4] C. M. Williams and N. C. Koon, "Anisotropy Energy Measurements on Single Crystal $Tb_{0.15}Ho_{0.85}Fe_2$," *AIP Conf. Proc.*, No. 18, pp. 1247-1248 (1973).

[5] N. C. Koon, A. I. Schindler, C. M. Williams, and F. L. Carter, "Magnetostrictive Properties of $Ho_xRb_{1-x}Fe_2$ Intermetallic Compounds," *J. Appl. Phys.* **45**, 5389-5391 (1974).

[6] R. W. Timme, "Magnetomechanical Characteristics of a Terbium-Holmium-Iron Alloy," *J. Acoust. Soc. Am.* **59**, 459-464 (1976).

[7] R. W. Timme and N. C. Koon, "Magnetostrictive Properties of Terbium-Holmium-Iron Compounds," *J. Acoust. Soc. Am.* **58S**, S74 (1975).

$$\frac{k_{33}^2}{1 - k_{33}^2} = \frac{d_{33}^2}{\mu_{33}^T s_{33}^B} \tag{1}$$

and from independent measurements of the magnetostrictive constant d_{33}, the incremental permeability μ_{33}^T, and the elastic compliance modulus s_{33}^B. The symbols used here are consistent with the "IEEE Standard on Magnetostrictive Materials."[8]

Figure 1 shows the coupling constant for the terbium-holmium-iron system as a function of rare-earth composition in the region of minimum magnetocrystalline anisotropy. Torque magnetometry measurements have indicated a zero first-order anisotropy coefficient near a composition of 14% terbium and 86% holmium, which leads to the expectation that the coupling would be maximum at that composition. As can be seen, this is not the case. The coupling reaches a maximum in the vicinity of 0.45 for a rare-earth composition of approximately 23% terbium and 77% holmium. The explanation must include a consideration of the different amounts of magnetostrain along the different crystallographic axes as well as magnetocrystalline anisotropy. For alloys more holmium-rich than 86%, the {100} are the easy axes of magnetization. For compositions containing between 86% and 80% holmium, the {110} are easy, and for less than 80% holmium, the {111} are easy. The magnetostrain is greatest along the {111} and least along the {100}. So, if anisotropy was low, a $TbHoFe_2$ alloy with {111} easy axes of magnetization would exhibit a larger d_{33} and a smaller incremental permeability than would an alloy with {100} easy axes. This would yield a larger k_{33} for the more terbium-rich than the holmium-rich alloy. However, the magnetocrystalline anisotropy energy is at a minimum at 86% holmium and increases as the holmium concentration decreases. The effect of the larger anisotropy is to decrease d_{33}, which causes a corresponding decrease in k_{33}. The net result of all this is that the magnetomechanical characteristics improve as the composition moves from holmium-rich toward terbium-rich, but a peak is quickly reached as the anisotropy increases very rapidly and becomes dominant.

The magnetostrictive constant d_{33} has a variation with composition similar to the curve shown in Fig. 1, but it reaches a maximum at a composition of 20% terbium and 80% holmium. The modulus s_{33}^B is relatively independent of composition in this range of composition with only a gradual increase of about 5% to a peak at 15% terbium and 85% holmium.

The magnetomechanical coupling as a function of rare-earth composition for the terbium-dysprosium-iron system has previously been reported by Savage, Clark, and Powers.[2] They found that with the more conventional method using impedance loci the terbium-dysprosium-iron system had a peak in coupling at a composition of about 26% terbium and 74% dysprosium. I have made subsequent measurements of

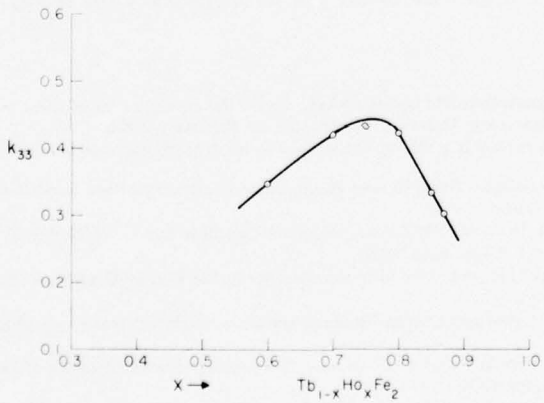

Fig. 1. Magnetomechanical coupling as a function of composition for $Tb_{1-x}Ho_xFe_2$

[8]Technical Committee on Transducers and Resonators of the IEEE Group on Sonics and Ultrasonics, "IEEE Standard on Magnetostrictive Materials: Piezomagnetic Nomenclature," IEEE Standard 319-1971 (1971).

the magnetostrictive properties and calculated the coupling as described on samples supplied by Clark and have obtained results in very good agreement.

A comparison of the coupling for two alloys near the optimum rare-earth composition is shown in Fig. 2. The properties are functions of the magnetic bias field, which must be externally applied because the alloys have only a small magnetic remanence. The $Tb_{0.3}Dy_{0.7}Fe_2$ alloy has a maximum k_{33} of 0.60, which is to be compared with 0.43 for $Tb_{0.25}Ho_{0.75}Fe_2$ and a maximum 0.27 for oxide-annealed nickel. These curves show the rare-earth iron alloys have a greater potential efficiency for energy conversion over a wider range of bias field than does nickel. The broad peak in the coupling implies that the alloys would retain their high values of coupling under high-power-drive conditions.

The magnetic permeability is important to the designer because it determines the reluctance of the flux path, the amount of magnetic field fringing, and the size of the current-carrying solenoids in addition to affecting the coupling constant. Generally, for a given coupling constant, it is desirable to have as large a permeability as possible. A striking difference is found between Tb-Ho-Fe and Tb-Dy-Fe alloys. In Fig. 3 is shown the static and incremental, or reversible, permeability of $Tb_{0.3}Dy_{0.7}Fe_2$ and $Tb_{0.25}Ho_{0.75}Fe_2$. The static permeability of the Tb-Dy-Fe reaches a maximum of 150 at 15 Oe (1,200 A/m) is still as high as 38 at 105 Oe (8.4 kA/m) where the Tb-Ho-Fe maximizes at 19. The incremental permeabilities are more similar in general shape, but the value for the Tb-Dy-Fe is again larger.

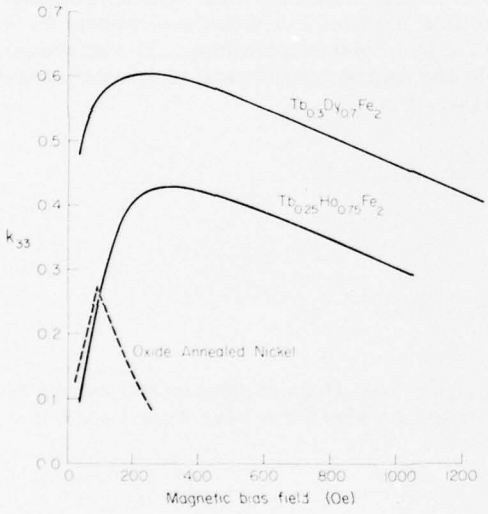

Fig. 2. Comparison of the magnetomechanical coupling as a function of magnetic bias field (1 Oe = 79.58 A/m)

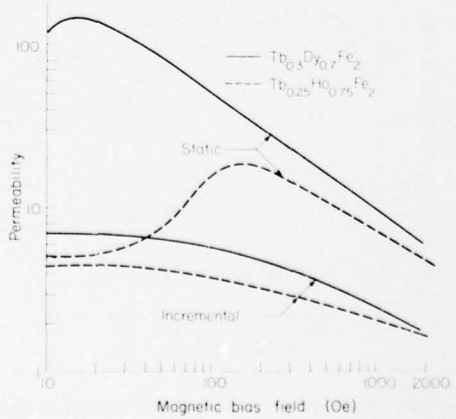

Fig. 3. Comparison of the magnetic permeability as a function of magnetic bias field (1 Oe = 79.58 A/m)

In magnetostrictive materials, the constant d_{33} is important for hydrophones as well as projector application. The sensitivity M (ratio of voltage V to incident sound pressure p) of a hydrophone that uses a sense coil with n turns to detect the change in flux density produced by a magnetostrictive element of cross-sectional area A in the presence of a sound pressure p is given by

$$M \equiv \frac{V}{p} = d_{33}\omega nA \, . \tag{2}$$

For a hydrophone using a piezoelectric element of thickness ℓ, the sensitivity is given by

$$M \equiv \frac{V}{p} = g_{33}\ell \, , \tag{3}$$

where g_{33} is the piezomagnetic stress constant. Each of these equations is derived with the assumption that the sound is incident only on the element surfaces in which the normal is parallel to the direction of magnetization or polarization. When this is not the case, the magnetostrictive and piezoelectric constants become more complicated because other elements of their respective tensors are included.

As can be seen from Eqs. (2) and (3), the sensitivity of a magnetostrictive or piezoelectric hydrophone depends on physical dimensions and, in the one case, frequency and number of sense coil turns. These factors make a direct comparison of the two dissimilar materials difficult. The hydrophone constant, as discussed by Woollett,[9] combines the electrical impedance Z with the sensitivity to provide a better comparison of the relative merit of materials for hydrophone application. This expression is given in Eqs. (4) and (5) and is shown reduced in both the magnetostrictive and piezoelectric cases to the same functional form. For magnetostrictive materials, it is

$$H \equiv \frac{M}{\sqrt{|Z|}} = \frac{d_{33}}{\sqrt{\mu}} \sqrt{\omega \ell A} \quad V/\text{Pa} - \Omega^{1/2} \, . \tag{4}$$

For piezoelectric materials, it is

$$H = \frac{d_{33}}{\sqrt{\epsilon}} \sqrt{\omega \ell A} \quad V/\text{Pa} - \Omega^{1/2} \, . \tag{5}$$

A comparison of the hydrophone factors for $Tb_{0.3}Dy_{0.7}Fe$, $Tb_{0.2}Ho_{0.8}Fe$, and oxide-annealed nickel to that of a piezoelectric ceramic is presented in Fig. 4. Typical values for a Navy Type I ceramic

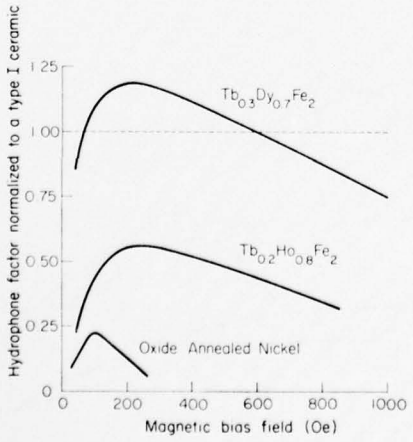

Fig. 4. Comparison of the hydrophone factor of the magnetostrictive alloys to that of a Type I ceramic (1 Oe = 79.58 A/m)

[9]R. S. Woollett, "Hydrophone Design for a Receiving System in Which Amplifier Noise is Dominant," *J. Acoust. Soc. Am.* **34**, 522-523 (1962).

($d_{33} = 2.8 \times 10^{-10}$ m/V and $\epsilon = 1.15 \times 10^{-8}$ F/m) were used in Eq. (5) to provide a value for the normalization of Eq. (4). The hydrophone factor of the Tb-Dy-Fe alloy is considerably larger than for the Tb-Ho-Fe and nickel and is shown to be comparable to the ceramic over a wide range of magnetic bias.

High-Power Drive

Until now, this paper has dealt only with low-field values of the material characteristics, but if the material is used in a sound projector operating under a high-power drive, these characteristics certainly will be different.

The room temperature magnetostrains of the $Tb_{0.3}Dy_{0.7}Fe_2$ and $Tb_{0.3}Ho_{0.7}Fe_2$ alloys and oxide-annealed nickel are compared in Fig. 5. The greater anisotropy of the rare-earth iron alloys is readily apparent from the more gradual increase of strain toward saturation; however, the much larger strains possible with the rare-earth iron alloys are evident. The oxide-annealed nickel saturates quickly to a strain of −38 ppm while the $Tb_{0.3}Ho_{0.7}Fe_2$ exhibits a strain of 480 ppm and the $Tb_{0.3}Dy_{0.7}Fe_2$ reaches a strain of 750 ppm at 1,900 Oe (150 kA/m), and both are still far from saturation.

It is this possibility of large strains that makes the rare-earth iron alloys attractive for underwater sound projectors. In an application as a projector, the alloy will be placed in a bias field because the magnetic remanence is too small and the dynamic strain will be produced by an applied alternating magnetic field. If a value of the bias field is selected and held constant and an alternating field is superimposed, the magnitude of the dynamic strain produced at the same frequency has been found to increase with alternating field magnitude until the mean-to-peak magnitude approaches about 80% of the bias field value. At this point some frequency distortion of the dynamic strain begins to occur. Because the sound pressure level generated is directly proportional to the displacement, the rare-earth iron alloys have significantly greater potential for generating sound than does the 35 ppm maximum dynamic strain of nickel.

When the amplitude of the drive field increases, the properties change from their low field values, and the cumulative effect of these changes can best be shown as the change in the coupling as is done in Fig. 6. Different bias fields were selected, and the alternating field was increased from 16 Oe (1,300 A/m) rms (the low field value) until mean to peak was 80% of the bias. Then the coupling was computed

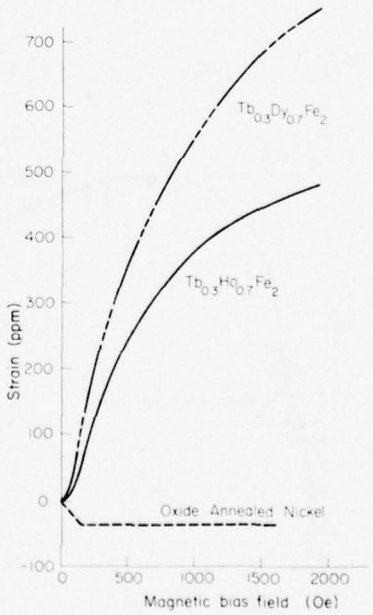

Fig. 5. Magnetostrain as a function of magnetic bias field (1 Oe = 79.58 A/m)

and displayed normalized to the low field values as a function of driving power also normalized to low field. The result is that the coupling actually increases by 5% to 10% before declining at higher power.

From these high-drive measurements of the rms magnetostrain, the elastic compliance constant, and frequency, and from the mechanical Q, an estimate can be made of the maximum power output P of which the material is capable. An example of this power capability is shown in Fig. 7 for a $Tb_{0.3}Ho_{0.7}Fe_2$ alloy. The maximum undistorted strain at 159 Hz for a given bias field was used to obtain the power at that bias. Because the mechanical Q, which involves the engineering application and not the material itself, is involved, the power output has been expressed in decibels relative to $Q/10$ W/cm^3. This rare-earth composition of 30% terbium and 70% holmium should be capable of generating at least 16 dB more power than nickel and the same amount of power as generated by a Type I piezoelectric ceramic under a

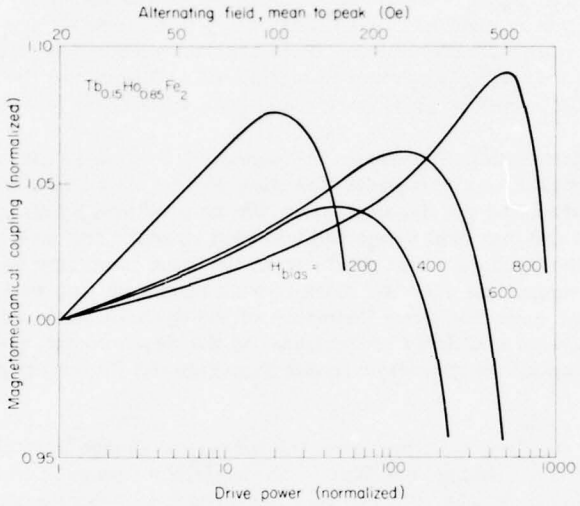

Fig. 6. Change in magnetomechanical coupling at high-power drive for various bias fields. Both drive power and magneto-coupling are normalized to low field operation.

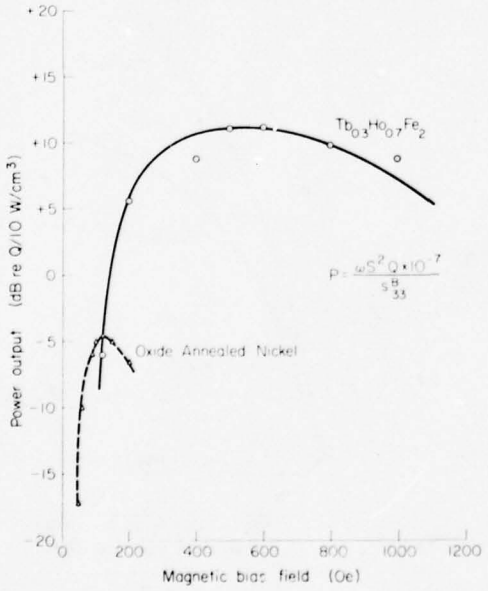

Fig. 7. Maximum undistorted power output at 159 Hz

5 kV/cm rms drive. Based on the greater magnetostrain of the Tb-Dy-Fe as shown in Fig. 5 and also on its lower stiffness moduli, a power output curve about 4.5 dB larger can be expected for Tb-Dy-Fe than that shown in Fig. 7 for the Tb-Ho-Fe.

EFFECTS OF BIAS STRESS

Normally, acoustic elements in an underwater sound projector are biased with a mechanical compressive stress. This is to prevent the element from undergoing tensile failure at high-drive levels, to shock harden, and to dampen spurious resonances. Thus it is likely these alloys will also be bias stressed in any operational design. For this reason the effects of one-dimensional compressive stress directed parallel to the direction of magnetic polarization have been investigated.

The results of the study on $Tb_{0.3}Dy_{0.7}Fe_2$ are shown in Fig. 8. A constant magnetic bias was maintained while the sample was stressed. The results shown are for a 200-Oe (16-kA/m) bias, but the changes appeared to be independent of magnetic bias. The magnetostrictive constant d_{33} and the permeability μ_{33}^T decreased while the elastic constant $1/s_{33}^B$ and the sound speed increased. The cumulative effect is that the coupling increases gradually to 113% at 17 MPa (2,500 psi) and then begins a slow decline.

Figure 9 shows the strain produced upon stressing the $Tb_{0.3}Dy_{0.7}Fe_2$ to failure. Catastrophic failure occurred without prior warning for two samples tested at almost the identical stress of 500 MPa (73,000 psi). This is about the same compressive failure point as that of a Type I ceramic.

CONCLUSIONS

This paper summarizes the investigation of the magnetostrictive properties of the ternary alloys of Tb-Ho-Fe and Tb-Dy-Fe as a function of composition, low- and high-power drives, and the effects of compressive bias stress. The following conclusions can be made:

- The terbium-dysprosium-iron alloy with a rare-earth composition of approximately 30% terbium and 70% dysprosium has been found to have a magnetomechanical coupling, hydrophone factor, maxium power output, magnetic permeability, and magnetostrain surpassing the best of the terbium-holmium-iron system. The Tb-Ho-Fe alloys were not annealed as were the Tb-Dy-Fe, and it is possible an annealing process will improve their performance somewhat.

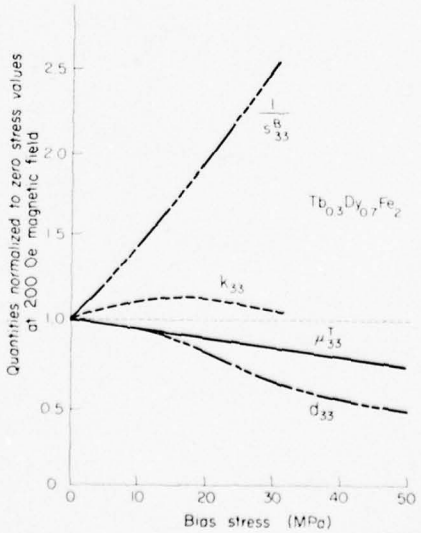

Fig. 8. Effects of bias stress on $Tb_{0.3}Dy_{0.7}Fe_2$ at constant 200-Oe (16-kA/m) magnetic bias field

- Both the Tb-Ho-Fe and the Tb-Dy-Fe alloys with about 30% terbium can compare favorably with piezoelectric ceramics as a projector material.

- For many reasons, not the least of which is familiarity, ceramics will not be replaced by these alloys, but a complementary role is quite feasible.

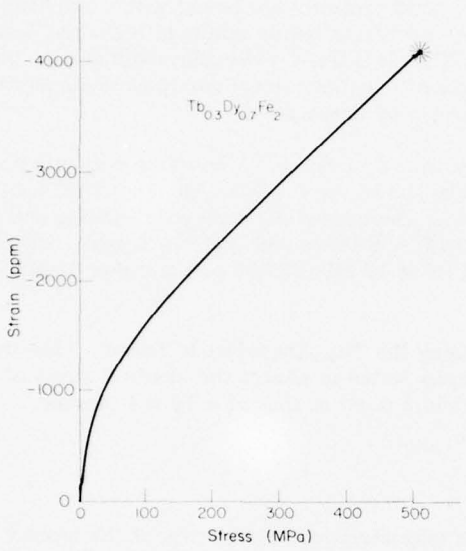

Fig. 9. Compressive stress-strain to failure for $Tb_{0.3}Dy_{0.7}Fe_2$

U.S. Navy Journal of Underwater Acoustics Volume 27, No. 1 January 1977

MICROSTRUCTURE AND MECHANICAL PROPERTIES OF THE IRON/RARE-EARTH INTERMETALLIC COMPOUNDS*

C. Robert Crowe
Naval Surface Weapons Center
Silver Spring, Maryland 20910

ABSTRACT

The recent discovery that the binary Fe_2Tb and ternary $Fe_2(Tb_xDy_{1-x})$ intermetallic compounds possess unusually large magnetostrictive responses makes these compounds attractive candidates as transducer materials for use in sonar systems. A difficulty associated with the use of these materials, however, is that in the as-cast and in the as-cast plus homogenized condition, the compounds exhibit low fracture toughness.

Typically, alloys have hardnesses in excess of Rc63 and compressive fracture strengths ranging from about 80 to 250 MPa. Observations of high sensitivity stress-strain curves and also fracture surfaces by scanning electron microscopy fail to reveal any signs of plastic deformation. The alloys fracture during elastic loading with fracture occurring exclusively by cleavage.

Attempts to increase the fracture toughness by metallurgical manipulation of the microstructure will be described and the results of some mechanical working experiments will be discussed.

INTRODUCTION

The recent discovery that the binary Fe_2Tb† and ternary $Fe_2(Tb_xDy_{1-x})$ intermetallic compounds possess unusually large magnetostrictive responses has prompted attempts to develop magnetostrictive transducers suitable for sonar applications using these materials. The magnetostrictive properties of a number of the alloys have been described in a series of papers by A. E. Clark, H. T. Savage, and J. M. Powers,[1-4] and application of the alloys as sonar transducers has been described in the contract reports of the Raytheon Company.[5-7]

A difficulty associated with the use of the rare-earth iron compounds is that they exhibit low fracture toughness in the as-cast and as-cast plus homogenized condition. Little or no quantative work appears in the literature on the mechanical properties of the alloys. In this investigation, preliminary mechanical properties and microstructures have been studied with the view toward increasing the fracture toughness of the alloys by metallurgical manipulation.

*Presented at the Workshop on Magnetostrictive Materials held under the sponsorship of the Underwater Sound Advisory Group and the Naval Research Laboratory, Orlando, Florida, 25-26 February 1976.

†A brief discussion of the rare-earth metals is given by Dr. Timme in his Introduction to the Theme in this issue.

[1] A. E. Clark, *AIP Conf. Proc.*, No. 18, p. 1015 (1974).
[2] H. T. Savage, A. E. Clark, and J. M. Powers, *J. Acoust. Soc. Am.* **56**, Suppl. S30 (1974).
[3] A. E. Clark and H. T. Savage, *IEEE Trans. Sonics Ultrason.* **54-22**, 50 (1975).
[4] H. T. Savage, A. E. Clark, and J. M. Powers, *IEEE Trans. Magn.* **mag-11**, 1355 (1975).
[5] J. L. Butler, Initial Bimonthly Report, Contract N00024-75-C-6137 (Raytheon Co., Portsmouth, R.I., (May 1975).
[6] J. L. Butler and S. J. Ciosek, Second Bimonthly Report, Contract N00024-75-C-6137 (Raytheon Co., Portsmouth, R.I., July 1975).
[7] J. L. Butler and S. J. Ciosek, Third Bimonthly Report, Contract N00024-75-C-6137 (Raytheon Co., Portsmouth, R.I., Sept. 1975).

TABLE I
Nominal Compositions of $Fe_2(Tb_xDy_{1-x})$ Alloys

Alloy	Fe(at.%)	Tb(at.%)	Dy(at.%)
23	66.7	9.0	24.3
24	66.1	9.2	24.7
25	65.5	9.3	25.2
27	63.0	10.0	27.0
A-1[a]	66.1	9.2	24.7
A-2[a]	66.1	9.2	24.7

[a]Melts produced from commercial grade raw materials.

EXPERIMENTAL PROCEDURES

Materials

Alloys used in this investigation were obtained from the Iowa State University, Ames, Iowa, in the form of arc-cast rods. The nominal rod compositions are listed in Table I.

Compression Specimens

Rods of alloys 23 through 27 were ground into rectangular cross sections and heat treated at 850° C for 6 days and slow cooled. Following this, the rods were heat treated at 1,000° C for 10 days and slow cooled.

Compression samples were cut and lapped to produce right prisms with aspect ratios of approximately 2.5 to 1. Samples with faces parallel to within 15 arcmin were obtained by mounting the cut specimen in a machined V-block and lapping them on standard metallographic equipment until the faces were flat and parallel.

Compression Testing

The specimens were tested in compression using a 10,000-kg floor model Instron testing machine at room temperature. The specimens were compressed between two hardened steel pistons that slid accurately in a close-fitting outer guide cylinder. Accurate positioning of the specimen along the axis of the pistons was achieved using an alignment disk and two O-rings. Load was transmitted to the pistons via a loading train mounted below the moving crosshead of the Instron. The loading train was attached to a stationary Instron FM tensile load cell by means of a pushrod that kept the load cell remote from the test assembly. The load train incorporated two hardened steel ball bearings, a Brinell plate, and a universal joint to achieve axial loading free from bending moments.

Displacement was measured using two Daytronics DS-200 linear variable differential transformers (LVDT) attached to the compression pistons by means of rigid horizontal bars. High sensitivity load-extension curves were plotted on a Hewlett-Packard 7035B x-y recorder. The extension axis signal was taken from the LVDT, processed, and fed to the x axis of the recorder to a sensitivity of 2.5 μ. This sensitivity was rather coarse for the experimental setup; its capabilities being three orders of magnitude more sensitive. The y axis signal was taken from the Instron load cell. The crosshead speed was 8.46×10^{-4} cm/s for all tests. A schematic of the jig and measuring system is shown in Fig. 1.

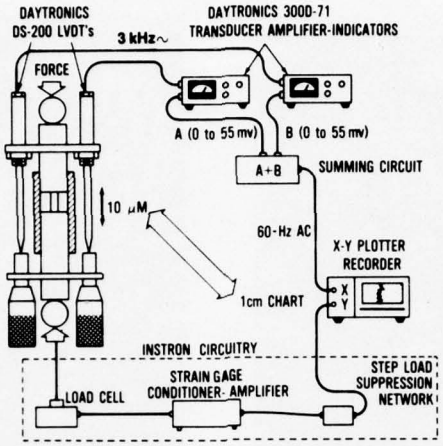

Fig. 1. A schematic of the experimental setup for measuring high sensitivity stress-strain curves in compression

Load extension curves were reduced to true stress-true strain curves by calculating the stress σ directly from the load F and separating the total length change $\Delta\ell_T$ into specimen and machine parts, $\Delta\ell_s$ and $\Delta\ell_m$, respectively, according to the relation:

$$\Delta\ell_T = \Delta\ell_s + \Delta\ell_m . \tag{1}$$

Because of elastic punching of the compression pistons by the specimen, $\Delta\ell_m$ is approximately

$$\Delta\ell_m \approx \frac{2P\ell_0}{E\pi\alpha^2} + \frac{(1-\nu^2)P}{E\sqrt{A/\pi}} , \tag{2}$$

where P is the load transmitted through the indenter, ℓ_0 is the length of a piston, E is Young's modulus of the piston material, α is the piston radius, ν is Poisson's ratio of the piston material, and A is the cross-sectional area. The specimen strain ϵ is then calculated approximately by

$$\epsilon = \frac{\Delta\ell_s}{\ell_s} \approx \frac{1}{\ell_s}\left[\Delta\ell_T - \frac{2P\ell_0}{E\pi\alpha^2} - \frac{(1-\nu^2)P}{E\sqrt{A/\pi}}\right]. \tag{3}$$

RESULTS

Metallographic Examinations

Figure 2(a) shows the microstructure of rod 25 after the 850° C heat treatment. This structure, which is typical of all the alloys after this heat treatment, consists of a partially decomposed dendritic structure of primary $Fe_2(Tb_{0.73}Dy_{0.27})$ dendrites with a divorced ternary eutectic structure in the grain boundaries. The rare-earth phase is dispersed in the grain boundaries in the form of spheres or sheets, and there is a fine dispersion of presumably nonmetallic inclusions in the primary grains.

Microstructures obtained after the 1,000° C heat treatment were somewhat different. Alloys 23, 24, and 25 exhibited extensive grain growth with a distinct Widmanstätten precipitate distributed throughout the primary grains. Widmanstätten structures result from precipitation and growth of second phase particles in a distinct geometric morphology. Therefore, to obtain the Widmanstätten structure as

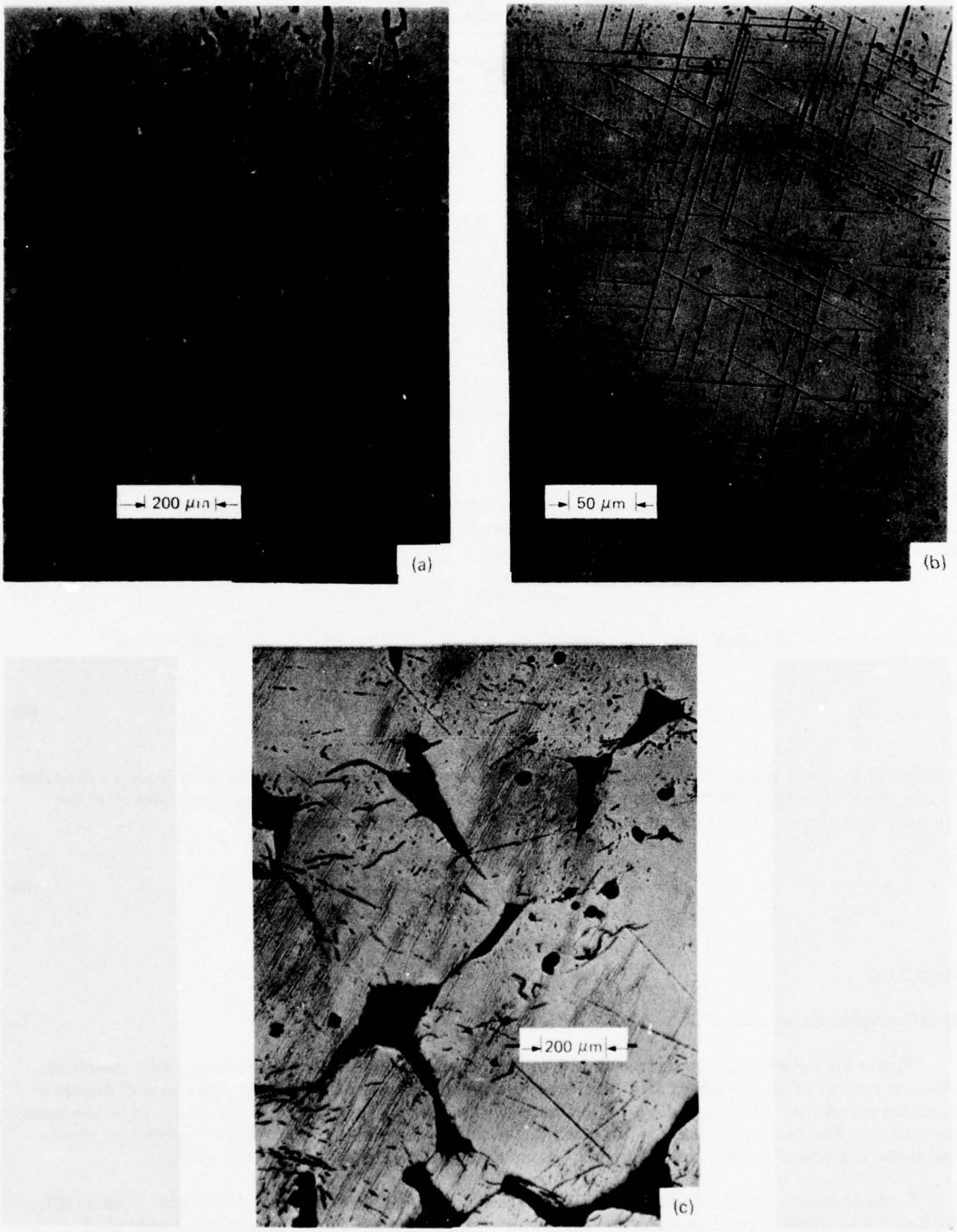

Fig. 2. Microstructures obtained in $Fe_2(Tb_xDy_{1-x})$ alloys. (a) As-cast plus 850° C for 6 days and slow cooled for alloy 25 (b) As-cast plus 850° C for 6 days and slow cooled plus 1,000° C for 10 days and slow cooled for alloys 23, 24, and 25 (c) Same heat treatment as in (b) for alloy 27 (Nital).

shown in Fig. 2(b) from the structure of Fig. 2(a) requires that the rare-earth phase distributed in the dendrite boundaries go into solid solution during the 1,000° C heat treatment for subsequent precipitation.

After the 1,000° C heat treatment, alloy 27 showed large rare-earth colonies distributed in the grain boundaries. The primary $Fe_2(Tb_xDy_{1-x})$ grains had become relatively uniaxial, and grain growth was not as extensive as in the other three rods. This morphology is shown in Fig. 2(c).

Scanning electron microphotographs (SEM) of the fracture surfaces of alloy 25 are shown in Figs. 3(a) and 3(b). As can be seen, there is no evidence of ductile flow associated with the fracture surface—fracture occurring exclusively by cleavage. Figure 4 is a SEM of alloy 27 showing the rare-earth phase dispersed as spheres.

Uniaxial Compression Tests

Stress-strain curves for the alloys are shown in Fig. 5. As can be seen, the modulus of all alloys increased with increasing stress. Alloys 23, 24, and 25 exhibited a final modulus of 2.9×10^{10} Pa at the highest stress levels. This compares with the value of 4.5×10^{10} Pa measured by Savage, Clark, and Powers[4] in magnetomechanical coupling experiments. Alloy 27 did not attain the degree of stiffness exhibited by the other alloys, its final modulus value being 5.95×10^9 Pa. This allows exhibited ideal elastic-plastic behavior, which is interpreted as grain boundary sliding rather than true plastic deformation of the $Fe_2(Tb_xDy_{1-x})$ matrix.

The compressive fracture strength as a function of the atomic percent excess rare-earth is shown in Fig. 6. Here it can be seen that the strongest alloys contain approximately 1.2% excess rare-earth.

Microhardness Results

In recent years a great deal of progress has been made in assessing the elastic-plastic behavior of materials, particularly brittle materials, by analysis of indentations produced during hardness testing.[8,9] The basic concepts are schematically shown in Fig. 7. It is assumed that the dark region A below the indentor has spherical symmetry that exerts a uniform hydrostatic pressure on the dotted surrounding area B. The region B is considered ideally plastic and constrained by the elastic matrix. If Y is the yield stress of the indented material, then

$$\frac{P_0}{Y} = h\left(\frac{E}{Y}\right)(\text{const}), \tag{4}$$

where P_0 is the mean contact pressure, $h(E/Y)$ is a slowly varying function of E/Y, and E is Young's modulus. Now $P_0 \approx H$, the hardness number, and H, according to Gilman,[9] is related to the shear stiffness on the glide plane G_{gp} by the relation

$$H = 0.167\, G_{gp}. \tag{5}$$

The critical resolved shear stress τ_{gd} is given approximately by

$$\tau_{gp} \approx 0.043\, G_{gp}. \tag{6}$$

[8] B. Lawn and R. Wilshaw, *J. Mater. Sci.* **10**, 1049 (1975).
[9] J. J. Gilman, *J. Appl. Phys.* **46**, 1435 (1975).

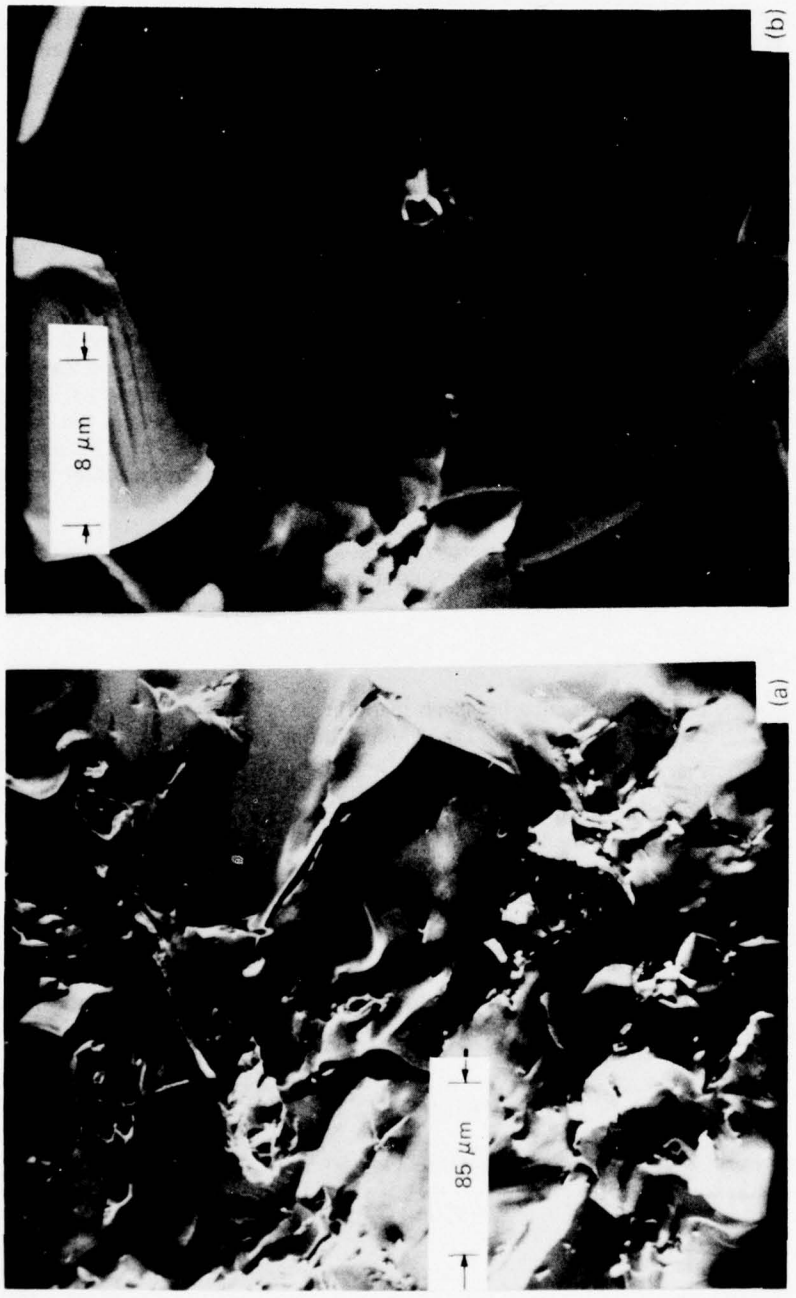

Fig. 3. SEM of the fracture surface of alloy 25 after the 85° C heat treatment. (a) At 240×. (b) At 2,400×

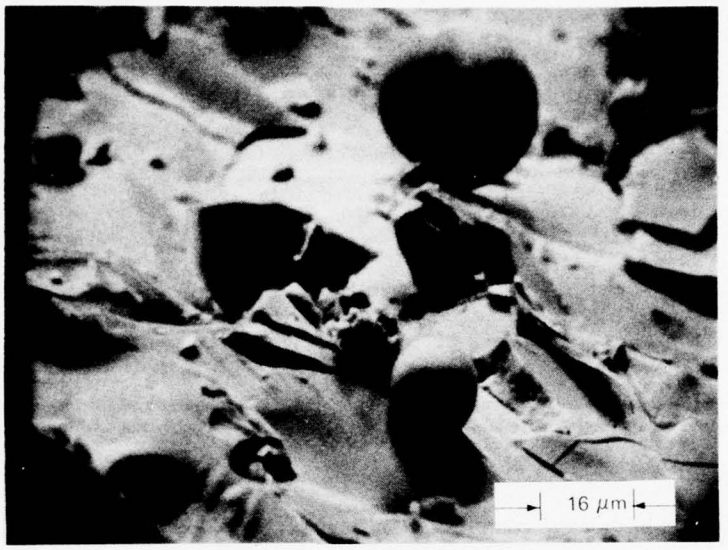

Fig. 4. SEM of the fracture surface of alloy 27 showing the rare-earth phase dispersed as spheres

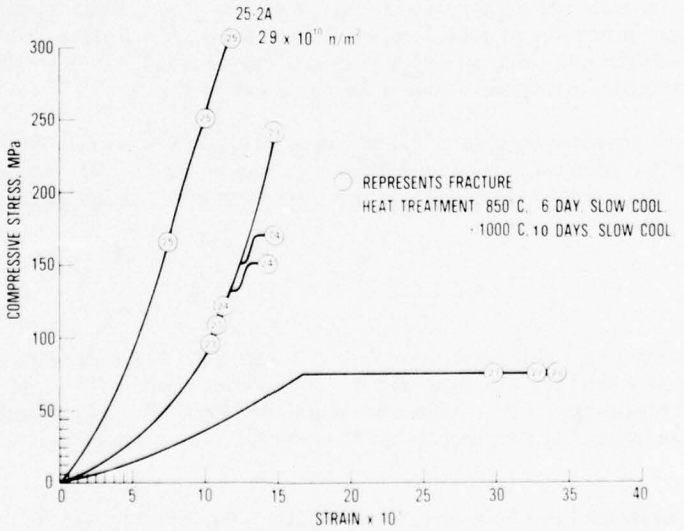

Fig. 5. Stress-strain curves for the $Fe_2(Tb_x Dy_{1-x})$ alloys

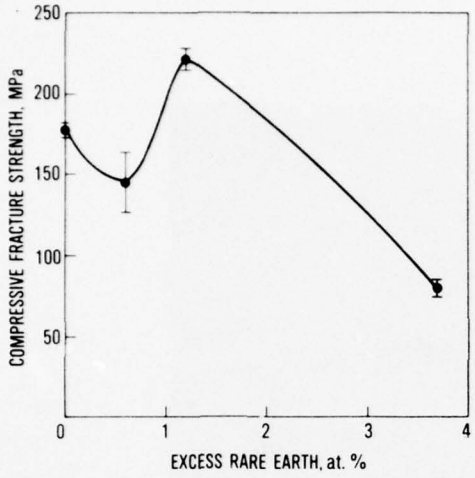

Fig. 6. The compressive fracture strength of $Fe_2(Tb_xDy_{1-x})$ alloys as a function of excess rare-earth content

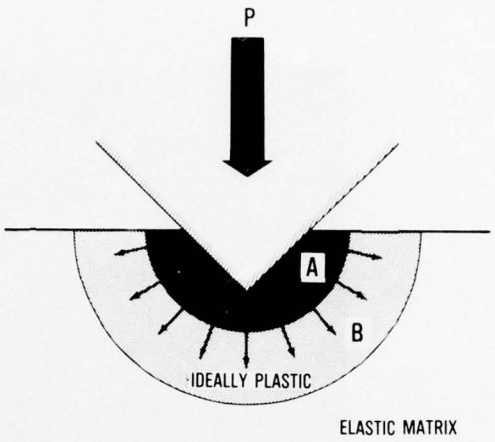

Fig. 7. A schematic of the model for a hardness indentation

Therefore, the yield stress in uniaxial compression σ_y is expected to be, roughly,

$$\sigma_y = 2\,\tau_{gp} \approx 0.515H. \tag{7}$$

Converting units, σ_y = 3,936 MPa for the 780 DPH hardness measured on all the $Fe_2(Tb_xDy_{1-x})$ alloys studied in this investigation. This compares with measured fracture strengths of about 250 MPa for the strongest of the alloys investigated.

A complication that accompanies this type of analysis is that the inelastic material suffers a permanent deterioration during a load-unload cycle. Therefore, a residual stress field remains in the unloaded solid after indentation. This stress field will generally contain significant tensile components that can cause fracture during unloading. Such a case is shown in Fig. 8.

Furthermore, if the indenter engages an existing microcrack in the material during loading, the specimen may fracture before a fully developed impression can be made. The regularity of the impressions observed in this study suggests that this was not a problem even though metallographic observations sometimes revealed microcracks.

Swaging Experiments

Swaging experiments were carried out using rods A-1 and A-2. The rods were spark machined to cylinders of approximately 0.51-cm diameter, and the ends were squared off. Close tolerance holes were drilled into lengths of high-purity, 1.27-cm-diameter aluminum rods. The alloys were fit into the holes and sealed with an aluminum plug that was epoxied into place. The parts of the assembly are shown in Fig. 9.

Two swaging experiments have been completed to date. The first, on rod A-1, was performed cold with the assembly being reduced from 1.27-cm diameter to 0.622-cm diameter in several passes at room temperature. The second experiment was performed warm, with the assembly containing rod A-2 being reduced from 1.27-cm diameter to 1.143-cm diameter in two passes at 350° C. Following the swaging, the assembly was given a stress relief anneal at 500° C for 24 hr in an inert atmosphere and was slow cooled over 48 hr to room temperature.

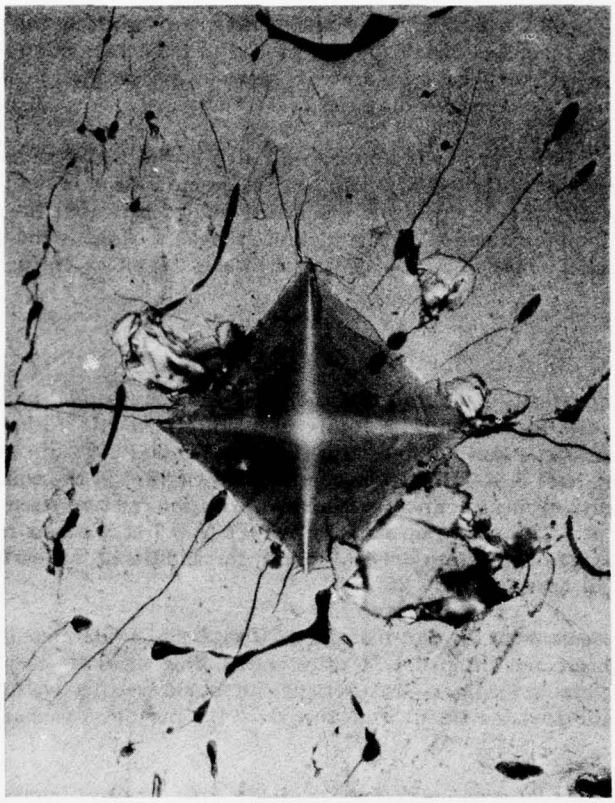

Fig. 8. A photomicrograph of a hardness indentation in alloy 27 (Nital) after the 850° C heat treatment (350X)

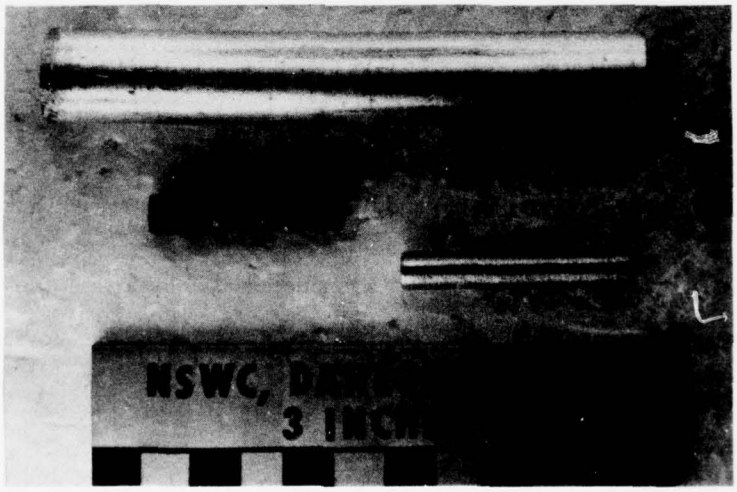

Fig. 9. A photograph showing the parts of the assembly used in swaging experiments

A radiograph of the results of the first swaging experiment is shown in Fig. 10. Some breakup of the rod occurred; however, some sections of the rod swaged to reductions in area in excess of 100% with no signs of internal cracks. A complication did occur, however. When the can was removed, the compressive stresses were relieved, causing the alloy rod to fracture.

The second swaging experiment was performed on rod A-2. In this experiment, the assembly was radiographed before swaging and after each of two passes. Again the rod broke in several pieces, with three fractures occurring after the first pass and one additional fracture after the second pass. Again, swaging was achieved with approximately 15% reduction in area. Following the second swaging pass, the assembly was stress-relief annealed at 500° C for 24 hr and was slow cooled.

DISCUSSION

The results of this investigation indicate that the most probable method of increasing the toughness of off-stoichiometric $Fe_2(Tb_xDy_{1-x})$ alloys is to obtain grain refinement. Although some increase in toughness results from structures that are rare-earth rich, this method is significant only with excess rare-earth concentrations of at least 3 at.%. There is considerable sacrifice in the compressive strength of the material when the rare-earth-element content is increased, with the fracture strengths decreasing from approximately 250 MPa at 1.2% excess rare-earth to 80 MPa at 3.7 at.% excess rare-earth. The strain to fracture, however, increases from 1.2% to only 3.2% with the additional rare-earth. This is equivalent to an increase in toughness of approximately 25%.

The basic problem stems from the fact that the $Fe_2(Tb_xDy_{1-x})$ intermetallic structure is inherently brittle. Fracture strengths on the order of 1/16 of estimated flow stress are observed with cleavage fracture occurring during elastic loading. Grain refinement should be effective in increasing the fracture strength to flow stress ratio to some extent, and, therefore, the resistance to cleavage fracture should increase.[10]

The purpose of the swaging experiments was twofold. First, because fracture does not occur under sufficient hydrostatic compression, swaging the $Fe_2(Tb_xDy_{1-x})$ while encapsulated would demonstrate the plastic properties of the alloys. This was demonstrated. Second, if plastic deformation could be induced, the possibility exists for obtaining grain refinement by recrystallization of the plastically deformed matrix. This possibility is currently being investigated.

CONCLUSIONS

The conclusions derived from this work are as follows:

- Adding excess rare-earth elements to a $Fe_2(Tb_xDy_{1-x})$ matrix toughens the alloys to a limited extent.
- Off-stoichiometric $Fe_2(Tb_xDy_{1-x})$ alloys can be plastically deformed under sufficient hydrostatic compression.
- $Fe_2(Tb_xDy_{1-x})$ alloys fracture by cleavage under uniaxial loads.
- The high-stress elastic modulus decreases by roughly 35% when the alloys are mechanically constrained.

ACKNOWLEDGMENT

This work was supported by the Naval Electronic Systems Command and the Naval Sea Systems Command.

[10] A. S. Tetelman and A. J. McEvily, *Fracture of Structural Materials* (John Wiley & Sons, Inc., New York, 1967), p. 340.

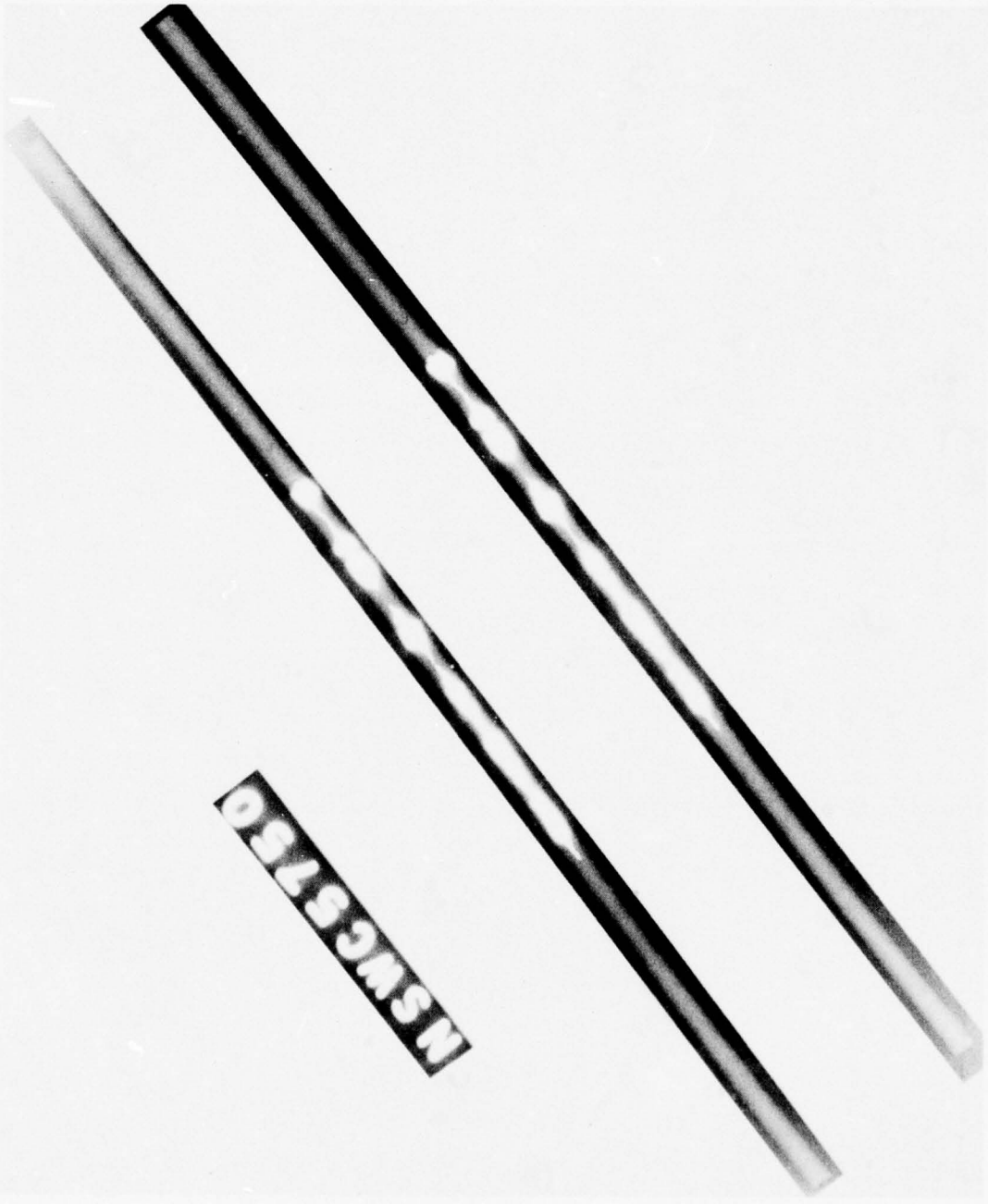

Fig. 10. A radiograph of assembly A-1 following cold swaging

U.S. Navy Journal of Underwater Acoustics Volume 27, No. 1 January 1977

AVAILABILITY AND COSTS OF RARE-EARTH METALS– ESPECIALLY THE HEAVY LANTHANIDES*

K. A. Gschneidner, Jr.
Ames Laboratory-ERDA and Department of Materials
Science and Engineering
Iowa State University
Ames, Iowa 50011

ABSTRACT

All the rare-earth elements fall into the 50th percentile of the abundances of the 83 naturally occurring elements. Projections of consumption patterns, known resources, and expected new rare-earth-element deposits indicate that it would take at least 200 years before a crisis similar to the recent petroleum and natural gas "shortage" would occur in the rare-earth industry. The cost of rare-earth materials has been on a downward trend for many years, but a leveling off and some increases have been seen in recent years. Future costs depend upon inflation and demand. Substantial decreases could result if a large market developed for one or two of the heavy lanthanide metals.

ABUNDANCES

The abundances of about half the 83 naturally occurring elements[1] are shown in Fig. 1, and it is seen that the 16 rare-earth elements† fall into the 50th percentile. Ce, Cerium, which is the most abundant, ranks 28th and thulium, Tm, the least abundant, ranks 63d. Collectively, if the rare earths were considered as one element, they would rank as the 22d most abundant (the demarcation line of the 75th percentile lies between the 21st and 22d elements). As a whole the heavy lanthanides, Gd to Lu, are less abundant than the light lanthanides, La to Eu, and thus are usually more expensive. Furthermore, the even atomic number metals (Ce, Nd, Sm, Gd, Dy, Er, and Yb) are more abundant than their neighboring odd atomic number elements (La, Pr, Pm (which is radioactive), Eu, Tb, Ho, Tm, and Lu). These variations will show up in the prices of the metals, which will be discussed later.

Thus, just from a point of view of abundances, one would be tempted to conclude that there are no availability problems with the rare earths, as there are many common elements (Hg, Cd, I, and Se, for example) less abundant and several more (W, Mo, Sn, Ge, and Pb) just as abundant. But there are other factors that also need to be considered: whether there are viable deposits, the amount of rare earths available in these deposits, and their current and projected consumptions.

CONSUMPTION

In 1973 the worldwide consumption was 27,000 metric tons of rare-earth oxide equivalent, and the known deposits contained at least 17 million metric tons of oxide. If the world consumption remained constant in the 1973 level, it would take about 625 years to use up these known deposits, assuming

*Presented at the Workshop on Magnetostrictive Materials held under the sponsorship of the Underwater Sound Advisory Group and the Naval Research Laboratory, Orlando, Florida, 25-26 February 1976.

†Further discussion of the rare-earth metals is given by Dr. Timme in his Introduction to the Theme in this issue.

[1]V. V. Cherdyntsev, *Abundances of Chemical Elements* (Univ. of Chicago Press, Chicago, 1961).

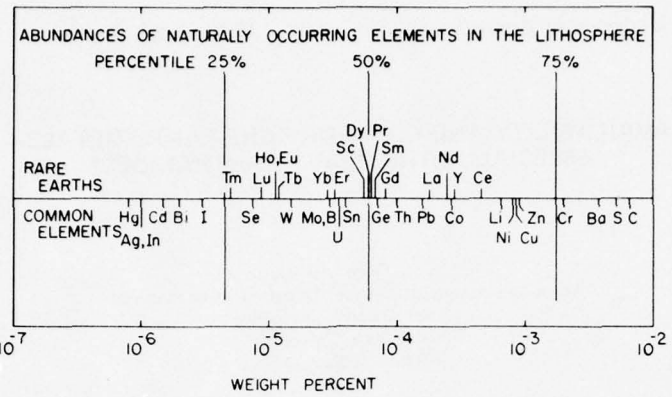

Fig. 1. The abundances of some of the 83 naturally occurring elements. For clarity the 12 most abundant elements, the 14 least abundant elements, and a few others in between have been omitted.

there would be no recycling of used rare-earth elements. But because the rare-earth consumption has increased at an annual rate of about 15% from 1965 through 1975 (the growth rate was about 20% through 1973, but the worldwide recession of the last 2 years has reduced this growth), one can easily show that all the rare-earths would be consumed by 2019 if the growth rate remained constant at 15%, if no recycling occurred, and if no discoveries of new rare-earth deposits were found. In approaching the end of the rare-earth supply, the first two assumptions would no longer hold. That is, the growth rate would level off and decrease and recycling would be prevalent, thereby pushing back the predicted "day of exhaustion." Finally, the last assumption is also incorrect, because new deposits are being found and will continue to be discovered for many years to come as the use of the rare-earth elements continues to grow. Indeed, between 1970 and 1974 the known resources in the world increased by 83%. Furthermore, these figures do not include mainland China, according to recent information published in Peking has the largest known deposits of the rare-earth elements in the world.[2]

All realistic projections indicate that the rare-earth industry is at least 200 years away from a crisis similar to that experienced by the world in its use of petroleum and natural gas. And the "day of exhaustion" is still beyond that.

Although the consumption of the rare earths is in the tens of thousands of tons per year, about 99% by weight of the rare-earth elements used is in the mixed or unseparated form, while 1% by weight is used as individual elements. In dollar amounts, the two (mixed versus separated) are about equal.

The nature of rare-earth applications is changing rapidly. In Fig. 2 it is seen that more than 50% of the rare-earth-element usage in the early 1970's is based on new developments since 1960 (shaded areas in the figure). Furthermore, a large change in the relative portions of the various markets occurred between 1970 and 1972. Although the fraction of the total market has decreased for glass polishing compounds and catalysts, the actual consumption for both increased in terms of the total amount of oxide sold. These rapid changes in the nature of the rare-earth markets also adds to the uncertainty of any projections one attempts to make about future trends.

RARE-EARTH SOURCES

The two major sources of the rare-earth elements are bastnasite (a fluorocarbonate) and monazite (a phosphate). Most of the bastnasite used in this country comes from Mt. Pass, Calif., which is 55 miles (88 km) southwest of Las Vegas, Nev. Monazite comes from beach sands (India, Brazil, and Australia) and as a byproduct from ilmenite mining in the southeastern part of the United States. The rare-earth distribution in these minerals is shown in Table I. It is seen that both these ores have low

[2] *RIC News* 11(1) (Rare-Earth Information Center (RIC), Iowa State University, Ames, Iowa 50011, Mar. 1976). [A brief summary is given in *RIC News*; the complete article (in English) is available from RIC and may be obtained by writing the center requesting a copy of "China Develops Rare Earth Industry."]

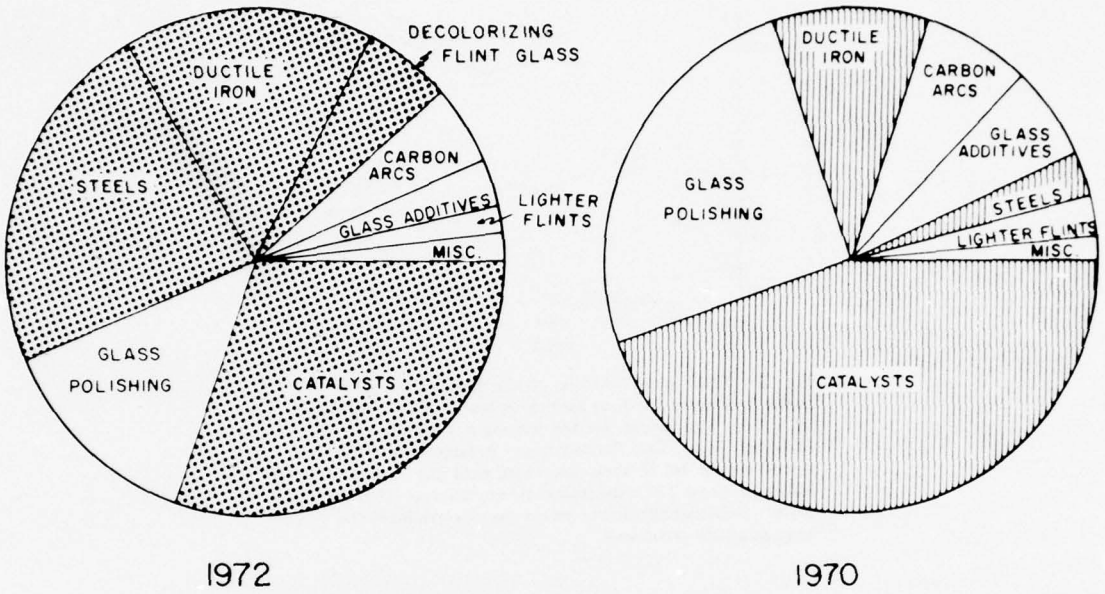

Fig. 2. Consumption of rare-earth elements in 1970 and 1972. The shaded areas are new major developments since 1960.

TABLE I
Rare-Earth Content of Source Minerals[a]

Rare Earth Element	Bastnasite, California (%)	Monazite, South Carolina (%)	Xenotime, Malaysia (%)	Uranium Residues, Ontario, Canada (%)
La	32.0	19.5	0.5	0.8
Ce	49.0	44.0	5.0	3.7
Pr	4.4	5.8	0.7	1.0
Nd	13.5	19.2	2.2	4.1
Sm	0.5	4.0	1.9	4.5
Eu	0.1	0.17	0.2	0.2
Gd	0.3	2.0	4.0	8.5
Tb	0.1	0.2	1.0	1.2
Dy		1.3	8.7	11.2
Ho		0.1	2.1	2.6
Er		0.5	5.4	5.5
Tm		—	0.9	0.9
Yb		0.2	6.2	4.0
Lu		—	0.4	0.4
Y	0.1	3.0	60.8	51.4

[a]From Ref. 3.

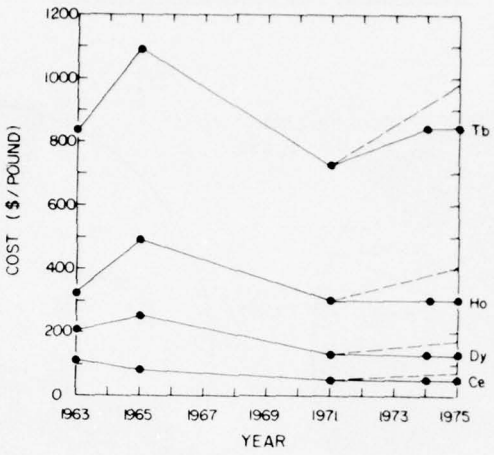

Fig. 3. The prices of one of the major rare-earth metal producers for four rare-earth metals from 1963 to 1975. The prices are for the ingot forms in 1-lb (0.45-kg) lots. The dashed lines indicate what the prices would be if they has risen with the rate of inflation since 1971 assuming an annual rate of 8%. Note: Substantially lower prices may be available for large quantity purchases.

concentrations of the heavy lanthanides and yttrium; generally they are not processed as a source material for the heavy lanthanides and yttrium (Y), although monazite is richer in these elements than bastnasite by a factor of about 15.

The major sources of the heavy lanthanides and yttrium are xenotime (a phosphate) and uranium mine tailings. The largest xenotime mining operation is in Malaysia, and the rare-earth elements obtained as byproducts from uranium mining come from Canada. The rare-earth-element distributions in these two sources are also given in Table I. The estimated reserves of the light rare earths in the United States are about 50% of the world's known resources (exclusive of mainland China), but those of the heavy lanthanides[3] constitute only 12%.

PRICES

The prices of rare-earth materials decreased significantly in the 1950's, and somewhat more gradually during the 1960's, but essentially remained constant in the 1970's. The large drop in prices in the 1950's occurred because the rare earths were being separated commercially for the first time on a large scale during the decade. In the 1960's the prices approached their minimum values as production, efficiency, and competition all increased. The variation in prices for four rare-earth metals (cheap: Ce; expensive: Tb; and intermediate: Ho and Dy) from 1963 to 1975 is shown in Fig. 3. If one takes into account inflation (dashed lines in Fig. 3), the rare-earth metals are actually cheaper in relation to the relative worth of the dollar today than they were in 1971. The prices in Fig. 3 are for the ingot form. The prices for other forms (such as powder, chips, and distilled) vary, generally upward. A more complete list of the current range of prices for the ingot and distilled forms is given in Table II. In general, the distilled metal is purer than the ingot. The heavy lanthanides, Y, and Sc (scandium) dissolve appreciable amounts of Ta (tantulum) when they are prepared, and they can be purified from Ta by distillation. The light lanthanides, La, Ce, Pr, and Nd, do not dissolve nearly as much Ta and thus do not need to be purified by distillation. That is indeed fortunate because they have very low vapor pressures, and

[3]"Trends in Usage of Rare Earths." National Materials Advisory Board, National Research Council Report NMAB-266 (Oct. 1970).

TABLE II
Range of Current Prices of the Rare-Earth Metals[a]

Rare Earth Element	Ingot ($/lb)	Distilled ($/lb)
La	50 - 160	[b]
Ce	50 - 160	[b]
Pr	170 - 310	[b]
Nd	110 - 230	[b]
Sm	155 - 530	145 - 460
Eu	3,000 - 5,530	2,500 - 5,050
Gd	220 - 460	1,050
Tb	850 - 1,610	1,600 - 2,520
Dy	130 - 500	300 - 560
Ho	300 - 800	700 - 1,020
Er	160 - 480	380 - 620
Tm	2,600 - 6,050	2,400 - 5,500
Yb	240 - 500	225 - 440
Lu	6,000 - 11,100	12,480 - 23,700
Sc	3,000 - 6,420	5,500 - 5,850
Y	150 - 330	770 - 1,140

[a]Claimed by vendor to be 99.9% pure. This generally means with respect to all metallic impurities only. In some cases this may mean only with respect to other rare-earth elements. The presence of nonmetallic impurities are usually not specified. Note: Substantially lower prices may be available for large quantity purchases.
[b]Not distilled.

distillation temperatures would have to be above 2,000° C. Although rare-earth metals are available as chips and powders, the author does not recommend the purchase of the metals in these forms because the rare-earth metals oxidize quite readily, especially the first four, La, Ce, Pr, and Nd, and the powder and chips may have an appreciable oxide content (up to as high as 50%). If one needs powders or chips it would be better to purchase the ingot or distilled form and then form the powders or chips in an inert atmosphere (He or Ar) just before use.

It is difficult to predict future prices, but with continued inflation there is little likelihood of any decreases in prices. Most likely they will rise, but probably at a slower rate than the rate of inflation. If a large demand for the heavy rare-earth oxides developed, a substantial decrease in the price of the oxide would result, but this would cause only a minimal reduction in the price of the metal. In general, the oxide cost is 1/2 to 1/3 of the ingot metal price and 1/4 to 1/8 of the distilled metal price. For the heavy lanthanides this translates into a $100 to $350 cost to prepare 1 lb (0.45 kg) of metal in the ingot form and a $250 to $1,000 cost to prepare the same amount of distilled metal. For the very expensive rare-earth metals, Sc, Eu, Tm, and Lu, the metal-making costs are much higher. If, however, a large demand arises in the future for the heavy rare-earth metals, a significant decrease in the price could be realized if the process was scaled up for more efficient operation. Indeed, both the oxide and metal price would fall, leading to a "double" reduction. A large-scale production operation (1 to 10 lb (0.45 to 4.5 kg) per day) could lower the price to about $50 per pound ($111 per kilogram) for preparing the metal in the ingot, and perhaps to as low as $100 per pound ($222 per kilogram) of distilled metal. Large price reductions for the light lanthanides are not as likely because La and Ce are being manufactured on a fairly large scale already.

This analysis is based on the assumption that the demand for the rare earths is "unbalanced." By "unbalanced," it is meant that a particular rare-earth element is produced by itself to meet a certain market without assured sales of associated rare-earths. In general, this is the condition of today's market.

If, however, the demands should become "balanced," all the individual elements would bear the cost of separation from one another, and, as a result, the oxide costs might be reduced by an additional 25% to 50%. In general, such a market situation would be unusual and is not likely to occur. If it should occur it would not be likely to remain that way for long because of new technological changes and advances involving rare-earth materials.

ACKNOWLEDGMENT

The author wishes to thank B. L. Evans and J. G. Cannon for their critical comments and valuable discussions. This paper was prepared for the U.S. Energy Research and Development Administration under Contract No. W-7405-eng.-82.

U.S. Navy Journal of Underwater Acoustics Volume 27, No. 1 January 1977

DEVELOPMENT OF TWO RARE-EARTH TRANSDUCERS*

John L. Butler† and Stanley J. Ciosek
Raytheon Company
Submarine Signal Division
Portsmouth, Rhode Island 02871

ABSTRACT

The results of our development on a piston-and-ring-type rare-earth transducer are presented. Both were made from Terfenol D rods and were designed for low-power operation. A comparison of the rare-earth piston transducer with a similar piezoelectric design showed that although the efficiency is somewhat less for the rare-earth model, it has approximately the same coupling coefficient and a lower resonant frequency for the same size.

INTRODUCTION

The large coupling coefficient and large potential displacement of rare-earth‡ magnetostrictive material make it attractive for underwater sound applications. As an initial step, we have developed two low-power rare-earth transducers in the form of a tonpilz and a ring. These forms are the most common ones in use in underwater acoustics and allow a comparison with transducers currently using piezoelectric material. Accordingly, we have also constructed a tonpilz of the same size as the rare-earth model but with piezoelectric ceramic as the driving element.

The magnetostrictive material is presently available in the form of rods as shown in Fig. 1. The rare-earth material used is Terfenol D ($Tb_{0.3}Dy_{0.7}Fe_2$).[1] The center bar was machined from the rather rough oval shaped bar shown above. The shorter but circular rod, shown below, required machining only at its two ends. Our task was to construct underwater sound transducers using this material.

As a first step, we wrapped a coil of wire around the oval bar and resonated it in air and water using the circuit in Fig. 2 for separating the dc bias current from the ac signal. The inductor L blocks the ac signal, and the capacitor C blocks the dc bias. Impedance measurements on the machined rod at longitudinal resonance confirmed that the speed of compressional waves in the rod is 2,300 m/s. This low velocity along with its density of 9,100 kg/m^3 yields a characteristic impedance of 20.9×10^6 mks rayls, much like that of the piezoelectric ceramic.

*Presented at the Workshop on Magnetostrictive Materials held under the sponsorship of the Underwater Sound Advisory Group and the Naval Research Laboratory, Orlando, Florida, 25-26 February 1976.
†Consultant for Raytheon Company.
‡A brief discussion of the rare-earth metals is given by Dr. Timme in his Introduction to the Theme in this issue.

[1]This material was supplied to us by Dr. Arthur E. Clark of NSWC, Silver Spring, Md.

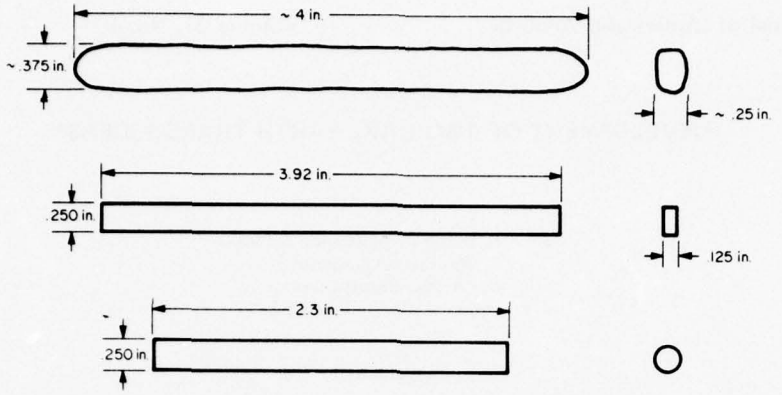

Fig. 1. Rare-earth iron alloy elements, Terfenol D, $Tb_{0.3}Dy_{0.7}Fe_2$

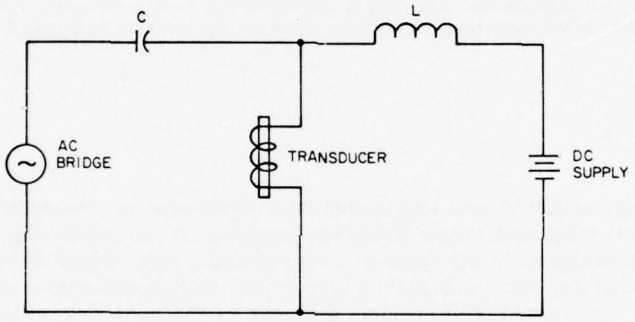

Fig. 2. Measurement circuit for transducer

TONPILZ TRANSDUCER

Construction

The lumped equivalent circuit of a magnetostrictive tonpilz transducer may be represented as shown in Fig. 3. The electromechanical turns ratio Z_{em} is equal to the product of the magnetostrictive constant h_{33} and the clamped core inductance L_0 divided by the total number of turns N. With this frequency-independent ideal transformer, the masses M and m become capacitors and the compliance becomes an inductor. Also, the equivalent radiation resistance is given by the reciprocal of the actual value. Some of the electrical losses may be represented by a resistor shunting the input.

Because the material is not presently available in laminations, the transducer was designed for low-frequency operation to keep the eddy-current losses small. The tonpilz design is shown in Fig. 4. Because these magnetostrictive legs are rather fragile, the transducer was initially assembled with a pliable cement along with a thin stress rod, enabling a series of design modifications without fracture.

The dimensions of the element are 6.15 in. (15.6 cm) in length with a rectangular radiating face 2 by 1 in. (5 by 2.5 cm). The tail mass-to-head-mass ratio is approximately four to one, and both were made of aluminum. The mass of the head (46 g) was chosen to resonate the transducer at 3.5 kHz. The resulting head-to-leg area transformation ratio is 32 for the 0.5-in. (1-cm) thick head. A smaller area transformation would have reduced the radiation area too much. With a the radius of an equivalent circular piston, the size parameter ka at resonance is approximately 0.3, which leads to a small but measurable radiation resistance (0.045 ρc per unit area).

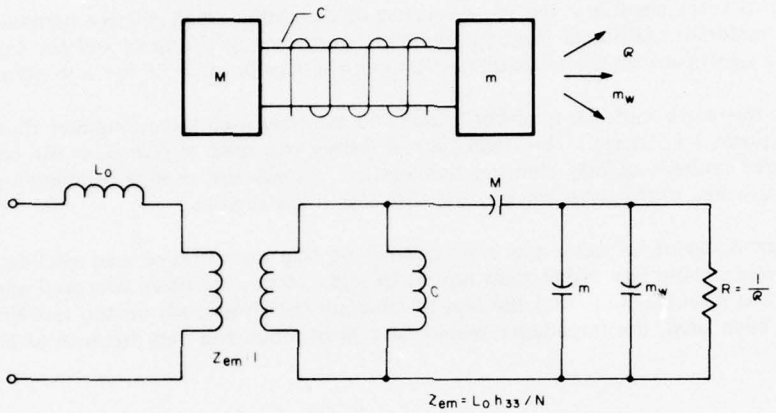

Fig. 3. Equivalent circuit of tonpilz transducer

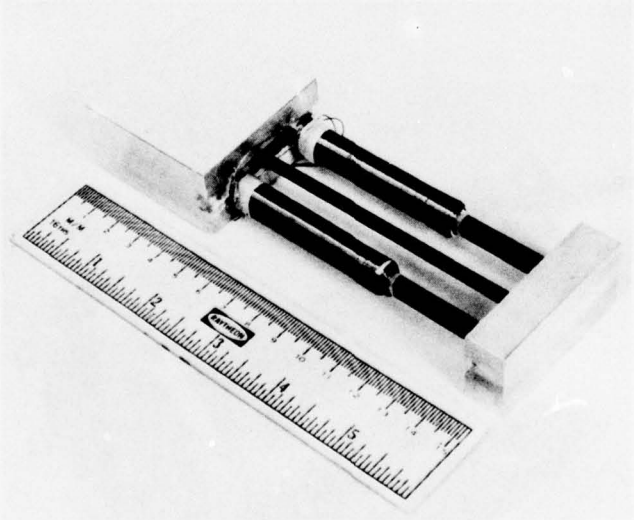

Fig. 4. Rare-earth iron tonpilz transducer

The choice of the coil length was a result of a series of measurements of the coupling coefficient and the mechanical Q. Although the plastic coil former was only in contact with the edges of each leg, there was excessive frictional loss when the entire length of the leg was covered. Because of this some of the coupling coefficient was sacrificed and a length of only 2.25 in. (5.72 cm) of the leg was covered with the six layers of No. 28 Formvar coated wire, with 860 turns on each leg.

The number of turns necessary was large because of the rather small relative permeability (approximately 5) of the material. Although magnetic couplers were used at the head and the tail ends of the legs, there was no significant magnetic coupling between the legs because of the low permeability.

Because this rare-earth material is rather brittle and the bars used were long and thin, great care was necessary to prevent breakage. The small tie rod shown was used to compress the unit while the epoxy cement cured under a slightly elevated temperature. It was not used to provide a significant compressive bias because this might have cracked the thin legs if misaligned.

A tonpilz transducer of the same size was constructed that consisted of lead zirconate titanate piezoelectric ceramic driving legs rather than rare-earth legs. Here a 31 drive was used and a proportional amount of silver was disconnected from the legs to simulate the short coils on the rare-earth transducer. If a 33 drive had been used, the impedance would have been much too high because of the shape factor.

Measurements

The transducers were each fitted into a heavy aluminum cylindrical housing shown in Fig. 5. An aluminum faceplate mask with a rectangular slot for the transducer head was used to prevent a pressure release (1.6 mm) condition. This entire front end was made watertight with a 1/16-in. neoprene rubber window. The tail mass and edge around the transducer face was isolated from the housing by corprene pads. Measurements were made with 0.5-A dc polarizing current. The beam pattern at 3.2 kHz in a plane through the long edge of the rare-earth transducer piston is shown in Fig. 6. The pattern is nearly omnidirectional because of the small size of the transducer piston, which is only one-tenth of a wavelength at these frequencies.

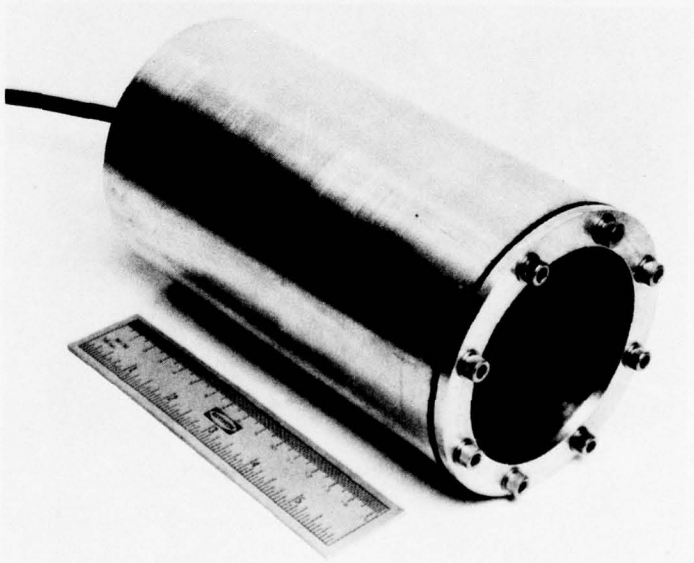

Fig. 5. Tonpilz transducer in pressure housing

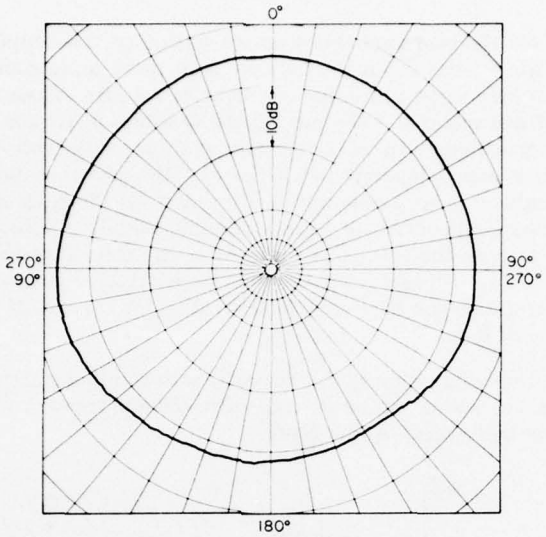

Fig. 6. Directivity pattern for tonpilz transducer at 3.2 kHz

The air and water impedance loci of the magnetostrictive transducer are shown in Fig. 7. As can be seen, there is considerable water radiation loading even though the transducer head is small compared to the wavelength of sound. The air resonance frequency is 3.6 kHz while the water-loaded resonance is 3.2 kHz. The mechanical Q values in air (Q_{mA}) and water (Q_{mW}) are 14.3 and 4.4, respectively, and the electrical Q in air (Q_{eA}) is 0.73, leading to an effective coupling coefficient of $k = 0.3$ from the formula

$$k = \frac{1}{\sqrt{1 + Q_{mA} Q_{eA}}} .$$

From the water and air resistance values, the estimated losses are one-third mechanical, one-third electrical loss in the No. 28 wire coil, and one-third hysteresis and eddy-current loss, leaving an overall efficiency of 30%.

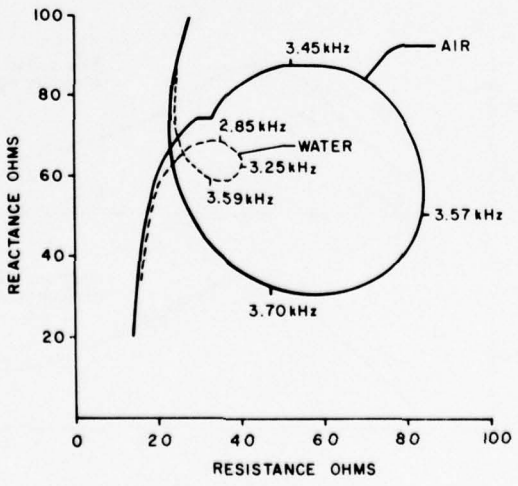

Fig. 7. Impedance loop near resonance for rare-earth iron tonpilz transducer

The admittance loci for the lead zirconate titanate version of this tonpilz are shown in Fig. 8, and except for the dip and displacement in Fig. 7, they are seen to be quite similar. Here, however, the air resonance frequency is 4.6 kHz while the water resonance is 4.4 kHz. These higher resonances are due to the higher sound speed of this material. The mechanical Q values in air and water are 32.7 and 9.2, respectively, which are approximately in the same ratio as those of the rare-earth transducer. From the Q_m values, this transducer is approximately 70% efficient. The two transducers have essentially the same mechanical losses, and the major reduction in efficiency for the magnetostrictive transducer is due to electrical losses. The coupling coefficient for the ceramic tonpilz is 0.18, which is due to its use of only part of the silver surface on the legs. For the case of complete silvering, the value of the coefficient was measured to be 0.24. Thus, if a full coil had been used for the magnetostrictive transducer, the coupling coefficient would be the measured value of 0.3 (for the partial coil) times the ratio 0.24/0.18, yielding a value of 0.4.

The transmitting and receiving responses for the rare-earth transducer are shown in Fig. 9. As can be seen from these responses, the results in the vicinity of resonance appear to be quite similar to those of sonar transducers currently being used by the Navy.

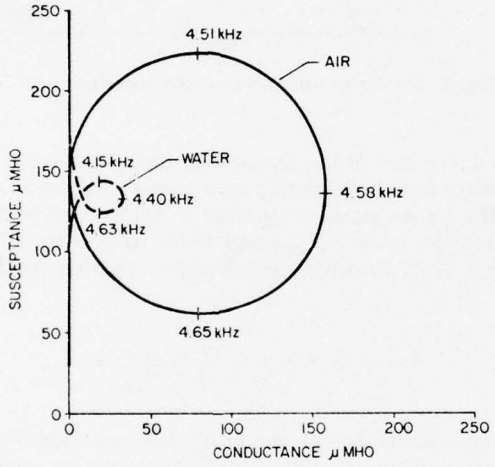

Fig. 8. Admittance loop near resonance for ceramic transducer

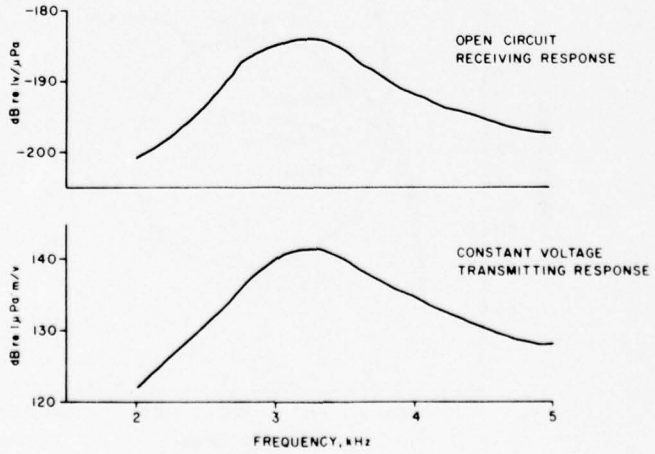

Fig. 9. Receiving sensitivity and transmitting response for rare-earth iron tonpilz transducer

The unit was driven with an ac current value up to one-half the dc bias value of 0.5 A with no significant nonlinear distortions. The corresponding responses for the ceramic unit are shown in Fig. 10. Here at resonance, the receiving sensitivity is 13 dB greater, but the transmitting value is down 20 dB for the same voltage. The receiving responses of the ceramic below resonance approach a flat condition while the rare-earth transducer response falls off at approximately 6 dB per octave. Above resonance, in the mass-controlled region, the rare-earth transducer approaches a flat transmitting response up to 10 kHz, except for a small variation in the vicinity of 6 kHz.

RING TRANSDUCERS

Piston transducers are usually combined as an array to form a unidirectional beam. Ring transducers are often coaxially stacked to yield a narrow beam in a plane through their axis and omnidirectionally in the perpendicular plane. The square ring transducer is shown in Fig. 11 and was constructed from four Terfenol D rods 1/4 in. (6 mm) in diameter with a length of 2.3 in. (5.8 cm). The mean diagonal distance of the ring is 4.0 in. (10.2 cm). The end connecting pieces are soft iron, and the wire is No. 28 with 750 turns for each leg. There is a screw hole in each end piece for attachment of interior stress wires and an exterior set of radiating pistons or cylinders. One advantage to this design is that the magnetic path from one end of the rod is more strongly coupled to the other end. With more rods, a larger ring and a better approximation to a ring could be made.

Surprisingly enough, however, this shape does conform to the resonance condition for a thin ring. If it were a pure ring, the fundamental ring resonance would be given by $f = c/\pi D$, where c is the sound speed and D the diameter. With c = 2,300 m/s and using D = 4 in. (10 cm), a resonance of 7.2 kHz is calculated. The air impedance locus of this ring is shown in Fig. 12, where it is noted that the resonance is 7.4 kHz. From this locus the mechanical and electrical values of Q are 7.44 and 0.67, respectively, yielding a coupling coefficient of 0.41. In this transducer design, full-length coils were used, yielding a high coupling coefficient but a low Q_{mA}.

The bias current for this locus was 0.7 A dc. A series of loci were taken from 0.1 A bias up through 0.8 A, at which time the ring became quite warm. From these curves the mechanical quality factor Q_{mA} and the electrical quality factor Q_{eA} were determined, and the effective coupling coefficient was calculated. These results are shown in Fig. 13. It can be seen here that the maximum coupling coefficient is essentially reached at 0.8 A. At low bias levels both values for Q begin to increase rapidly. The mechanical Q nearly doubles, indicating that half of these losses at large bias levels could be due to eddy currents unless the heating of the coil is introducing additional frictional losses.

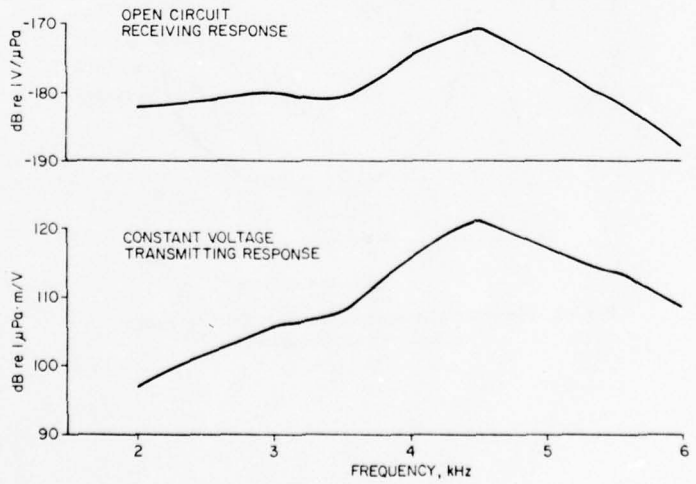

Fig. 10. Receiving sensitivity and transmitting response for ceramic tonpilz transducer

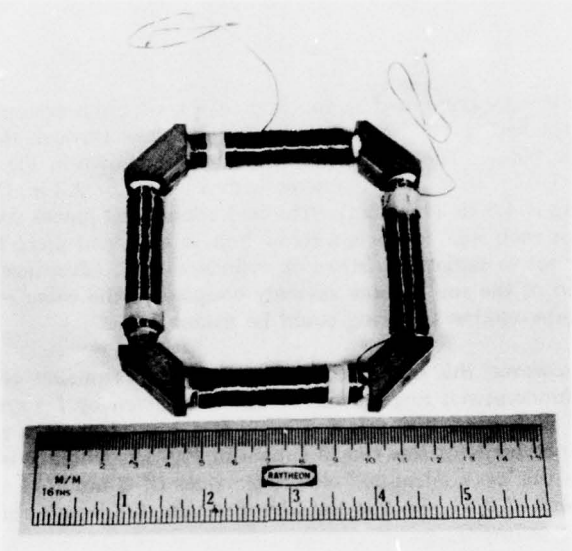

Fig. 11. Rare-earth iron square ring transducer

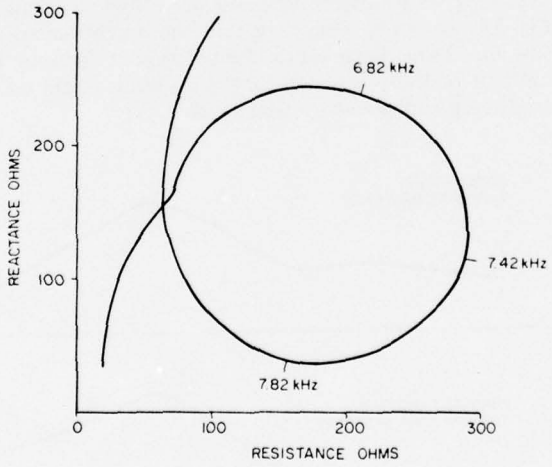

Fig. 12. Impedance loop near resonance for a rare-earth iron square ring transducer

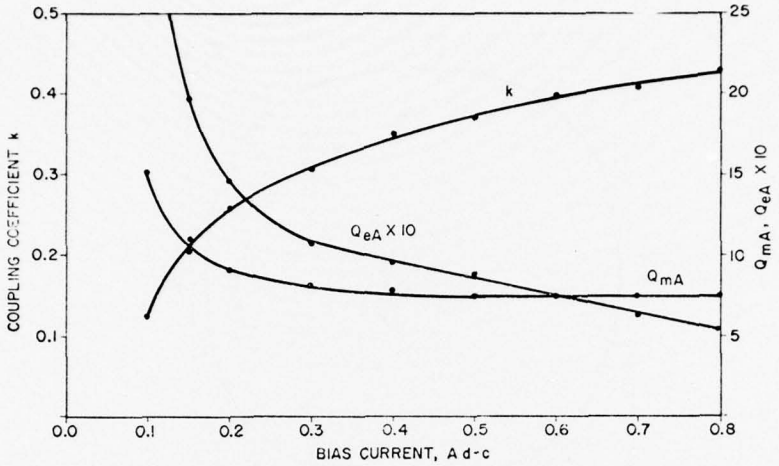

Fig. 13. Coupling coefficient and Q for the rare-earth iron square ring transducer

The ring transducer described is not an effective radiator because of its small surface area and the coils surrounding the rods. This loading can be improved by enclosing the ring with four curved pistons attached to the four connecting corner pieces.

Measurements, however, have been made for the square ring under free-flooded conditions with a 0.7-A bias. The beam pattern at resonance in the plane of the ring is shown in Fig. 14. The zero angular direction is along a line diagonally through two end pieces. The reduction here is presumably due to the acoustic phase difference over this distance. The pattern in a perpendicular plane was typical of free-flooded rings. The transmitting and receiving responses are shown in Fig. 15. The flat receiving response above resonance is consistent with the dipole-type radial motion of a free-flooded magnetostrictive ring.

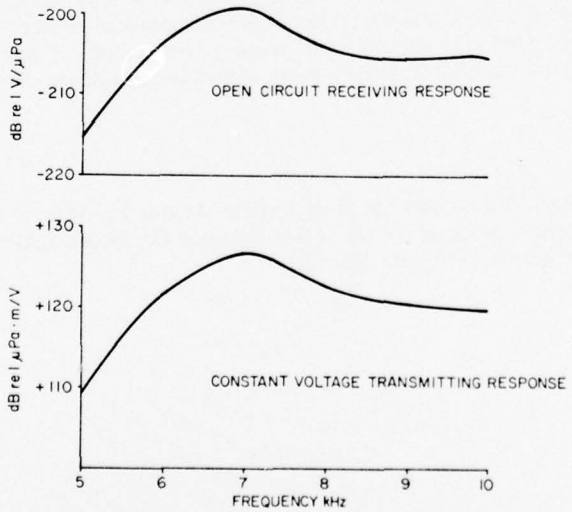

Fig. 14. Directivity pattern for a rare-earth iron square ring transducer at 6.8 kHz

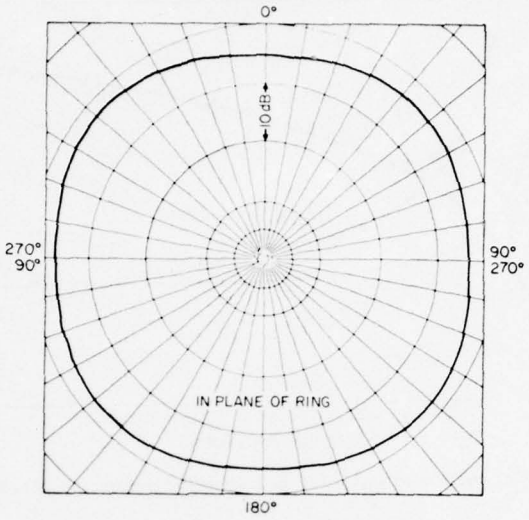

Fig. 15. Receiving sensitivity and transmitting response for a rare-earth iron square ring transducer

SUMMARY

We have presented results on two rare-earth low-powered transducers. The results indicate that a coupling coefficient on the order of 0.45 is attainable and that when compared to a ceramic transducer, the rare-earth transducer has a significantly lower mechanical Q and resonance frequency. Unfortunately, the efficiency was somewhat lower for our design; however, it is anticipated that this can be improved by use of a procedure similar to laminating, and also by adjusting the mechanical loading so that its electrical equivalent resistance is considerably greater than the losses in the coil.

Although the shapes and sizes of the two transducers presented here are somewhat uncommon, this is partly a result of the available sizes and shapes of the rare-earth material rather than wholly the result of its properties. We believe the next step should be to build a medium-power underwater transducer using considerably more rare-earth material in shapes more suited to transducer design.

ACKNOWLEDGMENTS

We would like to thank Stan Ehrlich of Raytheon and Dr. Arthur E. Clark of NSWC for their helpful discussions. This program was sponsored by Naval Sea Systems Command under Contract No. N 000 24-75-C-6137; C. Walker was the Program Manager.

U.S. Navy Journal of Underwater Acoustics Volume 27, Number 1 January 1977

DESIGN OF A TRANSDUCER USING RARE-EARTH MAGNETOSTRICTIVE MATERIALS*

Robert R. Smith and James C. Logan
Naval Undersea Center
San Diego, California 92132

ABSTRACT

This paper presents a transducer design with its conventional active ceramic element replaced by rods of the rare-earth magnetostrictive material Terfenol D. The major objective of this design is to allow a side-by-side comparison of piezoelectric ceramic and Terfenol D in an identical transducer. The transducer used is a small "folded-horn" unit designed by W. Angeloff of NUC. It was selected for two reasons. First, the dimensions are ideal for replacing the ceramic stack with two Terfenol D rods (currently available in only limited sizes) and their associated solenoids. Second, this source is strain- or electric-limited. Rare-earth magnetostrictive materials are expected to compare most favorably with piezoelectric ceramic for this type of transducer because of their larger ultimate strain. The details of the design of the magnetostrictive drive unit are presented, along with calibration results of a prototype transducer. The magnetostrictive unit exhibits less overall bandwidth and lower maximum output level than its piezoelectric counterpart, but has the desirable feature of resonating at lower frequencies. Based on the results from the prototype, recommendations are made for a future design that should improve maximum acoustic output and efficiency.

INTRODUCTION

This paper presents the rationale for a particular active transducer design that uses rare-earth† magnetostrictive material. Preliminary acoustic measurements are also presented, as well as a discussion of the results and recommended further work.

The purpose in conducting this work is to evaluate the rare-earth materials as replacement for piezoelectric ceramic for certain transducer types. A major advantage of the rare-earth compounds such as Terfenol D is the large ultimate strains that can be achieved. Savage, Clark, and Powers[1] report ultimate strains greater than 1,000 parts per million (ppm) for the compound $Tb_{0.28}Dy_{0.72}Fe_2$ (Terfenol D). A typical ceramic such as PZT-4 driven at maximum recommended electric field can produce a strain of only about 200 ppm peak to peak. Even though the rare-earth compounds may have other advantages over ceramic, it was decided to exploit the property of large magnetostrictive strain.

Based on these considerations, a survey of candidate transducers suitable for conversion to magnetostrictive drive was conducted. The following constraints were imposed in choosing a transducer design:

- The magnetostrictive material to be used was Terfenol D, available only in rods with 0.25-in. (0.635-cm) diameter and 2.4-in. (6.1-cm) length.

*Presented at the Workshop on Magnetostrictive Materials held under the sponsorship of the Underwater Sound Advisory Group and the Naval Research Laboratory, Orlando, Florida, 25-26 February 1976.

†A brief discussion of the rare-earth metals is given by Dr. Timme in his Introduction to the Theme in this issue.

[1]H. T. Savage, A. E. Clark, and J. M. Powers, "Magnetomechanical Coupling and ΔE Effect in Highly Magnetostrictive Rare Earth-Fe_2 Compounds," *IEEE Trans. Magn.* **mag-11**, 1355 (1975).

- The design was to be similar to an existing piezoelectric transducer, preferably only replacing the ceramic element with magnetostrictive material.

- The design was to allow high-drive levels for a comparison of maximum source level with piezoelectrics.

- The source was to be a strain-limited or voltage-limited device to take advantage of the added strain available from the magnetostrictive material.

This type of limitation is normally found in a low-frequency transducer. The most suitable transducer for conversion was found to be a "folded-horn" transducer, originally designed by W. Angeloff of the Naval Undersea Center. The transducer is a multiresonant device intended to operate in the band from 3 to 15 kHz. Although this band of operation is not low frequency, larger units of the folded-horn design can operate down to 100 Hz. The maximum drive is limited by the depolarization voltage. As shown in Fig. 1, the transducer consists of two bell-shaped housings placed end to end with a small air gap between the housings that is covered with a thin elastomer seal. A piezoelectric ceramic stack of rings normally extends the length of the transducer, with an internal stress member attached to the end of each housing to provide pre-stress.

The conversion of this design to magnetostrictive drive is described in the following section. Also given in this paper are some preliminary calibration results of a prototype unit. Although these results do not conclusively demonstrate the superiority of Terfenol D as a drive element for this transducer, they do indicate potential advantages of magnetostrictive drive. The results further suggest design changes that would improve the transducer performance, and these changes are summarized in the conclusions.

MAGNETOSTRICTIVE TRANSDUCER DESIGN

The basic design for the magnetostrictive drive element in the folded-horn transducer is shown in the cutaway schematic in Fig. 2. Unlike the piezoelectric design, there is no net pre-stress between the two housings. In the new design, the housings are connected to the drive element by nonstressed rods. The magnetostrictive material consists of two rods of Terfenol D, each driven by its own solenoid. Two circular stress plates are placed on the ends of the rods and the rods are pre-stressed by four stress bolts that pass through the stress plates parallel to the Terfenol D rods. A more detailed diagram of the pre-stress arrangement is shown in Fig. 3. Four aluminum stress bolts are used to allow the Terfenol D rods

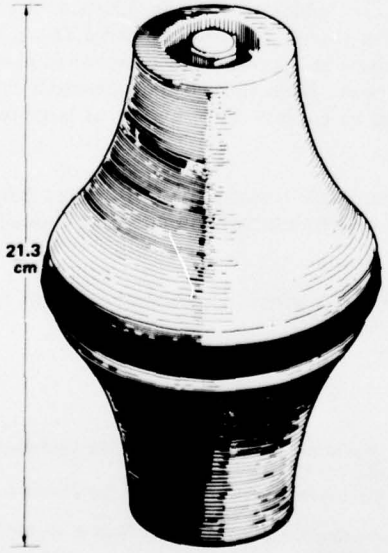

Fig. 1. Folded-horn transducer

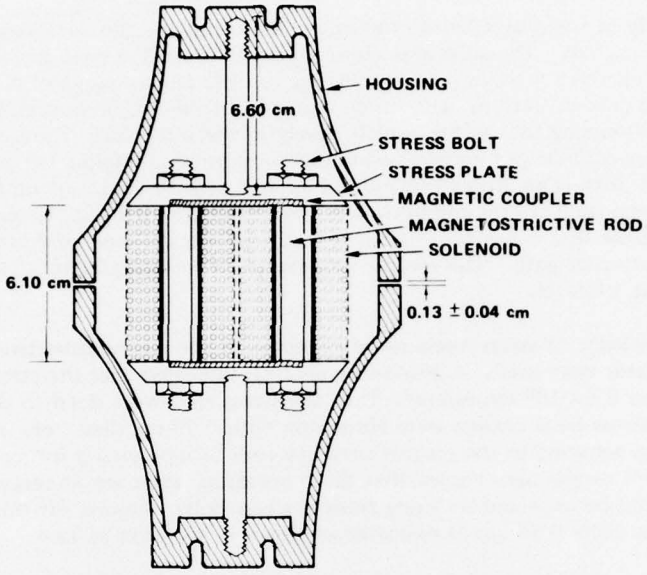

Fig. 2. Magnetostrictive drive unit as installed in transducer

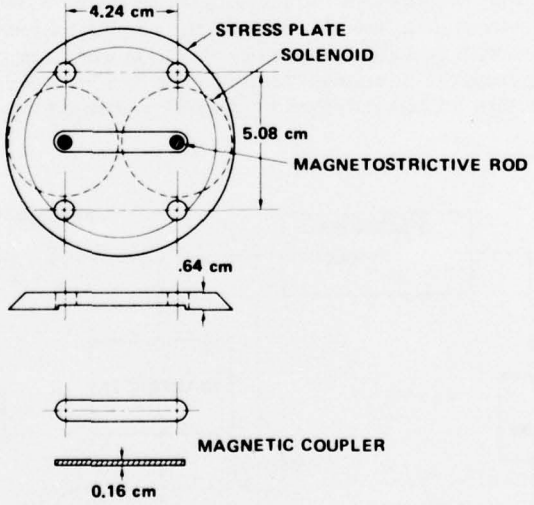

Fig. 3. Magnetostrictive rod pre-stress assembly

to be pre-stressed evenly with little net twisting force applied to the rods. This precaution was felt necessary because of the brittle nature of the rods. The stress plates are made of nonmagnetic stainless steel to prevent flux leakage. Also shown in Fig. 3 is a magnetic coupler made of laminated steel. The intent of this coupler is to allow a return path for the flux between the two magnetostrictive rods. Unfortunately, time has not permitted taking the measurements to determine the effectiveness of these magnetic couplers.

It was decided early in the design to use the solenoids to provide the necessary magnetic field bias rather than permanent magnets. The solenoids are designed to provide a peak magnetic field of 1,000 Oe (80 kA/m) without excessive heating. Each solenoid consists of 580 turns of No. 17 copper wire wound around a hollow core of Teflon. The inside diameter of the Teflon is slightly greater than the diameter of the rods, permitting the rods to vibrate freely in the solenoids. The field produced by each solenoid is approximately 125 Oe per ampere, assuming no magnetic coupling between the two rods. The maximum intended drive is an alternating current of 4 A zero to peak superimposed on a 4-A dc bias, producing a magnetic field alternating between 0 and 1,000 Oe (0 to 80 kA/m). The two solenoids are wired in series to insure that the fields applied to each rod are the same and in alternate rotational sense to promote a return flux path. The electric impedance of the transducer is largely inductive and has the value of 24 Ω at 1,000 Hz.

Without prior knowledge of stress levels to be expected in the magnetostrictive rods during operation, conservative estimates were used. A worst-case analysis indicated that the stress in a free rod driven to saturation could reach 5.5×10^8 dynes/cm^2. Thus the stress rods were sized to allow pre-stress to at least these levels. The stress bolts chosen were aluminum with 0.79-cm diameter. A pre-stress of 5.5×10^8 dynes/cm^2 was achieved in the magnetostrictive rods by applying a torque of 1.4×10^7 dyne-cm to each bolt. Subsequent results have shown that these pre-stress levels are unnecessarily high, and improved performance could be expected by using thinner stress bolts. Results for this unit and for a modified unit with stress bolts 0.48 cm in diameter are given in the next section.

EXPERIMENTAL RESULTS

The prototype transducers described in the previous section were tested at NUC's TRANSDEC calibration facility. The electrical drive was provided by the amplifier circuit shown in Fig. 4. Separate dc and ac sources were used with an inductor to block the ac power from the dc source and a capacitor to block the dc bias power from the ac source. Although the dc source was capable of supplying up to 10 A, the ac source was voltage limited at higher frequencies and could not deliver 4 A to the transducer across the operating band.

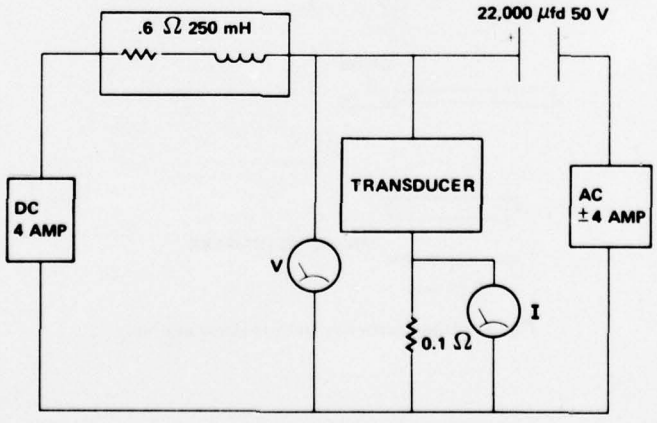

Fig. 4. Magnetostrictive amplifier circuit for dc-biased operation

Figure 5 shows the transmitting response of the original magnetostrictive transducer over the frequency band. The response was measured at a constant ac current of 0.35 A rms and a dc current of 2 A. The transmitting response is given in units of decibels relative to 1 μPa-m/Oe to remove the dependence on the solenoid design. To obtain the response in decibels relative to 1 μPa-m/A, the values in Fig. 5 should be increased by 41.9 dB. For comparative purposes, the transmitting voltage response of the piezoelectric version of this transducer is given in Fig. 6. A comparison of the transmitting responses for both designs is made in the following section.

The complex impedance of the magnetostrictive transducer was also measured and is shown in Fig. 7. The impedance was measured for 0.35 A rms ac and 2.0 A dc. As seen from the figure, the impedance is largely inductive. The real part of the impedance is relatively large at all frequencies, implying the existence of losses such as solenoid heating, material damping, and hysteresis losses.

The original prototype was subsequently modified by replacing the 0.79-cm diameter stress bolts with bolts 0.48 cm in diameter. The elastomer seal around the unit was also replaced by one similar to that used in the piezoelectric unit. The modified prototype had essentially the same low-frequency

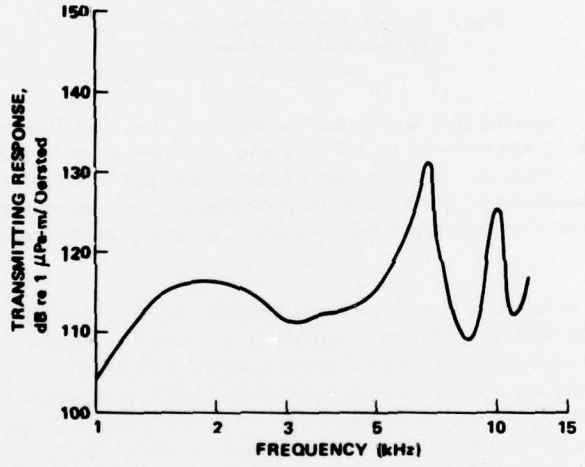

Fig. 5. Transmitting response of magnetostrictive transducer

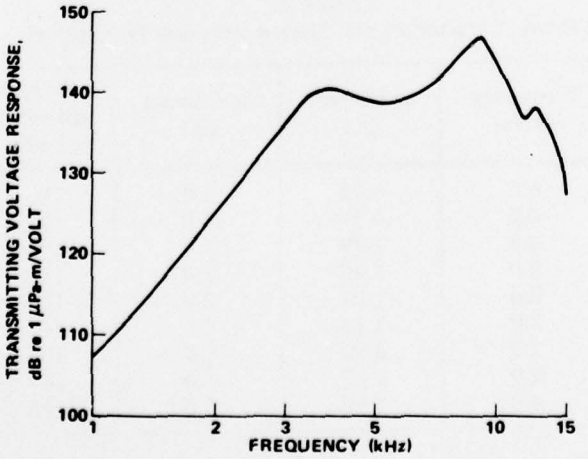

Fig. 6. Transmitting voltage response of piezoelectric transducer

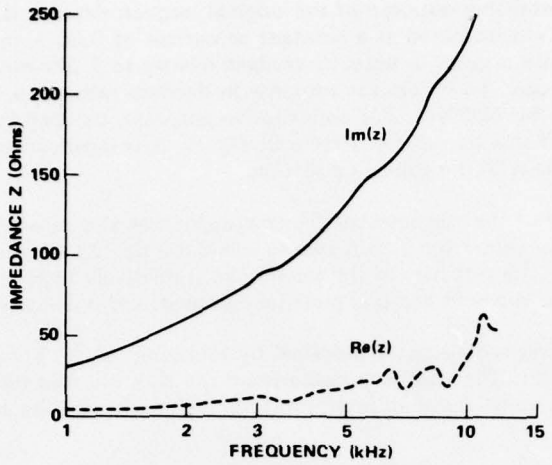

Fig. 7. Complex electrical impedance of magnetostrictive transducer

response as the original unit, implying that the broad resonance at 2 kHz is determined by the housings. The sharp resonance at 6.5 kHz was reduced to 5.5 kHz and increased in level, indicating that the stress bolts are significant for this resonance. The real part of the impedance was significantly reduced at lower frequencies indicating that the losses in the original magnetostrictive unit were largely due to the elastomer seal. The phase measurements were not taken with sufficient accuracy to determine the efficiency of the modified unit.

These measurements were taken at low-drive levels because the output of the amplifier was limited in the higher frequency range; however, some measurements were taken at higher drive levels and are summarized in Table I. Here unit 1 is the original magnetostrictive unit and unit 2 is the unit with modified stress bolts and elastomer seal. Although there were insufficient measurements to quantify the degree of linearity of the devices, the output pressure level is approximately proportional to input current level. Note in particular the increase in output level with dc bias. This behavior is consistent at all frequencies, with a 2.5-dB increase between 2.0- and 4.0-A dc, and a 1.5-dB increase and between 4.0- and 6.0-A.

TABLE I
High-Drive Characteristics of Magnetostrictive Transducers

Unit	Frequency (kHz)	ac Current (A)	dc Current (A)	Pressure (dB relative to 1 μPa-m)
1	6.5	0.35	4.0	165.5
1	6.5	0.70	4.0	172.0
1	6.5	1.29	4.0	178.2
2	2.0	0.42	2.0	149.0
2	2.0	1.07	2.0	159.0
2	2.0	1.14	4.0	161.5
2	2.0	2.03	4.0	166.8
2	2.0	1.17	6.0	163.0
2	2.0	2.09	6.0	168.3

CONCLUSIONS

The folded-horn transducer chosen for this study appears to be a good candidate for evaluating the rare-earth magnetostrictive materials, at least for the rod shapes currently available. The major purpose of the first magnetostrictive prototype was to demonstrate that the design concept was valid and that reasonable pressure output levels could be obtained, and these goals have been met. The broader question as to whether the rare-earth magnetostrictive materials are competitive with piezoelectric ceramic has not been answered either affirmatively or negatively by this work. The magnetostrictive material may also perform better in other geometric shapes, such as hollow cylinders, a question that has not been addressed in this paper.

Comparison of Figs. 5 and 6 shows certain similarities. Both transducers exhibit a broad low-frequency resonance at about 3.5 kHz for the piezoelectric unit and 2.0 kHz for the magnetostrictive unit. Both units exhibit a multiresonant behavior, but the higher frequency resonances of the piezoelectric unit are broader and occur at different frequencies. Some of this difference may be due to the different seals used to seal the air gap between the two housings. Experience[2] has shown that transducer performance is highly sensitive to the seal used. Another significant difference is the stiffness of the drive element in the two units; the piezoelectric stack is much stiffer than the magnetostrictive rods with their stress bolts, accounting for the higher resonant frequencies seen for that unit.

The maximum recommended drive for the piezoelectric unit is 50 dB relative to 1 V, above which excessive heating and depolarization can occur. Likewise, the maximum drive for the magnetostrictive unit is 50 dB relative to 1 Oe (80 A/m) (corresponding to a magnetic field varying between 0 and 1,000 Oe (0 to 80 kA/m)), above which solenoid heating and magnetic saturation can occur. Thus, Figs. 5 and 6 provide a rough comparison of the maximum output levels to be expected from each transducer. Note that the levels of Fig. 5 can be increased by 4 dB by using a 6-A dc bias. Of course, if the device is significantly nonlinear, it may not be possible to extrapolate the values in Fig. 5 by 50 dB. The results of Table I suggest this extrapolation may be valid, and on this assumption one sees that the magnetostrictive unit is capable of less output (up to 20 dB less) than the piezoelectric unit except at the lower frequencies. These lower levels seem to be due to two factors: the magnetostrictive unit has too much stiffness in its stress rods relative to the stiffness of the active material and the volume of active material in the magnetostrictive unit is 42 times less than that in the piezoelectric unit, thus limiting the amount of electromechanical energy conversion that can be expected. One would expect, on the basis of the recommendations in the following paragraph, that much greater output levels could be achieved in the magnetostrictive unit.

The results on the first prototype described in this paper suggest several design iterations that could improve the performance of that unit. One modification that has been partially tested would be to reduce the stiffness of stress bolts. A more thorough analysis of expected stress levels should be performed, using models for an impedance-loaded rod. Results indicate that the stress bolt stiffness could be chosen to optimize output at the higher frequencies. Another desirable modification would be to use more magnetostrictive material, although the amount of material is ultimately limited by the large solenoids required to drive the material to near saturation. The use of permanent magnets rather than a dc bias should be considered to improve efficiency and maximum output, reduce solenoid size, and simplify the amplifier design. Measurements should be made to determine the extent of magnetic flux coupling, and more effective coupling techniques should be investigated. Finally, the stainless steel stress plate should be replaced by a thicker aluminum plate to minimize plate bending. Once a second iteration design is fabricated, an extensive set of measurements could be performed to determine efficiency of the unit and linearity of the device under various drive and bias levels.

ACKNOWLEDGMENTS

The authors are indebted to Leonard Reavis and Richard Dettmer, who fabricated the prototype magnetostrictive transducer under severe time constraints. Arthur Clark and Howard Savage provided the magnetostrictive rods and much useful information on material characteristics. This work was sponsored by the Naval Sea Systems Command, Code SEA 06H1; Charles Walker was the Program Manager.

[2]W. L. Angeloff, Naval Undersea Center, private communication.

U.S. Navy Journal of Underwater Acoustics Volume 27, Number 1 January 1977

RARE-EARTH MAGNETOSTRICTIVE TRANSDUCER AND MATERIAL DEVELOPMENT STUDIES*

Orrill L. Akervold and David L. Hutchins
Honeywell Marine System Division
Seattle, Washington 98107

and

R. G. Johnson and B. G. Koepke
Honeywell Corporate Research Center
Minneapolis, Minnesota 55408

ABSTRACT

Rare-earth magnetostrictive material and transducer studies conducted at Honeywell in 1975 are reviewed. The topics discussed include preliminary measurements of the magnetostrictive effect in arc-cast unannealed specimens of $Tb_{0.3}Dy_{0.7}Fe_2$, an electropolishing and etching procedure developed for the metallographic examination of the compound surface, and an experimental transducer configuration.

INTRODUCTION

Several new magnetostrictive materials have been developed at the Naval Surface Weapons Center and the Naval Research Laboratory. These materials are metals consisting of combinations of iron and various rare-earth elements,† such as dyprosium, terbium, and holmium. They exhibit very high magnetostrictive strains and are, therefore, attractive candidates for use in high-power transducers.

The state of the art of these new materials has reached the point where a transducer can and should be designed, built, and tested. The fundamental physical properties (magnetostrictive strain, anisotropy constants, etc.) have been measured, as have such acoustic-related properties as coupling coefficient. The actual performance obtainable with these materials can, however, only be assessed by constructing and evaluating a suitable transducer.

Honeywell has conducted material and transducer studies to begin to assess the utility of these materials in practical transducers. An experimental transducer has been designed and built at the Marine Systems Division, and the Corporate Research Center has initiated a research effort into the metallurgy of the rare-earth compounds. The progress and status of these efforts is summarized in this paper.

EXPERIMENTAL TRANSDUCER

Design

Dr. Arthur Clark of the Naval Surface Weapons Center supplied the Honeywell Marine Systems Division with four rods (2-1/4 in. (5.72 cm) long by 1/4 in. (6.3-mm) in diameter) of Terfenol. (Terfenol is the Naval Surface Weapons Center abbreviation for $Tb_{0.3}Dy_{0.7}Fe_2$.) These rods were incorporated into the simple longitudinal vibrator transducer illustrated in Fig. 1. A photograph of the actual transducer is shown in Fig. 2. This experimental transducer has the following features:

*Presented at the Workshop on Magnetostrictive Materials held under the sponsorship of the Underwater Sound Advisory Group and the Naval Research Laboratory, Orlando, Florida, 25-26 February 1976.
†A brief discussion of the rare-earth metals is given by Dr. Timme in his Introduction to the Theme in this issue.

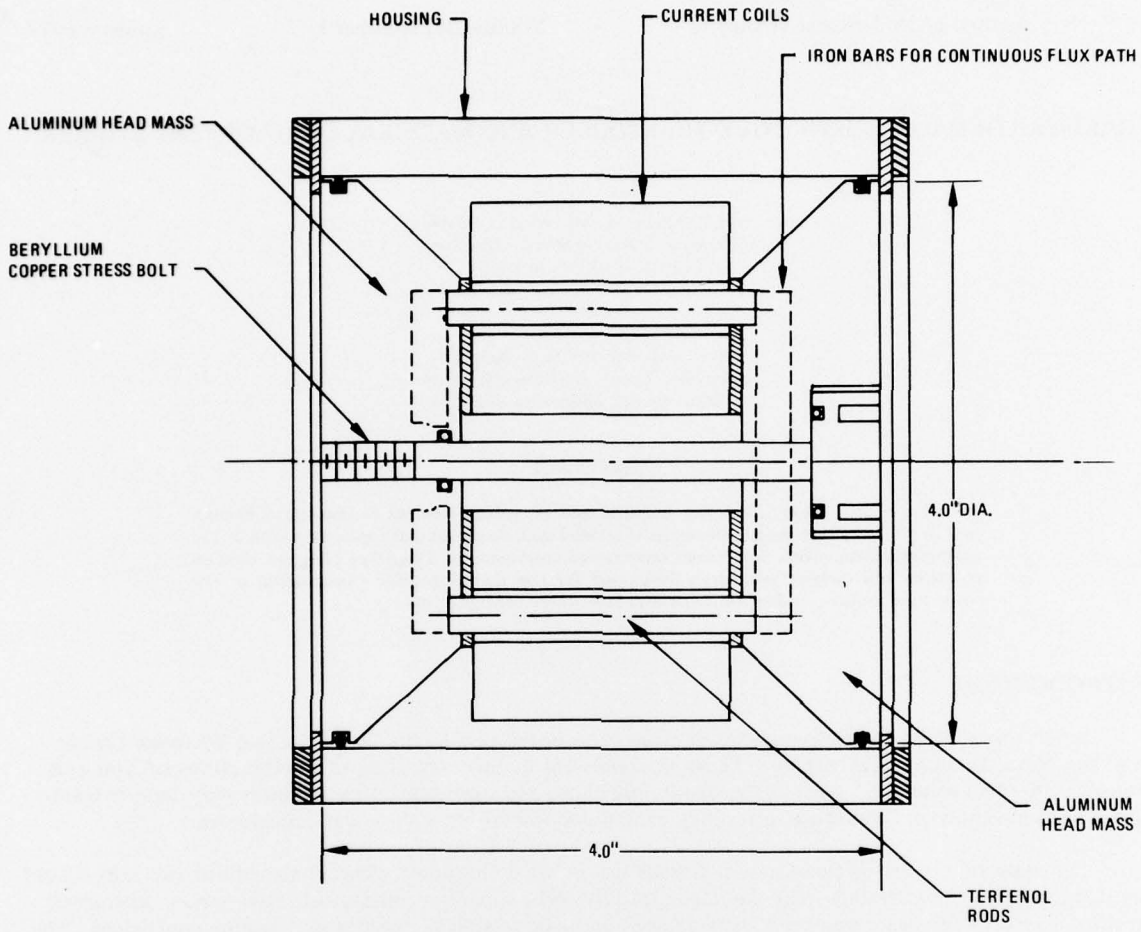

Fig. 1. Magnetostrictive transducer

- It is experimentally flexible in that the magnetostrictive rods, the bias coils, and the drive coils can easily be changed.

- It is a conceptually simple, double-ended, longitudinal vibrator and is, therefore, relatively easy to model mathematically.

- The magnetostrictive active element can easily be replaced with a comparable ceramic element.

This simple transducer provides a vehicle for measurement of the acoustic capabilities of the new rare-earth magnetostrictive materials and facilitates comparison of the capabilities with both theoretical predictions and with the capabilities of comparable ceramic materials.

Test Results

Preliminary test results obtained with this transducer are shown in Figs. 3 and 4. The ac drive signal in all cases was 30 V_{rms}. Under these drive conditions the maximum sound pressure level reached was 174 dB relative to 1 μPa at 1 yard (1 m). This was achieved at 3.5 kHz at the 10-A dc bias drive. The ac efficiency was about 14%, and the overall efficiency was approximately 1%.

Fig. 2. Rare-earth magnetostrictive transducer

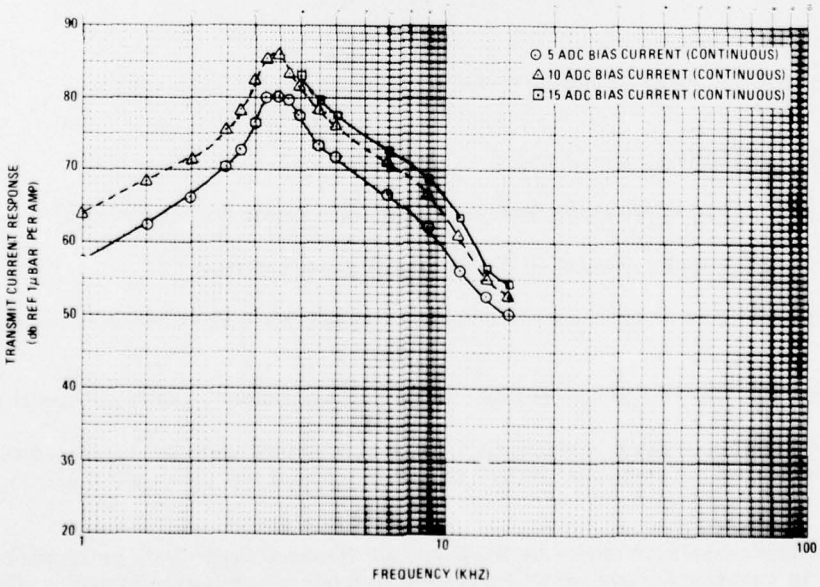

Fig. 3. Rare-earth magnetostrictive transducer transmit current acoustic response

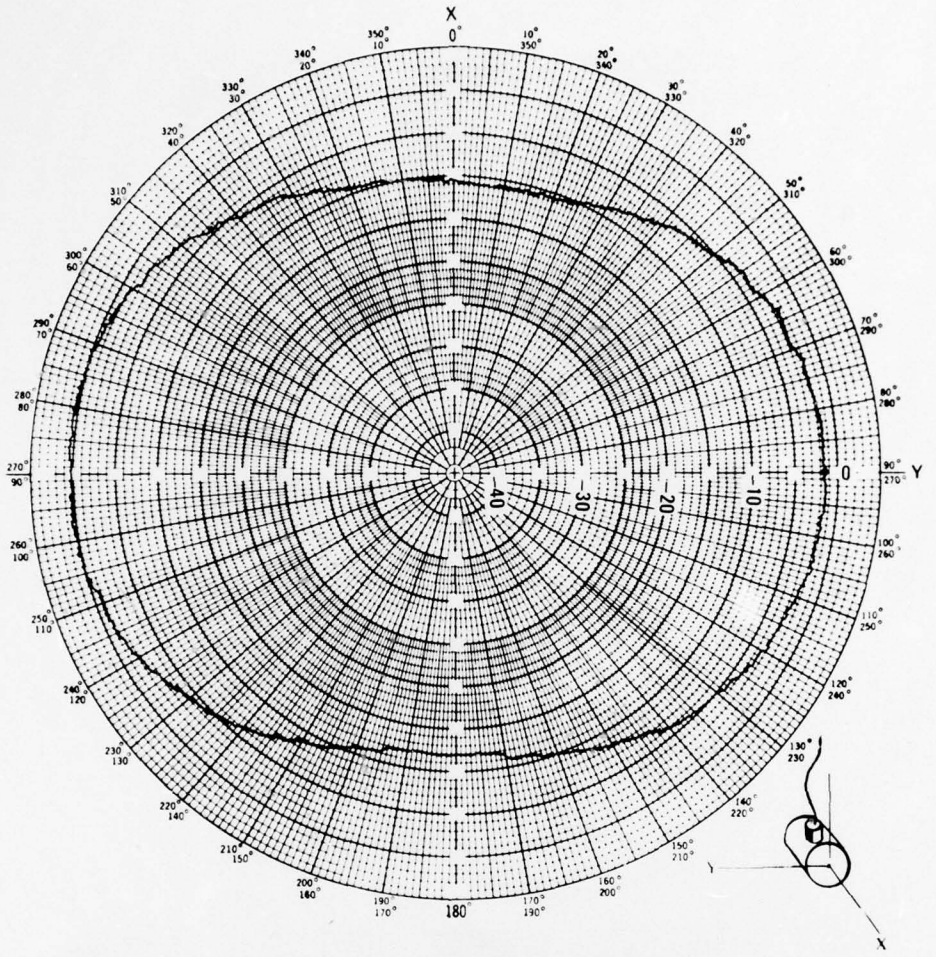

Fig. 4. Rare-earth magnetostrictive directivity pattern at 3.5 kHz in x, y plane

METALLURGICAL STUDIES

The goals of the 1975 effort at the Honeywell Corporate Research Center were to—

- Develop techniques for fabricating the magnetostrictive materials
- Develop techniques of polishing and etching for metallurgical examination in the resulting materials
- Fabricate magnetostrictive rods suitable for use and evaluation in the experimental transducer.

The results were as follows: (1) an electropolishing and etching procedure was developed for the metallographic examination of the compound surface and (2) compound test pieces up to 1-1/2 in. (3.81 cm) long were cast.

A ternary compound was produced by the Corporate Research Center with composition near $Tb_{0.3}Dy_{0.7}Fe_2$ to minimize the anisotropy energy and to retain a large magentostrictive effect. The objective of the first part of the investigation was to make the compound with all, or as much as possible, of the material in the Laves phase, which has the desired large magnetostrictive properties. If the

Tb and Dy behave in a chemically similar way (as is often the case with rare-earth elements), then the ternary compound can be described by a pseudobinary diagram similar to the Dy-Fe binary phase diagram in Fig. 5. Preliminary work indicates that this is the case and that only three phases, characteristic of a binary compound, are distinguishable in the unannealed cast material.

Figures 6 and 7 show the result of electropolishing and etching an unannealed specimen of the stoichiometric material $Tb_{0.3}Dy_{0.7}Fe_2$. The dominant surface is $(Tb, Dy)_1 Fe_2$, the slightly deeper etched long narrow structures are $(TbDy)_1 Fe_3$, and the bright crosslike formation that is hardly attacked by the acid is the (Tb, Dy) oxide or nitride impurity phase with no detectable iron. The excess rare-earth phase appears only in compounds having less than the stoichiometric amount of iron. These identifications are based on the EDAX identification of the elements and the indicated relative amounts of each element in the three different phases that are present.

Preliminary magnetostriction measurements as a function of applied field for unannealed compounds are shown in Fig. 8. Although high values of λ_{11} are obtained, the desired saturation effect at low applied fields was not always present in the preliminary runs.

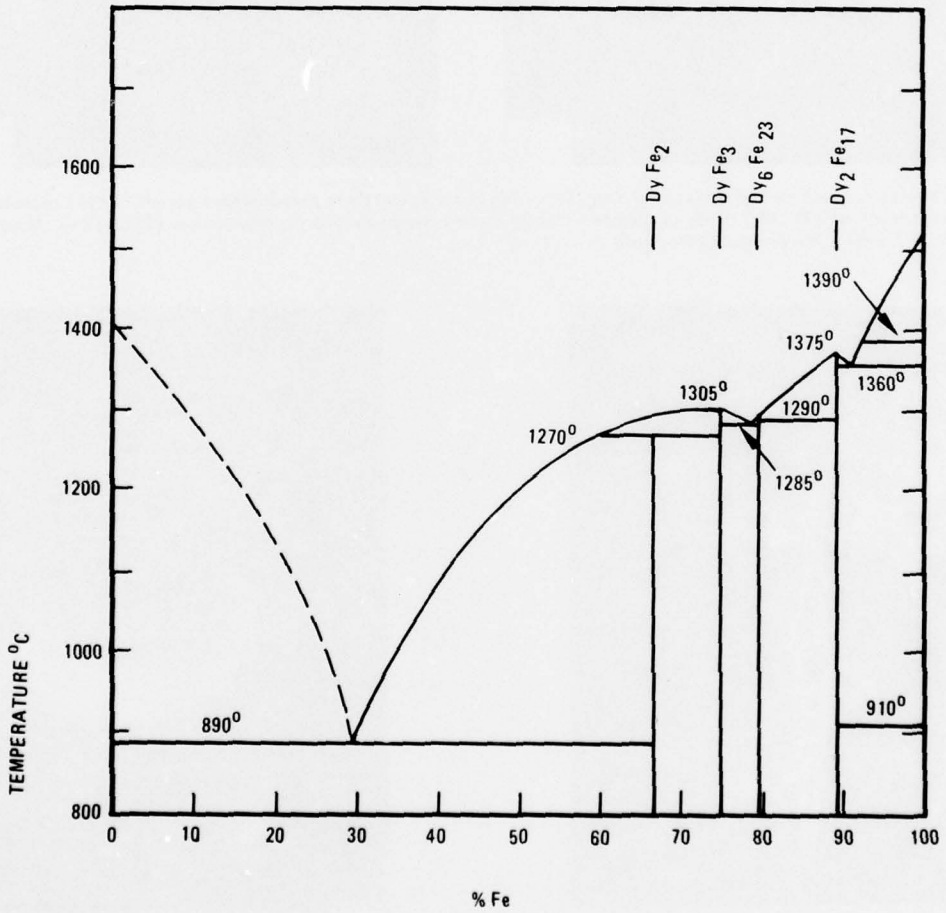

Fig. 5. The dysprosium-iron binary system. (This phase diagram appears to be a satisfactory guide in the study of the pseudobinary system: (Tb, Dy) = Fe, particularly when terbium is the minor constituent as in the compound $Tb_{0.3}Dy_{0.7}Fe_2$.)

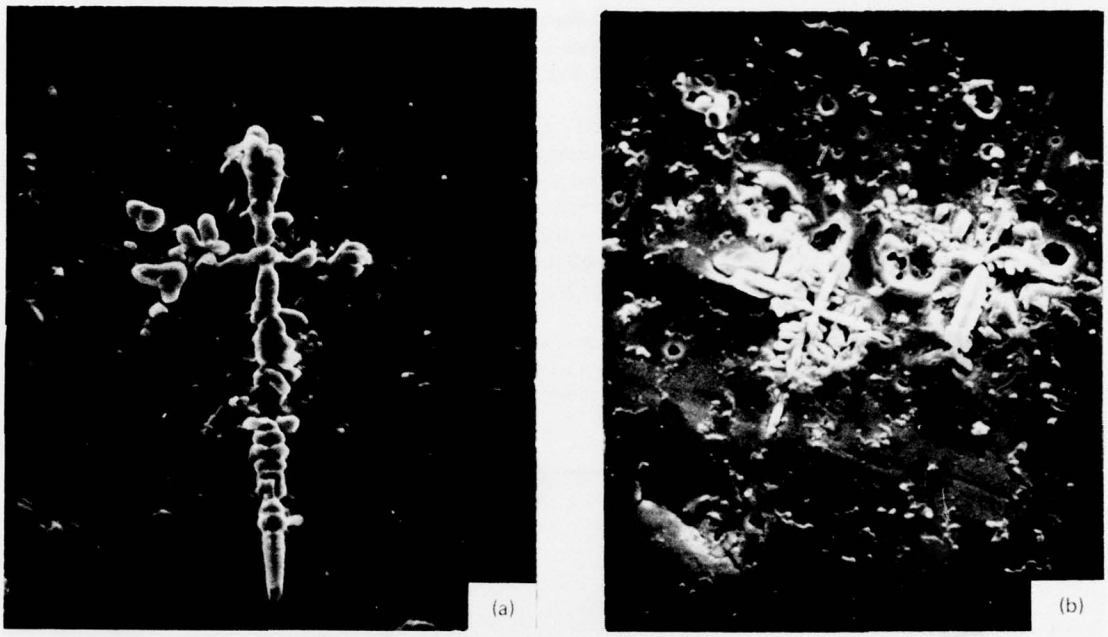

Fig. 6. "Two examples of etched surfaces of $Tb_{0.3}Dy_{0.7}Fe_2$ showing the three pseudobinary phases. Bright cross-like structures in sharp relief are (Tb, Dy) oxide or nitride. Slightly etched needle-shaped depressions are $(TbDy)Fe_3$. Major smooth surface is $(Tb, Dy)Fe_2$, the desired Laves phase.

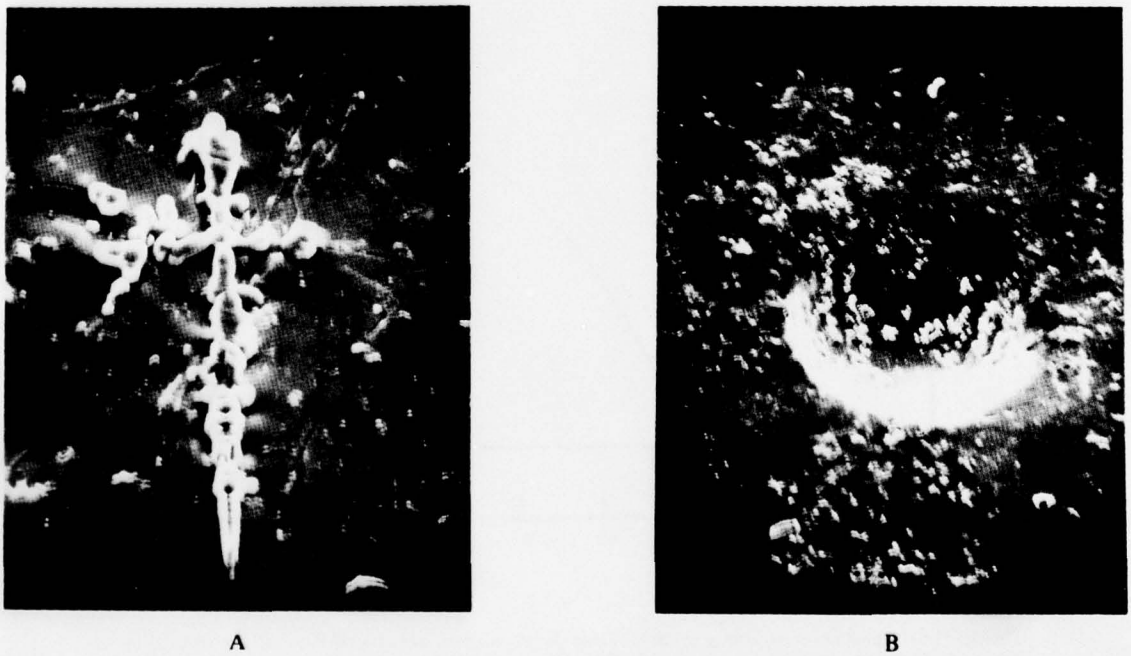

Fig. 7. A polished and etched specimen of $Tb_{0.3}Dy_{0.7}Fe_{1.8}$. A dendrite of (TbDy) composition stands out in sharp relief. The long, shallow etched zones are $(TbDy)Fe_3$. The general field is $(TbDy)Fe_2$. Scanning electron microscope photograph. (a) At 1,150×. (b) At 100×.

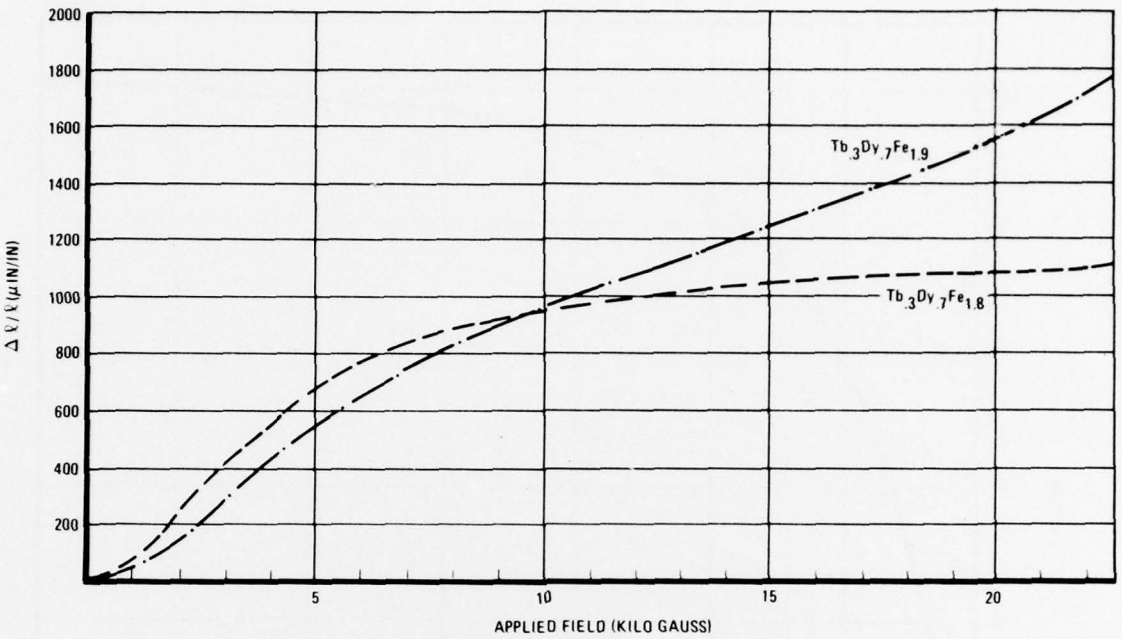

Fig. 8. Examples of magnetostrictive elongation in unannealed melts of TbDyFe compounds

Ten rods of $Tb_{0.3}Dy_{0.7}Fe_{1.8}$ were fabricated for use in the experimental transducer. These rods are each about 1-1/4 in. (3.18 cm) long by 1/4 in. (6.3 mm) in diameter. The strain characteristics of these rods are shown in Fig. 9.

SUMMARY

The experimental transducer worked well from a mechanical and acoustical standpoint and is a useful test bed for further studies of its measured and potential electrical properties. Comparison must be made of its performance to the performance resulting when the magnetostrictive rods are replaced with a ceramic driver producing a resonance at the same frequency. If the electroacoustic performance of the rare-earth materials warrants its use, the metallurgical studies are needed to develop practical methods of fabricating rare-earth iron parts with the desired configurations for transducer applications.

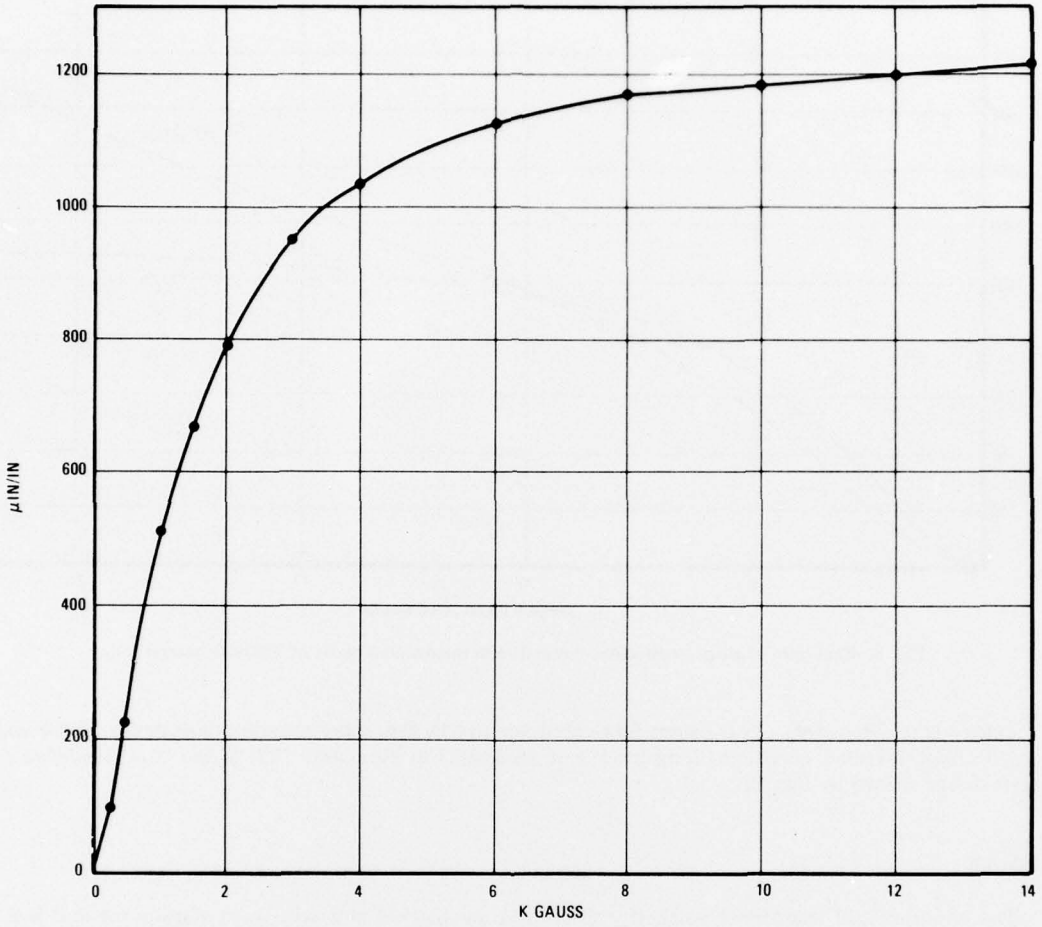

Fig. 9. Magnetostrictive strain in an arc-cast unannealed specimen having an overall composition of $Tb_{0.3}Dy_{0.7}Fe_{1.85}$